Design, Synthesis, and Evaluation of Thymidine Derivatives as Inhibitors of a
Thymidylyltransferase Enzyme, Cps2L

by

Alana M. M. Rangaswamy

Submitted in partial fulfilment of the requirements
for the degree of Master of Science

at

Dalhousie University
Halifax, Nova Scotia
July 2020

"The definition of insanity

is repeating the same thing over and over

and expecting a different result."

-A quote most likely misattributed to Albert Einstein.

This document serves as a testament to the notion

that scientific pursuits require at least a small degree of insanity.

Table of Contents

iii

List of Tables

List of Figures

List of Schemes

Abstract

The inhibition of thymidylyltransferase enzymes has long been studied as a potential avenue for antibiotic development. Several thymidine derivatives were designed, synthesized, and evaluated for binding and inhibition against Cps2L, a thymidylyltransferase enzyme present in the bacteria *Streptococcus pneumoniae*. Compounds that were evaluated via WaterLOGSY binding studies indicated binding. Furthermore, most compounds demonstrated reversible inhibition, with many of those displaying K_i values within micromolar ranges. Compounds **4d** and **4e** bearing aldehydes, and compounds **4a** and **4b** bearing ortho-formylarylboronic acid pinacol esters, have the potential to covalently modify lysine residues at the active site of Cps2L. Particular potency was observed from compounds **4d** and **4f**; structure-activity relationship studies with these compounds may provide future directions for the iterative design of these inhibitors.

List of Abbreviations and Symbols Used

2-MeTHF	2-Methyltetrahydrofuran
APCI	Atmospheric pressure chemical ionization
APS	Ammonium persulfate
ATP-Glc	Adenosine-5′-triphosphate- α-D-glucose
AU	Absorbance units
B_2Pin_2	Bis(pinacolato)diboron
BPin	Pinacolboronate
COMU	(1-Cyano-2-ethoxy-2-oxoethylidenaminooxy)dimethylamino-morpholino-carbenium hexafluorophosphate
COSY	Correlation spectroscopy
CuAAC	Copper-catalyzed azide-alkyne cycloaddition
DCC	Dicyclohexylcarbodiimide
DCM	Dichloromethane
DIPEA	N-Ethyl-N,N-diisopropylamine
DMSO	Dimethylsulfoxide
DMF	N,N-Dimethylformamide
dTDP	2′-Deoxythymidine-5′-diphosphate
dTDP-glucose	2′-Deoxythymidine-5′-diphosphate-α-D-glucose
dTDP-rhamnose	2′-Deoxythymidine-5′-diphosphate-β-L-rhamnose
dTMP	2′-Deoxythymidine-5′-monophosphate
dTP_4	2′-Deoxythymidine-5′-tetraphosphate
dTTP	2′-Deoxythymidine-5′-triphosphate
EDC	1-Ethyl-3-(3-dimethylaminopropyl)carbodiimide
eq.	Equivalents
ESI	Electrospray ionization
EtOAc	Ethyl acetate
G1P	α-D-Glucose-1-phosphate
g	Gravity of earth

HATU	Hexafluorophosphate azabenzotriazole tetramethyl uronium (1-[bis(dimethylamino)methylene]-1H-1,2,3-triazolo[4,5-b]pyridinium 3-oxid hexafluorophosphate)
HMBC	Heteronuclear multiple bond correlation
HPLC	High-performance liquid chromatography
hPNP	Human purine nucleoside phosphorylase
HSQC	Heteronuclear single quantum correlation
IPP	Inorganic pyrophosphatase
IPTG	Isopropyl-β-D-1-thiogalactopyranoside
K[23]	Lysine at position [23] in a polypeptide
K_D	Dissociation constant
K_i	Inhibition constant
K_{iC}	Competitive-mode inhibition constant
K_M	Michaelis constant
K_S	Substrate inhibition constant
K_{iU}	Uncompetitive-mode inhibition constant
LB [media]	Lysogeny broth [media]
LB_{kan}	Lysogeny broth containing kanamycin
LB [plot]	Lineweaver-Burk [plot]
Me	Methyl
MESG	7-methyl-6-thioguanosine
MOPS	3-(N-Morpholino)propanesulfonic acid
NMR	Nuclear magnetic resonance
o-FABA	ortho-Formylarylboronic acid
ORTEP	Oak Ridge thermal ellipsoid plot
P_i	Inorganic phosphate
PP_i	Inorganic pyrophosphate
SAD	Sum of absolute differences
SAR	Structure-activity relationship

r.t.	Room temperature
SDS	Sodium dodecyl sulfate
SDS-PAGE	Sodium dodecyl sulfate polyacrylamide gel electrophoresis
SPAAC	Strain-Promoted azide-alkyne cycloaddition
TBTA	Tris(benzyltriazolylmethyl)amine
TBTU	N,N,N′,N′-Tetramethyl-O-(benzotriazol-1-yl)uronium tetrafluoroborate
TFA	Trifluoroacetic acid
THF	Tetrahydrofuran
TLC	Thin-layer chromatography
TMEDA	Tetramethylethylenediamine
Tris	Tris(hydroxymethyl)aminomethane
UP$_4$-Glc	Uridine-5′-tetraphosphate-α-D-glucose
UTP-Glc	Uridine-5′-triphosphate-α-D-glucose
UV-vis	Ultraviolet-visible
v	Initial reaction rate
V_{max}	Maximum reaction rate
WaterLOGSY	Water-ligand observed through gradient spectroscopy
XO	Xanthine oxidase

Acknowledgements

I would first like to acknowledge my supervisor, Dr. David Jakeman, for providing guidance as I began independent research, and always being willing and available to offer advice. I would like to thank the members of the Jakeman group: thanks particularly to past members Dr. Stephanie Forget, Dr. Jian-She Zhu, and Madison Carroll, who welcomed me into the group and taught me several techniques in synthetic chemistry and microbiology. I would also like to thank present members Dr. Michael Beh, Dr. Ebrahim Soleimani, and Julie Cormier, who all contributed in various ways to this project. I would also like to acknowledge past undergraduate students Steve Sequeira and Firi Adam, who taught me as much as I hopefully taught them.

I would like to thank my supervisory committee, Dr. Alex Speed and Dr. Stephen Bearne, for providing guidance, support, and helpful advice throughout the course of this challenging project.

I would like to thank the incredible staff in the Dalhousie Department of Chemistry. Thanks especially to Dr. Mike Lumsden of the NMR facility for providing any help I needed in acquiring or interpreting NMR data, and Xiao Feng of the Mass Spectrometry facility, who acquired all of the mass spectrometry data for this project. Thanks also to Lea Gawne, for helping me stay on track and always providing prompt and helpful information whenever I needed it. Additionally, I would like to thank Dr. Katherine Robertson of the the Saint Mary's University Chemistry Department, who performed all X-ray crystallography experiments on compounds I synthesized for this project.

I would like to thank the various sources who contributed to funding for this project, specifically the Natural Sciences and Engineering Research Council, the Canadian Institutes of Health Research, and the CREATE BioActives program.

Finally, I would like to thank my family, who has always supported me, and my friends. Thanks especially to Dr. Sarah Greening, who taught me how to be a graduate student and a leader, and Roberto Diaz-Rodriguez, for everything.

If you are a researcher in need of encouragement, I would like to acknowledge you, as well.

Chapter 1. Introduction

1.1. Background

Streptococcus pneumoniae is an infectious Gram-positive species of bacteria, and a common human pathogen. It resides in human mucosal surfaces, and is responsible for many diseases such as pneumonia, sepsis, and meningitis, depending on its location of residence within the human body.[1] *S. pneumoniae* has been long known as an antibiotic-resistant strain,[2] with clinical resistance to penicillin reported as early as 1965.[3] This antibiotic resistance is likely due in part to its natural competence,[1] i.e., its ability to uptake external plasmids in order to modify its own genome. *S. pneumoniae* has evolved a vast arsenal of mechanisms to deal with a variety of antimicrobials, including modifying target proteins to decrease their affinity for the antibiotic (as in β-lactams), or developing improved efflux mechanisms to flush out the undesirable compound (as in macrolides).[4] Furthermore, genes coding for these modifications are highly mutable and have been found across several strains, suggesting that heightened resistance can be passed not only between organisms but horizontally between other streptococci.[4]

Antibiotic resistance is a force to be reckoned with, and appears at the forefront of modern medical research.[5] The issue has been exacerbated by misuse of antibiotics, both in medical cases such as over- and mis-prescribing[6] and in agriculture, where resistant bacteria are spread to soil, water, and humans through consumption and waste run-off.[7] The World Health Organization now considers antibiotic resistance to be one of the overall greatest threats to human health.[8] It is, therefore, essential that new antibiotics are developed with novel targeting strategies and mechanisms of action.[9]

1.2. Rhamnose Biosynthesis as a Therapeutic Target

Rhamnose is a sugar commonly found in bacteria, serving varied functions dependent upon the bacterial species. Rhamnose is biosynthesized from glucose and is responsible for the viability and virulence of several pathogens, including *S. pneumoniae*, strains within the *Pseudomonas* and *Mycobacterium* genera, and others.[10] In streptococci, rhamnose plays a significant structural role in the capsular polysaccharide, which replaces teichoic acid polymers in the cell wall.[10] Critically, while rhamnose is found in bacteria and plants, it is not known to be produced, used, or metabolized by humans.[11] The rhamnose biosynthesis

pathway is, therefore, an attractive target for new antibiotics, as sufficiently selective drugs are less likely to interfere with human metabolic processes.

Biosynthesis of rhamnose from α-D-glucose-1-phosphate (G1P) follows a 4-step process (Scheme 1.1),[12] catalyzed by enzymes generally named RmlA-D. In the first step, RmlA catalyzes the transfer of thymidine monophosphate (dTMP) onto G1P to form dTDP-α-D-glucose (dTDP-glucose) with the release of pyrophosphate from the thymidine triphosphate (dTTP) substrate. RmlB, in conjunction with coenzyme NAD$^+$, oxidizes the 4′-hydroxyl to the corresponding ketone, followed by dehydration at the 6′ carbon. RmlC performs a double-epimerization to obtain the ring-flipped sugar with opposite stereochemistry at the 3′ and 5′ carbons, then RmlD reduces the ketone at the 4′ position to afford dTDP-β-L-rhamnose (dTDP-rhamnose), the formal building block of rhamose-containing polymers in bacteria.[9] dTDP-rhamnose performs a secondary function, acting as a feedback-loop inhibitor of RmlA by binding at its allosteric site.
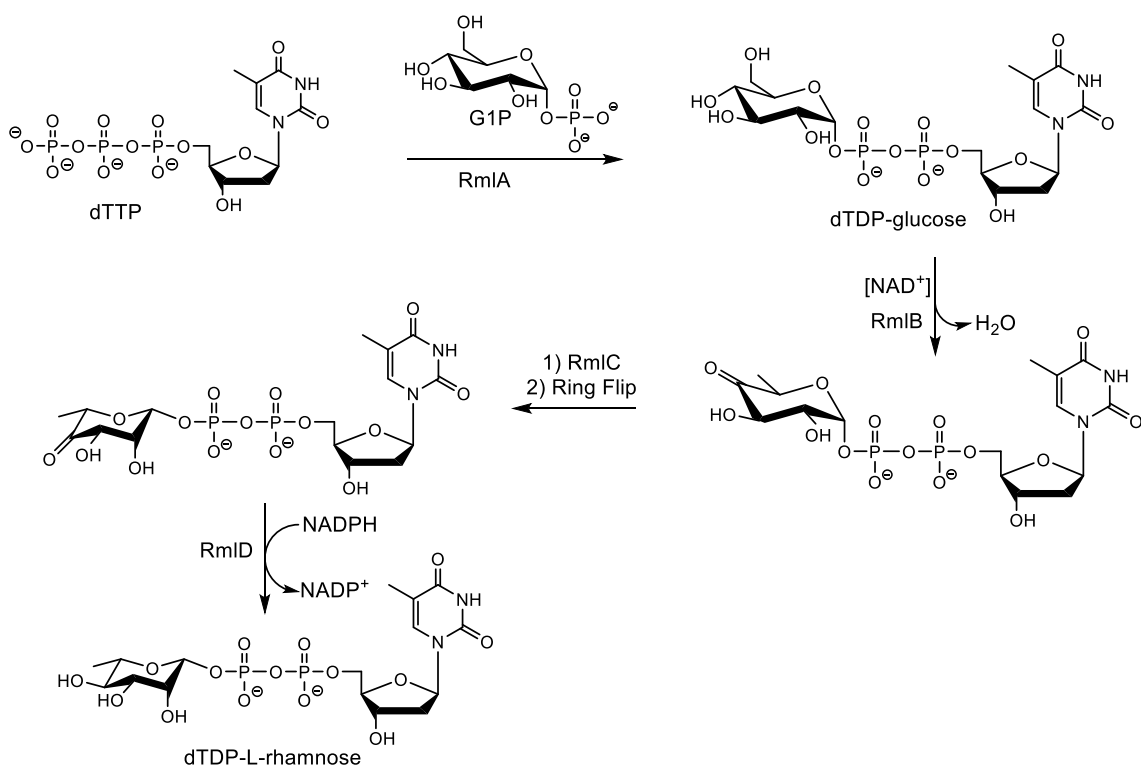
Scheme 1.1: Biosynthesis of dTDP-β-L-rhamnose.

Any of the four Rml enzymes may be viable therapeutic targets when seeking to inhibit the biosynthesis of rhamnose; in fact, substrate analogues may well inhibit more

than one simultaneously. We have chosen to direct our focus to RmlA; specifically, the homologue of RmlA found in *S. pneumoniae*, named Cps2L. Cps2L has been the subject of in-depth study in the Jakeman lab in the past,[13–15] and therefore serves as a reasonable starting point for this project. Furthermore, Cps2L has a high degree of homology with corresponding RmlA enzymes from other bacterial strains, demonstrating, for example, 67% amino acid identity with RmlA from *Pseudomonas aeruginosa*.[a] Therefore, potent inhibitors of Cps2L may also inhibit RmlA enzymes from other pathogens, thus acting as broad-spectrum antibiotics.
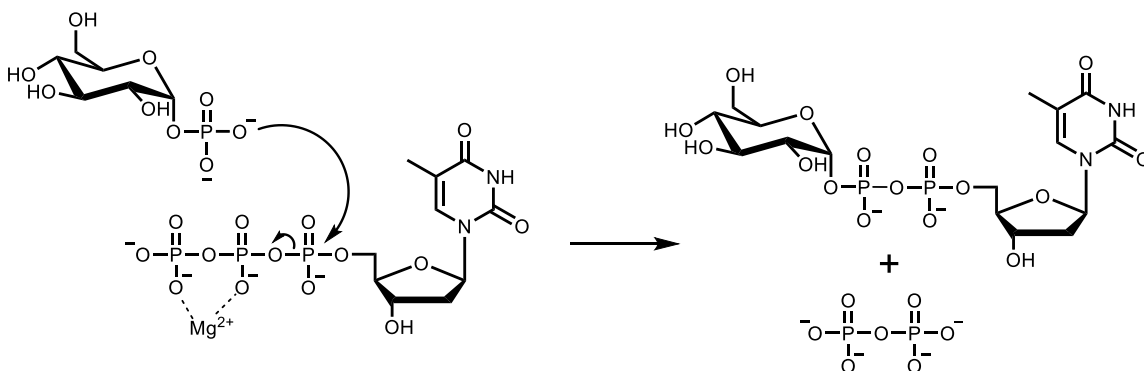
Scheme 1.2: Mechanism of the physiological reaction catalyzed by Cps2L.

1.3. Targeting Cps2L

The mechanism for the reaction catalyzed by Cps2L is shown in Scheme 1.2. A logical first step in designing inhibitors of an enzyme is to derivatize one of the natural substrates (and/or, as the case may be, natural inhibitors) of the enzyme. The Jakeman group has thus far focused largely on developing analogues of G1P[13–15] but has only done preliminary work in determining the inhibition of Cps2L by molecules bearing a thymidine moiety.[16] In the latter study, analogues of the product, dTDP-glucose, were synthesized with a varying number of phosphate units (see Figure 1.1). They determined that a 4-phosphate linker led to the most potent inhibitor, which informs us that the enzyme will accept, and potentially prefer, a larger molecule than the product, dTDP-glucose. With this in mind, herein we report the first in-depth study focusing on thymidine derivatives as inhibitors of

---

[a] The amino acid sequences from Cps2L from *S. pneumoniae* (GenBank no. AVN85499.1) and RmlA from *P. aeruginosa* (GenBank no. ARU35951.1) were accessed from the NCBI Protein Database and compared using Clustal Omega alongside those of RmlA from *E. coli* and *M. tuberculosis*.[70] See Appendix A.

Cps2L, which are expected to impart improved selectivity for thymidylyltransferases (i.e. RmlA) over other enzymes.

8 - 20 % yield

dTDP–Glc 2	UTP–Glc 5
dTTP–Glc 3	UP$_4$–Glc 6
dTP$_4$–Glc 4	ATP–Glc 7
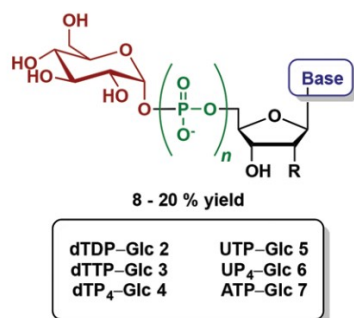
Figure 1.1: Inhibitors previously synthesized by the Jakeman group. Compounds 2, 3, and 4 bear a thymine base. Figure adapted from Smithen *et al.* 2015.[16]

Cps2L, as well as all other RmlA homologues, has a tetrameric quaternary structure (see Figure 1.2), where each monomer bears an active site and an allosteric site (where the aforementioned dTDP-rhamnose binds as a feedback inhibitor). Cps2L has been sequenced, and through comparison with RmlA of *Pseudomonas aeruginosa*,[17] the amino acid residues present in the active site that are relevant for binding of substrates have been determined. The thymidine imide moiety participates in H-bonding with a proximal glutamine residue,[18] but no residues directly participate in catalysis. Therefore, when designing active site inhibitors, we seek to optimize interactions between the inhibitor and noncatalytic residues, with the hope that this will produce a molecule with a higher binding affinity than the substrate for which it is an analogue, dTTP.

One way to increase the binding affinity is to incorporate a functional group "warhead", a moiety on the inhibitor which can covalently modify a residue of interest. Covalent protein modification has been used extensively not only for inhibition studies, but also for tagging proteins (with, for instance, fluorophores for observation using fluorescence microscopy). The most common amino acid target is cysteine, a residue with a highly nucleophilic methanethiol sidechain, which will readily undergo reactions with soft electrophiles such as maleimides,[19] alkyl halides[20] or acrylamides.[21] Cysteine targeting has been used to great effect in some cancer drugs, where mutations often lead to acquired cysteine residues in proteins.[22] However, cysteine has a low natural abundance (<2%)[19]

and electrophiles that interact with cysteine may also be subject to nucleophilic attack by glutathione, which is ubiquitous in living systems.[19]
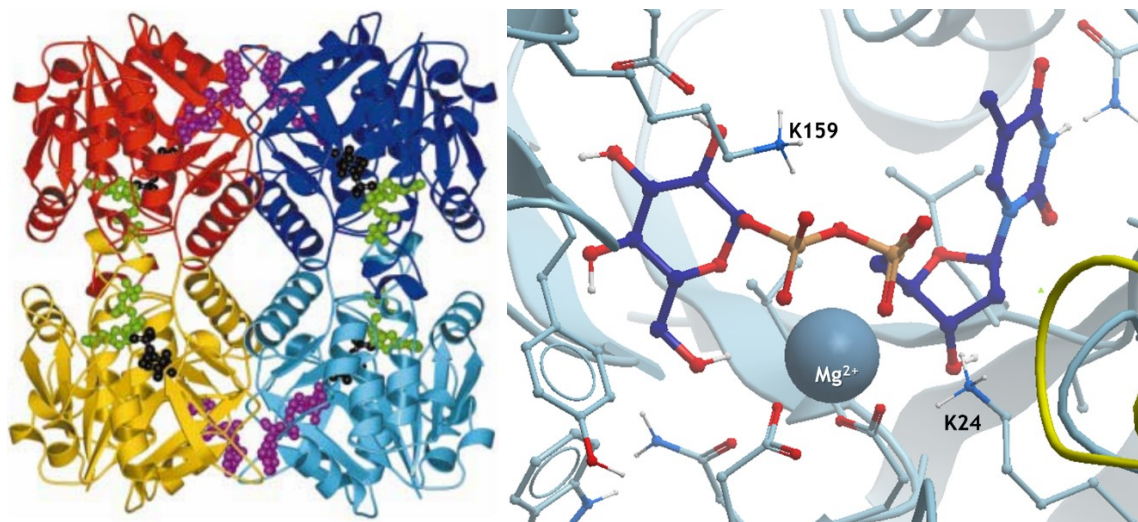
Figure 1.2: Crystal structures of RmlA homologues. Left: ribbon structure of RmlA,(*P. aeruginosa*) binding dTTP (green) and G1P (black) at the active sites, and dTDP-rhamnose (magenta) at the allosteric sites.[18] Each monomeric unit is indicated in red, dark blue, yellow, and light blue. Right: active site of RmlA (*M. tuberculosis*) binding dTDP-glucose. The location of the active site lysine residues are indicated (note the specific residue numbers vary between homologues).[b]

The active site of our enzyme of interest, Cps2L, does not contain cysteine residues, but fortunately does contain another nucleophilic residue: the alkyl amine, lysine. There are two lysine residues (K23 and K160) in the active site of Cps2L, which are conserved across RmlA homologues (albeit in slightly different positions, see Figure 1.2). Lysine is a harder nucleophile than cysteine,[21] and is known to interact preferentially with harder electrophiles such as sulfonyl chlorides or isothiocyanates.[19] Lysine is basic (pKa~10.5), and is thus usually protonated under physiological conditions. It is only nucleophilic when neutral, as in an enzyme binding pocket where bulk water may be excluded; therefore, electrophiles targeting lysine may be less likely to experience off-target binding events, as covalent modification is more likely to occur within the site of interest. Several studies have been performed to assess the reactivity of lysine with various electrophiles such as sulfonyl fluorides, acrylates and acrylamides, dichlorotriazines, and others.[23] Many of

---

[b] Figure generated by Dr. David Jakeman using ICMbrowser from RSCB Protein DataBank entry no. 6B5E.[71] Crystal structure acquired by Holden et al.[49]

these functional groups have been used in the synthesis of potent irreversible enzyme inhibitors.[24]

While irreversible covalent modification is a powerful tool for enzyme inhibition, it comes with a significant drawback, which is that off-target binding is also irreversible, and may lead to more severe side-effects in a drug.[25] It is thus desirable to maintain a degree of reversibility in the binding mechanism. In that case, theoretically, a selective reversible-covalent inhibitor will bind the target enzyme with a high degree of affinity due to non-covalent interactions, and the covalent modification will strengthen the association. Conversely, in an off-target binding event, a lower affinity between the inhibitor and enzyme, due to the absence of specific noncovalent interactions, would promote dissociation via reversal of the covalent reaction. One such covalent interaction could be achieved through conjugation of lysine with a ketone or aldehyde, to form an imine[26] (see Figure 1.3a). In an aqueous environment, this interaction is easily hydrolyzed, making it effectively reversible. Despite this, a study performed by Neri *et al.* demonstrated that high affinities can be achieved between lysine and aryl aldehydes if the electronic properties of the aryl aldehyde are appropriately tuned.[27] However, as aforementioned, lysine nucleophilicity can vary in aqueous environments, and in some cases the reaction may favour the reverse direction (hydrolysis), negating the benefits of the covalent interaction. Improved binding and stability of the adduct[28] has been observed when a proximal boronic acid is installed in range of the carbonyl,[26] such that the imine is stabilized by a dative bond into the boronic acid's empty p-orbital (see Figure 1.3b). Such an interaction, termed an "iminoboronate", is the only prominently employed *reversible* covalent modifier of lysine in the literature today,[26–28] and is the subject of this study.
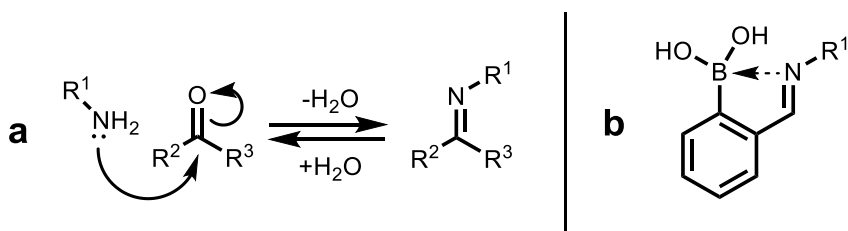
Figure 1.3: a) Reversible formation of an imine by reaction of an amine and a carbonyl. b) An example of an iminoboronate (boron-stabilized imine) formed from an amine and 2-formylphenylboronic acid.

1.4. Research Aims

In this project, we aim to:

1) Synthesize a library of thymidine derivatives bearing warheads which may reversibly, covalently modify K23 and/or K160 in the active site of Cps2L. This will be achieved by linking an ortho-formylarylboronic acid warhead to thymidine through various linker functionalities.

2) Evaluate the binding potential of these molecules through WaterLOGSY NMR, an NMR technique which can be used to characterize ligand-macromolecule interactions.

3) Evaluate the inhibitory activity of these molecules against Cps2L by employing a coupled enzyme assay previously reported by the Jakeman group.[29]

4) Confirm proposed binding events using X-ray crystallographic studies.

Chapter 2. Results and Discussion of the Synthesis of Inhibitors

2.1. Targeting Iminoboronate-Forming Thymidine Derivatives

The target compound for reversible covalent inhibition of Cps2L is shown in a general form in Figure 2.1a, where X represents the linker between the ortho-formylarylboronic acid (o-FABA) and thymidyl moieties. We considered several options for X, and decided to pursue linkage via 1,4-substituted 1,2,3-triazole (Figure 2.1b) due to its ease of synthesis from the correspondingly substituted azide and alkyne. The retrosynthesis for this type of compound is shown in Scheme 2.1, where the azide is first installed at the 5′-position of thymidine, and the alkyne on the o-FABA.
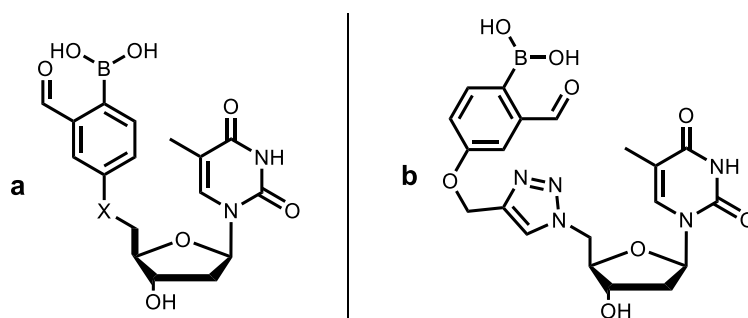
Figure 2.1: a) General structure of iminoboronate-forming target compounds, where X = various linker functionalities; b) iminoboronate-forming compound with a 1,4-substituted triazole linker.
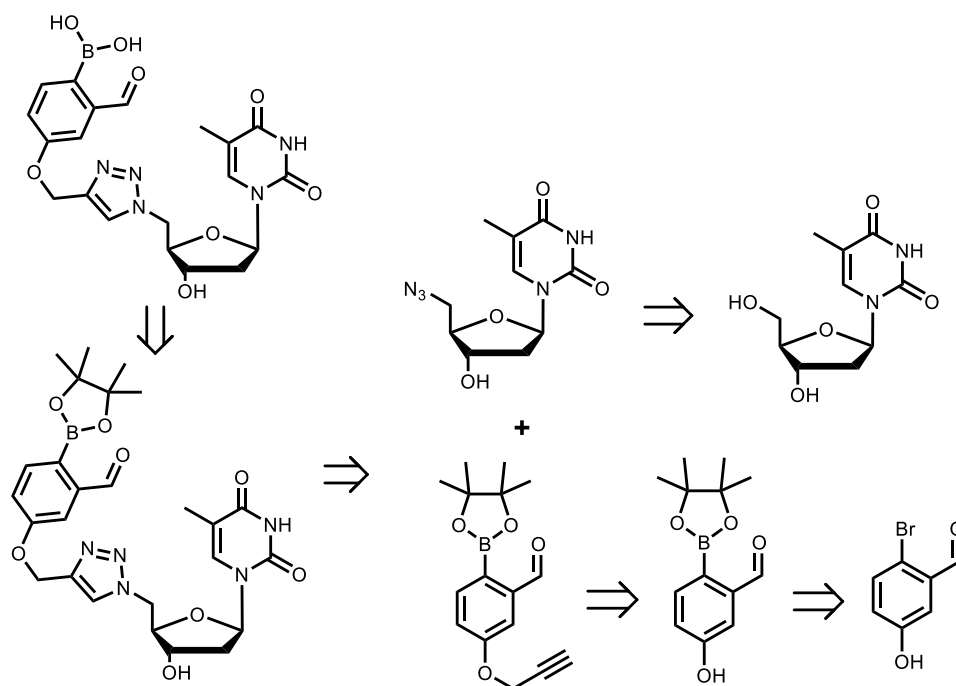
Scheme 2.1: Retrosynthetic analysis for triazole-linked compounds.

8

Scheme 2.2 shows the synthesis of two constitutional isomers we targeted with this strategy. The first step involved the installation of a pinacolboronate (BPin) group through a Miyaura-type cross-coupling based on conditions reported by Sella et al.[30] to make compound **2**. This was first performed on **a** to prepare compound **2a**. Prior to optimization of the reaction, we observed poor conversion to the desired product by NMR analysis of reaction mixtures, in addition to low isolated yields, indicating that the reaction was inefficient under the reported conditions. Furthermore, monitoring the reaction by TLC proved challenging due to overlapping spots and streaking on the TLC plate with simple eluent systems (e.g. ethyl acetate / hexanes). I determined that a solvent system of 10% EtOAc, 45% hexanes, and 45% DCM significantly improved the resolution of the TLC plates, clearly separating the starting material and product spots, and facilitating the monitoring of this reaction. Furthermore, we determined that an increase in catalyst loading to 5% and an excess of B_2Pin_2 (1.8 equivalents) led to cleaner conversion. After optimization of reaction conditions and purification steps, compounds **2a** and **2b** were acquired reliably in excellent yields.
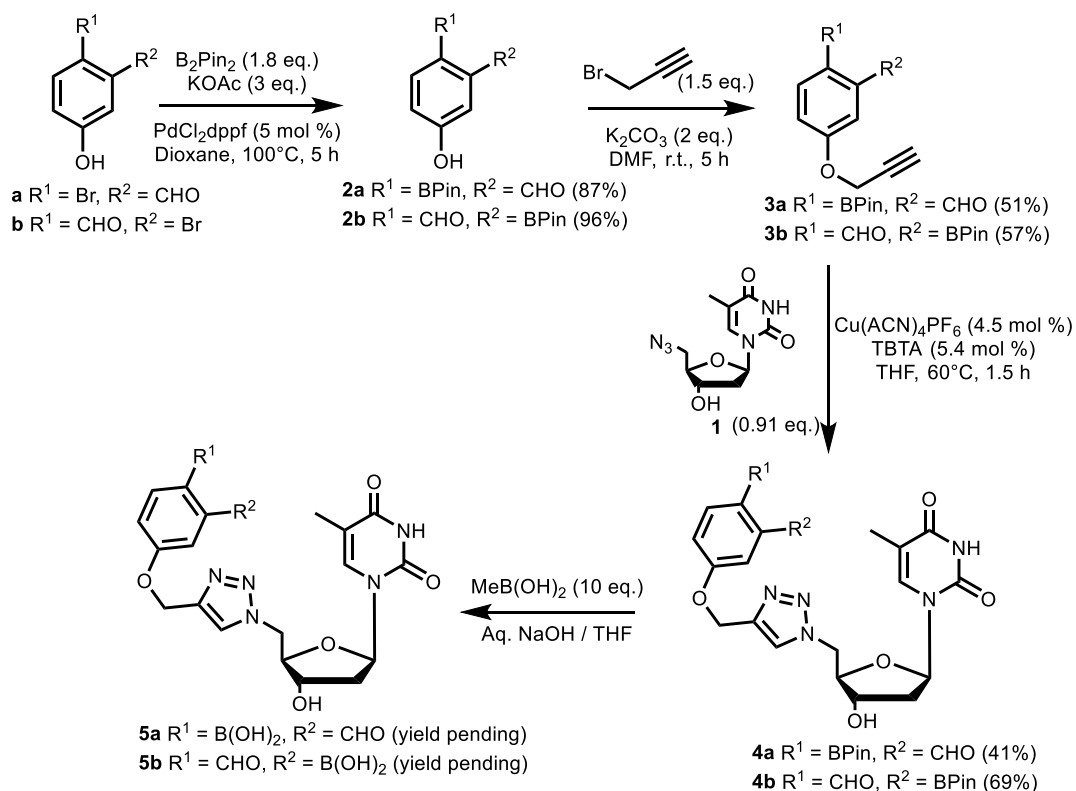
Scheme 2.2: Synthesis of triazole-linked iminoboronate-forming inhibitors **4a** and **4b**, en route to target compounds **5a** and **5b**.

9

The next step, the S$_N$2 reaction of compounds **2a** and **2b** with propargyl bromide, has been well-reported,[31–33] and following the reported methods gave compounds **3a** and **3b** in fair yields, although complete conversion to the ether was observed by TLC analysis. Loss of material was attributed to the workup by extraction, wherein the Lewis-acidic boron has an affinity for the aqueous phase, made basic by residual K$_2$CO$_3$. This was the case even after back-extraction of the aqueous phase with organic solvent. Preliminary attempts to improve the yield of **3a/b** by neutralizing the aqueous layer led to some decomposition of the material as observed by TLC analysis, and, therefore, was not further pursued.

5′-Azido-5′-deoxythymidine (**1**) was used as the azide component for the triazole-formation reaction, and was synthesized from 5′-tosylthymidine, a commercially available electrophilic thymidine species, based on literature procedures.[34,35] Some optimization of the purification method was required to improve the yield of this reaction. The reaction solvent, DMF, needed to be removed in vacuo prior to extraction, as the product is partially water-soluble and would partition into the aqueous phase if any residual DMF was present during the extraction step. 2-Methyltetrahydrofuran (2-MeTHF) was used as an extraction solvent due to its enhanced polarity compared to common extraction solvents such as diethyl ether, ethyl acetate, or DCM. Furthermore, due to the water solubility of **1**, the aqueous phase was supplemented with sodium sulfate to promote salting out of the product,[36] and was thoroughly extracted in order to optimize the yield. Using this method provided **1** reliably, cleanly, and in near-quantitative yield without further purification.

The Copper-catalyzed Azide-Alkyne Cycloaddition (CuAAC) reaction (to convert **3** to **4**, see Scheme 2.2) is often employed for the selective formation of 1,4-substituted triazoles, from correspondingly substituted azides and alkynes.[37] The active copper (I) species is usually obtained by combining a copper (II) species with a 1-electron reducing agent such as sodium ascorbate, and these conditions have been used to great effect with 5′-azidothymidine and various alkynes.[35,38,39] We employed these conditions successfully on several aryloxy-substituted terminal alkynes (to be discussed later), and attempted to use them to react **1** with **3a** or **3b** to make compound **4a/b**. Under those conditions, the triazole was formed as intended, but the BPin was lost through protodeborylation. This result was attributed to the propensity of copper to cleave C-B bonds through insertion.[40]

Teichert et al.[41] circumvented this issue through the use of tris(benzyltriazolylmethyl)amine (TBTA), a coordinating ligand[42] which inhibits C-B insertion by copper (I) due to steric bulk of the coordination complex. The presence of TBTA also provides the benefit of requiring less copper, as the coordination complex helps stabilize the copper (I) species[43] (Figure 2.2), and increases the rate of catalysis due to electron donation from the tertiary amine nitrogen.[44] We were successful in applying the conditions of Teichert et al. to the reaction of **3a/b** and **1** to form **4a/b**, and although several new spots were observed when the reaction was monitored by TLC, ^{1}H NMR analysis of the crude material showed complete and exclusive conversion to the desired product. However, purification by silica gel chromatography (0-20% acetonitrile in DCM) provided the protodeborylated product (i.e. compound **4d**, see Scheme 2.3) which suggested that the product was unstable on silica. Fortunately, we determined that the product could be purified by precipitation from DCM, and consequently, this method was used to access **4a** and **4b** (Scheme 2.2).
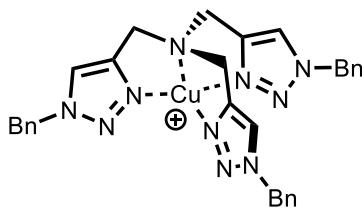
Figure 2.2: Copper (I) – TBTA coordination complex.

The final step to access the target compound (**5a** or **5b**) involves hydrolysis of the BPin ester to its corresponding boronic acid. The Jakeman group has previously had success deprotecting a BPin group (unpublished results) using methylboronic acid through a transesterification reaction reported by Hinkes et al.[45] The volatility of the reagents and byproducts theoretically removes the necessity for chromatographic purification which, as previously mentioned, leads to protodeborylation of these products. We applied the reported conditions to **4b** with 5% trifluoroacetic acid (TFA) relative to the solvent, THF, and increasing the proportion of MeB(OH)$_2$ from 5 to 10 equivalents. Consumption of the starting material was observed after 3 days by ^{1}H NMR analysis of the reaction mixture, although some side products were present as indicated by several peaks in the aldehyde region of the spectrum. Therefore, unfortunately, purification could not be performed simply through evaporation of volatiles. However, a single product (as indicated by ^{1}H

NMR analysis) was isolated from the mixture with relative ease by washing the solid with THF followed by DCM, as the boronic acid is less soluble in organic solvents than the ester precursor. However, the expected 3′-hydroxyl signal of the deoxyribose ring was not observed in the ^{1}H NMR spectrum of the purified material (Figure 2.3a). Given that the reaction is acid-catalyzed, a plausible outcome was that the 3′-alcohol had reacted with TFA to form a trifluoroacetate ester. To confirm this hypothesis, a ^{19}F NMR spectrum was acquired (d_6-DMSO, 500 MHz), and a singlet was observed at -74.4 ppm (Figure 2.3b), which is a chemical shift consistent incorporation of the proposed trifluoroacetate ester. Comparison to a standard sample of TFA in d_6-DMSO showed a difference in chemical shift of -1.1 ppm, indicating that the signal was not merely residual TFA.

Due to this result, we sought alternative reaction conditions to cleave the BPin esters of **4a** and **4b**, as an additional deprotection step to remove the TFA ester was not desirable. The work by Hinkes et al. demonstrates that aqueous base can be used instead of TFA for the BPin deprotection.[45] These conditions, when applied to compound **4b**, showed some conversion to the desired product, **5b** (as observed by NMR analysis of the reaction mixture) however, at the time of writing, neither of the target compounds **5a** or **5b** have been isolated.
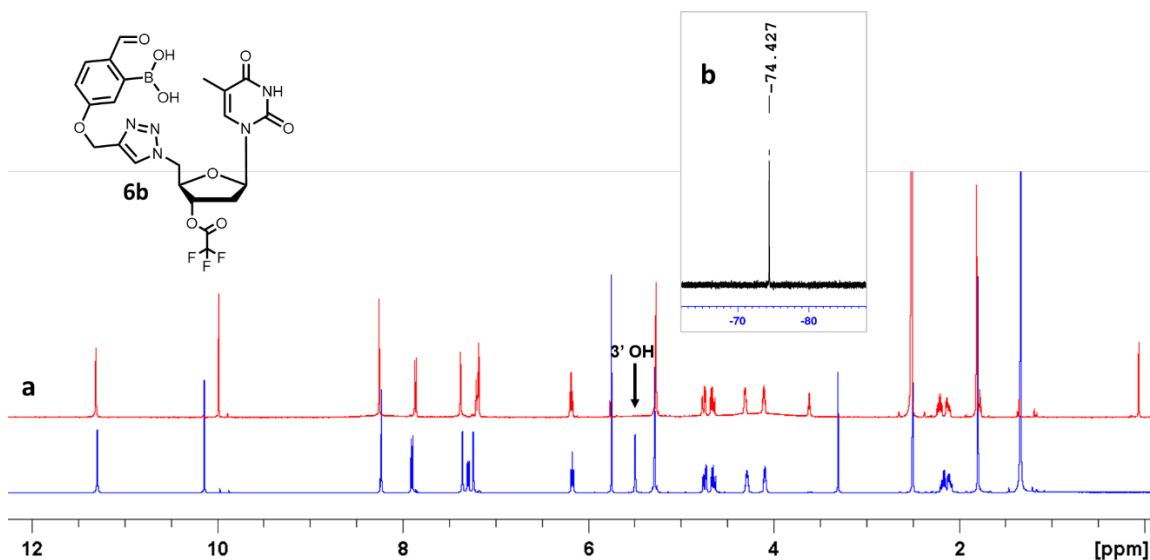
Figure 2.3: a) Comparison by ^{1}H NMR (d_6-DMSO, 500 MHz) of **4b** (lower spectrum) and **6b** (upper spectrum). b) ^{19}F NMR spectrum (d_6-DMSO, 471 MHz) of **6b**.

2.2. Synthesis of Other Thymidine Derivatives for Cps2L Targeting

During optimization of the synthesis of iminoboronate-forming targets, we were successful in developing a library of compounds for a preliminary structure-activity relationship (SAR) study. Synthesis of these compounds will be discussed here.

2.2.1. Aryloxy-Substituted Triazolylthymidine Compounds

Compounds **4c-g** were synthesized as shown in Scheme 2.3. Substituted phenols **c-g** were subjected to the same reaction conditions as in the synthesis of **3a** and **3b** (Scheme 2.2) to give **3c-g** in fair to excellent yields, and required no further purification as determined by ^{1}H NMR analysis following aqueous-organic extraction.

Reaction of alkynes **3c-g** with **1** were carried out successfully using classical CuAAC conditions: namely, in the presence of a catalytic amount of copper (II) and reducing agent. CuSO$_4$ and ascorbic acid were chosen as they are both inexpensive, easy to handle, and easy to remove in workup steps due to their high aqueous solubility. The reaction conditions were optimized for these substrates in the following ways: first, we experimented with proportions relative to the limiting reagent, azide **1.** We determined that 0.5 equivalents of CuSO$_4$ and 0.55 equivalents of ascorbic acid demonstrated high rates of reaction with most alkyne substrates, and that a slight excess of alkyne (1.1 equivalents relative to **1**) ensured complete conversion. Secondly, the solvent system (3:1 THF:H$_2$O) was chosen to solubilize both organic compounds and inorganic salts. Reactions were also tested in methanol/water and neat methanol due to the desirable solvation properties of the alcohol, but aldehyde-containing alkynes were subject to acetal formation, and THF mitigated this issue. Thirdly, the reaction was found to proceed somewhat inefficiently when all reagents were combined at the same time. Instead, alkyne **3** and azide **1** were combined and dissolved in THF. Separately, CuSO$_4$ and ascorbic acid were dissolved together in H$_2$O, then the aqueous solution added to the organic solution to initiate the reaction. This ensured that all copper was dissolved, and the colour change from blue to green gave a qualitative indicator that copper (II) was reduced to copper (I) by ascorbic acid. Additionally, compound **1** is soluble in THF but benefits from gentle heating to fully dissolve. Initially, the azide and alkyne were dissolved at 50 °C but the reaction run at room temperature; however, the reaction was found to proceed more smoothly if conducted at 50 °C throughout. Finally the reaction was found to proceed best under anaerobic

conditions, as can be expected due to the oxidative conversion of active copper (I) to inactive copper (II), and correspondingly the reaction vessel was purged with nitrogen once all reagents were combined.
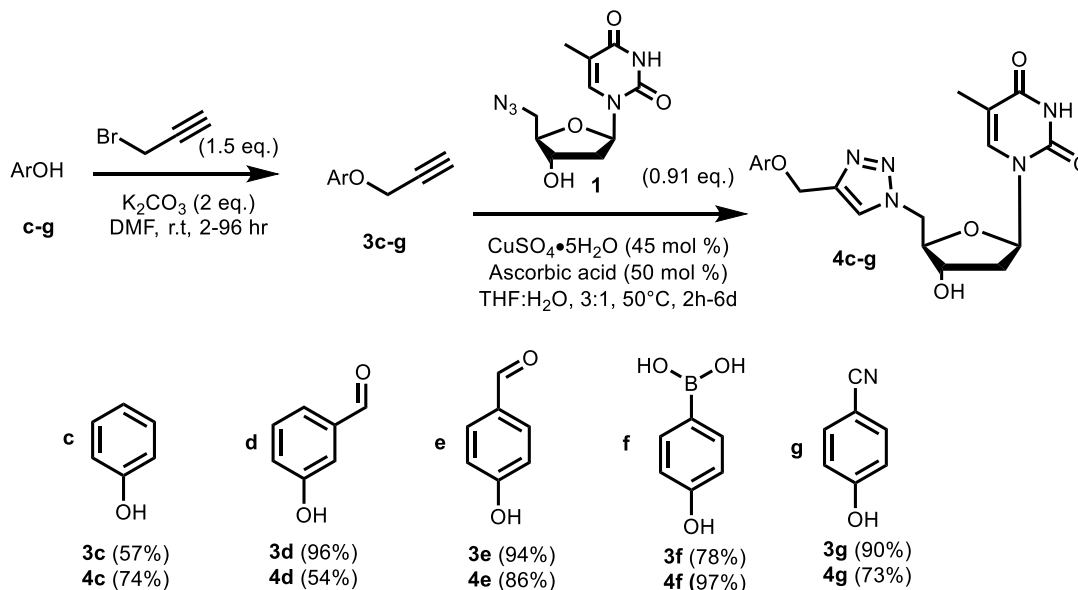
Scheme 2.3: Synthesis of aryloxy-substituted thymidine derivatives **4c-g**, bearing 1,4-substituted triazole linkers.

The reaction progress was monitored by TLC, wherein it was once again necessary to optimize the solvent system (in this case, 10% MeOH, 45% DCM, 45% hexanes) to give adequate separation between the limiting reagent, **1**, and the product (**4c-g**). Preliminary purification protocols involved extraction followed by silica column chromatography (which was performed to purify **4c**), but this was found to be challenging for certain products with very low solubility in our available extraction solvents (i.e. diethyl ether, DCM, EtOAc, or 2-MeTHF) as well as being insoluble in water. An alternative method of purification was developed for products with low organic solubility: first the reaction solvent was evaporated, then the residual solid was resuspended in water and stirred until the copper and ascorbic acid were dissolved. The aqueous-soluble material was removed by filtration, and the collected solid was dried at 37 °C. The material was then resuspended in DCM, which served to dissolve any excess alkyne. The solid was once again filtered, washed with DCM, and dried under vacuum. This method gave clean product by NMR analysis, and was less wasteful than purification by column chromatography. It, therefore, became the standard for purification of all CuAAC reactions we conducted in this way.

14

Compounds **4c-f** were synthesized as control compounds to probe the steric and electronic effects of the constituent parts (scaffold and functional groups) of **5a** and **5b**. **4c** bears an unsubstituted phenyl group and thus serves to demonstrate how steric contributions alone affect binding of, and inhibition by, this series of substrates. This compound was used in preliminary binding studies by WaterLOGSY NMR (see Chapter 3.3). Both **4d** and **4e** bear an aldehyde, at either the meta- or para- positions of the aryl ring, respectively, and were designed to demonstrate how the electronic properties of the aldehyde contribute to binding. Aldehydes may react with amines reversibly to form imines in the absence of a Lewis acid, but this interaction is known to be less stable than that of an iminoboronate.[28] Finally, **4f**, bearing a para-substituted arylboronic acid, was synthesized in order to probe whether the boronic acid may interact with any polar residues in the active site, as in the formation of a Lewis acid-base pair with either of the lysine residues.

2.2.2. Nitriles as Electrophiles

Smith et al. recently reported a modified arylomycin bearing a nitrile functionality which reacts covalently with a lysine residue within its target enzyme, signal peptidase LepB.[46] Inspired by these results, we sought to synthesize a small series of nitrile-functionalized thymidine derivatives which may react with either of the lysine residues (Figure 2.4a) within the active site of Cps2L. Nitriles are also stable to polar protic solvents whereas aldehydes readily form acetals or hemiacetals, therefore substituting a nitrile may simplify the synthetic process, as methanol and ethanol dissolve thymidine derivatives more readily than aprotic solvents. Compound **4g** (Scheme 2.3), a para-substituted aryl nitrile, was the first of these compounds.
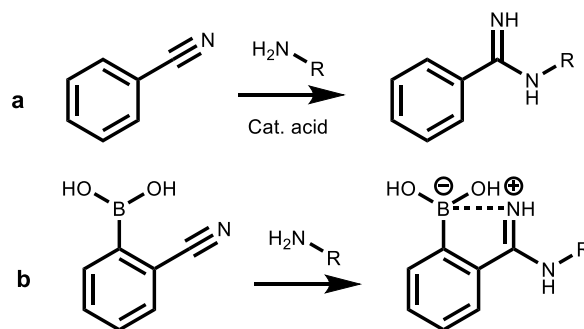
Figure 2.4: General synthesis of amidines; a) catalyzed by an external acid, b) potential reaction catalyzed by an internal boronic acid.

Scheme 2.4 shows the synthesis **7**, an alkyl nitrile-bearing triazolylythymidine derivative. Synthesis of **7** from **1** proceeded in the same manner as for compounds **4c-g**, although the resulting solid, isolated after washing with H$_2$O and DCM, was purified by column chromatography.
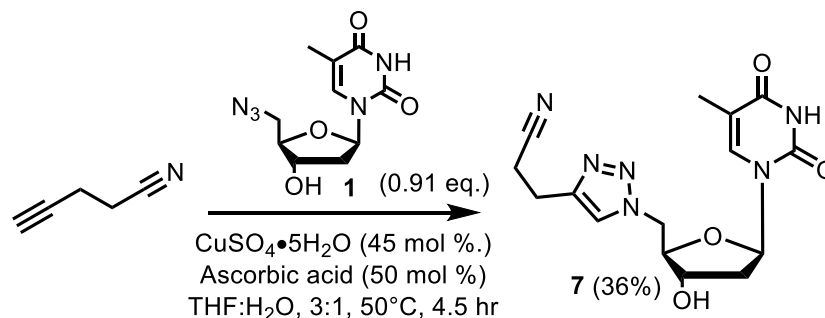
Scheme 2.4: Synthesis of compound **7**.

In addition to the alkyl and aryl nitrile compounds, we were interested to see if a proximal boronic acid could help catalyze the formation of an amidine from a nitrile and lysine (Figure 2.4b). An amidine can be accessed synthetically from a nitrile and an amine in the presence of a Brønsted or Lewis acid,[47,48] and a boronic acid may provide an alternative, biocompatible catalyst. This proposed reaction has not been reported to date, and we considered it a reasonable avenue to explore.
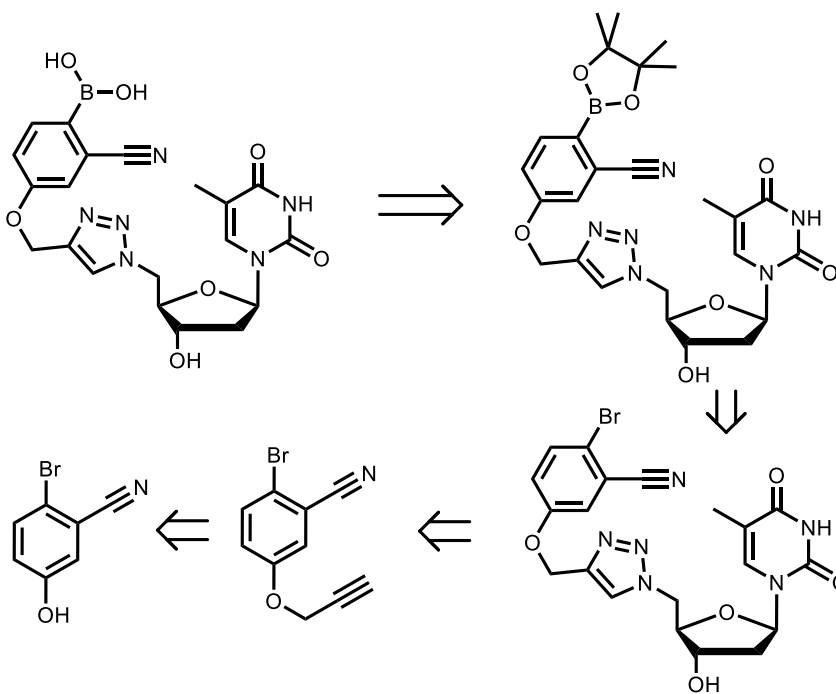
Scheme 2.5: Retrosynthesis of a thymidine derivative bearing a boronic acid and ortho-nitrile.

Retrosynthesis of a proposed "amidinoboronate"-forming thymidine derivative is shown in Scheme 2.5. When designing the synthesis of this compound, we were aware of the protodeborylation caused by Cu, but had not yet discovered the solution of using TBTA. We, therefore, planned to perform the CuAAC reaction prior to the installation of boron.

The synthesis of **8**, the meta-substituted isomer of **4g**, is shown in Scheme 2.6. Synthesis of precursor **4h** was performed as described above for compounds **3** and **4** (see Scheme 2.3). **8** was not the intended product when **4h** was subjected to Miyaura borylation conditions, though not entirely unexpected. In preliminary experiments, we had observed protodeborylation when ortho-formylaryl bromide-containing thymidine derivatives were subjected to various borylation conditions. We hoped that since the corresponding nitrile-bearing substrate provided less steric interference, the borylation reaction may proceed; however, deborylation still occurred. This reaction indicated to us that the electron-withdrawing nature of both the nitrile, and the aforementioned aldehyde, may destabilize the C-B bond. Despite this, **8** was a valuable compound, and was collected. In future studies, an analogous route to that described in Scheme 2.1 would be used to obtain the target compound (i.e. the final compound shown in Scheme 2.5).
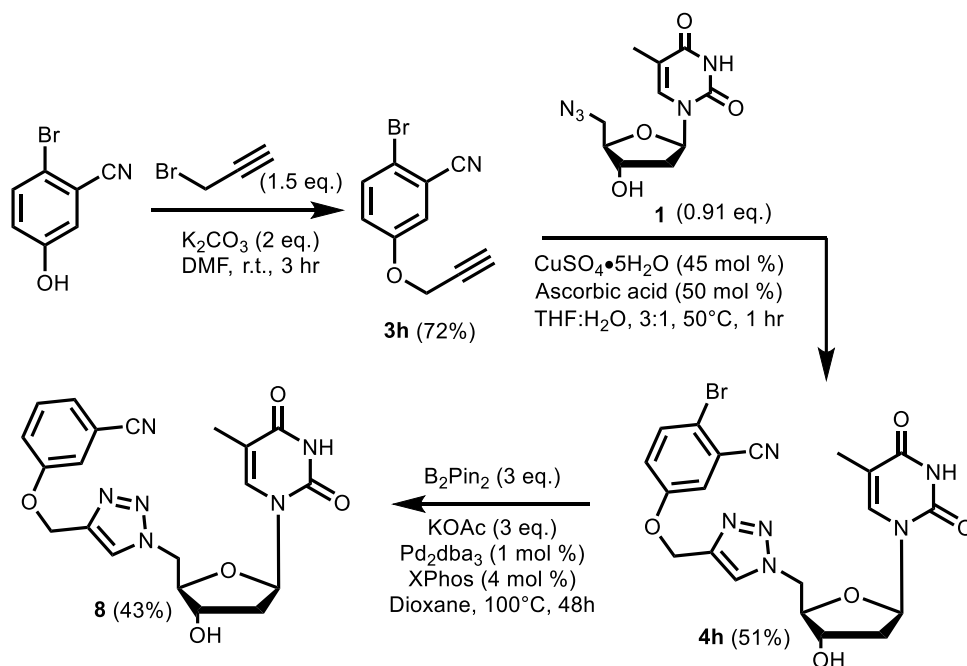
Scheme 2.6: Synthesis of **8**.

To date, there has been only one substrate, of those we attempted to borylate, for which installation of a BPin group was successful following the CuAAC reaction. Compound **9** was synthesized from **4i** according to Scheme 2.7, employing conditions suggested by Dr. Craig Smith, a post-doctoral fellow in the research group of Professor Alison Thompson. Compound **9** was successfully isolated by silica gel column chromatography, indicating that the C-B bond of **9** is more stable to silica than that of compound **4b**, which bears an ortho-formyl group. This result reinforced the hypothesis that ortho-electron-withdrawing groups are detrimental to the formation and stability of the C-B bond. Although this serves mainly as a mechanistic proof-of-concept, comparing the activity of **9** and **4f** (the former bearing a BPin group; the latter a $B(OH)_2$) against Cps2L will aid in SAR studies and inform future directions for synthesis.
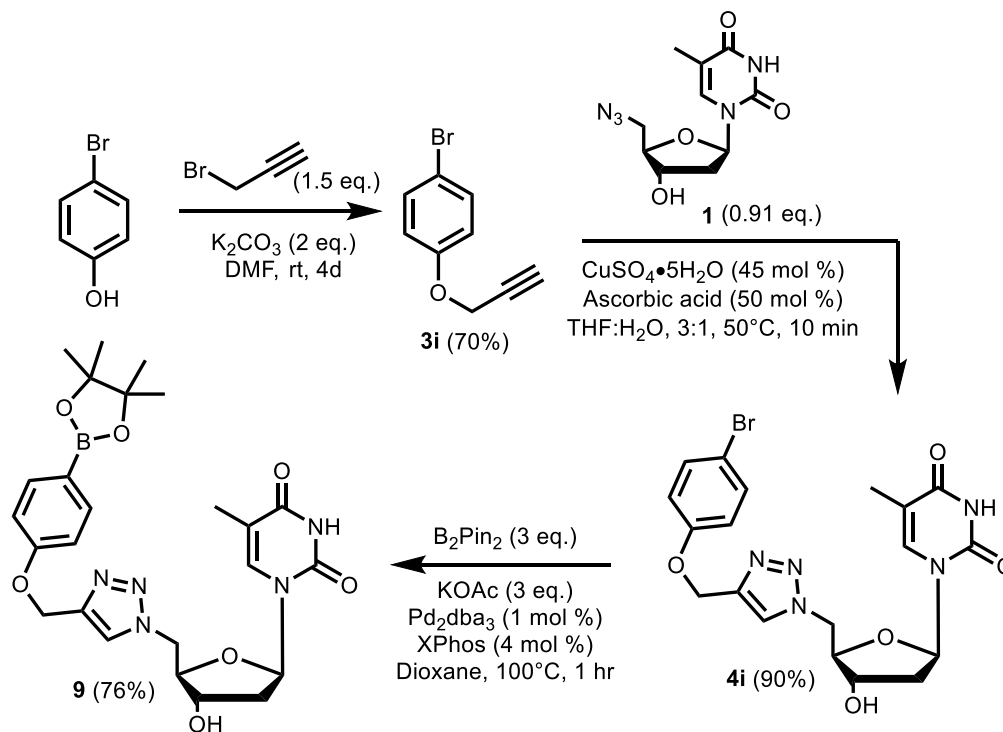
Scheme 2.7: Synthesis of **9**.

2.2.3. Ketone-Linked Compounds

Scheme 2.8 shows the synthesis of **10a**, an alternative triazolylthymidine scaffold from **1** with the same conditions for CuAAC as described for compounds **4c-g**. This model integrates a ketone into the linker, which may potentially react with lysine in the active site of Cps2L.

18
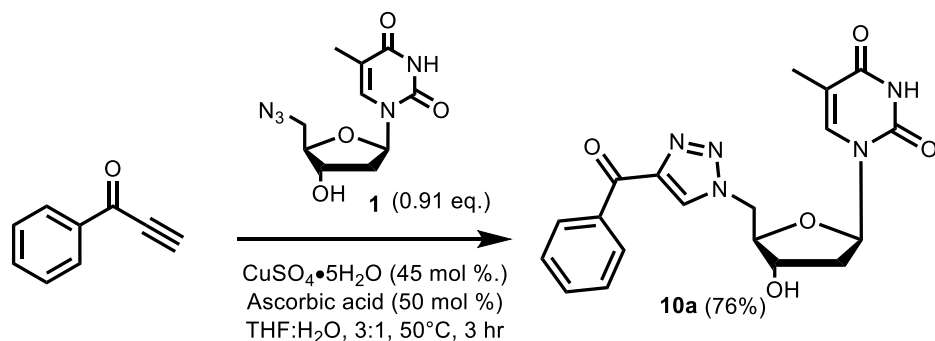
Scheme 2.8: Synthesis of **10a**.

Substitution of an ortho-boronic acid on the phenyl ring of **10a** may help autocatalyze the potential reaction between the ketone and lysine, and stabilize the resulting imine if it were to form. Retrosynthesis of such a compound is shown in Scheme 2.9, however, we attempted synthesis of **10b** according the slightly altered route described in Scheme 2.10.
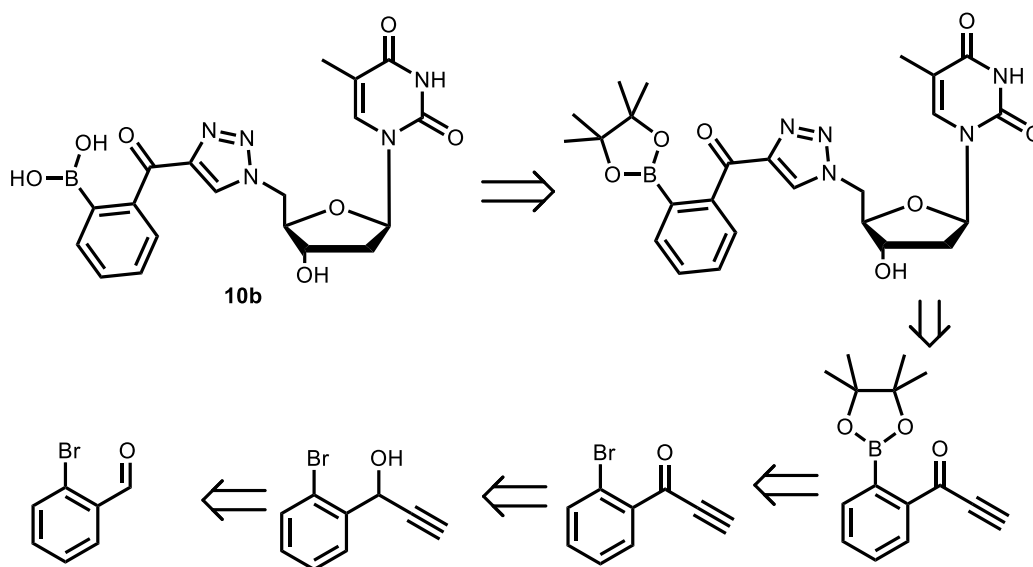
Scheme 2.9: Retrosynthesis of **10b** from 2-bromobenzaldehyde.

We chose the latter route because at the time of synthesis, we were unaware of the use of TBTA enabling the CuAAC reaction in the presence of a C-B bond. Alkyne **12** was prepared in two steps from 2-bromobenzaldehyde: a Grignard reaction with commercial ethynylmagnesium bromide gave alcohol **11** in quantitative yield, which was then oxidized to the corresponding ketone (**12**) using Dess-Martin periodinane. Formation of triazole **13** was successful when catalyzed by the system of copper (II) sulfate reduced by ascorbic acid. However, when subjected to either set of borylation conditions shown in Scheme

2.10, protodeborylation occurred to give **10a** instead of **10b**. This is consistent with our previous observations that a proximal carbonyl group may destabilize the C-B bond. In future studies, borylation of the alkyne should be performed prior to the CuAAC reaction (as suggested by the retrosynthetic analysis in Scheme 2.9), using $Cu(ACN)_4PF_6$ and TBTA, which were successful in synthesizing compounds **4a** and **4b**.
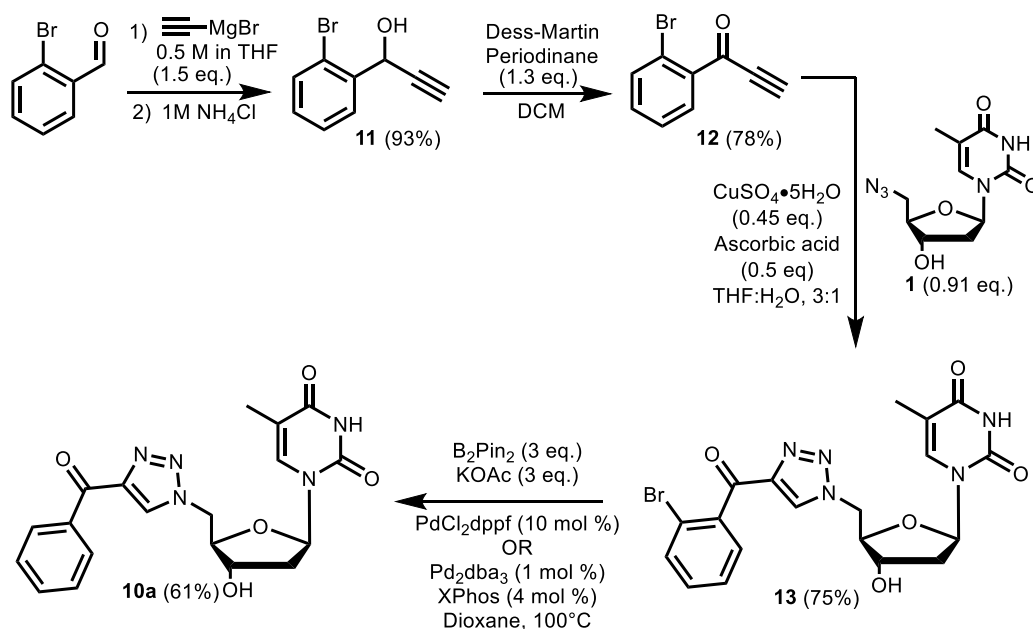
Scheme 2.10: Attempted synthesis of **10b**. Protodeborylation led to the accidental recovery of **10a**.

2.2.4. Dithymidine Compounds

RmlA-type enzymes have a tetrameric structure[17,49] as shown in Figure 2.5. The monomers are oriented such that each active site is pointed towards another. This inspired us to synthesize symmetrical compounds with two thymidyl units, which, we hypothesized, may bind both active sites simultaneously and improve affinity. We built two such dithymidyl compounds, as shown in Schemes 2.11 and 2.12.
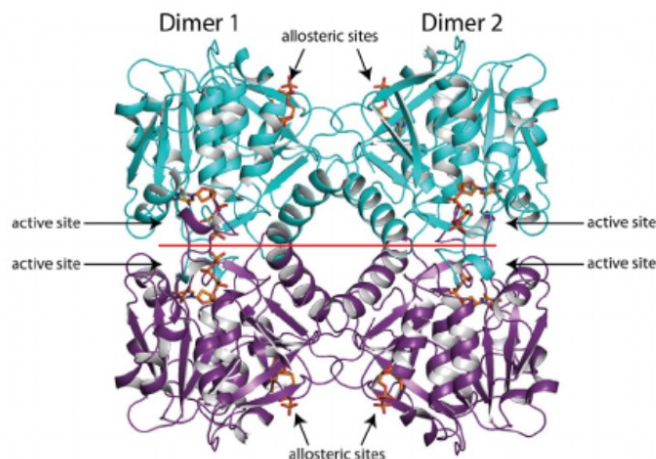
Figure 2.5: Tetrameric structure of RmlA from *Mycobacterium tuberculosis*.[50]
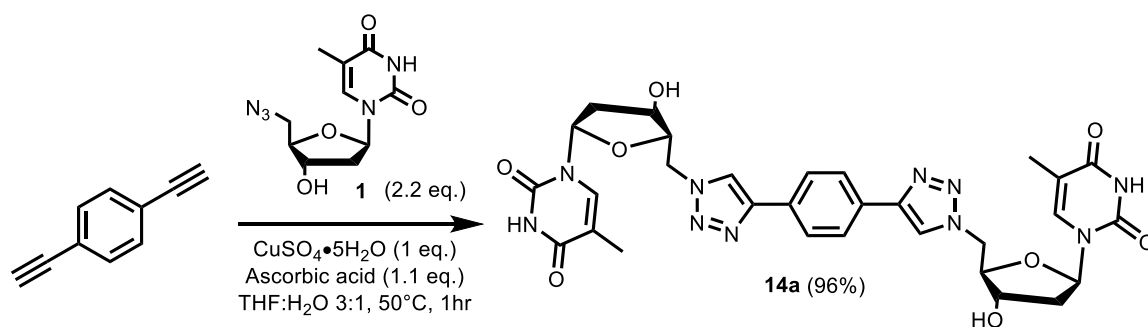
Scheme 2.11: Synthesis of **14a**, one two dithymidyl compounds.

Synthesis of **14a** was performed using analogous conditions as for compounds **4c-g** (see Scheme 2.3 for reference). The product was found to be highly insoluble in most solvents, making purification by filtration trivial. The residual solid was washed with MeOH rather than DCM to remove excess 5′-azidothymidine, and **14a** was recovered in near-quantitative yield. The ^{1}H NMR spectrum of **14a** demonstrates the symmetry of this compound about the central phenyl ring (Figure 2.6). The singlet at 7.92 ppm integrating to 4H represents the phenyl ring protons, and the lack of splitting shows that each proton is exactly equivalent.
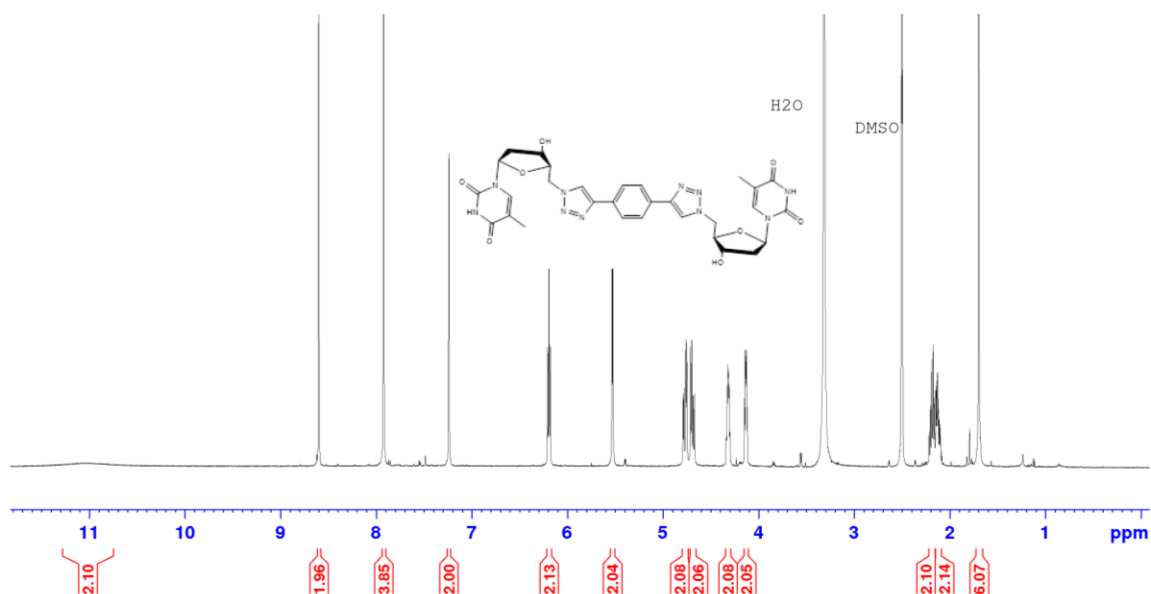
Figure 2.6: ^{1}H NMR spectrum (d_6-DMSO, 500 MHz) of **14a**.

Compound **14b** has a similar structure to **14a**, but with an extended linker (bearing ether linkages about the central phenyl ring). Synthesis was performed in 2 steps as shown in Scheme 2.12. Two alkynes were installed on 1,4-dihydroxybenzene using the same conditions as for **3a-i** but doubling the proportions of reagents. Similarly, the CuAAC reaction was performed with slightly over two equivalents of **1**, as in the synthesis of **14a**. The product was once again isolated by filtration although the solid was a fine precipitate and some material was lost in the filtrate. The product that was recovered was pure by ^{1}H NMR analysis of the solid.
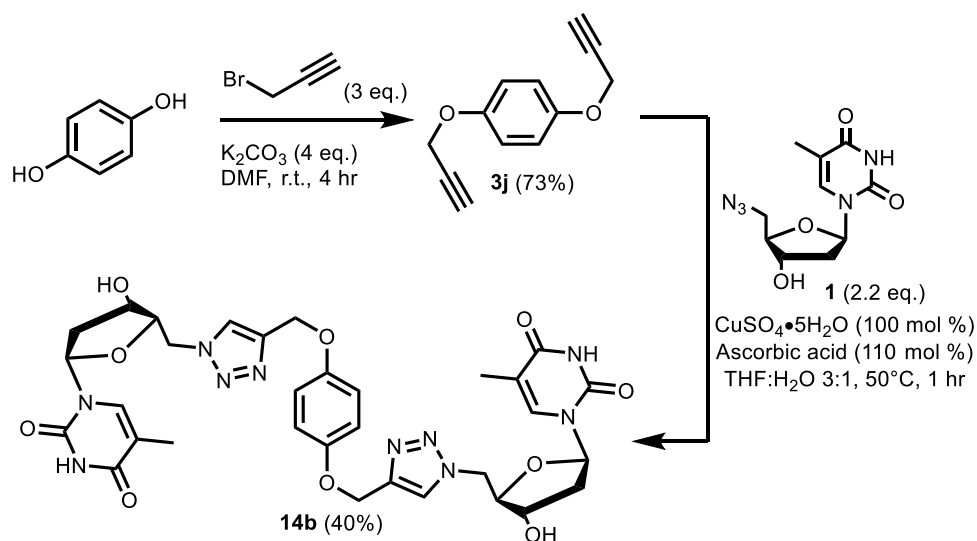
Scheme 2.12: Synthesis of **14b**.

2.2.5. SPAAC Reaction With 5′-Azidothymidine

Given the ease of synthesis of **1**, we wanted to attempt an alternative "click"-type reaction: namely, SPAAC, the Strain-Promoted Azide-Alkyne Cycloaddition. In this reaction, a cyclic alkyne reacts with an azide without catalysis to form a bicyclic system. Synthesis of such a compound, **15**, is shown in Scheme 2.13. We selected the cyclooctyne shown due to its commercial availability, and the reaction proceeded as expected, though complete conversion was not observed by TLC analysis despite increasing time and equivalents of alkyne. Compound **15** was purified by column chromatography rather than filtration, as the material was more soluble in organic solvents than the other triazolylthymidine derivatives, and was recovered in fair yield.
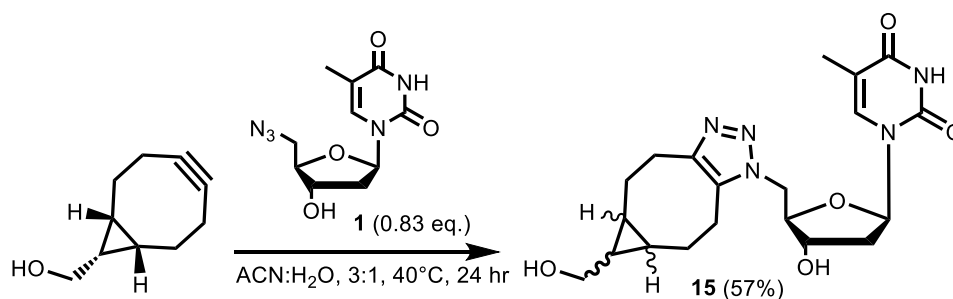
Scheme 2.13: Synthesis of **15** via SPAAC.

Since the thymidine precursor is chiral, and the cyclooctyne is prochiral, a mixture of diastereomers was observed by NMR analysis of **15**, in a 1:1 mixture according to peak integration (Figure 2.7). By all chromatographic methods we attempted (TLC, preparative chromatography, HPLC) the two diastereomers were inseparable, so we chose to assess the binding and inhibitory capacity of these two compounds as a mixture. Binding of this compound was assessed using WaterLOGSY NMR (See Chapter 3.3).
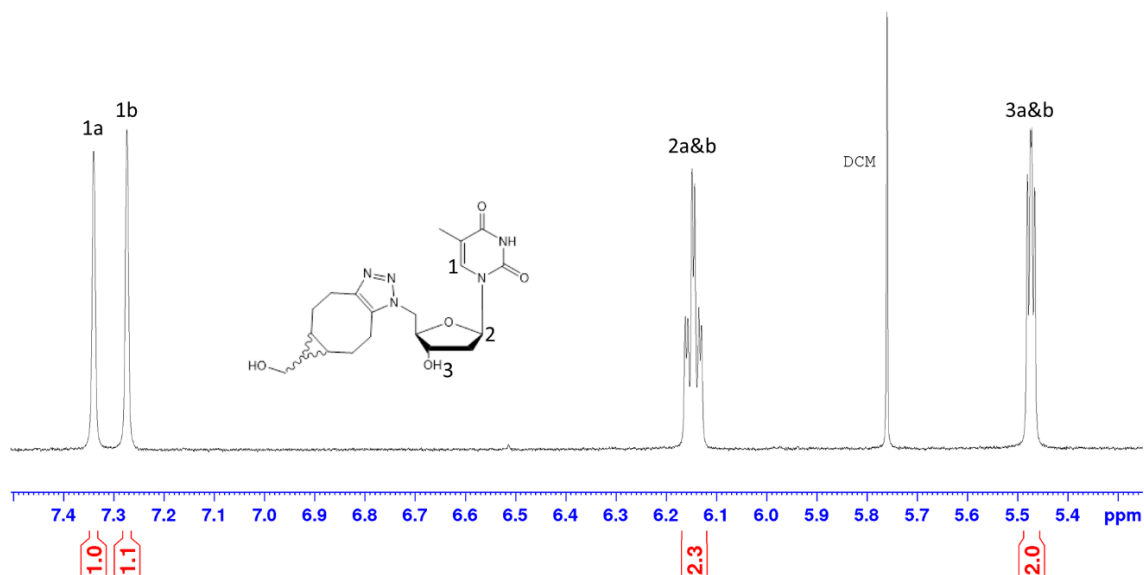
Figure 2.7: Cropped ^{1}H NMR spectrum (d_6-DMSO, 500 MHz) of **15**, showing a 1:1 mixture of diastereomers a and b (relative stereochemistry not assigned) by integration.

2.2.3. Amide Scaffold

We were interested in preparing compounds with alternative linkers to determine whether the triazole itself affects binding of the substrates. We chose to pursue amide-linked compounds due to their purported ease of synthesis and biological stability. The most common method of preparing amides is by combining an amine and a carboxylic acid in the presence of a coupling agent.[50,51] Scheme 2.14 shows the synthesis of **18**, an amide-linked thymidine derivative bearing an unsubstituted phenyl ring. Contributions of the linker towards inhibitory capacity will be assessed by comparing the binding affinity of **18** and **4c**, the unsubstituted phenyl-bearing triazolylthymidine derivative.
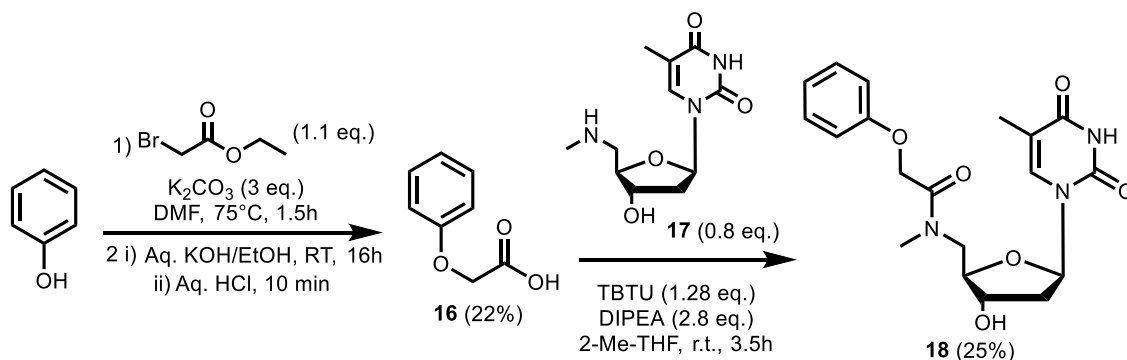
Scheme 2.14: Synthesis of amide **18**.

24

Acid **16** was prepared from phenol according to a reported procedure,[52] as was amine **17**.[53] We screened several coupling agents (DCC, EDC, SOCl$_2$, oxalyl chloride, HATU, TBTU, COMU) and found cleanest conversion by TLC analysis with the benzotriazole derivatives (HATU and TBTU) when the reactions were performed on analytical scale. The best method devised for the preparation of **18** was achieved by pre-stirring **16** with TBTU and DIPEA in 2-MeTHF, followed by addition of **17** after an hour. **18** showed greater solubility in organic solvents than the triazole-linked compounds, and was thus collected by extraction with 2-MeTHF and subsequent purification by column chromatography (rather than filtration). The ^{1}H NMR spectrum of **18** demonstrates the apparent presence of two entities (Figure 2.8). The two sets of signals represent two rotational isomers caused by the barrier of rotation due to resonance about the amide bond. **18** was crystallized to confirm identity, and a crystal structure is shown in Figure 2.9. Only the Z isomer is apparent in the crystal macrostructure (Figure 2.9b).
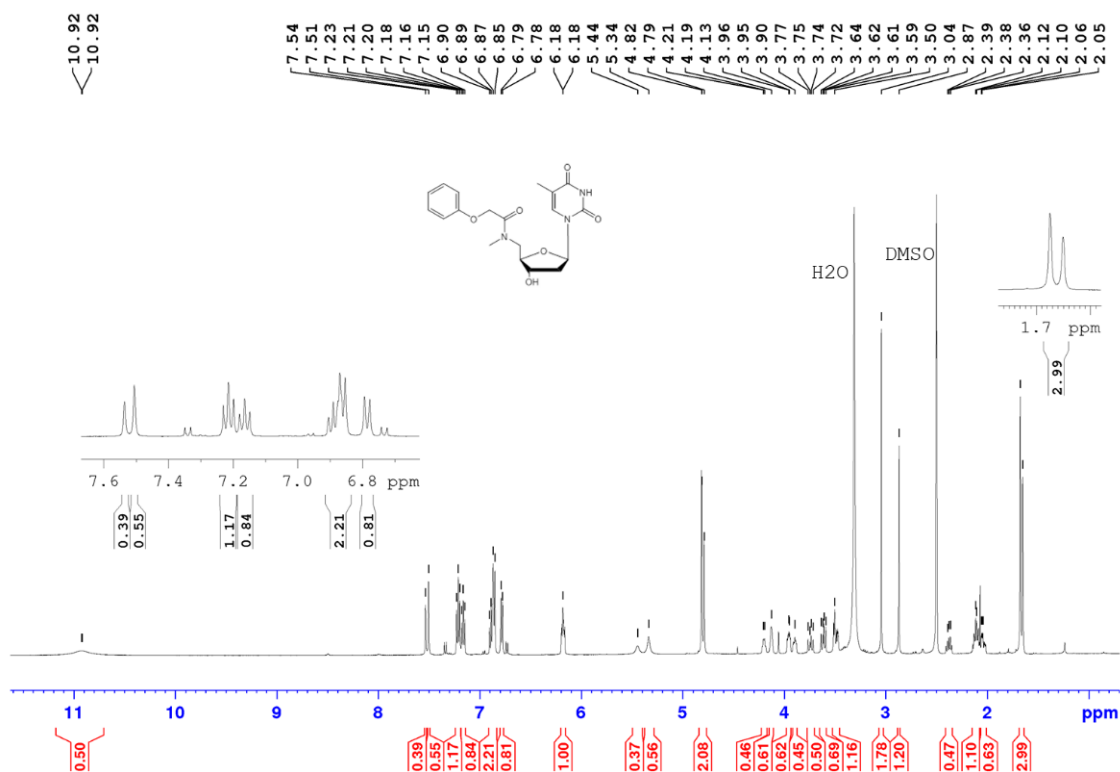
Figure 2.8: ^{1}H NMR spectrum (d_6-DMSO, 500 MHz) of **18**. Two sets of signals are observed, each with the same pattern but different chemical shifts (e.g. the singlets at 1.65 and 1.68 ppm both correspond to the thymine methyl group) indicating the presence of rotational isomers.
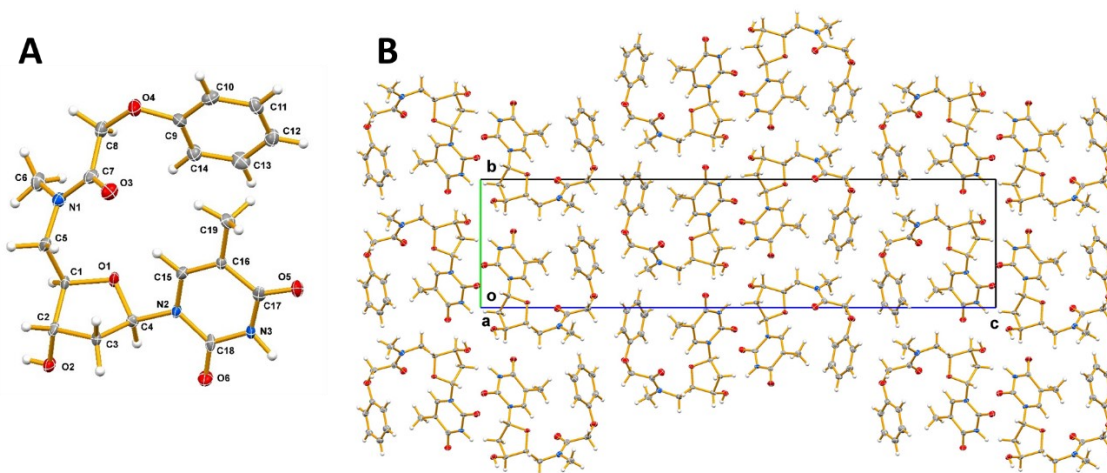
Figure 2.9: X-ray crystallographic analysis of **18**. A) ORTEP diagram; B) crystal packing (viewed along the x-axis) indicating one rotational isomer participates in crystal packing.

2.3. Summary

We have synthesized 15 thymidine derivatives which potentially target Cps2L and other RmlA-type thymidylyltransferase enzymes. Of these compounds, eight have the potential to modify the enzyme covalently through reaction with a noncatalytic lysine residue: those bearing aldehyde (**4a**, **b**, **d**, and **e**), ketone (**10a**), or nitrile (**4g**, **7**, and **8**) functionalities. Furthermore, we have synthesized two potential iminoboronate-forming compounds (**4a** and **b**) albeit bearing boronate esters rather than boronic acids. Future directions in synthesis of inhibitors would seek to optimize a method for the deprotection of pinacolboronate esters, use the alternative CuAAC conditions to synthesize analogues of **10a** and **8** with proximal boronic acids, and explore alternative linkers to join the warhead and thymidine moieties.

Chapter 3. Results and Discussion of WaterLOGSY Experiments With Synthesized Potential Inhibitors of Cps2L.

3.1. Introduction

WaterLOGSY NMR is a straightforward and convenient method of assessing the ability of a ligand to bind a macromolecule. WaterLOGSY studies have previously been performed successfully in the Jakeman group,[13,14,54] and as such, we decided to use this method as a preliminary assessment of binding of our synthesized potential inhibitors to Cps2L.

WaterLOGSY is a proton observe experiment wherein bulk water is irradiated, and magnetization is transferred to the ligand.[55] The signal is amplified when rotational relaxation pathways are limited due to binding interactions with the macromolecule;[56] therefore, even at low concentrations of the host (e.g. enzyme), signals corresponding to the bound ligand are visible in the spectrum. The technique requires bulk water, and, therefore, the sample is (unusually, for an NMR experiment) made in 10% D_2O in H_2O (the former for the spectrometer's solvent lock). The experiment, consequently, includes a water suppression sequence to ensure that the water signal does not obscure the ligand peaks.

Despite the complex dynamics of the system under observation, interpretation of WaterLOGSY spectra is quite simple: the phasing of the ligand peaks in the spectrum indicates whether or not that ligand binds the enzyme. This is usually achieved relative to a reference compound, where the phasing (either above or below the baseline) of the reference compound peak(s) is defined "non-binding", and peaks that phase opposite are considered "binding". This technique is optimal for ligands with moderate affinity for the enzyme: if the association is too weak, insufficient magnetization is transferred to the ligand and signal enhancement is minimal. Conversely, if the compound has a very high affinity for the enzyme, fast exchange cannot occur and the "non-binding" signal for the residual compound overrides the "binding" signal.[57] As such, false-negative responses must be taken into consideration, but a "positive" result can be claimed with a greater degree of confidence: a signal phased opposite to a non-binding standard most likely indicates binding.

As aforementioned, WaterLOGSY studies have been reported by the Jakeman group on multiple occasions to probe binding interactions between enzymes and

synthesized ligands. In 2013, sugar-1C-phosphonate analogues and sugar nucleotides were evaluated for binding of Cps2L in the presence and absence of dTTP, as well as binding RmlB-D.[54] Loranger *et al.* determined that their phosphonate analogues demonstrated binding to Cps2L, however, the rhamnose-1C-phosphonate analogue did not bind in the presence of dTTP. This suggests that the conformational change induced by the binding of dTTP prevented access to the binding site of the phosphonate analogue. They also demonstrated that dTDP-rhamnose bound RmlC in addition to its natural target, which may suggest that similar analogues may indeed inhibit multiple enzymes within the rhamnose pathway.[54] Another study, reported in 2015 by Forget *et al.*, used WaterLOGSY to acquire a dissociation constant for an ethylphosphonate derivative of glucose, which demonstrated inhibition against Cps2L. The compound, which bound only in the presence of dTTP, was titrated into an NMR sample containing a solution of dTTP and Cps2L. To a plot of signal intensity (of two characteristic peaks) vs. concentration of the phosphonate was fitted a binding model, which enabled the extraction of a K_D value for that compound.[14] These examples demonstrate that WaterLOGSY is a powerful tool which can provide both mechanistic insight and quantitative analysis of enzyme-ligand interactions, and may thus serve as a valuable complement to inhibition studies in this project.

3.2. Analysis of Natural Cps2L Substrates by WaterLOGSY NMR

A full procedure for conducting WaterLOGSY experiments can be found in Chapter 5.2. The pH for all WaterLOGSY experiments was maintained at 7.5 using 100 mM deuterated Tris•HCl buffer (dTris). Therefore the dTris residual signal, which appears at 3.67 ppm, was used as a "non-binding" signal in lieu of spiking the sample with a non-binding standard compound. In all experiments performed for this project, the dTris signal was phased above the baseline, thereby defining "phase-down" peaks as indicative of binding. Concentrations of enzyme (0.05 mM), MgCl$_2$ (2 mM) and ligand (2.5 mM) were chosen based on previously reported WaterLOGSY experiments.[14] Experimentation with ligand concentration determined that any single-digit millimolar concentration tested was sufficient to acquire the binary "binding/no binding" signal. Experiments with each compound tested included samples in the absence and presence of dTTP. Each sample was made separately (i.e., dTTP was not added to the NMR tube after acquisition of a "zero-

dTTP" spectrum) and thus comparison of the two spectra should not be considered as a titration experiment.

The first set of WaterLOGSY experiments for this project were performed with each of the two natural substrates for Cps2L: G1P and dTTP. Given the generally accepted ordered Bi-Bi mechanism of RmlA-type enzymes,[18] G1P is known to bind Cps2L only in the presence of dTTP. Therefore, a WaterLOGSY experiment with G1P and Cps2L alone demonstrates non-binding signals. Figure 3.1 shows the water-suppression proton NMR and WaterLOGSY spectrum of G1P. As expected, signals corresponding to G1P phase upward, indicating non-binding. Conversely, dTTP is known to bind Cps2L first, and will therefore bind in the absence of G1P. Figure 3.2 shows the proton NMR and WaterLOGSY spectra of dTTP. The phase-down peaks corresponding to dTTP indicate that it binds Cps2L. These two sets of spectra (Figures 3.1 and 3.2) are exemplary of the expected "nonbinding" and "binding" sets of signals. Note that the signals for dTTP show broader peaks relative to those of, for example, G1P. This has been observed previously,[14] and is likely due to interactions with the enzyme, which affects the relaxation time of the nuclei.

Figure 3.1: WaterLOGSY experiment with G1P and Cps2L. A) Water suppression ^{1}H NMR spectrum; B) WaterLOGSY NMR spectrum (500 MHz, 9:1 H_2O : D_2O) of G1P. Sample composition: 2.5 mM G1P, 2 mM $MgCl_2$, 0.05 mM Cps2L, 100 mM dTris•HCl. *residual imidazole from protein purification/His-tag; ^{a}HOD signal; ^{b}dTris residual.

Figure 3.2: WaterLOGSY experiment with dTTP and Cps2L. A) Water suppression ^{1}H NMR spectrum; B) WaterLOGSY NMR spectrum (500 MHz, 9:1 H_2O : D_2O) of dTTP. Sample composition: 2.5 mM dTTP, 2 mM $MgCl_2$, 0.05 mM Cps2L, 100 mM dTris•HCl. ^{a}HOD signal; ^{b}dTris residual.

Many of the compounds synthesized had limited solubility in aqueous buffer, so tolerance of the WaterLOGSY experiment to the presence of d_6-DMSO was probed. Figure 3.3 shows the ^{1}H and WaterLOGSY spectra of dTTP in the presence of 0, 5, and 10% d_6-DMSO. At 10% d_6-DMSO, characteristic peaks are invisible. Conversely, at 5% d_6-DMSO, all dTTP peaks are identifiable, and appear at the same chemical shift as the spectrum with 0% d_6-DMSO, indicating that a sample containing 5% d_6-DMSO should be permissible.
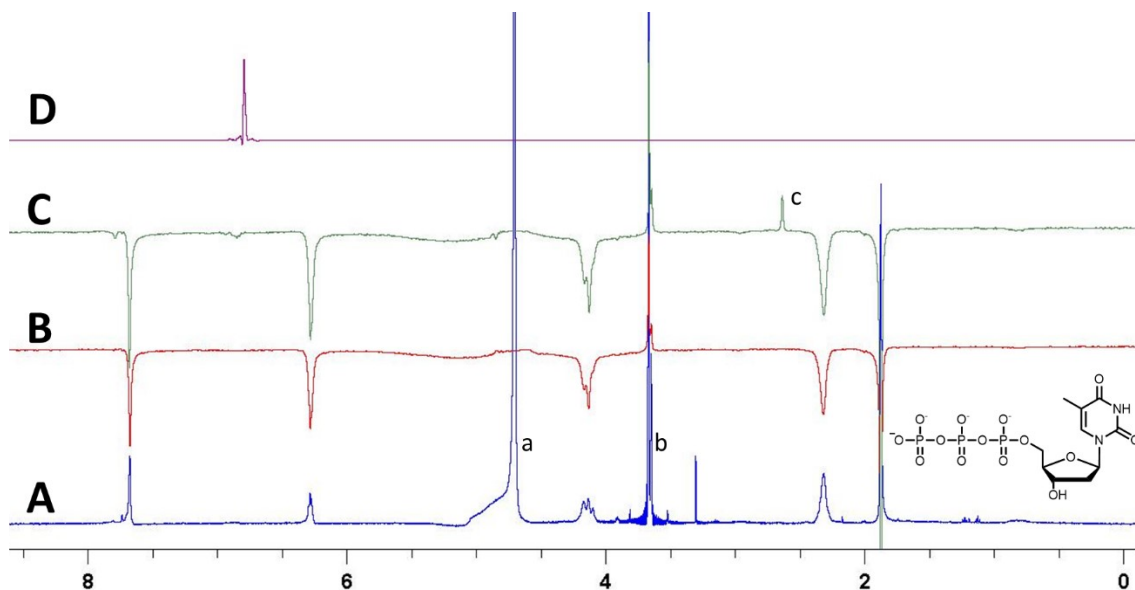
Figure 3.3: WaterLOGSY experiment with dTTP and Cps2L, and varying concentration of d_6-DMSO. A) Water suppression ^{1}H NMR spectrum; B-D) WaterLOGSY NMR spectra (500 MHz, 9:1 H_2O : D_2O) of dTTP with 0% (A, B), 5% (C) or 10% (D) d_6-DMSO. Sample composition: 2.5 mM dTTP, 2 mM $MgCl_2$, 0.05 mM Cps2L, 100 mM dTris•HCl. *dTTP signals; ^{a}HOD signal; ^{b}dTris residual; ^{c}DMSO residual.

30

3.3. Evaluation of Synthesized Compounds as Ligands for Cps2L by WaterLOGSY NMR

NMR samples were prepared as described in Chapter 5.2.1. As discussed above, a 5% aqueous solution of d_6-DMSO did not interfere with the WaterLOGSY experiment. Therefore, 50 mM stock solutions of each potential ligand were made in d_6-DMSO, and added to the WaterLOGSY sample solution such that the final concentrations of d_6-DMSO and ligand were 5% and 2.5 mM respectively. Four compounds were tested in this experiment (see Figure 3.4). Compounds **15**, **18**, and **4c** were chosen to represent different linker scaffolds (amide, fused triazole, and 1,4-substituted triazole, respectively), and **4f** was chosen to probe whether changes in the electronics of the warhead would influence binding, when compared to **4c**.
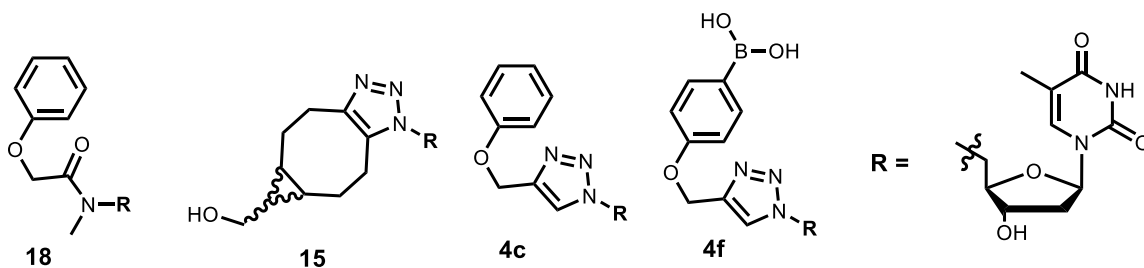
Figure 3.4: Synthesized compounds evaluated by WaterLOGSY NMR.

Figure 3.5 shows the ^{1}H and WaterLOGSY NMR spectra for compound **18**, in the absence and presence of dTTP. The latter is a competition experiment, which has previously been used to probe the mechanism of binding of ligands to Cps2L.[54] In the absence of dTTP (Figure 3.5B), **18** demonstrates binding, but in the presence of one equivalent of dTTP (Figure 3.5C), signals corresponding to **18** phase up, indicating non-binding. This could suggest that **18** binds in a competitive manner, with a sufficiently lower affinity for the active site than dTTP that it is outcompeted, or else that the binding of dTTP induces a conformational change of the enzyme that precludes binding of **18**. It should also be noted that the signals indicating "nonbinding" for compound **18** appear significantly weaker than those of dTTP (Figure 3.5C), even though they are present in equimolar amounts. This is due to the signal enhancement through increased magnetization transfer by the enzyme-ligand interaction, leading to an apparently larger signal for dTTP. While WaterLOGSY can be used for quantitative measurements in certain cases, only the qualitative measurement (phase direction) is considered in this experiment.

Figure 3.6 shows the ^{1}H and WaterLOGSY NMR spectra of compound **15**, once again, in the absence (B) and presence (C) of 1 equivalent of dTTP. Like compound **18**, **15** exhibits nonbinding in the presence of dTTP, suggesting that the latter may exclude binding of **15**.
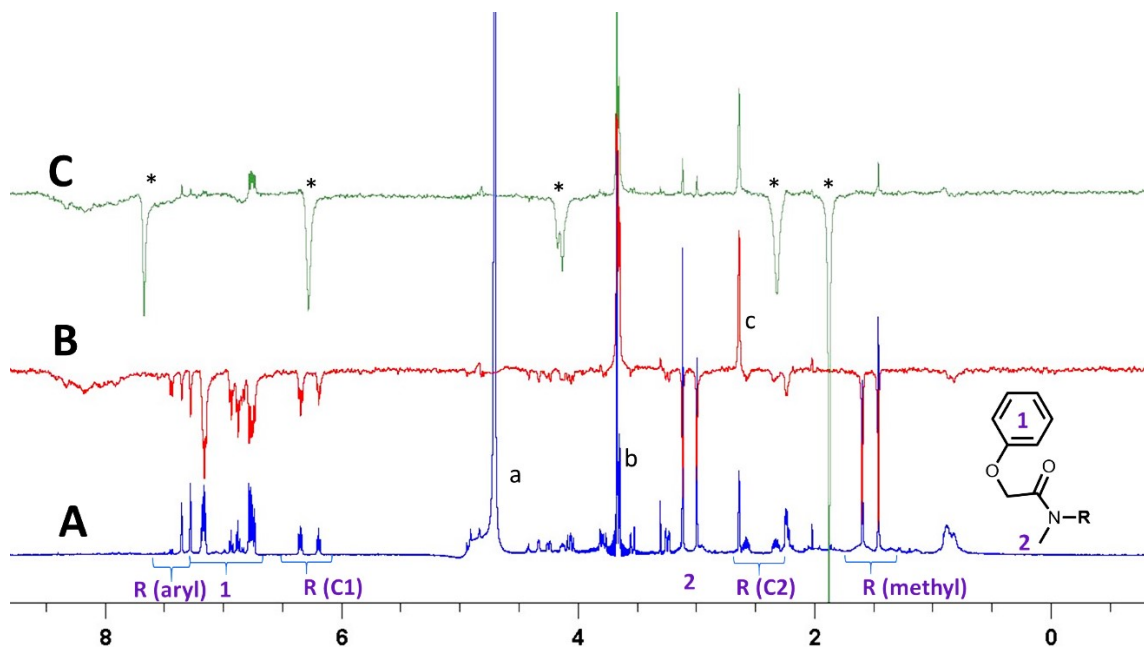
Figure 3.5: WaterLOGSY experiment with **18** and Cps2L. A) Water suppression ^{1}H NMR spectrum; B,C) WaterLOGSY NMR spectra (500 MHz, 17:2:1 H_2O : D_2O : d_6-DMSO) of **18** with 0 (A, B), or 1 (C) equivalent of dTTP. Sample composition: 2.5 mM **18**, 2 mM $MgCl_2$, 0.05 mM Cps2L, 0 or 2.5 mM dTTP, 100 mM dTris•HCl. *dTTP signals; [a]HOD signal; [b]dTris residual; [c]DMSO residual.
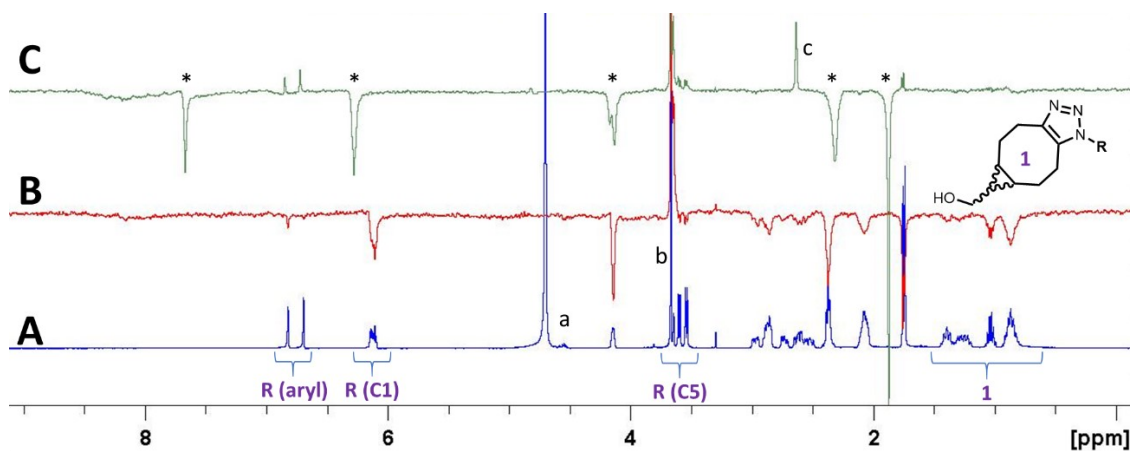
Figure 3.6: WaterLOGSY experiment with **15** and Cps2L. A) Water suppression ^{1}H NMR spectrum; B,C) WaterLOGSY NMR spectra (500 MHz, 17:2:1 H_2O : D_2O : d_6-DMSO) of **15** with 0 (A, B), or 1 (C) equivalent of dTTP. Sample composition: 2.5 mM **15**, 2 mM $MgCl_2$, 0.05 mM Cps2L, 0 or 2.5 mM dTTP, 100 mM dTris•HCl. *dTTP signals; [a]HOD signal; [b]dTris residual; [c]DMSO residual. The sample giving rise to spectra A and B were prepared without d_6-DMSO.

32

Figure 3.7 shows the ^{1}H and WaterLOGSY spectra of compound **4c** in the absence (B) and presence of 1 equivalent (C) or 10 equivalents (D) of dTTP. In all cases, **4c** binds Cps2L, suggesting that dTTP does not completely outcompete, or preclude, its binding. Note that in Figure 3.7C, the signals for dTTP are larger than those for **4c**, despite being present at the same concentration. This may indicate that dTTP has a greater affinity for Cps2L than **4c** does. However, the signals demonstrating binding of **4c** in the presence of a significant excess of dTTP indicates either a significantly higher affinity, or a different binding mode than that of **15** or **18**. Cps2L is tetrameric, with a total of four active and four allosteric sites, so it is possible that, for example, **4c** binds the allosteric site, enabling it to bind without either binding event (**4c** or dTTP with Cps2L) precluding the other.
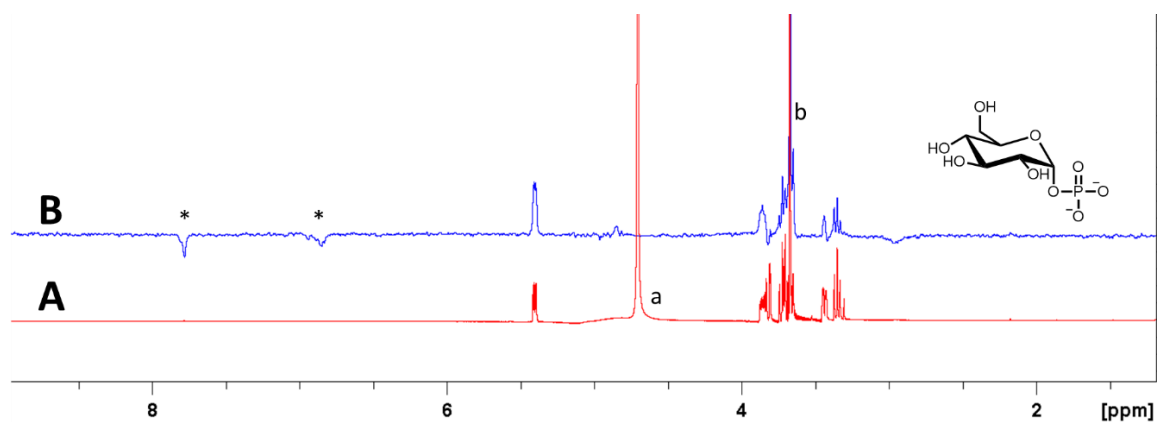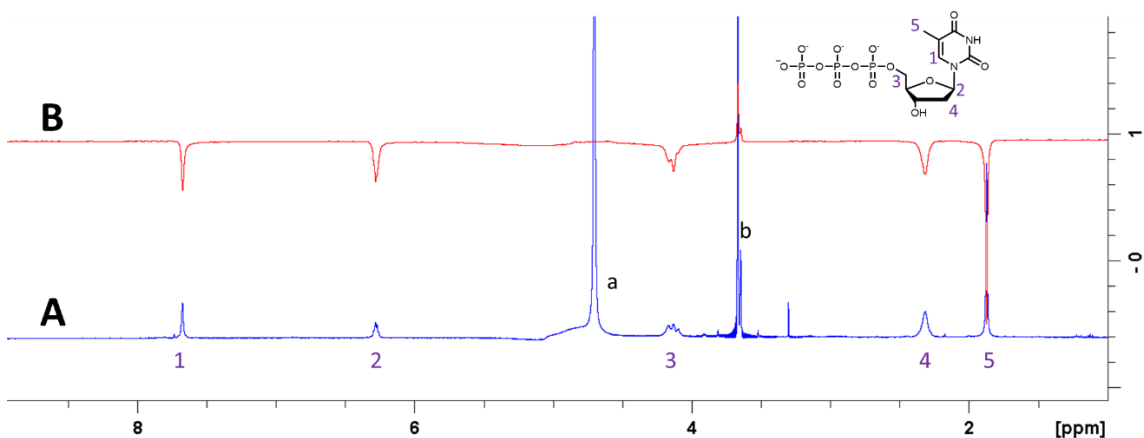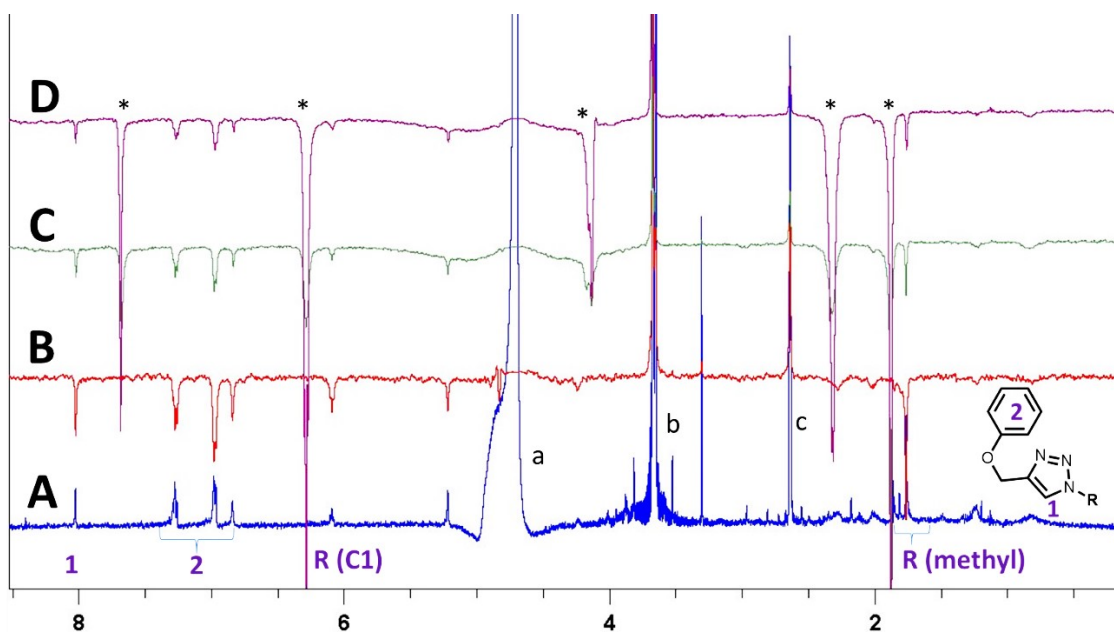

Figure 3.7: WaterLOGSY experiment with **4c** and Cps2L. A) Water suppression ^{1}H NMR spectrum; B-D) WaterLOGSY NMR spectra (500 MHz, 17:2:1 H$_2$O : D$_2$O : d_6-DMSO) of **4c** with 0 (A, B), 1 (C) or 10 (D) equivalents of dTTP. Sample composition: 2.5 mM **4c**, 2 mM MgCl$_2$, 0.05 mM Cps2L, 0, 2.5, or 25 mM dTTP, 100 mM dTris•HCl. *dTTP signals; ^{a}HOD signal; ^{b}dTris residual; ^{c}DMSO residual.

Given this result, compound **4f**, with the same 1,4-substituted triazole linker as **4c**, was evaluated. Figure 3.8 shows the ^{1}H and WaterLOGSY NMR spectra of **4f** which, like **4c**, were acquired in the presence of 0 (B), 1 (C), and 10 (D) equivalents of dTTP. Similarly to **4c**, **4f** gave a binding signal both in the presence of one and 10 equivalents of dTTP, reinforcing the possibility that the 1,4-substitued triazole scaffold has a unique binding mechanism compared to the scaffolds present in compounds **15** and **18**.
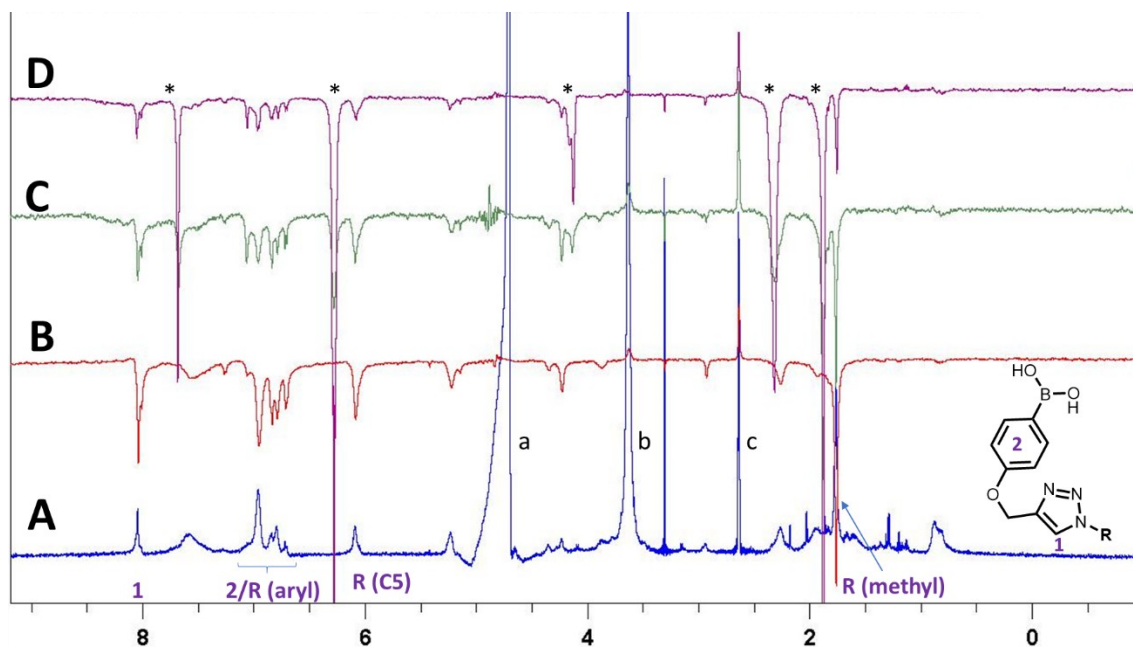
Figure 3.8: WaterLOGSY experiment with **4f** and Cps2L. Water suppression ^{1}H NMR spectrum (A) and WaterLOGSY NMR spectra (B-D) (500 MHz, 17:2:1 H_2O : D_2O : d_6-DMSO) of **4f** with 0 (A, B), 1 (C) or 10 (D) equivalents of dTTP. Sample composition: 2.5 mM **4f**, 2 mM $MgCl_2$, 0.05 mM Cps2L, 0, 2.5, or 25 mM dTTP, 100 mM dTris•HCl. *dTTP signals; ^{a}HOD signal; ^{b}dTris residual; ^{c}DMSO residual.

3.4. Summary

WaterLOGSY NMR was used to assess four compounds (**15, 18**, **4c**, and **4f**), representing three different structural scaffolds, for their ability to bind Cps2L. This study demonstrates that while all of the tested compounds bind and are, therefore, reasonable candidates for inhibitors, only the 1,4-substituted triazole scaffolds (**4c** and **4f**) demonstrated binding in the presence of dTTP. Furthermore, both **4c** and **4f** demonstrate binding in the presence of 10 equivalents of dTTP. These results suggest that compounds with 1,4-substituted triazole scaffolds may exhibit different modes of binding than the other scaffolds. A plausible explanation for this may be that binding of the 1,4-substituted triazole-bearing compounds occurs at the allosteric site, which may permit simultaneous binding of dTTP at the active site.

Chapter 4.   Results and Discussion of the Evaluation of Synthesized Compounds as Inhibitors of Cps2L.

4.1. Introduction

The reaction catalyzed by Cps2L has been studied extensively in the Jakeman lab, and as such, several inhibitor evaluation methods have previously been devised.[14,54,58,59] NMR studies (for example, using ^{31}P NMR) may be used to determine *if* the desired reaction has occurred,[59] but the method is too slow to observe initial reaction rates. The reaction could also be quenched at regular intervals and observed by integration of HPLC or ^{31}P NMR signals.[58] This method has merit in determining the substrate scope of an enzyme, but is inefficient in terms of time and solvent for determining kinetic parameters. Ideally, UV-vis spectroscopy would be used for rapid data acquisition, but the reaction catalyzed by Cps2L does not produce any change in absorbance over time. Therefore, a coupled assay was designed,[14] wherein a chromophore is produced which absorbs at a unique wavelength from that of the reactants and products. Scheme 4.1 shows the coupled enzyme reaction.
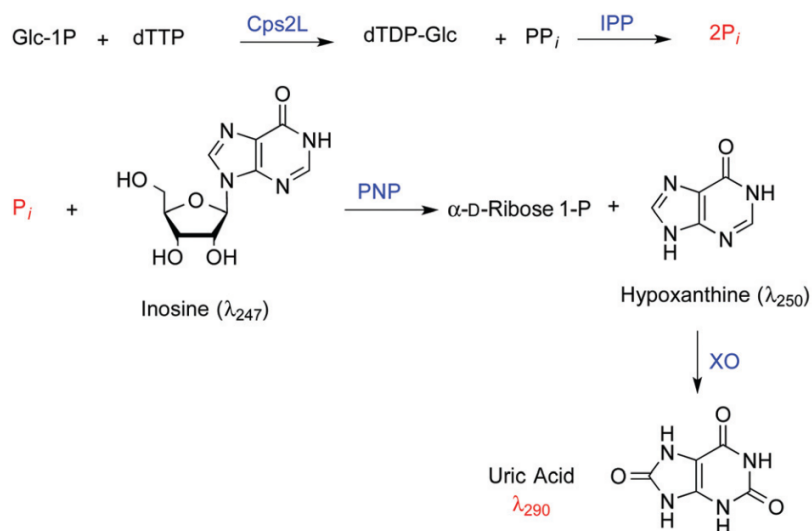
Scheme 4.1: Coupled enzyme reaction to produce the chromophore, uric acid, which absorbs uniquely at 290 nm.[14]

The reaction takes advantage of the production of inorganic pyrophosphate (PP$_i$) which, in this coupled assay, is hydrolysed to phosphate (P$_i$) by inorganic pyrophosphatase (IPP). P$_i$ then reacts with inosine, catalyzed by human purine nucleoside phosphorylase (hPNP), to release hypoxanthine. Finally, hypoxanthine is oxidized to uric acid by xanthine oxidase (XO). The concentration of reagents and enzymes are chosen such that the reaction

of Cps2L is rate-limiting, and an increase in absorbance at 290 nm correlates to the production of dTDP-glucose over time. This method was developed as a more robust alternative[14] to the commonly-used MESG-based assay[54] for detecting inorganic phosphate.

This assay requires the use of four enzymes, two of which (XO and IPP) are commercially available, and two of which (Cps2L and hPNP) need to be overexpressed and isolated in the lab. New stocks of Cps2L and hPNP were prepared for the evaluation of the inhibitors synthesized for this project, as well as new stock solutions of each reagent required for the assay.

4.2. Substrate Inhibition by dTTP

While the reaction catalyzed by Cps2L involves two substrates, a pseudo-first-order reaction is achieved by maintaining a constant high concentration of one substrate and variable low concentrations of the other substrate. In previous studies, dTTP was kept at a high concentration and G1P was varied; however, given that the compounds for this project are dTTP analogues, we chose to vary dTTP instead. dTTP analogues are more likely to mimic the binding of dTTP, which binds Cps2L before G1P does. Performing the assay in this manner also provides us with a K_M value for dTTP which can then be compared to K_i values for our inhibitors.

Before the inhibitors were evaluated, the parameters of the reaction with dTTP as a limiting reagent were determined. As this assay is relatively complex, it required both practice and method optimization in order to acquire consistent data. The optimized method is described in Chapter 5.4.2. It was essential to make new 20 mM stock solutions of dTTP every week, and new dilutions every day. Furthermore, Cps2L loses activity shortly after dilution and therefore must be diluted within minutes of measuring kinetics. Additionally, given that many of our synthesized inhibitors had low water solubility, stock solutions of inhibitor were made in 70% DMSO/water. Therefore, DMSO was added to this "zero inhibitor" assay at the same concentration as it would be present in the inhibition assays. Finally, all solutions must be incubated together prior to addition of Cps2L, so that any excess phosphate from dTTP and G1P solutions is consumed.
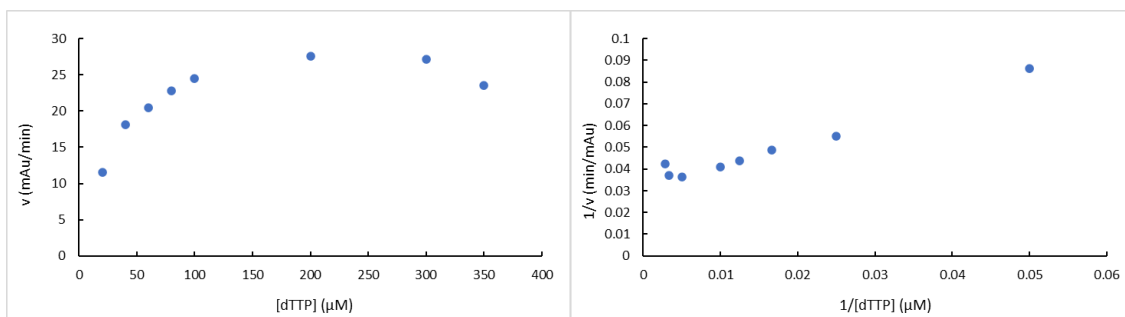
Figure 4.1: Left: Michaelis-Menten plot for the reaction rate of Cps2L with increasing concentration of dTTP. Right: Lineweaver-Burk plot of reciprocal rate vs. reciprocal concentration of dTTP.

Figure 4.1 shows the Michaelis-Menten plot of initial reaction rate (*v*) vs. concentration of dTTP. In standard Michaelis-Menten kinetics, the rate will increase with increasing substrate, until it plateaus at high concentrations. However, this plot shows a marked decrease in rate at high concentrations of dTTP. This pattern, which corresponds to curvature in the corresponding Lineweaver-Burk plot (Figure 4.1, right), suggests that substrate inhibition is occuring,[60] wherein a second substrate molecule binds the enzyme-substrate complex, most likely allosterically,[61] and inhibits the reaction. This has not been observed in previous studies with Cps2L where G1P was the limiting reagent, but unpublished results from a study performed by Dr. Jian-She Zhu from the Jakeman lab provided further evidence that dTTP inhibits Cps2L almost completely at high concentrations. Furthermore, Cps2L is known to have an allosteric site which binds dTDP-rhamnose, which is structurally similar to dTTP and therefore would reasonably accept dTTP as a guest molecule.

Given that we observed substrate inhibition for this reaction, the data cannot accurately be described by the standard Michaelis-Menten equation (Equation 1). We therefore used a modified Michaelis-Menten equation which incorporates an inhibition constant for the substrate. Such an equation (Equation 2) has been reported previously[60,61] and is derived in Appendix D based upon an "uncompetitive"-type inhibition model, where the "inhibitor" substrate molecule may bind the allosteric site of the substrate-bound enzyme.

$$v = \frac{V_{max}[S]}{K_M+[S]} \tag{1}$$

$$v = \frac{V_{max}[S]}{K_M+[S]\left(1+\frac{[S]}{K_S}\right)} \tag{2}$$

Using Equation 2, we determined K_M (Michaelis constant), V_{max} (maximum rate), and K_S (inhibition constant of the substrate) values by employing the Solver function of Excel, which optimizes the values so that the fit matches the datapoints as closely as possible. The method for this optimization can be found in Appendix C. Figure 4.2 shows the optimized fit for this dataset.
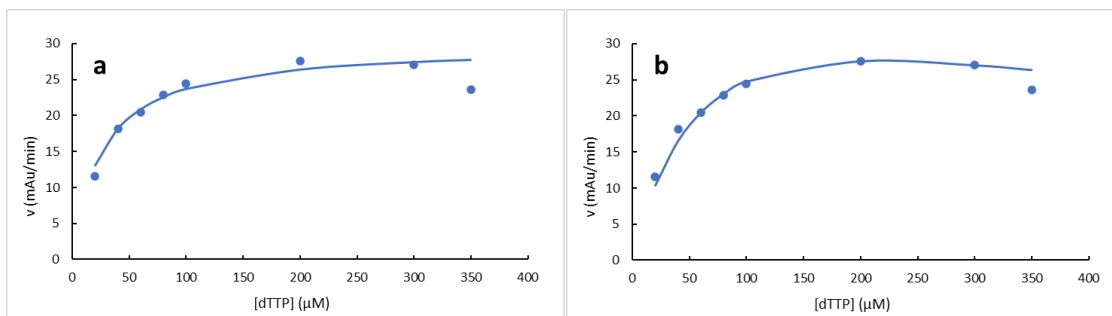
Figure 4.2: Comparison of mathematical models to fit rate data from the reaction of Cps2L with varying dTTP. a) Data (points) with overlaid fit (line) according to Equation 1 with optimized parameters: K_M = 25.7 µM, V_{max} = 29.8 mAu/min. Sum of absolute differences (SAD) = 8.6 mAu/min. b) Data (points) with overlaid fit (line) according to Equation 2 with optimized parameters: K_M = 64.9 µM, V_{max} = 44.4 mAu/min, K_S = 704 µM. SAD = 6.2 mAu/min.

The relative "goodness of fit" can be assessed using the Sum of Absolute Differences (SAD) between the fit values and data values for each datapoint. This sum is the value minimized in optimizing the fit. The smaller the SAD, the better the fit. This method can only be used to compare different models for the same dataset, but can provide a quantitative measure of which model most accurately describes the system. The fit shown in Figure 4.2a shows the fit for the standard Michaelis-Menten equation (Equation 1), optimized by the Solver algorithm, which has a SAD of 8.6 rate units (mAu/min). Comparing this to the modified Michaelis-Menten described by Equation 2, the optimized fit (Figure 4.2b) gives a SAD of 6.2 mAu/min. The SAD of the latter is lower than that of the former, indicating that the latter is a better fit. It should be noted that the significance of the difference (in this case 2.4 mAu/min) is itself qualitative: we must decide on a case-to-case basis whether a small difference in SAD constitutes a truly improved fit. This is an important consideration when using the SAD to choose which inhibition model is most probable.

4.3. Evaluation of Synthesized Compounds as Reversible Inhibitors of Cps2L

4.3.1. Data Acquisition Using the Coupled Enzyme Assay for Cps2L.

To determine inhibition constants (K_i) for each inhibitor, the same procedure to the assay discussed in Section 4.2 (above) was followed, except that four assays were run simultaneously: one with no inhibitor (as before), and three with different inhibitor concentrations (see Chapter 5.4.3 for full method). It was necessary to perform a "zero inhibitor" assay alongside the assays with inhibitor present, as the same dilution of Cps2L was used for all four assays, and there is variation in activity between dilutions of Cps2L. Therefore, the "inhibitor-present" data could not simply be combined with, for example, the data shown in Figure 4.1, as the activity of that particular dilution of Cps2L may be different.

The preliminary evaluation of each compound was performed using 200, 400, and 800 µM of inhibitor. Based on the results from the first assay, the concentrations were adjusted iteratively, until clear separation between each series of datapoints (corresponding to each concentration of inhibitor) was observed when the entire dataset was plotted in a Michaelis-Menten type graph.

An important difference in the inhibition assay method was implemented partway through the period when assays were being conducted. We discovered that Tris buffer, which was used in the assay and in enzyme stock solutions, may react with o-FABA moieties,[62] thus potentially inactivating some of our inhibitors. We therefore dialyzed our enzyme solutions in 3-(N-morpholino)propanesulfonic acid (MOPS), and ran future assays in MOPS instead of Tris. Figure 4.3 shows a comparison between inhibition by **4a** in Tris buffer and MOPS buffer. We found generally significantly improved data quality, and apparently increased inhibition when MOPS buffer was used, and all future assays were performed in MOPS buffer for consistency.
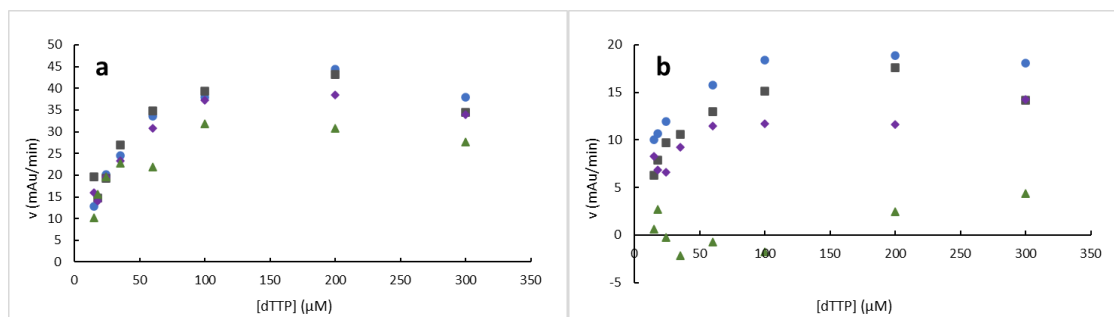
Figure 4.3: Inhibition of Cps2L by **4a** at 0 (●), 200 (■), 400 (◆) and 800 (▲) µM in a) Tris buffer and b) MOPS buffer.

Unfortunately, high quality data was not acquired for each compound discussed in Chapter 2 for several reasons. Primarily among these is the technical challenge of running the assay. Each well in the 96-well plate (1 well = 1 datapoint) contained twelve components, and as there was error associated with each addition and dilution, preparation and execution of the assay were difficult and time-consuming. Practice was required in order to optimize the timing of each addition, especially that of Cps2L. Secondarily, due to the variations in activity between each dilution of Cps2L as aforementioned, each dataset, even with the same concentrations of inhibitor, may produce drastically different results. Therefore, data could not be averaged (which would correct for inconsistencies in individual errant datapoints) and any individual dataset that gave low quality results could not contribute to replicates. Finally, closure of labs due to the COVID-19 pandemic interrupted data acquisition, and therefore not all compounds could be evaluated. Even for those compounds that were evaluated, the optimal range of concentrations were often not determined, and preliminary data could not be used to determine K_i values. Evaluation of compound **10a**, however, gave sufficiently high-quality data and will be discussed presently. Figure 4.4 shows the Michaelis-Menten plot for the inhibition of Cps2L by **10a**.
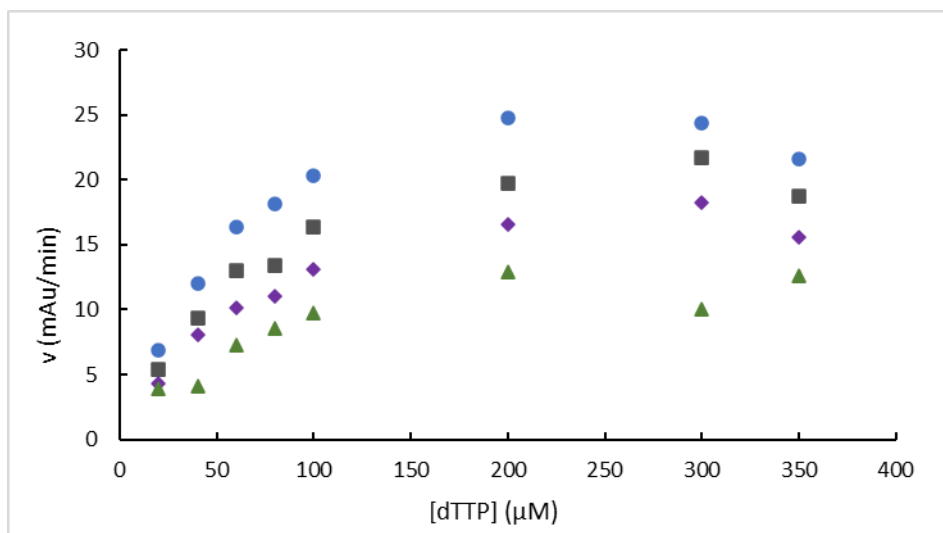
Figure 4.4: Reaction rate of Cps2L at varying dTTP concentration in the presence of 0 (●), 200 (■), 400 (◆) and 800 (▲) μM of **10a**.

4.3.2. Mathematical Determination of Inhibition Mechanisms

There are four standard modes of reversible inhibition, which describe the inhibitor's affinity for the substrate-unbound enzyme, substrate-bound enzyme, both equally, or both unequally. These modes are referred to as competitive, uncompetitive, noncompetitive, and linear-mixed inhibition respectively, and are mathematically described in Equations 3, 4, 5, and 6 respectively. Note that in Equation 6, there are two inhibition constants: K_{iC} and K_{iU} which refer to the inhibitor's affinity for the free enzyme (competitive-type) and substrate-bound enzyme (uncompetitive type) respectively.

$$v = \frac{V_{max}[S]}{K_M(1+\frac{[I]}{K_I})+[S]} \tag{3}$$

$$v = \frac{V_{max}[S]}{K_M+[S](1+\frac{[I]}{K_I})} \tag{4}$$

$$v = \frac{V_{max}[S]}{K_M(1+\frac{[I]}{K_I})+[S](1+\frac{[I]}{K_I})} \tag{5}$$

$$v = \frac{V_{max}[S]}{K_M(1+\frac{[I]}{K_{IC}})+[S](1+\frac{[I]}{K_{IU}})} \tag{6}$$

However, as previously discussed, and as is evident in qualitative observation of Figure 4.4, inhibition by **10a** does not preclude substrate inhibition, which is not considered

41

in Equations 3-6. I therefore derived four compound equations which comprise both substrate inhibition, and the mode of inhibition of interest. The derivations for equations describing competitive, uncompetitive, noncompetitive, and mixed inhibition, each in the presence of substrate inhibition, are found in Appendix D. Equations 7, 8, 9, and 10, describe the four compound inhibition modes, respectively. Note that the equations are based on a scheme which assumes that the substrate inhibition occurs independently of the inhibition by the compound of interest. To my knowledge, no such compound inhibition expressions have yet been reported, although my mathematical method is consistent with the derivation of equations expressing several simultaneous inhibition events in the general case.[63]

$$v = \frac{V_{max}[S]}{K_M(1+\frac{[I]}{K_I})+[S](1+\frac{[S]}{K_S})} \tag{7}$$

$$v = \frac{V_{max}[S]}{K_M+[S](1+\frac{[I]}{K_I}+\frac{[S]}{K_S})} \tag{8}$$

$$v = \frac{V_{max}[S]}{K_M(1+\frac{[I]}{K_I})+[S](1+\frac{[I]}{K_I}+\frac{[S]}{K_S})} \tag{9}$$

$$v = \frac{V_{max}[S]}{K_M(1+\frac{[I]}{K_{IC}})+[S](1+\frac{[I]}{K_{IU}}+\frac{[S]}{K_S})} \tag{10}$$

The Solver algorithm was used to determine K_i values by fitting each model (i.e. Equations 7-10) to the data. Figure 4.5 shows the data and each overlaid fit. I chose to first determine values for K_M, V_{max} and K_S by fitting only the "zero inhibitor" dataset (similarly to the plot shown in figure c) from each experiment, as this minimized unnecessary variation between fits. Assuming independent substrate inhibition, these values should be the same regardless of the mode of inhibition. Then, the values obtained from the "zero inhibitor" fit were inserted into each equation as constants, and only K_i (or in the case of mixed inhibition, K_{iC} and K_{iU}) were varied.

It should be acknowledged that one standard method of estimating the mode of inhibition is by producing a LB plot of reciprocal rate ($1/v$) against reciprocal concentration ($1/[dTTP]$). Mathematically, the reciprocal of the Michaelis Menten equation gives a linear relationship between $1/v$ and $1/[S]$. Consequently, Equations 3-6, variations upon the

Michaelis-Menten equation, give LB plots wherein inhibition alters the slope, y-intercept, or both, relative to a no-inhibitor curve. Therefore, qualitative observation of the LB plots of inhibition data, if it follows Michaelis-Menten kinetics, can give an indication as to which mode of inhibition is being exhibited by a given compound. For our data, however, the presence of substrate inhibition leads to a second-order dependence upon [S], leading to non-linearity in the LB plot (e.g. Figure 4.1, right). This confounds the convergence point (or lack thereof) in the LB plots for inhibition by a given compound at different concentrations. LB plots are included in Appendix E, where linear fits were applied by excluding the nonlinear datapoints. However, the analysis provided herein is based upon nonlinear regression with Equations 7-10 as previously discussed.
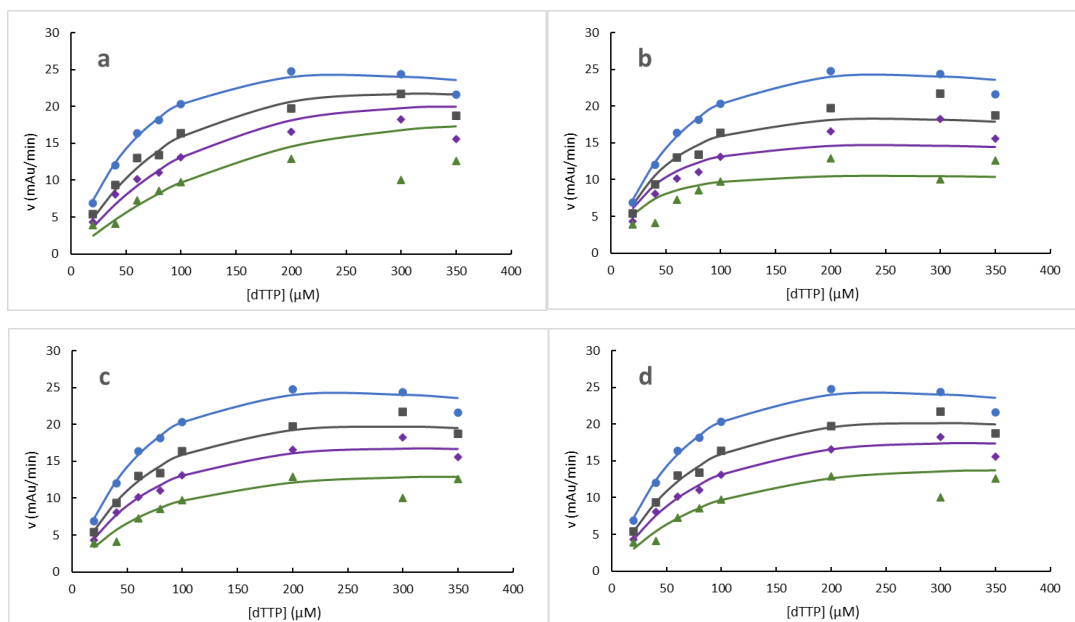
Figure 4.5: Inhibition data of **10a** at 0 (●), 200 (■), 400 (◆) and 800 (▲) µM; and overlaid optimized fits (lines) for a) competitive, b) uncompetitive, c) noncompetitive, and d) mixed inhibition models.

Table 4.1 shows the K_i value(s) and SAD for each inhibition model, based on the data from compound **10a**, with pre-optimized values $V_{max} = 43.7$ mAu/min; $K_M = 98.9$ µM; $K_S = 616.5$ µM. Note that all of the inhibition constants are denoted "K_{iC}" or "K_{iU}", where, in competitive inhibition, only the competitive inhibition constant, K_{iC} is present in the equation, and is thus generally referred to as only "K_i". The same is true of K_{iU} in uncompetitive inhibition.

Table 4.1: Optimized inhibition constants according to each model of inhibition, for the inhibition of Cps2L by **10a**.

Mode of inhibition	K_{iC} (μM)	K_{iU} (μM)	(SAD) (mAu/min)
Competitive (a)	332.3	-	34.3
Uncompetitive (b)	-	339.9	37.7
Noncompetitive (c)	668.5		19.9
Mixed (d)	556.2	858.6	19.2

The relatively low SAD values indicate that noncompetitive and mixed inhibition modes give the closest fits for this dataset. Observing the K_{iC} and K_{iU} values for the mixed inhibition mode, it appears that **10a** has a slightly higher affinity for the unbound enzyme, but still binds the substrate-bound enzyme, and therefore likely binds the allosteric site.

Based on this type of analysis, the probable mode of inhibition was determined, along with corresponding K_i values, for each of the synthesized compounds we were able to evaluate. Table 4.2 provides a summary of the calculated K_i values and probable modes of inhibition. All plots, K_i values, and SAD values for each compound can be found in Appendix F, and Excel sheets containing all raw data and calculated constants are included in Appendix G.

Table 4.2: Summary of results for all reversible inhibition studies.

Compound	Probable mode of inhibition	K_i value(s) (μM)
4a	Uncompetitive	503.3
4b	Mixed	162.0 (K_{iC}) / 240.0 (K_{iU})
4d	No fit	<<25[c]
4e	Uncompetitive	272.3
4f	No fit	<<200[c]
4g	Noncompetitive	3429[a]
7	Uncompetitive	2319
8	No inhibition at 800 μM	>>800[b]
10a	Mixed	556.2 (K_{iC}) / 858.6 (K_{iU})

[a]The mixed model gives a very slightly improved fit but the difference in K_{Ii} values is insignificant. [b]The estimate provided is greater than the highest inhibitor concentration tested. [c]These compounds gave apparent complete inactivation, and the estimate provided is less than the lowest concentration tested.

While only preliminary data were obtained, certain conclusions may be drawn from these results. For example, none of the nitrile-bearing compounds (**7**, the aliphatic nitrile, or **8** and **4g**, the meta- and para-substituted aryl nitriles) were particularly potent inhibitors. Indeed, **8** provided no observable inhibition whatsoever at the concentrations tested. Therefore, the nitrile functionality does not appear to improve binding, at least not within the timescale of these measurements.

Compound **10a** demonstrates moderate, but not notably potent, inhibition of Cps2L. According to the mixed inhibition model, it will bind either the free or substrate-bound enzyme, but slightly prefers the competitive mechanism. Note that the structure of **10a**, bearing a compound triazole-ketone linker, is different than most of the other compounds indicated in Table 4.2, and, therefore, poses a challenge in performing SAR studies in this preliminary test.

Compound **4f**, bearing a para-substituted arylboronic acid, demonstrates high potency against Cps2L among the tested compounds. This may suggest that electronics at the para- position are significant: note that the two other triazole-scaffold compounds bearing para-substituted aryl rings (compounds **4g** and **4e**) show lower inhibition, and indeed as the electron-deficiency of the para-substituted group increases, so does the apparent potency of the compound (i.e. $ArB(OH)_2 > ArCHO > ArCN$). This may suggest that in future studies, placing a highly electrophilic group at that position may improve inhibition.

However, conclusions are difficult to draw when comparing the four aldehyde-bearing compounds, **4a**, **4b**, **4d** and **4e**. A summary of the data accrued for these compounds can be found in Figure 4.6. Comparing compounds **4a** and **4b**, which have identical functional groups but at different positions, not only show significantly different potency, but also different apparent modes of inhibition. **4a** demonstrates a high degree of preference for the uncompetitive model, with a SAD of 17.5, compared to 21.8, 28.3, and 28.0 for competitive, noncompetitive, and mixed models, respectively. Meanwhile, **4b** is apparently more potent, but shows mixed inhibition (SAD = 30.0 compared to 45.6, 38.6, and 31.3 for competitive, uncompetitive, and noncompetitive models, respectively). In fact, according to the K_i values, **4b** shows a slightly higher affinity for the active site (i.e. the competitive mechanism). This suggests that the steric bulk afforded by the BPin group does

not appear to dictate which site the compound prefers, as both **4a** and **4b** bear a BPin group. Furthermore, there is no discernible pattern in either potency or mode of inhibition when comparing the positioning of the aldehyde. For example, both **4a** and **4d** bear meta-functionalized aldehydes (relative to the ether group linking the aryl ring and the rest of the molecule) but have the lowest and highest potency of the four compounds in Figure 4.6, respectively. Additionally, **4b** and **4e** both bear an ortho-substituted aldehyde, but **4e** demonstrates uncompetitive inhibition (SAD = 48.4 compared to 80.9, 57.9, and 48.4 for competitive, noncompetitive, and mixed models respectively – note that in the mixed model, $K_{iC} > 50\ 000$ μM, so the only true inhibition is coming from the uncompetitive component) whereas, as aforementioned, **4b** demonstrates mixed inhibition.
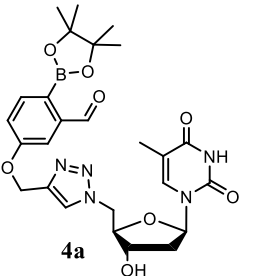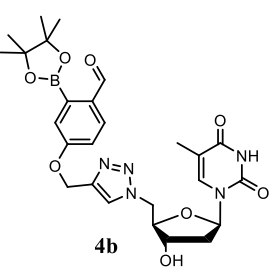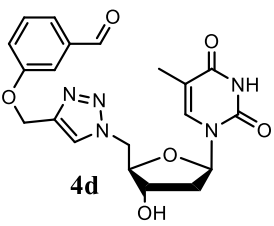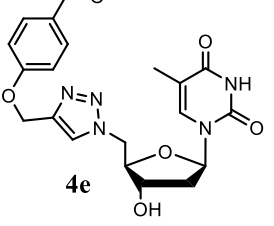
4a	Inhibition mode: **uncompetitive** K_{iU}: **503 μM** Preferred binding site: **Allosteric**	**4b**	Inhibition mode: **Mixed** K_{iC}: **162 μM** K_{IU}: **240 μM** Preferred binding site: **Active**
4d	Inhibition mode: **unknown** K_i: **<< 25 μM** Preferred binding site: **Unknown**	**4e**	Inhibition mode: **uncompetitive** K_{iU}: **272 μM** Preferred binding site: **Allosteric**

Figure 4.6: Summary of K_i values and presumed inhibition modes for aldehyde-containing compounds.

The size of the inhibitor also seems to have no bearing on its potency. As aforementioned, **4d** is by far the most potent inhibitor, but the second-most potent is compound **4b**, although the difference between potencies of compound **4b** and **4e** may not be significant, given the limited nature of our results. Therefore, I must conclude only that it is too early to conclude anything as it pertains to structure-activity relationship with this set of molecules. Obtaining more consistent and higher quality data will be important future steps in the analysis of these molecules as inhibitors.

It is evident that further studies need be performed in order to draw firm conclusions, but the following are some general observations. First, while any amount of inhibition is informative from these exploratory experiments, a preliminary measure of the "goodness" of an inhibitor is comparison of its calculated K_i value(s) to the K_M of the limiting substrate (in this case, dTTP). The K_M values were measured separately for each experiment, but the average value and standard deviation for calculated K_M values is 57.2 µM and 19.3 µM respectively. Based on this measure, only **4d**, and possibly **4f** indicate comparable or improved potency. Secondly, it is notable that none of the compounds displayed selective, competitive inhibition. However, given the observation that dTTP consistently demonstrates substrate inhibition and is known to bind the allosteric site,[17] along with the knowledge that the natural feedback-loop inhibitor, dTDP-rhamnose, binds allosterically, it is unsurprising that our thymidine derivatives have an affinity for the allosteric site, sometimes even over the active site. Combined with the WaterLOGSY studies discussed in Chapter 3, these data provide further evidence that the triazole-bearing thymidine derivatives bind at the allosteric site in preference to the active site. This may indicate that future work may include intentional targeting of the allosteric site to improve the selectivity of the inhibitors. Currently, the most potent inhibitors of RmlA thus far are thymine derivatives that bind at the allosteric site (according to co-crystallization with the enzyme)[17] supporting the possibility that this mechanism could be demonstrated by our thymidine derivatives. Furthermore, we only tested triazole-bearing compounds in kinetic studies. It is possible that the amide series or compounds bearing other linkers may demonstrate competitive binding, as the amide (**18**) and fused-triazole (**15**) compounds were fully displaced by dTTP in WaterLOGSY binding studies. Finally, while we were unable to synthesize target compounds **5a** and **5b**, the two most potent compounds we tested, **4d** and **4f**, bore the composite functional groups of **5a**, suggesting that it potentially may be a very potent compound if it is synthetically accessible. Therefore, not only will it be valuable to determine the K_i values and mechanisms of inhibition of **4d** and **4f**, but also to synthesize and evaluate compounds **5a** and **5b**.

4.4. Exploration of Potential Covalent Inactivators Through Time-Dependent Inhibition Studies

The inhibition mechanisms discussed in Chapter 4.3.2 (above) only describe fully reversible inhibition, where the interaction between the host and guest can be interrupted by dilution. Some of our compounds (i.e., aldehydes **4d** and **4e**, as well as BPin-aldehyde compounds **4a** and **4b**) are designed to react covalently with lysine residues to form imines or iminoboronates, respectively. As such, this type of may not be observed easily using kinetic studies which rely on fast, reversible binding. Instead, slow-binding studies are used.

In slow-binding studies, the compound is allowed to interact with the enzyme for an extended period of time, and increased inhibition (i.e., decreased enzyme activity) is demonstrated over time. This may be done by preincubating the inhibitor with the enzyme, then performing the coupled assay at several timepoints throughout the incubation (the specific time period would vary based on how slow the binding was). In this case, a plot of reaction rate vs. time would show datapoints which decreased either linearly or as a decay function, and this method has previously been used successfully in the Jakeman group.[64] However, due to the propensity of Cps2L to lose activity rapidly after dilution, we found that even in the absence of inhibitor, activity would decrease over time.

We therefore opted for an alternative method to observe slow binding, which uses not the rate data, but the raw data acquired from the assay, plotting absorbance (proportional to product formation) over time. Theoretically, in the presence of a slow, "tight-binding" inhibitor, the rate of reaction will decrease over time, whereas the same reaction in the absence of inhibitor should show no decrease in rate over the same period of time.[65] Naturally, as the substrate is consumed, the reaction rate will begin to decrease; so a relatively high concentration of substrate must be chosen, as well as an appropriate time period over which the reaction rate remains linear.

Jakeman group members Julie Cormier, Dr. Michael Beh and I began to conduct the slow-binding assay prior to lab closures (the full procedure can be found in Chapter 5.4.4), but no conclusive data have yet been collected. Most commonly, curvature in the "zero inhibitor" trace occurs, indicating that the time period is too long, and the substrate is being consumed. We have also observed immediate inhibition rather than inhibition over

time (see Figure 4.7) which visually confounds the expected observation (curvature, or lack thereof). Given the kinetic studies, we know that most of the compounds we test give some degree of fast, reversible inhibition which explains this result. Future studies will determine optimal parameters for this assay so that any covalent interactions can be identified and characterized.
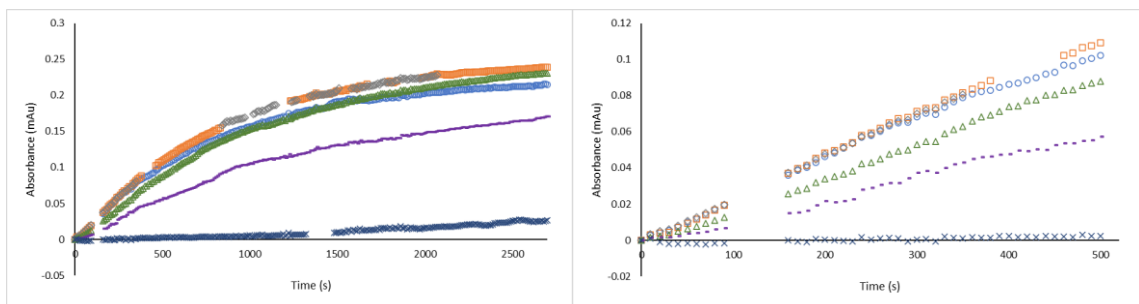
Figure 4.7: Formation of product (proportional to absorbance) by Cps2L over time in the presence of **4d** at 0 (○), 2 (□), 4 (◇), 6 (△), 8 (━) and 12.5 (✕) μM over the course of (left) 2700 s and (right) 500 s. Errant datapoints due to artifacts during acquisition were removed for clarity. Immediate inhibition is evident by the decreased initial slope at increasing concentrations of inhibitor. Additionally, curvature is evident at 0 μM, confounding the expected result. Data collected by Dr. Michael Beh.

4.5. Summary

Nine of the compounds synthesized for this project were analyzed for reversible inhibition of Cps2L. Kinetic models were devised to incorporate multiple instances of inhibition (by the substrate and the compound of interest), for each of the four standard reversible inhibition models. Preliminary data suggest that all but one compound demonstrated at least some inhibition at the concentrations tested, with particular potency demonstrated by compound **4d**. Exploratory work into probing slow-binding inhibition was also performed. Future work will involve acquiring consistent and high-quality kinetic data for each of the compounds synthesized so that accurate kinetic parameters and mechanisms of inhibition can be determined.

Chapter 5.   Experimental Procedures

5.1. Procedures for the Synthesis of Inhibitor Compounds and Intermediates

5.1.1. General Remarks

Reactions were conducted using oven-dried glassware and stir bars. Reaction solvents were purchased anhydrous and used without further purification. All reagents were obtained from commercial sources and used without further purification except for 2-bromo-5-hydroxybenzaldehyde, which was purified by column chromatography before use. Reaction progress was monitored using glass-backed silica TLC plates, and visualized using UV light, or p-anisaldehyde, dinitrophenylhydrazine, or potassium permanganate stain. NMR spectra were acquired using a Bruker 500 MHz (11.7 T) NMR spectrometer at Dalhousie University's NMR-3 facility. NMR chemical shifts were reported in ppm relative to TMS (^{1}H and ^{13}C nuclei) or BF_3OEt_2 (^{11}B nucleus) or $CFCl_3$ (^{19}F nucleus). Mass spectra were acquired by Xiao Feng using a Bruker microTOF Focus Mass Spectrometer, using an ESI (+ or -) or APCI (+ or -) ionization source.

5.1.2. General Procedure 1 (GP1) for the Alkyne Substitution Reaction of Phenols

Phenol **1** (1 equiv.) and potassium carbonate (2 equiv.) were dissolved in anhydrous DMF to a final concentration of approximately 0.75 M with respect to phenol, then propargyl bromide (1.5 equiv., 80% v/v solution in toluene) was added. The reaction mixture was covered with a septum and stirred at room temperature until complete as determined by TLC analysis (eluent = 3:1 hexane : ethyl acetate). Upon completion, the reaction solvent was removed in vacuo under a 50 mbar atmosphere while maintained at 50 °C. The crude material was redissolved in ~20 mL ethyl acetate, then washed with water (2 × 20 mL) and saturated aqueous sodium sulfate solution (1 × 20 mL). The organic phase was dried with anhydrous magnesium sulfate, filtered, and evaporated in vacuo to give the product. No further purification was required except where noted.

5.1.2. General Procedure 2 (GP2) for the CuAAC Reaction With CuSO$_4$ and Ascorbic Acid

5′-Deoxy-5′-azidothymidine (1 equiv.) and alkyne (1.1 equiv.) were stirred in THF (approx. 0.12 M with respect to azide) at 50 °C until both were fully dissolved. Copper (II) sulfate pentahydrate (0.5 equiv.) and ascorbic acid (0.55 equiv.) were dissolved in water (1/3 volume of THF), then the aqueous solution was added to the THF solution. The

reaction mixture was purged with nitrogen, and stirred at 50 °C. After consumption of 5′-deoxy-5′-azidothymidine as determined by TLC analysis (10% MeOH, 45% hexane, 45% DCM), the reaction mixture was evaporated to dryness in vacuo. The residue was triturated with H_2O (5-10 mL) then filtered and washed several times with water to remove copper salts and ascorbic acid. The solid was dried, washed with DCM to remove excess alkyne, and collected to give the product. No further purification was required except where noted.

5.1.3. Synthesis of Compounds

5′-Deoxy-5′-azidothymidine (**1**)
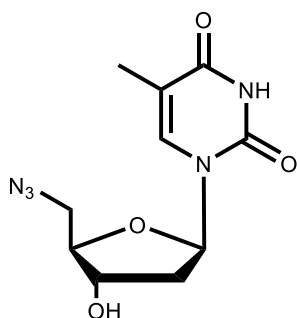
5′-O-(p-Toluenesufonyl)thymidine (500 mg, 1.261 mmol) and sodium azide (123 mg, 1.892 mmol) were solvated in N,N-dimethylformamide (DMF, 3 mL). The reaction mixture was stirred at 70 °C for 3 h, and monitored by thin-layer chromatography (silica, 5% methanol in dichloromethane). Upon completion, the solvent was removed in vacuo, then the crude material was redissolved in a mixture of 1:1 H_2O/saturated aqueous Na_2SO_4. The aqueous solution was extracted 4x with 2-methyltetrahydrofuran (Me-THF). The organic layers were combined and dried with anhydrous $MgSO_4$, filtered, and evaporated in vacuo to give the product as a crystalline white solid (333 mg, 99%). TLC: R_F = 0.46. Characterization data are consistent with literature.[35]

2-Formyl-4-hydroxyphenylboronic acid pinacol ester (**2a**)
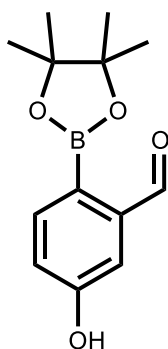
2-Bromo-5-hydroxybenzaldehyde (1300 mg, 6.467 mmol), bis(pinacolato)diboron (2956 mg, 11.614 mmol) and ([1,1′-Bis(diphenylphosphino)ferrocene]dichloropalladium(II) (236 mg, 0.323 mmol) were combined, followed by potassium acetate (1904 mg, 19.401 mmol). The solids were dissolved in dioxane (10 mL), then the reaction mixture was purged with nitrogen and stirred at 100 °C under nitrogen atmosphere. The reaction was monitored by TLC (SiO_2, 10% EtOAc, 45% hexane, 45% DCM) and found to be compete after 3.5 h. The reaction mixture was evaporated to dryness in vacuo, then redissolved in EtOAc (50 mL) and transferred to a separatory funnel. The organic phase was washed with water (3 × 50 mL), then collected,

dried with MgSO$_4$, and filtered. The dissolved crude material was adsorbed directly onto Celite®, dry-loaded onto a silica column, and purified by flash chromatography (0-10% EtOAc in hexane) to give the product (1393g, 87%). ^{1}H NMR (500 MHz, CDCl$_3$) δ 10.65 (s, 1H), 7.86 (d, J = 8.2 Hz, 1H), 7.51 (d, J = 2.6 Hz, 1H), 7.10 (dd, J = 2.6, 8.2 Hz, 1H), 6.04 (s, 1H), 1.37 (s, 12H). ^{13}C NMR (126 MHz, CDCl$_3$) δ 195.22, 158.45, 143.54, 138.43, 120.43, 113.22, 84.21, 24.85. ^{11}B NMR (160 MHz, CDCl$_3$) δ 30.78. HRMS - ESI+ (m/z) calc'd for C$_{13}$H$_{17}$BNaO$_4$: 271.1112; found 271.1109.

2-Formyl-5-hydroxyphenylboronic acid pinacol ester (**2b**)
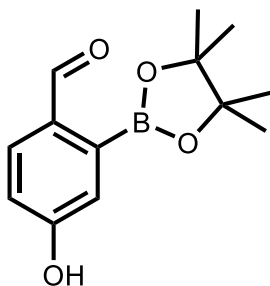
2-Bromo-4-hydroxybenzaldehyde (1000 mg, 4.974 mmol), bis(pinacolato)diboron (2274 mg, 8.954 mmol) and ([1,1′-Bis(diphenylphosphino)ferrocene]dichloropalladium(II) (182 mg, 0.249 mmol) were combined, followed by potassium acetate (1464 mg, 14.922 mmol). The solids were dissolved in dioxane (8 mL), then the reaction mixture was purged with nitrogen and stirred at 100 °C under nitrogen atmosphere. The reaction was monitored by TLC (SiO$_2$, 10% EtOAc, 45% hexane, 45% DCM) and found to be complete after 5 h. The reaction mixture was evaporated to dryness in vacuo, redissolved in EtOAc (40 mL), the organic phase washed with water (2 × 40 mL), then the aqueous phases reextracted with EtOAc (20 mL). The organic phases were combined, washed with a solution of 1:1 H$_2$O: brine (20 mL), then dried with MgSO$_4$, filtered, and evaporated. The residue was adsorbed onto Celite®, dry-loaded onto a silica column, and purified by flash chromatography (0-20% EtOAc in hexane). Fractions containing product were evaporated to dryness, then the material was washed with cold hexane to give the product as a white solid (1180 mg, 96%). Characterization data are consistent with literature.[66]

2-Formyl-4-(2-propyn-1-yloxy)-phenylboronic acid pinacol ester (3a)
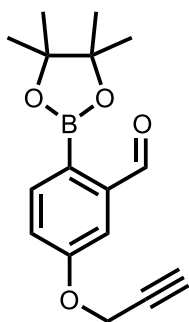
Compound **3a** was prepared according to **GP1** with 1000 mg (4.031 mmol) of **2a**. The reaction was complete after 4 h. Following extraction, the organic material was filtered through a short plug of silica and evaporated to dryness to give an off-white solid (592 mg, 51%). $R_F = 0.42$. ^{1}H NMR (500 MHz, CDCl$_3$) δ 10.67 (s, 1H), 7.89 (d, J = 8.3 Hz, 1H), 7.57 (d, J = 2.6 Hz, 1H), 7.19 (dd, J = 2.7, 8.3 Hz, 1H), 4.77 (d, J = 2.4 Hz, 2H), 2.53 (t, J = 2.4 Hz, 1H), 1.37 (s, 12H). ^{13}C NMR (126 MHz, CDCl$_3$) δ 194.54, 159.82, 143.55, 137.97, 120.51, 111.57, 84.24, 77.78, 76.06, 55.82, 24.87. Characterization data are consistent with literature.[66]

2-Formyl-5-(2-propyn-1-yloxy)phenylboronic acid pinacol ester (3b)
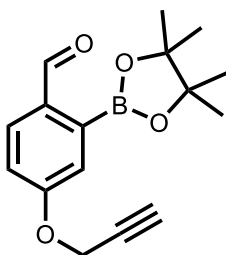
Compound **3b** was prepared according to **GP1** with 1000 mg (4.031 mmol) of **2b**. The reaction was complete after 5 h. The product was recovered as a reddish crystalline solid (655 mg, 57%). ^{1}H NMR (500 MHz, CDCl$_3$) δ 10.39 (s, 1H), 7.95 (d, J = 8.6 Hz, 1H), 7.37 (d, J = 2.7 Hz, 1H), 7.11 (dd, J = 2.5, 8.5 Hz, 1H), 4.78 (d, J = 2.4 Hz, 2H), 2.54 (t, J = 2.4 Hz, 1H), 1.39 (s, 12H). ^{13}C NMR (126 MHz, CDCl$_3$) δ 192.94, 161.14, 135.32, 130.48, 121.19, 116.68, 84.48, 77.66, 76.07, 55.89, 24.83. HRMS – ESI+ (m/z) calc'd for C$_{16}$H$_{19}$BNaO$_4$: 309.1269; found 309.1268.

5′-(4-((3-Formyl-4-(pinacolborono)phenoxy)methyl)-1H-1,2,3-triazol-1-yl)-5′-deoxythymidine (4a)
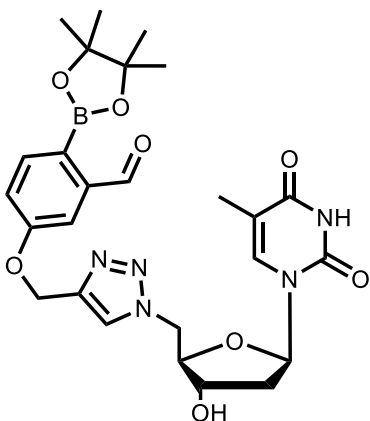
Tetrakis(acetonitrile)copper(I) hexafluorophosphate (14 mg, 0.037 mmol) and Tris[(1-benzyl-1H-1,2,3-triazol-4-yl)methyl]amine (24 mg, 0.045 mmol) were stirred in anhydrous THF (24 mL). 5′-deoxy-5′-azidothymidine (200 mg, 0.748 mmol) and **3a** (236 mg, 0.823 mmol) were each dissolved in 6 mL THF, and added sequentially to the reaction mixture. The solution was purged with nitrogen and heated to 60 °C. After 1 hour, the azide starting material was consumed by TLC analysis (SiO$_2$,

53

10% MeOH, 45% DCM, 45% hexane), and the reaction mixture was evaporated to dryness in vacuo. The resulting solid was stirred in DCM (20 mL) and the solid collected by filtration to give the product (160 mg, 39%). ^{1}H NMR (500 MHz, d_6-DMSO) δ 11.29 (s, 1H), 10.44 (s, 1H), 8.22 (s, 1H), 7.74 (d, J = 8.3 Hz, 1H), 7.50 (d, J = 2.6 Hz, 1H), 7.34 (m, 2H), 6.17 (t, J = 7.0 Hz, 1H), 5.49 (d, J = 4.4 Hz, 1H), 5.26 (s, 2H), 4.73 (dd, J = 4.3, 14.3 Hz, 1H), 4.64 (dd, J = 7.6, 14.3 Hz, 1H), 4.28 (q, J = 3.3 Hz, 1H), 4.09 (m, J = 3.8 Hz, 1H), 2.16 (m, 1H), 2.09 (m, 1H), 1.79 (d, J = 0.7 Hz, 3H), 1.33 (s, 12H). ^{13}C NMR (126 MHz, d_6-DMSO) δ 193.78, 163.59, 160.12, 150.35, 142.81, 142.22, 137.24, 136.00, 125.35, 119.94, 112.43, 109.82, 84.03, 83.94, 81.31, 70.73, 61.19, 51.24, 37.86, 24.56, 24.44, 12.00. ^{11}B NMR (160 MHz, d_6-DMSO) δ 32.39, 22.33. HRMS – ESI+ (m/z) calc'd for $C_{26}H_{32}BN_5NaO_8$: 576.2236; found 576.2241.

5′-(4-((4-Formyl-3-(pinacolborono)phenoxy)methyl)-1H-1,2,3-triazol-1-yl)-5′-deoxythymidine (4b)
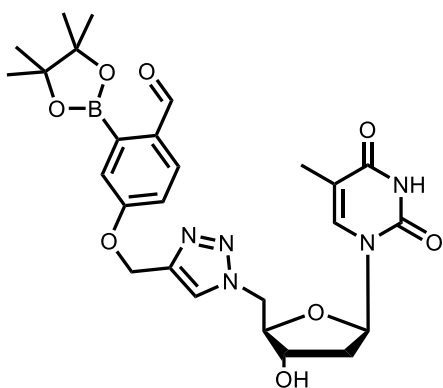
Tetrakis(acetonitrile)copper(I) hexafluorophosphate (14 mg, 0.037 mmol) and Tris[(1-benzyl-1H-1,2,3-triazol-4-yl)methyl]amine (24 mg, 0.045 mmol) were stirred in anhydrous THF (24 mL). 5′-deoxy-5′-azidothymidine (200 mg, 0.748 mmol) and 3b (236 mg, 0.823 mmol) were each dissolved in 6 mL THF and added sequentially to the reaction mixture. The solution was purged with nitrogen and heated to 60 °C. After 1 hour, 5′-deoxy-5′-azidothymidine was consumed by TLC analysis (SiO$_2$, 10% MeOH, 45% DCM, 45% hexane), and the reaction mixture was evaporated to dryness in vacuo. The resulting solid was stirred in DCM (20 mL) and the solid collected by filtration to give the product as a red-brown solid (284 mg, 69%). ^{1}H NMR (500 MHz, d_6-DMSO) δ 11.29 (s, 1H), 10.14 (s, 1H), 8.23 (s, 1H), 7.90 (d, J = 8.6 Hz, 1H), 7.35 (d, J = 0.9 Hz, 1H), 7.29 (q, J = 3.7 Hz, 1H), 7.24 (d, J = 2.6 Hz, 1H), 6.17 (t, J = 7.0 Hz, 1H), 5.49 (d, J = 4.4 Hz, 1H), 5.28 (s, 2H), 4.74 (dd, J = 4.3, 14.3 Hz, 1H), 4.65 (dd, J = 7.6, 14.3 Hz, 1H), 4.29 (m, 1H), 4.09 (m, 1H), 2.17 (m, 1H), 2.10 (m, 1H), 1.80 (s, 3H), 1.34 (s, 12H). ^{11}B NMR (160 MHz, d_6-DMSO) δ 33.13.

2-(Propyn-1-yloxy)benzene (3c)
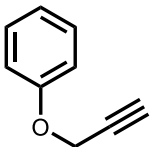
Compound **3c** was prepared according to **GP1** with 100 mg (1.06 mmol) of phenol. The reaction was complete after 2 h, and extraction was performed using diethyl ether as the organic phase instead of ethyl acetate. The product was recovered as a colourless oil (80 mg, 57%). ^{1}H-NMR (500 MHz, CDCl₃) δ 2.51 (1H, t, J = 2.38 Hz), 4.70 (2H, d, J = 2.15 Hz), 7.00 (3H, m, J = 4.44 Hz), 7.31 (2H, t, J = 7.98 Hz). Characterization data are consistent with literature.[31]

3-(2-Propyn-1-yloxy)benzaldehyde (3d)
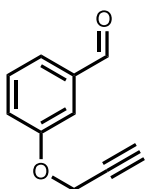
Compound **3d** was prepared according to **GP1** with 250 mg (2.047 mmol) of 3-hydroxybenzaldehyde. The reaction was complete after 3 h. The product was recovered as a pale oil (316 mg, 96%). R_F = 0.49. ^{1}H NMR (500 MHz, CDCl₃) δ 9.99 (s, 1H), 7.50 (m, J = 8.1 Hz, 3H), 7.26 (qd, J = 1.2, 8.1 Hz, 2H), 4.76 (d, J = 2.4 Hz, 2H), 2.55 (t, J = 2.4 Hz, 1H). Characterization data are consistent with literature.[32]

4-(2-Propyn-1-yloxy)benzaldehyde (3e)
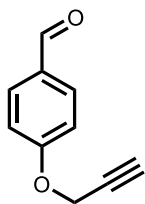
Compound **3e** was prepared according to **GP1** with 250 mg (2.047 mmol) of 4-hydroxybenzaldehyde. The reaction was complete after 3 h. The product was recovered as an off-white solid (307 mg, 94%). ^{1}H NMR (500 MHz, CDCl₃) δ 9.91 (s, 1H), 7.86 (d, J = 8.8 Hz, 2H), 7.10 (d, J = 8.8 Hz, 2H), 4.78 (d, J = 2.5 Hz, 2H), 2.56 (t, J = 2.4 Hz, 1H). Characterization data are consistent with literature.[32]

4-(2-Propyn-1-yloxy)phenylboronic acid (3f)
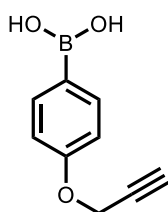
Compound **3f** was prepared according to **GP1** using 200 mg (1.450 mmol) of 4-hydroxyphenylboronic acid. The reaction was complete after 16 h. After workup, the product was collected as a light brown crystalline solid (199 mg, 78%). ^{1}H NMR (500 MHz, CDCl₃) δ 8.18 (d, J = 8.7 Hz, 2H), 7.09 (d, J = 8.7 Hz, 2H), 4.78 (d, J = 2.4 Hz, 2H), 2.56 (t, J = 2.4 Hz, 1H). ^{13}C NMR (126 MHz, CDCl₃) δ 161.16, 137.47, 123.08, 114.38, 78.24, 75.77, 55.63. ^{11}B NMR (160 MHz, CDCl₃) δ 29.27. Molecular ion was not found when analyzed by mass spectrometry.

4-(2-Propyn-1-yloxy)benzonitrile (**3g**)

Compound **3g** was prepared according to **GP1** with 300 mg (2.518 mmol) of 4-hydroxybenzonitrile. The reaction was complete after 2 h. The product was recovered as a tan solid (358 mg, 90%). ^{1}H NMR (500 MHz, CDCl$_3$) δ 7.61 (d, J = 8.9 Hz, 2H), 7.04 (d, J = 8.9 Hz, 2H), 4.75 (d, J = 2.4 Hz, 2H), 2.56 (t, J = 2.4 Hz, 1H).). Characterization data are consistent with literature.[33]

5′-(4-Phenoxymethyl-1H-1,2,3-triazol-1-yl)-5′-deoxythymidine (**3c**)

Compound **4c** was prepared from **3c** according to **GP2** with 147 mg (0.550 mmol) of 5′-deoxy-5′-azidothymidine. The reaction was complete after 2 h, after which the reaction mixture was adsorbed directly onto Celite®, dry-loaded onto a silica column and purified by flash chromatography (0-10% MeOH in DCM). The product was recovered as a light brown solid (163 mg, 73%). ^{1}H NMR (500 MHz, d_6-DMSO) δ 11.29 (s, 1H), 8.19 (s, 1H), 7.35 (s, 1H), 7.29 (t, J = 8.0 Hz, 2H), 7.02 (d, J = 8.0 Hz, 2H), 6.94 (t, J = 7.3 Hz, 1H), 6.17 (t, J = 7.0 Hz, 1H), 5.49 (d, J = 4.3 Hz, 1H), 5.13 (s, 2H), 4.73 (dd, J = 4.4, 14.3 Hz, 1H), 4.63 (dd, J = 7.6, 14.3 Hz, 1H), 4.29 (m, 1H), 4.09 (m, 1H), 2.17 (m, 1H), 2.09 (m, 1H), 1.79 (s, 3H). ^{13}C NMR (126 MHz, d_6-DMSO) δ 164.09, 158.47, 150.84, 143.24, 136.49, 129.92, 125.65, 121.27, 115.10, 110.31, 84.51, 84.41, 71.22, 61.37, 51.68, 38.31, 12.49. HRMS: APCI+ Calculated: 400.1615, found: 400.1622.

5′-(4-((3-Formylphenoxy)methyl)-1H-1,2,3-triazol-1-yl)-5′-deoxythymidine (**4d**)

Compound **4d** was prepared from **3d** according to **GP2** with 180 mg (0.674 mmol) of 5′-deoxy-5′-azidothymidine. The reaction was complete after 30 min. Following washing steps, the product was recovered as a white solid (234 mg, 54%). ^{1}H NMR (500 MHz, d_6-DMSO) δ 11.29 (s, 1H), 9.97 (s, 1H), 8.22 (s, 1H), 7.54 (q, J = 2.9 Hz, 2H), 7.52 (s, 1H), 7.36 (m, J = 3.9 Hz, 2H), 6.16 (t, J = 7.0 Hz, 1H), 5.49 (d, J = 4.4 Hz, 1H), 5.24 (s, 2H), 4.74 (dd, J = 4.4, 14.3 Hz, 1H), 4.64 (dd, J = 7.6, 14.3 Hz, 1H), 4.29 (m, J = 3.3 Hz, 1H), 4.09 (m, J = 3.8 Hz, 1H), 2.17 (m, 1H), 2.09 (m, 1H), 1.79 (s, 3H). ^{13}C NMR (126 MHz,

d_6-DMSO) δ 193.30, 158.98, 142.84, 138.10, 136.49, 130.84, 125.81, 123.08, 121.97, 114.64, 110.31, 84.51, 84.40, 71.23, 61.76, 51.72, 38.33, 12.48. HRMS - ESI+ (m/z) calc'd for $C_{20}H_{21}N_5NaO_6$: 450.1384; found 450.1397.

5′-(4-((4-Formylphenoxy)methyl)-1H-1,2,3-triazol-1-yl)-5′-deoxythymidine (4e)
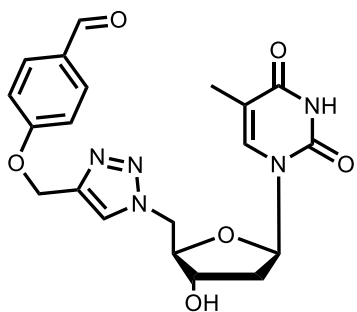
Compound **4e** was prepared from **3e** according to **GP2** with 180 mg (0.674 mmol) of 5′-deoxy-5′-azidothymidine. The reaction was complete after 5 h. After washing steps, the product was recovered as a white solid (370 mg, 86%). ^{1}H NMR (500 MHz, d_6-DMSO) δ 11.33 (s, 1H), 9.87 (s, 1H), 8.25 (s, 1H), 7.87 (d, J = 8.7 Hz, 2H), 7.36 (s, 1H), 7.23 (d, J = 8.7 Hz, 2H), 6.17 (t, J = 7.0 Hz, 1H), 5.52 (d, J = 4.3 Hz, 1H), 5.27 (s, 2H), 4.74 (dd, J = 4.3, 14.3 Hz, 1H), 4.64 (dd, J = 7.7, 14.3 Hz, 1H), 4.29 (q, J = 3.2 Hz, 1H), 4.09 (q, J = 3.8 Hz, 1H), 2.18 (m, 1H), 2.09 (m, 1H), 1.79 (s, 3H). ^{13}C NMR (126 MHz, d_6-DMSO) δ 191.78, 164.10, 163.37, 150.84, 142.51, 136.53, 132.22, 130.29, 126.01, 115.62, 110.33, 84.48, 84.38, 71.20, 61.82, 51.73, 38.28, 12.52. HRMS - ESI+ (m/z) calc'd for $C_{20}H_{21}N_5NaO_6$: 450.1384; found 450.1392.

5′-(4-((4-Boronophenoxy)methyl)-1H-1,2,3-triazol-1-yl)-5′-deoxythymidine (4f)
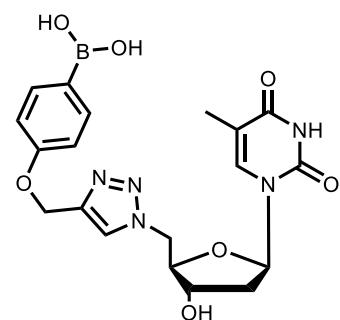
Compound **4f** was prepared from **3f** according to **GP2** with 131 mg (0.490 mmol) of 5′-deoxy-5′-azidothymidine. The reaction was complete after 5 h. After washing steps, the product was stirred overnight in DCM, filtered, and collected as a light brown solid (217 mg, 95%). ^{1}H NMR (500 MHz, d_6-DMSO) δ 11.29 (s, 1H), 8.21 (s, 1H), 7.82 (s, 2H), 7.73 (d, J = 8.2 Hz, 2H), 7.35 (s, 1H), 6.98 (d, J = 8.2 Hz, 2H), 6.17 (t, J = 6.9 Hz, 1H), 5.49 (d, J = 3.9 Hz, 1H), 5.14 (s, 2H), 4.73 (dd, J = 4.2, 14.2 Hz, 1H), 4.64 (dd, J = 7.6, 14.2 Hz, 1H), 4.29 (m, 1H), 4.09 (m, 1H), 2.18 (m, 1H), 2.10 (m, 1H), 1.79 (s, 3H). ^{13}C NMR (126 MHz, d_6-DMSO) δ 164.09, 160.18, 150.85, 143.33 (determined by 2D data), 136.51, 136.27, 126.46 (determined by 2D spectra), 125.73, 114.07, 110.32, 84.53, 84.41, 71.23, 61.22, 51.72, 38.32, 12.49. ^{11}B NMR (160 MHz, d_6-DMSO) δ 30.28. Molecular ion was not found for this compound when analyzed by mass spectrometry.

5′-(4-((4-Cyanophenoxy)methyl)-1H-1,2,3-triazol-1-yl)-5′-deoxythymidine (4g)
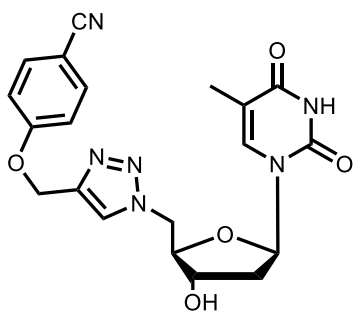
Compound **4g** was prepared from **3g** according to **GP2** with 100 mg (0.374 mmol) 5′-deoxy-5′-azidothymidine. The reaction mixture was stirred at 30 °C for 6 days. Following full conversion, the reaction mixture was diluted in water (~15 mL) and extracted 3x with equal volumes of 2-Me-THF. The organic phases were combined, dried with MgSO$_4$, filtered, and evaporated to give a white solid. The solid was suspended in DCM (~10 mL), filtered, and collected to give the product (116 mg, 73%). ^{1}H NMR (500 MHz, d_6-DMSO) δ 11.31 (s, 1H), 8.25 (s, 1H), 7.79 (d, J = 8.8 Hz, 2H), 7.36 (s, 1H), 7.23 (d, J = 8.9 Hz, 2H), 6.18 (t, J = 7.0 Hz, 1H), 5.51 (d, J = 4.3 Hz, 1H), 5.26 (s, 2H), 4.75 (dd, J = 4.3, 14.3 Hz, 1H), 4.65 (dd, J = 7.6, 14.3 Hz, 1H), 4.30 (q, J = 3.4 Hz, 1H), 4.10 (m, J = 3.9 Hz, 1H), 2.20 (m, 1H), 2.11 (m, 1H), 1.80 (s, 3H). ^{13}C NMR (126 MHz, d_6-DMSO) δ 164.08, 161.92, 150.84, 142.39, 136.53, 134.62, 126.01, 119.50, 116.26, 110.31, 103.61, 84.54, 84.38, 71.22, 61.86, 51.74, 38.31, 12.49. HRMS - APCI+ (m/z) calc'd for C$_{20}$H$_{21}$N$_6$O$_5$: 425.1568; found 425.1578.

5′-(4-(2-Cyanoethyl)-1H-1,2,3-triazol-1-yl)-5′-deoxythymidine (7)
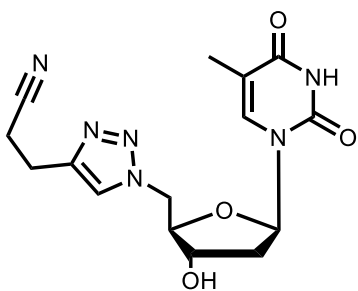
Compound **7** was prepared from 4-pentynenitrile according to **GP2** with 100 mg (0.374 mmol) of 5′-deoxy-5′-azidothymidine. The reaction was complete after 4.5 h. Following washing steps, the material was further purified by column chromatography (0-10% MeOH in DCM) to give the product as a white solid (47 mg, 36%). ^{1}H NMR (500 MHz, d_6-DMSO) δ 11.29 (s, 1H), 7.96 (s, 1H), 7.35 (s, 1H), 6.16 (t, J = 7.0 Hz, 1H), 5.48 (d, J = 4.0 Hz, 1H), 4.70 (dd, J = 4.3, 14.3 Hz, 1H), 4.60 (dd, J = 7.4, 14.4 Hz, 1H), 4.27 (m, 1H), 4.05 (m, 1H), 2.95 (t, J = 7.1 Hz, 2H), 2.83 (t, J = 7.1 Hz, 2H), 2.16 (m, 1H), 2.09 (m, 1H), 1.80 (s, 3H). ^{13}C NMR (126 MHz, d_6-DMSO) δ 164.09, 150.84, 144.47, 136.53, 123.67, 120.54, 110.28, 84.46 (2 overlapping C signals), 71.16, 51.60, 38.34, 21.71, 16.92, 12.50. HRMS - APCI+ (m/z) calc'd for C$_{15}$H$_{19}$N$_6$O$_4$: 347.1462; found 347.1457.

2-Bromo-5-(2-propyn-1-yloxy)benzonitrile (**3h**).
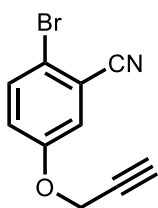
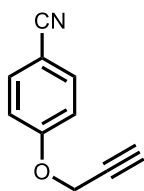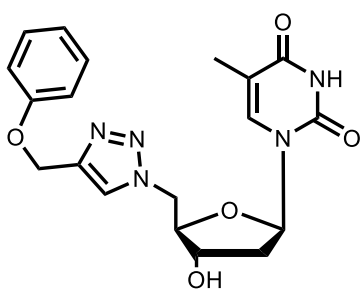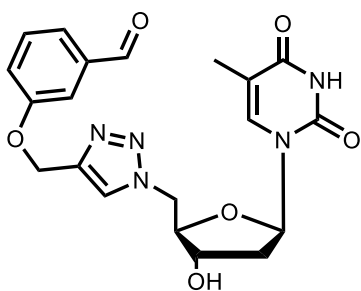Compound **3h** was prepared according to **GP1** with 200 mg (1.010 mmol) of 2-bromo-5-hydroxybenzonitrile. The reaction was complete after 3 h. After workup, purification by flash chromatography (9:1 hexane / ethyl acetate) was performed. The product was recovered as a white solid (172 mg, 72%). ^{1}H NMR (500 MHz, CDCl$_3$) δ 7.57 (d, J = 9.0 Hz, 1H), 7.26 (d, J = 2.6 Hz, 1H), 7.09 (dd, J = 3.0, 9.0 Hz, 1H), 4.71 (d, J = 2.4 Hz, 2H), 2.57 (t, J = 2.4 Hz, 1H). ^{13}C NMR (126 MHz, CDCl$_3$) δ 156.50, 134.05, 121.67, 120.13, 116.89, 116.71, 116.36, 76.92, 56.34. HRMS - APCI+ (m/z) calc'd for C$_7$H$_{10}$BrNO: 235.9706; found 235.9706.

5′-(4-((4-Bromo-3-cyanophenoxy)methyl)-1H-1,2,3-triazol-1-yl)-5′-deoxythymidine (**4h**)
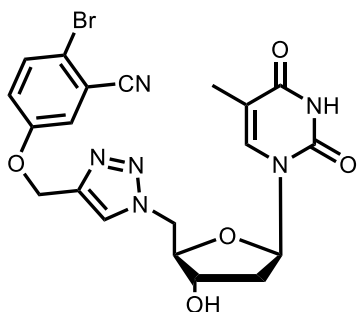
Compound **4h** was prepared from **3h** according to **GP2** with 155 mg (0.578 mmol) of 5′-deoxy-5′-azidothymidine. The reaction was complete after 1 hour. Following washing, the product was collected as a light yellow solid (150 mg, 51%). ^{1}H NMR (500 MHz, d_6-DMSO) δ 11.29 (s, 1H), 8.23 (s, 1H), 7.75 (d, J = 9.0 Hz, 1H), 7.70 (d, J = 2.9 Hz, 1H), 7.34 (s, 1H), 7.32 (dd, J = 3.0, 9.0 Hz, 1H), 6.17 (t, J = 6.9 Hz, 1H), 5.50 (d, J = 4.3 Hz, 1H), 5.22 (s, 2H), 4.74 (dd, J = 4.2, 14.2 Hz, 1H), 4.64 (dd, J = 7.6, 14.3 Hz, 1H), 4.29 (q, J = 3.2 Hz, 1H), 4.08 (m, J = 3.8 Hz, 1H), 2.18 (m, 1H), 2.10 (m, 1H), 1.79 (s, 3H). ^{13}C NMR (126 MHz, d_6-DMSO) δ 164.10, 157.79, 150.84, 142.27, 136.49, 134.55, 126.05, 122.94, 120.87, 117.49, 115.57, 115.43, 110.32, 84.53, 84.38, 71.23, 62.20, 51.75, 38.34, 12.50. HRMS - APCI+ (m/z) calc'd for C$_{20}$H$_{20}$BrN$_6$O$_5$: 503.0673; found 503.0687.

5′-(4-((3-Cyanophenoxy)methyl)-1H-1,2,3-triazol-1-yl)-5′-deoxythymidine (**8**)
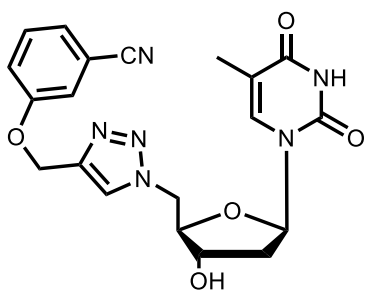
Compound **4h** (100 mg, 0.199 mmol), bis(pinacolato)diboron (151 mg, 0.596 mmol), potassium acetate (58 mg, 0.596 mmol), tris(dibenzylideneacetone)dipalladium(0) (2 mg, 0.002 mmol) and XPhos (4 mg, 0.008 mmol) were stirred under vacuum for 5 min, purged with nitrogen, then dissolved in

dioxane (1.5 mL) and stirred at 100 °C. After 48 h, the temperature was reduced to 23 °C and stirred for another 48 h until the starting material was consumed by TLC analysis (10% MeOH, 45% hexane, 45% DCM). The reaction mixture was diluted in water (~20 mL) and washed twice with an equal volume of 2-Me-THF. The organic phases were combined, dried with $MgSO_4$, filtered, and evaporated. The organic residue was adsorbed onto Celite®, dry-loaded onto a silica column and purified by flash chromatography (0-5% MeOH in DCM/Hexane (1:1)). The product was collected as a white solid. Although the reaction was conducted with the intent to install a BPin group, NMR analysis revealed the protodeborylated product (36 mg, 43%). ^{1}H NMR (500 MHz, d_6-DMSO) δ 11.29 (s, 1H), 8.23 (s, 1H), 7.55 (d, J = 1.4 Hz, 1H), 7.49 (t, J = 8.0 Hz, 1H), 7.41 (d, J = 7.6 Hz, 1H), 7.37 (dd, J = 2.5, 8.4 Hz, 1H), 7.35 (s, 1H), 6.17 (t, J = 7.0 Hz, 1H), 5.50 (d, J = 4.3 Hz, 1H), 5.22 (s, 2H), 4.74 (dd, J = 4.4, 14.3 Hz, 1H), 4.64 (dd, J = 7.7, 14.3 Hz, 1H), 4.29 (q, J = 3.2 Hz, 1H), 4.09 (m, J = 3.9 Hz, 1H), 2.18 (m, 1H), 2.10 (m, 1H), 1.79 (s, 3H). ^{13}C NMR (126 MHz, d_6-DMSO) δ 164.09, 150.84, 142.55, 139.28, 136.50, 131.29, 125.95, 125.27, 121.04, 119.06, 118.10, 112.68, 110.32, 84.53, 84.40, 71.23, 61.86, 51.74, 38.33, 12.49. HRMS - APCI+ (m/z) calc'd for $C_{20}H_{21}N_6O_5$: 425.1568; found 425.1570.

1-Bromo-4-(2-propynyloxy)benzene (3i)
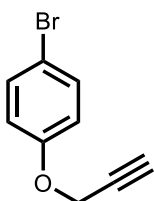
Compound **3i** was prepared according to **GP1** with 432 mg (2.500 mmol) of 1-bromo-4-hydroxybenzene. The reaction was complete after 96 h. The product was recovered as a yellow oil (368 mg, 70%). ^{1}H NMR (500 MHz, CDCl₃) δ 7.40 (td, J = 2.7, 10.3 Hz, 2H), 6.87 (td, J = 2.8, 10.1 Hz, 2H), 4.67 (d, J = 2.4 Hz, 2H), 2.52 (t, J = 2.4 Hz, 1H). Characterization data are consistent with literature.[32]

## 5′-(4-((4-Bromophenoxy)methyl)-1H-1,2,3-triazol-1-yl)-5′-deoxythymidine (4i)
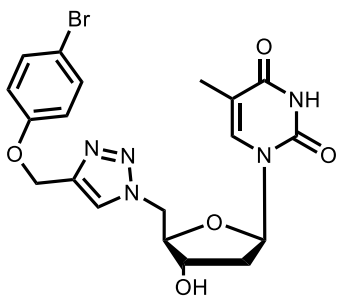
Compound **4i** was prepared from **3i** following **GP2** with 334 mg (1.250 mmol) of 5′-deoxy-5′-azidothymidine. The reaction was complete after 10 min. Following washing steps, the product was recovered as a solid (537 mg, 90%). ^{1}H NMR (500 MHz, d_6-DMSO) δ 11.29 (s, 1H), 8.20 (s, 1H), 7.45 (d, J = 8.9 Hz, 2H), 7.34 (s, 1H), 7.01 (d, J = 8.9 Hz, 2H), 6.17 (t, J

= 7.0 Hz, 1H), 5.49 (d, J = 4.3 Hz, 1H), 5.13 (s, 2H), 4.73 (dd, J = 4.4, 14.3 Hz, 1H), 4.63 (dd, J = 7.6, 14.3 Hz, 1H), 4.28 (q, J = 3.3 Hz, 1H), 4.08 (m, J = 3.9 Hz, 1H), 2.17 (m, 1H), 2.10 (m, 1H), 1.79 (s, 3H). ^{13}C NMR (126 MHz, d_6-DMSO) δ 163.58, 157.26, 150.33, 142.35, 135.99, 132.06, 125.28, 116.99, 112.22, 109.80, 84.01, 83.88, 70.71, 61.21, 51.20, 37.81, 11.99. HRMS - APCI+ (m/z) calc'd for $C_{19}H_{20}BrN_5O_5$: 478.0721; found 478.0706.

5′-(4-((4-(Pinacolborono)phenoxy)methyl)-1H-1,2,3-triazol-1-yl)-5′-deoxythymidine (9)
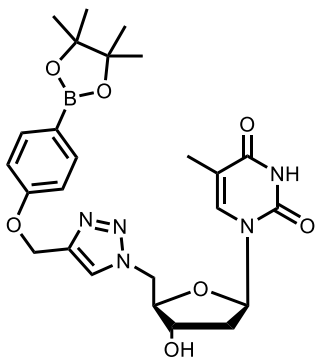
Compound **4i** (86 mg, 0.180 mmol), bis(pinacolato)diboron (137 mg, 0.540 mmol), potassium acetate (53 mg, 0.540 mmol), tris(dibenzylideneacetone)dipalladium(0) (1.6 mg, 0.002 mmol) and XPhos (3.3 mg, 0.007 mmol) were stirred under vacuum for 5 min, purged with nitrogen, then dissolved in dioxane (1.25 mL) and stirred at 100 °C. The reaction was complete after 1 hour by TLC analysis (10% MeOH, 45% hexane, 45% DCM), and was diluted in MeOH (5 mL) and filtered through Celite®. The resulting solution was adsorbed onto Celite®, dry-loaded onto a silica column, and purified by flash chromatography (0-10% MeOH in DCM/Hexane (1:1)). The product was collected as an off-white solid (72 mg, 76%). ^{1}H NMR (500 MHz, d_6-DMSO) δ 11.28 (s, 1H), 8.21 (s, 1H), 7.60 (d, J = 8.5 Hz, 2H), 7.34 (s, 1H), 7.02 (d, J = 8.5 Hz, 2H), 6.17 (t, J = 7.0 Hz, 1H), 5.51 (br. s, 1H), 5.17 (s, 2H), 4.73 (dd, J = 4.4, 14.3 Hz, 1H), 4.63 (dd, J = 7.5, 14.3 Hz, 1H), 4.28 (m, J = 3.3 Hz, 1H), 4.09 (m, J = 3.9 Hz, 1H), 2.16 (m, 1H), 2.09 (m, 1H), 1.79 (s, 3H), 1.28 (s, 12H).

5′-(4-Benzoyl-1H-1,2,3-triazol-1-yl)-5′-deoxythymidine (10a)
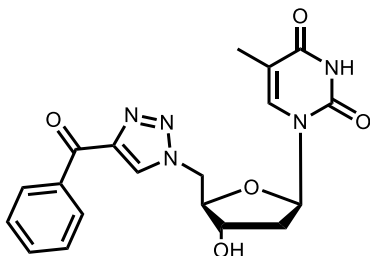
Compound **10a** was prepared from 1-phenylprop-2-yn-1-one according to **GP2** with 120 mg (0.449 mmol) 5′-deoxy-5′-azidothymidine. Upon completion by TLC analysis, the reaction mixture was evaporated in vacuo, redissolved in H$_2$O (20 mL) and extracted with 2-Me-THF (3x20 mL). The organic phases were combined, dried with MgSO$_4$, filtered, and evaporated in vacuo. The residue was adsorbed onto Celite®, dry-loaded onto a silica column, and purified by flash chromatography (50 mL hexane, then 0-10% MeOH in DCM). The product was

recovered as a white solid (135 mg, 76%). ^{1}H NMR (500 MHz, d_6-DMSO) δ 11.30 (s, 1H), 8.85 (s, 1H), 8.23 (d, J = 7.2 Hz, 2H), 7.70 (t, J = 7.4 Hz, 1H), 7.58 (t, J = 7.7 Hz, 2H), 7.33 (s, 1H), 6.18 (t, J = 7.0 Hz, 1H), 5.52 (d, J = 4.1 Hz, 1H), 4.84 (dd, J = 4.7, 14.2 Hz, 1H), 4.76 (dd, J = 7.2, 14.2 Hz, 1H), 4.32 (q, J = 3.4 Hz, 1H), 4.17 (m, 1H), 2.23 (m, 1H), 2.12 (m, 1H), 1.74 (s, 3H). ^{13}C NMR (126 MHz, d_6-DMSO) δ 184.96, 163.54, 150.35, 146.40, 136.52, 135.99, 133.20, 130.64, 129.80, 128.47, 109.81, 84.01, 83.44, 70.59, 51.27, 37.70, 11.94. HRMS - APCI+ (m/z) calc'd for $C_{19}H_{20}N_5O_5$: 398.1495; found 398.1467.

1-(2-Bromophenyl)-prop-2-yn-1-ol (**11**)
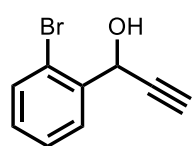
To an oven-dried, sealed flask purged with nitrogen was added ethynylmagnesium bromide solution (0.5 M in THF; 9 mL/4.5 mmol). The solution was stirred on ice for 5 min, following which, 2′-bromobenzaldehyde (350 μL, 3 mmol) was added to the THF solution dropwise. The starting material was consumed after 10 min by TLC analysis (3:1 hexane : ethyl acetate). The reaction mixture was quenched with 20 mL of 1M aqueous ammonium chloride, then extracted with 20 mL EtOAc. The organic phase was washed twice with brine, dried with MgSO₄, filtered, and evaporated in vacuo to give the product as a yellow oil (592 mg, 93%). ^{1}H NMR (500 MHz, CDCl₃) δ 7.79 (dd, J = 1.6, 7.8 Hz, 1H), 7.58 (dd, J = 1.0, 8.0 Hz, 1H), 7.37 (td, J = 11.3, 0.9 Hz, 1H), 7.20 (td, J = 1.6, 11.5 Hz, 1H), 5.81 (dd, J = 2.2, 5.4 Hz, 1H), 2.67 (d, J = 2.3 Hz, 1H), 2.47 (d, J = 5.5 Hz, 1H). Characterization data are consistent with literature.[67]

1-(2-Bromophenyl)prop-2-yn-1-one (**12**)
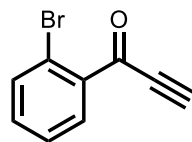
Compound **11** (590 mg, 2.795 mmol) and Dess-Martin periodinane (1541 mg, 3.634 mmol) were dissolved in dichloromethane (10 mL) and stirred at 23 °C. The reaction was complete after 5 min by TLC analysis (3:1 hexane : ethyl acetate). The reaction mixture was washed with water (3x10 mL), then the organic phase was dried with MgSO₄ and evaporated to dryness. The crude material was adsorbed onto silica, then the silica was washed with hexane (50 mL) and the product eluted (3:1 hexane : ethyl acetate, 50 mL). The solution containing product was evaporated in vacuo to give an orange crystalline solid (458 mg, 78%). ^{1}H NMR (500 MHz, CDCl₃) δ

8.11 (dd, J = 1.8, 7.7 Hz, 1H), 7.70 (dd, J = 1.1, 7.9 Hz, 1H), 7.45 (td, J = 1.3, 7.5 Hz, 1H), 7.39 (td, J = 1.8, 7.6 Hz, 1H), 3.47 (s, 1H). Characterization data are consistent with literature.[67]

5′-(4-((2-Bromophenyl)oxomethyl)-1H-1,2,3-triazol-1-yl)-5′-deoxythymidine (13)
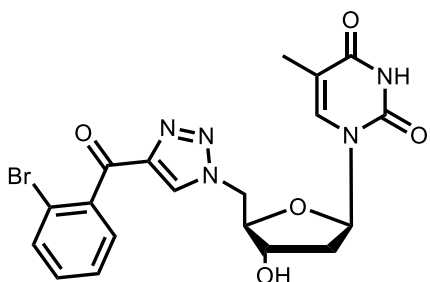
Compound **13** was prepared from **12** according to **GP2** with 300 mg (1.123 mmol) 5′-deoxy-5′-azidothymidine. The reaction was complete after 2 h by TLC analysis. Following washing with H_2O, the organic material was dissolved in MeOH, adsorbed onto Celite®, dry-loaded onto a column, and purified by flash chromatography (0-10% MeOH in DCM/Hexane (1:1)). The product was collected as a yellow foam (404 mg, 75%). ^{1}H NMR (500 MHz, d_6-DMSO) δ 11.30 (s, 1H), 8.83 (s, 1H), 7.75 (dd, J = 7.7, 1.1 Hz, 1H), 7.52 (m, 3H), 7.37 (d, J = 1.1 Hz, 1H), 6.17 (t, J = 7.0 Hz, 1H), 5.51 (s, 1H), 4.81 (dd, J = 4.5, 14.2 Hz, 2H), 4.72 (dd, J = 7.6, 14.2 Hz, 1H), 4.30 (s, 1H), 4.15 (m, J = 3.9 Hz, 1H), 2.21 (m, 2H), 2.11 (m, 2H), 1.77 (d, J = 0.7 Hz, 3H). ^{13}C NMR (126 MHz, d_6-DMSO) δ 187.00, 163.56, 150.34, 145.77, 139.81, 136.02, 132.94, 132.00, 130.36, 129.41, 127.48, 118.55, 109.82, 84.10, 83.45, 70.67, 51.47, 37.71, 11.97. HRMS was not acquired for this compound.

1,4-Bis(1-(5′-deoxy-5′-thymidyl)-1H-1,2,3-triazol-4-yl)benzene (14a)
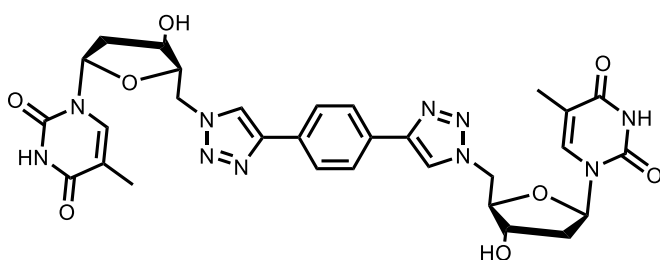
1,4-Diethynylbenzene (43 mg, 0.340 mmol) and 5′-deoxy-5′-azidothymidine (200 mg, 0.748 mmol) were stirred in THF (4 mL) at 50 °C until both reagents were dissolved. Copper sulfate pentahydrate (85 mg, 0.340 mmol) and ascorbic acid (66 mg, 0.374 mmol) were dissolved in water (1.5 mL) and added to the THF solution. The reaction mixture was sealed with a septum, purged with N_2, and stirred under nitrogen atmosphere. The reaction was complete by TLC analysis (3:1 hexanes : ethyl acetate) and the produced significant precipitation. The solid was collected by filtration, washed with water (~20 mL) followed by MeOH (~20 mL) and dried to give the product as a light orange solid (216 mg,

96%). ^{1}H NMR (500 MHz, d_6-DMSO) δ 11.01 (s, 2H), 8.60 (s, 2H), 7.92 (s, 4H), 7.24 (d, J = 1.2 Hz, 2H), 6.19 (t, J = 6.9 Hz, 2H), 5.53 (d, J = 4.4 Hz, 2H), 4.77 (dd, J = 4.6, 14.4 Hz, 2H), 4.69 (dd, J = 6.6, 14.4 Hz, 2H), 4.32 (m, 2H), 4.13 (m, 2H), 2.18 (m, 2H), 2.13 (m, 2H), 1.69 (d, J = 1.0 Hz, 6H). ^{13}C NMR (126 MHz, d_6-DMSO) δ 164.04, 150.85, 146.52, 136.42, 130.52, 126.06, 122.76, 110.29, 84.31, 84.19, 71.00, 51.58, 38.36, 12.44. HRMS – ESI- (m/z) calc'd for $C_{30}H_{31}N_{10}O_8$: 659.2332; found 659.2327.

1,4-Bis(2-propyn-1-yloxy)benzene (3j)
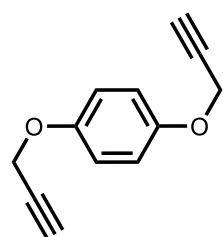
1,4-Dihydroxybenzene (200 mg, 1.816 mmol) and potassium carbonate (1004 mg, 7.264 mmol) were stirred in DMF (2 mL), then propargyl bromide (80% w/w in toluene; 607 μL, 5.449 mmol) was added to the solution. The reaction was complete after 4 h by TLC analysis (3:1 hexane: ethyl acetate), and the solvent was removed in vacuo. The crude material was dissolved in ethyl acetate (20 mL) and washed with H_2O (3x20 mL). The organic material was adsorbed onto silica and the product eluted with a solution of 25% EtOAc in hexane. The product was collected after evaporation as a pale yellow oil (248 mg, 73%). ^{1}H NMR (500 MHz, CDCl$_3$) δ 6.93 (s, 4H), 4.65 (d, J = 2.4 Hz, 4H), 2.51 (t, J = 2.4 Hz, 2H). Characterization data are consistent with literature.[68]

1,4-Bis((1-(5′-deoxy-5′-thymidyl)-1H-1,2,3-triazol-4-yl)methoxy)benzene (14b)
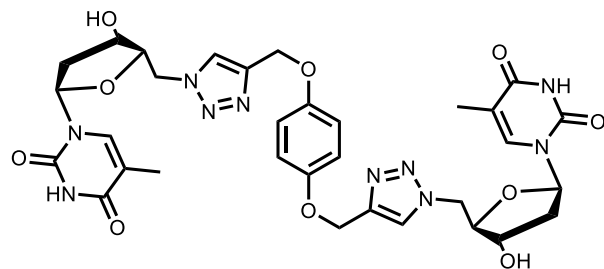
3j (93 mg, 0.500 mmol) and 5′-deoxy-5′-azidothymidine (294 mg, 1.100 mmol) were stirred in THF (6 mL) at 50 °C until both reagents were dissolved. Copper sulfate pentahydrate (125 mg, 0.501 mmol) and ascorbic acid (97 mg, 0.551 mmol) were dissolved in water (2 mL) and then the aqueous solution was added to the THF solution. The reaction was complete after 1 hour by TLC analysis (3:1 EtOAc/hexane). The solution was diluted in H_2O (5 mL). The precipitate was collected by filtration and washed with water (10 mL), then dried under vacuum to give the product as a white solid (144 mg, 40%). ^{1}H NMR (500 MHz, d_6-DMSO) δ 11.29 (s, 2H), 8.17 (s, 2H), 7.34 (s, 2H), 6.94 (s, 4H), 6.17 (t, J = 7.0 Hz, 2H), 5.50 (d, J = 4.3 Hz, 2H), 5.06 (s, 4H), 4.73 (dd, J = 4.4, 14.3 Hz, 2H), 4.63 (dd, J = 7.5,

14.3 Hz, 2H), 4.28 (m, 2H), 4.09 (m, 2H), 2.17 (m, 2H), 2.10 (m, 2H), 1.79 (s, 6H). ^{13}C and HRMS not available for this compound due to lab closures as a result of the COVID-19 pandemic.

(5aR,6S,6aS)-rel-1,4,5,5a,6,6a,7,8-Octahydro-1-(5′-deoxy-5′-thymidyl)cyclopropa[5,6]cycloocta[1,2-d]-1,2,3-triazole-6-methanol (15)
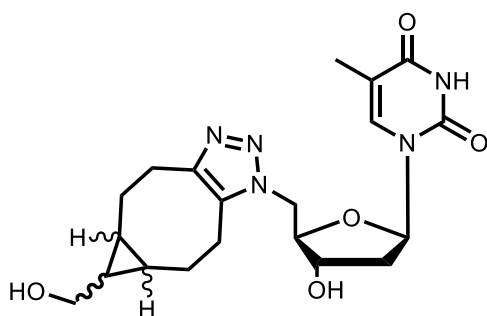
5′-Deoxy-5′-azidothymidine (50 mg, 0.187 mmol) and (1R,8S,9S)-Bicyclo[6.1.0]non-4-yn-9-ylmethanol (34 mg, 0.224 mmol) were dissolved in acetonitrile (1.5 mL) and water (0.5 mL). The reaction was stirred at 40 °C for 24 h, after which the reaction mixture was adsorbed directly onto Celite®, dry-loaded onto a silica column, and purified by flash chromatography (0-10% MeOH in DCM). The product was recovered as a clear residue, and lyophilized to give a white, amorphous solid (45 mg, 57%). 2 diastereomers, 1:1 molar ratio by ^{1}H NMR integration. ^{1}H NMR (500 MHz, d_6-DMSO) δ 11.29 (s, 2H), 7.34 (s, 1H), 7.27 (s, 1H), 6.14 (app. td, J = 2.6, 10.2 Hz, 2H), 5.76 (s, 2H), 5.47 (app. dd, J = 3.0, 4.3 Hz, 2H), 4.59 (app. td, J = 5.3, 14.7 Hz, 2H), 4.50 (app. ddd, J = 2.7, 6.9, 14.7 Hz, 2H), 4.33 (m, 2H), 4.27 (app. q, J = 5.3 Hz, 2H), 4.08 (q, J = 5.3 Hz, 1H), 4.02 (s, 1H), 3.99 (m, 2H), 3.45 (app. q, J = 4.2 Hz, 1H), 3.18 (app. d, J = 5.3 Hz, 3H), 2.93 (m, 4H), 2.72 (m, 2H), 2.66 (m, 3H), 2.27 (m, 2H), 2.07 (m, 7H), 1.79 (app. d, 4.5 Hz, 6H) 1.49 (m, 5H), 0.96 (m, 2H), 0.79 (m, 4H). ^{13}C NMR (126 MHz, d_6-DMSO) δ 164.07, 154.35, 150.87, 143.94, 143.85, 136.51, 134.55, 129.03, 128.86, 110.15, 98.90, 98.84, 84.79, 84.67, 84.27, 71.06, 57.77, 49.08, 49.04, 38.13, 26.00, 25.95, 22.92, 22.40, 22.28, 21.76, 21.63, 21.15, 19.31, 19.26, 18.90, 18.65, 12.47. HRMS – ESI+ (m/z) calc'd for $C_{20}H_{27}N_5NaO_5$: 440.1904; found 440.1898.

Phenoxyacetic acid (16)
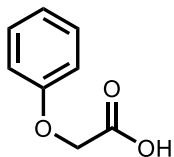
Phenol (500 mg, 5.313 mmol) and potassium carbonate (2.2g, 15.939 mmol) were dissolved in DMF (4 mL). To this solution was added ethyl bromoacetate (648 μL, 5.844 mmol), and the mixture was stirred at 75 °C. The reaction was complete after 1.5 h by TLC analysis, upon which the reaction mixture

was filtered. The filtrate was stirred in 3 mL EtOH and 3 mL 7% aqueous KOH. Upon full hydrolysis of the ester by TLC analysis, the ethanol was removed in vacuo, then 2M HCl was added to the remaining aqueous solution dropwise until white crystals formed. Crystals were collected by filtration to give the product (215 mg, 22%). ^{1}H NMR (500 MHz, CDCl$_3$) δ 7.32 (t, J = 8.0 Hz, 2H), 7.03 (t, J = 7.4 Hz, 1H), 6.93 (d, J = 7.9 Hz, 2H), 4.69 (s, 2H). Characterization data are consistent with literature.[69]

5′-Deoxy-5′-aminothymidine (17)
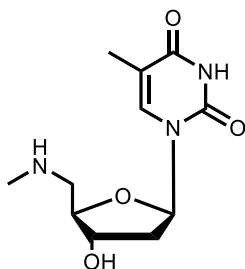
5′-O-(p-Toluenesufonyl)thymidine (300 mg) was dissolved in a solution of methylamine (33% in EtOH). The reaction mixture was purged with N$_2$ and stirred, covered from light, for 48 h. The reaction was monitored by TLC (9:1 dioxane : NH$_4$OH), and upon completion, the solvent was removed in vacuo. The residue was dissolved in 5 mL H$_2$O, filtered, and purified by column chromatography using an H$^+$-charged Dowex-80 ion exchange resin (eluent = 0-20% NH$_4$OH in H$_2$O). Fractions containing product were concentrated in vacuo, then lyophilized to give **17** as a fluffy, light yellow amorphous solid (125 mg, 86%). Characterization data are consistent with literature.[53]

5′-(N-(Phenoxyacetyl)-N-methylamino)-5′-deoxy-thymidine (18)
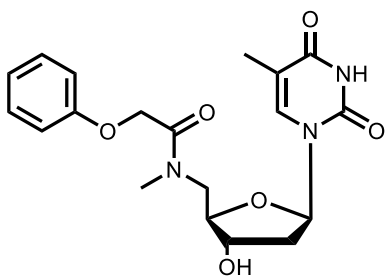
A solution of phenoxyacetic acid (88 mg, 0.490 mmol), 2-(1H-benzotriazole-1-yl)-1,1,3,3-tetramethylaminium tetrafluoroborate (TBTU) (200 mg, 0.627 mmol) and diisopropylethylamine (DIPEA) (239 μL, 1.372 mmol) in 2-MeTHF (3 mL) and DMF (0.5 mL) was stirred at 23 °C for 45 min, after which 5′-deoxy-5′-methylaminothymidine (100 mg, 0.392 mmol) was added. The reaction was complete by TLC analysis 3.5 h after addition of 5′-deoxy-5′-aminothymidine, following which the reaction mixture was poured into brine (20 mL) and extracted with 2-MeTHF (3 × 20 mL). The organic layers were combined, dried with MgSO$_4$, filtered, and evaporated. The residue was adsorbed onto Celite®, dry-loaded onto a silica column, and purified by flash chromatography (0-10% MeOH in DCM) to give the product as a tan solid (38 mg, 25%).

5.2. Procedure for Conducting WaterLOGSY Experiments

5.2.1. Preparation of NMR Samples

Stock solutions of deuterated Tris buffer (1 M, pH adjusted to 7.5) and $MgCl_2$ (20 mM) were made in distilled, deionized water. A stock solution of the compound to be tested (50 mM) was made in d_6-DMSO. A stock solution of Cps2L (1.44 mM in 50 mM Tris buffer) was previously expressed and isolated (see Section 5.3). NMR samples were prepared by combining stock solutions in an Eppendorf tube along with D_2O, and diluted in distilled, deionized water to 650 µL to the final concentrations: dTris: 100 mM, $MgCl_2$: 2 mM, Cps2L: 0.05 mM; d_6-DMSO: 5% v/v, compound to test: 2.5 mM, and D_2O: 10% v/v. For solutions containing substrates dTTP or G1P, a stock solution of the substrate (50 mM) was also added to a final concentration of 2.5 mM (1 equivalent) or 25 mM (10 equivalents).

5.2.2. Data Acquisition and Processing

Data was acquired using a Bruker 500 MHz NMR spectrometer. A water-suppression ^1H NMR spectrum of each sample was collected (16 scans) followed by a WaterLOGSY spectrum (256 scans, mixing time = 1.5 s). Fourier transformed data was phased such that the dTris residual signal pointed upwards in all spectra, thus defining phased-up peaks as "non-binding" and phased down peaks as "binding".

5.3. Microbiology Procedures

5.3.1. Preparation of Buffers and Solutions

LB media

Bio-tryptone (10 g/L), NaCl (10 g/L), and yeast extract (5g/L) were dissolved in distilled, deionized water. The pH was adjusted to 7.5 with NaOH (1 M) and HCl (1 M). The solution was autoclaved before use.

LB agar

Agar (1.5 g) was dissolved in LB media (100 mL) and autoclaved. The solution was cooled to 50 °C before 50 mg/mL kanamycin solution (100 µL) was added.

Lysis buffer

Glycerol (3 mL), Triton X-100 (1 mL, 10%) and wash buffer (16 mL) were combined in a falcon tube and vortexed.

Wash buffer

NaH_2PO_4 (20 mM), NaCl (300 mM) and imidazole (10 mM) were dissolved in distilled, deionized water. The pH was adjusted to 7.5 with NaOH (1 M) and HCl (1 M).

Elution buffer

NaH_2PO_4 (20 mM), NaCl (300 mM) and imidazole (250 mM) were dissolved in distilled, deionized water. The pH was adjusted to 7.5 with NaOH (1 M) and HCl (1 M).

Resolving buffer

Tris (1.5 M) was dissolved in distilled, deionized water. The pH was adjusted to 8.8 with NaOH (1 M) and HCl (1 M).

Bis-acrylamide

Acrylamide (29 g) and N,N-methylenebisacrylamide (1g) were dissolved in distilled, deionized water (100 mL). The solution was protected from light and stored at 4 °C.

Stacking buffer

Tris (0.5 M) was dissolved in distilled, deionized water. The pH was adjusted to 6.8 using NaOH (1 M) and HCl (1 M).

Tris-HCl

Tris (500 mM) was dissolved in distilled, deionized water. The pH was adjusted to 7.5 using NaOH (1 M) and HCl (1 M). Solutions of Tris-HCl at lower concentrations were diluted from this stock with distilled, deionized water.

Loading dye

Glycerol (2 mL), SDS (6 mL, 10%), stacking buffer (2.5 mL), and aqueous Bromophenol blue (42 μL, 1% w/v) were combined and vortexed. The solution was separated into 100 μL aliquots and frozen. When ready for use, an aliquot was thawed and 2-mercaptoethanol (25 μL per 100 μL dye solution) was added.

SDS running buffer (10X)

SDS (10 g/L), Tris (300 g/L) and glycine (144 g/L) were dissolved in Millipore water. This solution was diluted 10x to make the SDS running buffer (1X) used in gel electrophoresis.

MOPS buffer

MOPS (500 mM) was dissolved in distilled, deionized water. The pH was adjusted to 7.5 using NaOH (1 M) and HCl (1 M). Lower concentrations of MOPS buffer were obtained by diluting this solution in distilled, deionized water.

5.3.2. Overexpression of Cps2L

Cps2L was produced according to a previously reported procedure.[58] A glycerol stock of BL21-DE3 competent *E. coli* harbouring plasmid pSK001 (coding for Cps2L) was grown on LB agar plates containing kanamycin (50 µg/mL) at 37 °C for 18 h. LB_{kan} (LB media containing 50 µg/mL kanamycin, 25 mL) was inoculated with a single culture isolated from the agar plate using a sterile loop, and the culture was grown overnight with shaking (200 rpm) at 37 °C. Then, 3 mL of the small growth solution was added to each of 3 flasks containing 330 mL LB_{kan}. The large growths were incubated at 37 °C with shaking, and monitored by UV-Vis (600 nm) until an optical density (OD) of 0.6-0.8 was observed (approximately 3 h). Then, isopropyl β- D-1-thiogalactopyranoside (IPTG) solution (300 µL, 1 M) was added to each flask (to a final IPTG concentration of 1 mM) to induce production of Cps2L. The growths were incubated with shaking (200 rpm) overnight at 18 °C. The resulting solution was centrifuged (3700 rpm, 1 hour, 4 °C), and the resulting cell pellet collected. The supernatant was discarded.

5.3.3. Cell Lysis

The cell pellet, isolated from the overexpression step, was added to a solution of lysis buffer (20 mL), DNAse (1µg/mL, 20 µL), and lysozyme (10 mg). The mixture was stirred for 30 min at 0 °C, and the resulting lysate sonicated (5 × 5 s, 50% amplitude) using a microprobe sonicator (Autotune High Intensity Ultrasonic Processor, 750 W). The material was centrifuged (13000 rpm, 15 min, 4 °C), and the supernatant collected. 200 µL of the supernatant was set aside for analysis by gel electrophoresis.

5.3.4. Purification of Cps2L

A Hi-trap affinity HP column was primed by washing with 15 mL distilled water, then charged with an aqueous solution of nickel (II) sulfate (0.1 M, 2.5 mL) and washed with distilled water (15 mL). The column was loaded with the supernatant collected from cell lysis, then impurities removed with wash buffer (30 mL). The protein was eluted using a

gradient of 10-100% elution buffer in wash buffer. Fractions were collected and concentrated using a Macrosep Advance centrifugal filtration device (4700*g*, 45 min, 4 °C) and stored at 4 °C.

5.3.5. Preparation of 0.1% SDS-Polyacrylamide Gels (SDS-PAGE) for Protein Electrophoresis

Sodium dodecyl sulfate (SDS) polyacrylamide gels were prepared[c] using a 1 mm cast, resolving gel solution, and stacking gel solution. The resolving gel solution was prepared by combining distilled water (2.8 mL), resolving buffer (3.75 mL), SDS solution (100 µL, 10% w/v), bis-acrylamide solution (3.3 mL, 30% w/v), freshly prepared ammonium persulfate (APS) solution (100 µL, 10% w/v) and tetramethylethylenediamine (TMEDA, 15 µL). Immediately after addition of TMEDA, the solution was stirred briefly, then added to the cast. The gel was covered with a layer of ethanol. The stacking gel solution was prepared by combining distilled water (2.75 mL), stacking buffer (0.47 mL), SDS solution (37.5 µL, 10% w/v), bis-acrylamide solution (0.5 mL, 30% w/v), APS solution (20 µL, 10% w/v), and TMEDA (6 µL). Immediately upon addition of TMEDA, the mixture was stirred, the ethanol drained from the set resolving gel, and the stacking gel added to the cast. A comb was inserted, and the stacking gel allowed to set at room temperature. The compound gel was stored, sealed to contain moisture, at 4 °C.

5.3.6. Analysis of Nickel Column Fractions by SDS-PAGE

Fractions collected from the Nickel affinity chromatography column following addition of elution buffer, as well as the aliquot of cell lysate collected prior to enzyme purification, were analyzed by SDS-PAGE to determine the presence and purity of the desired protein. Samples were prepared in the following way: to a 500 µL Eppendorf tube was added a sample of column fraction (2.5 µL), Tris-HCl buffer (20 µL, 10 mM) and pre-prepared loading dye (5 µL). The tubes were vortexed briefly (a colour change from yellow to blue was observed), then suspended in boiling water for 3 min to promote denaturation of proteins.

---

[c]Acknowledgement to Mr. Brendan McKeown of Dr. Kerry Goralski's research group for help preparing and running SDS-PAGE.

The SDS-PAGE gel was installed in the electrophoresis apparatus, which was filled with SDS-PAGE running buffer (1X). Prepared fraction samples were loaded into the wells of the gel (20 µL each), alongside commercially available prestained standard protein ladder (New England Biolabs, 11-245 kDa). A voltage of 150V was applied for 1 hour, monitored by the progress of the bromophenol blue indicator. The gel was washed with distilled water, and the bands visualized by overnight staining with commercially available EZBlue™ gel staining reagent.

5.3.7. Collection, Dialysis, Analysis, and Storage of Protein-Containing Fractions

Clean fractions, as indicated by a single band in the corresponding lane of the polyacrylamide gel, were combined and concentrated using a Macrosep Advance centrifugal filtration device (4700g, 45 min, 4 °C). The concentrated protein solution was diluted to 15 mL with 25 mM Tris-HCl buffer, then recentrifuged. The process was repeated 3x to replace the phosphate buffer with Tris-HCl buffer. The concentration of Cps2L in Tris-HCl buffer was determined by UV-Vis analysis (280 nm) using a previously determined extinction coefficient of 29300 $M^{-1}cm^{-1}$.[58] The protein solution was separated into 400 µL aliquots and stored at -70 °C. When in use, an aliquot was thawed, stored at 4 °C, and used for up to a month. Aliquots were not refrozen once thawed.

5.3.8. Overexpression, Purification, and Analysis of Human Purine Nucleoside Phosphorylase (hPNP)

The enzyme, hPNP, was obtained following the same general procedure as with Cps2L, but using an extinction coefficient of 29800 $M^{-1}cm^{-1}$ to determine final concentration.[54] The concentrated solution of hPNP contained excess PO_4^{3-}, which interfered with the coupled enzyme assay, and was repurified by nickel affinity column chromatography using wash buffer and elution buffer prepared from Tris-HCl instead of phosphate buffer. After concentration by centrifugation, the concentration of protein was once again determined, then the solution was separated into 400 µL aliquots and stored at -70 °C. When in use, an aliquot was thawed and stored at 4 °C. Aliquots were not refrozen once thawed.

5.3.9. Preparation of Xanthine Oxidase (XO) and Inorganic Pyrophosphatase (IPP)

Microbial XO and recombinant IPP were obtained from Sigma Aldrich. Stock solutions of IPP were made in Millipore water from a lyophilized powder containing buffer salts (1

EU/µL) and were stored in 400 µL aliquots at -30 °C. XO stock solutions (591 µM) were made in 25 mM Tris-HCl from lyophilized powder containing BSA and glutamate as stabilizers, and were stored in 400 µL aliquots at -70 °C. Once thawed, aliquots were stored at 4 °C and used for up to a month after thawing. IPP was diluted to 0.1 EU/µL in 25 mM Tris-HCl before use in the coupled assay.

5.3.10. Dialysis of Enzymes in 3-(N-morpholino)propanesulfonic acid (MOPS) Buffer

Cps2L, IPP, XO and hPNP were dialyzed in MOPS buffer due to the potential interference of Tris-HCl with binding of iminoboronates. A Pur-A-Lyzer™ Maxi Dialysis kit was utilized, with PURX60015 dialysis tubes. The tubes were primed by soaking in distilled water for 5 min, then each tube was loaded with either Cps2L, IPP, XO, or hPNP enzyme solutions in Tris-HCl (approx. 2 mL). The tubes were suspended in stirred MOPS buffer (1 L, 50 mM) for 3 h. Each solution was analyzed by UV-Vis before and after dialysis (280 nm for Cps2L, IPP and hPNP, 450 nm for XO) to ensure no change in concentration had occurred. Each enzyme solution was separated into 400 µL aliquots and stored at -70 °C. When used for enzyme assays, the solutions were stored at 4 °C and used for up to a month after thawing.

5.4. Procedure for Conducting the Coupled Enzyme Assay

5.4.1. General Notes for the UV-vis Assay

Assays were performed in 96-well plates, monitored spectrophotometrically using a SPECTRAmax Plus Microplate Reader spectrometer, with SoftMax Pro version 4.8 software. Measurements were acquired with irradiation of the wells at 290 nm, and data was acquired every 5 s for 300 s. Non-linear regression analysis was performed with Microsoft Excel, using the Solver plugin.

Stock solutions of MgCl$_2$ (500 mM), inosine (20 mM), G1P (20 mM) and buffer (Tris-HCl or MOPS) (500 mM) were prepared from distilled, deionized water (ddH$_2$O). A solution of 70% DMSO in water was also prepared in ddH$_2$O. Solutions of enzymes Cps2L (351 µM), hPNP (163 µM), XO (591 µM), and IPP (0.1 EU/µL) were prepared as described in Chapter 5.3. All solutions were stored at 4 °C.

2′-deoxythymidine-5′-triphosphate (dTTP) stock solution (20 mM) was prepared in ddH$_2$O and the pH adjusted to 7.5. This solution was stored at 4 °C for up to a week. From

this stock solution were prepared dilutions (either 20, 40, 60, 80, 100, 200, 300, 350 μM; or 15, 18, 24, 35, 60, 100, 200, 300 μM) in ddH$_2$O. Fresh dilutions were prepared daily.

5.4.2. Determination of Cps2L Kinetic Parameters With Varying [dTTP]

To an Eppendorf tube was added stock solutions of buffer (Tris-HCl or MOPS) (60 μL), inosine (60 μL), G1P (60 μL), MgCl$_2$ (14 μL), IPP (15 μL), hPNP (7.5 μL), XO (3 μL) 70% DMSO solution (96 μL) and ddH$_2$O (134 μL). The tube was sealed and inverted several times, then 45 μL of this solution was added to each of 8 wells containing 60 μL of dTTP at different dilutions. The resulting solutions were pre-incubated for 5 min. An intermediate, 100-fold dilution of Cps2L stock was made in 25 mM buffer (Tris-HCl or MOPS), then from the intermediate dilution, a further 40-fold dilute solution was made in 25 mM buffer. This solution (4000-fold dilute overall) was added to the 8 wells (15 μL each) using an Eppendorf Repeater M4 Pipette. Immediately upon addition of Cps2L, UV measurements were acquired. The final concentration of each component in each well was as follows: buffer: 25 mM, inosine: 1 mM, G1P: 1 mM, MgCl$_2$: 5.8 mM, IPP: 1.25 EU/mL, hPNP: 1 μM, XO: 1.5 μM, DMSO: 5.6%, dTTP (varied) and Cps2L: 0.011 μM.

The data acquired gave curves of increasing absorbance over time. The slopes of the initial, linear regions of these curves were recorded as the rate of reaction (mAu/min). A Michaelis-Menten curve was produced by plotting the measured rates against the corresponding concentration of dTTP, and the Michaelis-Menten equation was fit to the data in order to extract kinetic parameters.

5.4.3. Determination of Inhibition Parameters of Synthesized Compounds Against Cps2L

Inhibitor compounds were dissolved in a solution of 70% DMSO in ddH$_2$O to make stock solutions (10 mM).

The assay was run in the same way as in the determination of Cps2L kinetic parameters, except that inhibitor was added to the initial mixture of stock solutions (see Table 5.1). Generally, 4 assays were run simultaneously, measuring the effects of 3 different inhibitor concentrations, plus an assay where zero inhibitor is present.

All rate data were plotted against the corresponding concentration of dTTP. Models were fit to the data to estimate the mode of inhibition (Excel sheets are included in appendices for each compound and inhibition model).

Table 5.1: Volume of inhibitor stock solution added to effect a corresponding final inhibitor concentration in enzyme assays.

Final concentration (inhibitor) (µM)	Volume (inhibitor) (µL)	Volume (70% DMSO) (µL)
800	96	0
600	72	24
400	48	48
300	36	60
200	24	72
100	12	84
50	6	90
25	3	93
10	1.2	95

5.4.4. Determination of Time-Dependent Inhibition by Potential-Covalent Inhibitors

Dilutions of 10 mM stock inhibitor were prepared according to Table 5.2. 60 µL of each solution were added to wells.

To an Eppendorf tube was added MOPS buffer (60 µL), inosine (60 µL), G1P (60 µL), $MgCl_2$ (14 µL), IPP (15 µL), XO (3 µL), hPNP (7.5 µL), dTTP (9 µL), and ddH_2O (221 µL). 45 µL of this solution was added to each well, and the resulting solutions were incubated for 5 min. A 4000-fold dilution of Cps2L in MOPS buffer was prepared as described above, through an intermediate 100-fold dilution. 15 µL of this solution was added to each well using a repeater pipette. Measurements were acquired for an extended period (7-30 min, depending on the individual experiment).

Table 5.2: Standard dilutions of stock inhibitor prepared to evaluate the time-dependent inhibition of Cps2L.

$C_{f\ (stock)}$ (μM)	$C_{f\ (assay)}$ (μM)	$V_{inh\ sol'n}$ (μL)	$V_{70\%\ DMSO\ /\ H2O}$ (μL)	V_{H2O} (μL)	V_{tot} (μL)
0	0	0	20	480	500
40	20	2	18	480	500
80	40	4	16	480	500
120	60	6	14	480	500
160	80	8	12	480	500
200	100	10	10	480	500
300	150	15	5	480	500
400	200	20	0	480	500

Chapter 6.   Conclusion

The work reported in this thesis has represented the first deliberate effort by the Jakeman group to synthesize and evaluate a library of thymidine derivatives as potential inhibitors of Cps2L. We have successfully synthesized 15 compounds, comprising varied scaffolds (bearing triazole and amide linker moieties), and varied warhead functionalities (bearing aldehyde, nitrile, and o-FABA groups). The major goal of this project was to synthesize thymidine derivatives which covalently modify lysine residues through formation of an iminoboronate. Two compounds, **4a** and **4b**, have the theoretical potential to react with lysine in this manner, although they bear BPin groups rather than boronic acids.

Of the synthesized molecules, four were evaluated for their ability to bind Cps2L using WaterLOGSY NMR. This experiment indicated that each of the evaluated compounds (**4c**, **4f**, **15** and **18**) bound Cps2L in the absence of the substrate, dTTP. Of those, **4c** and **4f** both bound in the presence of both equimolar and excess dTTP, suggesting that the scaffold that both compounds bear (i.e. the 1,4-substituted triazole) allows the compounds to participate in a unique mode of binding compared to the other two.

Of the synthesized molecules, nine were evaluated for reversible inhibition of Cps2L (**4a**, **4b**, **4d**, **4e**, **4f**, **4g**, **7**, **8**, and **10a**). Of these, all but nitrile-bearing compound **8** demonstrated inhibition against Cps2L, although nitrile-bearing compounds **4g** and **7** gave weak inhibition relative to the other tested compounds. The most potent compounds tested were **4f**, bearing a para-substituted arylboronic acid warhead, and **4d**, bearing a meta-substituted aryl aldehyde warhead. Kinetic models representing four modes of reversible inhibition were developed to account for the substrate inhibition by dTTP, and using these models, preliminary estimates of binding modes were determined for each compound.

This work is exploratory in nature, and begins to probe the complex system that is the reaction of thymidylyltransferase enzymes; as such it concludes little but provides much direction for future research. Due to the current global pandemic and halting of research efforts, we were unable to complete the synthesis of the initial target compounds, **5a** and **5b**. Kinetic assay results suggest that compound **5a** may be a highly potent inhibitor, as the two highest-potency inhibitors tested (**4d** and **4f**) bore the constituent functionalities present in **5a**. Similarly, our data acquisition of WaterLOGSY and kinetic assays was incomplete, leading to gaps in our understanding of whether and how the compounds of

interest bind. For example, there was no overlap in compounds tested by WaterLOGSY NMR and those evaluated for kinetic inhibition, except for **4f** whose kinetic parameters and thus mechanism of binding were not ascertained.

As mentioned, the reaction (and inhibition) of Cps2L is a complex system. Natural thymidine derivatives are known to bind both the active and allosteric sites of the enzyme, giving rise to substrate inhibition among other effects, which may explain our conflicting WaterLOGSY and kinetic assay data. While all compounds bind Cps2L in the absence of dTTP according to WaterLOGSY studies, indicating a potential competitive mode of inhibition, none of the compounds assayed for reversible inhibition indicated a preference for competitive inhibition. Instead, some compounds gave a strong preference for uncompetitive inhibition, which should theoretically preclude binding of the substrate-unbound enzyme. In order to elucidate the mechanism of action of these compounds, further studies by WaterLOGSY NMR and acquisition of consistent kinetic data will be necessary. Future work may include mutation of certain residues within the active or allosteric sites of Cps2L, which may influence binding at either site and aid in determination of binding mechanisms. Further studies may also include co-crystallization of the inhibitors with Cps2L. We are currently in collaboration with Dr. Hazel Holden's research group at the University of Wisconsin-Madison, who have previously reported crystal structures of RmlA from *Mycobacterium tuberculosis*, and whom we have sent several synthesized compounds (**4e**, **4g**, **7**, **8**, **10a**, **14a**, **14b**, and **15**). Once university operations reopen, obtaining the crystal structures of our compounds (hopefully) binding RmlA will certainly elucidate the binding modes.

Finally, developing a robust method for probing covalent modification of the enzyme will be valuable for future compounds which may exhibit time-dependent inactivation of Cps2L. Currently, all of the inhibitors with the potential to covalently modify the lysine residues of Cps2L (i.e. aldehyde and o-FABA bearing compounds) demonstrate fast, reversible inhibition. It will be important to distinguish this alternative mode of covalent inactivation, if it is present, in order to fully understand the system.

References

(1) Weiser, J. N.; Ferreira, D. M.; Paton, J. C. Streptococcus Pneumoniae: Transmission, Colonization and Invasion. *Nat. Rev. Microbiol.* **2018**, *16* (6), 355–367. https://doi.org/10.1038/s41579-018-0001-8.

(2) Baquero, F.; Beltren, J. M.; Loza, E. A Review of Antibiotic Resistance Patterns of Streptococcus Pneumoniae in Europe. *J. Antimicrob. Chemother.* **1991**, *28* (suppl C), 31–38. https://doi.org/10.1093/jac/28.suppl_c.31.

(3) Appelbaum, P. C. Antimicrobial Resistance in Streptococcus Pneumoniae: An Overview. *Clin. Infect. Dis.* **1992**, *15* (1), 77–83. https://doi.org/10.1093/clinids/15.1.77.

(4) Charpentier, E.; Tuomanen, E. Mechanisms of Antibiotic Resistance and Tolerance in Streptococcus Pneumoniae. *Microbes Infect.* **2000**, *2* (15), 1855–1864. https://doi.org/10.1016/S1286-4579(00)01345-9.

(5) Wang, W.; Arshad, M. I.; Khurshid, M.; Rasool, M. H.; Nisar, M. A.; Aslam, M. A.; Qamar, M. U. Antibiotic Resistance : A Rundown of a Global Crisis. *Infect. Drug Resist.* **2018**, 1645–1658.

(6) Ventola, C. L. The Antibiotic Resistance Crisis. *Pharm. Ther.* **2015**, *40* (4), 277–283.

(7) Thanner, S.; Drissner, D.; Walsh, F. Antimicrobial Resistance in Agriculture. *MBio* **2016**, *7* (2), 1–7. https://doi.org/10.1128/mBio.02227-15.

(8) Antibiotic resistance https://www.who.int/news-room/fact-sheets/detail/antibiotic-resistance (accessed Jun 2, 2020).

(9) C Reygaert, W. An Overview of the Antimicrobial Resistance Mechanisms of Bacteria. *AIMS Microbiol.* **2018**, *4* (3), 482–501. https://doi.org/10.3934/microbiol.2018.3.482.

(10) van der Beek, S. L.; Zorzoli, A.; Çanak, E.; Chapman, R. N.; Lucas, K.; Meyer, B. H.; Evangelopoulos, D.; de Carvalho, L. P. S.; Boons, G. J.; Dorfmueller, H. C.; et al. Streptococcal DTDP-L-Rhamnose Biosynthesis Enzymes: Functional Characterization and Lead Compound Identification. *Mol. Microbiol.* **2019**, *111* (4), 951–964. https://doi.org/10.1111/mmi.14197.

(11) Giraud, M. F.; Naismith, J. H. The Rhamnose Pathway. *Curr. Opin. Struct. Biol.* **2000**, *10* (6), 687–696. https://doi.org/10.1016/S0959-440X(00)00145-7.

(12) Babaoglu, K.; Page, M. A.; Jones, V. C.; McNeil, M. R.; Dong, C.; Naismith, J. H.; Lee, R. E. Novel Inhibitors of an Emerging Target in Mycobacterium Tuberculosis; Substituted Thiazolidinones as Inhibitors of DTDP-Rhamnose Synthesis. *Bioorganic Med. Chem. Lett.* **2003**, *13* (19), 3227–3230. https://doi.org/10.1016/S0960-894X(03)00673-5.

(13) Forget, S. M.; Bhattasali, D.; Hart, V. C.; Cameron, T. S.; Syvitski, R. T.; Jakeman, D. L. Synthesis and Enzymatic Evaluation of Ketose Phosphonates: The

Interplay between Mutarotation, Monofluorination and Acidity. *Chem. Sci.* **2012**, *3* (6), 1866–1878. https://doi.org/10.1039/c2sc01077a.

(14) Forget, S. M.; Jee, A.; Smithen, D. A.; Jagdhane, R.; Anjum, S.; Beaton, S. A.; Palmer, D. R. J.; Syvitski, R. T.; Jakeman, D. L. Kinetic Evaluation of Glucose 1-Phosphate Analogues with a Thymidylyltransferase Using a Continuous Coupled Enzyme Assay. *Org. Biomol. Chem.* **2015**, *13* (3), 866–875. https://doi.org/10.1039/C4OB02057J.

(15) Zhu, J. S.; McCormick, N. E.; Timmons, S. C.; Jakeman, D. L. Synthesis of α-Deoxymono and Difluorohexopyranosyl 1-Phosphates and Kinetic Evaluation with Thymidylyl- and Guanidylyltransferases. *J. Org. Chem.* **2016**, *81* (19), 8816–8825. https://doi.org/10.1021/acs.joc.6b01485.

(16) Smithen, D. A.; Forget, S. M.; Mccormick, N. E.; Syvitski, R. T.; Jakeman, D. L. Polyphosphate-Containing Bisubstrate Analogues as Inhibitors of a Bacterial Cell Wall Thymidylyltransferase. *Org. Biomol. Chem.* **2015**, *13* (11), 3347–3350. https://doi.org/10.1039/c4ob02583k.

(17) Alphey, M. S.; Pirrie, L.; Torrie, L. S.; Boulkeroua, W. A.; Gardiner, M.; Sarkar, A.; Maringer, M.; Oehlmann, W.; Brenk, R.; Scherman, M. S.; et al. Allosteric Competitive Inhibitors of the Glucose-1-Phosphate Thymidylyltransferase (RmlA) from Pseudomonas Aeruginosa. *ACS Chem. Biol.* **2013**, *8* (2), 387–396. https://doi.org/10.1021/cb300426u.

(18) Blankenfeldt, W.; Asuncion, M.; Lam, J. S.; Naismith, J. H. The Structural Basis of the Catalytic Mechanism and Regulation of Glucose-1-Phosphate Thymidylyltransferase (RmlA). *EMBO J.* **2000**, *19* (24), 6652–6663. https://doi.org/10.1093/emboj/19.24.6652.

(19) Spicer, C. D.; Davis, B. G. Selective Chemical Protein Modification. *Nat. Commun.* **2014**, *5*. https://doi.org/10.1038/ncomms5740.

(20) DeGruyter, J. N.; Malins, L. R.; Baran, P. S. Residue-Specific Peptide Modification: A Chemist's Guide. *Biochemistry* **2017**, *56* (30), 3863–3873. https://doi.org/10.1021/acs.biochem.7b00536.

(21) Lonsdale, R.; Ward, R. A. Structure-Based Design of Targeted Covalent Inhibitors. *Chem. Soc. Rev.* **2018**, *47* (11), 3816–3830. https://doi.org/10.1039/c7cs00220c.

(22) Visscher, M.; Arkin, M. R.; Dansen, T. B. Covalent Targeting of Acquired Cysteines in Cancer. *Curr. Opin. Chem. Biol.* **2016**, *30*, 61–67. https://doi.org/10.1016/j.cbpa.2015.11.004.

(23) Cuesta, A.; Taunton, J. Lysine-Targeted Inhibitors and Chemoproteomic Probes. *Annu. Rev. Biochem.* **2019**, *88* (1), 365–381. https://doi.org/10.1146/annurev-biochem-061516-044805.

(24) Pettinger, J.; Carter, M.; Jones, K.; Cheeseman, M. D. Kinetic Optimization of Lysine-Targeting Covalent Inhibitors of HSP72. *J. Med. Chem.* **2019**, *62* (24),

11383–11398. https://doi.org/10.1021/acs.jmedchem.9b01709.

(25)   Bradshaw, J. M.; McFarland, J. M.; Paavilainen, V. O.; Bisconte, A.; Tam, D.;
       Phan, V. T.; Romanov, S.; Finkle, D.; Shu, J.; Patel, V.; et al. Prolonged and
       Tunable Residence Time Using Reversible Covalent Kinase Inhibitors. *Nat. Chem.
       Biol.* **2015**, *11* (7), 525–531. https://doi.org/10.1038/nchembio.1817.

(26)   Cal, P. M. S. D.; Vicente, J. B.; Pires, E.; Coelho, A. V.; Veiros, L. F.; Cordeiro,
       C.; Gois, P. M. P. Iminoboronates: A New Strategy for Reversible Protein
       Modification. *J. Am. Chem. Soc.* **2012**, *134* (24), 10299–10305.
       https://doi.org/10.1021/ja303436y.

(27)   Dal Corso, A.; Catalano, M.; Schmid, A.; Scheuermann, J.; Neri, D. Affinity
       Enhancement of Protein Ligands by Reversible Covalent Modification of
       Neighboring Lysine Residues. *Angew. Chemie - Int. Ed.* **2018**, *57* (52), 17178–
       17182. https://doi.org/10.1002/anie.201811650.

(28)   Akçay, G.; Belmonte, M. A.; Aquila, B.; Chuaqui, C.; Hird, A. W.; Lamb, M. L.;
       Rawlins, P. B.; Su, N.; Tentarelli, S.; Grimster, N. P.; et al. Inhibition of Mcl-1
       through Covalent Modification of a Noncatalytic Lysine Side Chain. *Nat. Chem.
       Biol.* **2016**, *12* (11), 931–936. https://doi.org/10.1038/nchembio.2174.

(29)   Forget, S. M.; Jee, A.; Smithen, D. A.; Jagdhane, R.; Anjum, S.; Beaton, S. A.;
       Palmer, D. R. J.; Syvitski, R. T.; Jakeman, D. L. Kinetic Evaluation of Glucose 1-
       Phosphate Analogues with a Thymidylyltransferase Using a Continuous Coupled
       Enzyme Assay. *Org. Biomol. Chem.* **2015**, *13* (3), 866–875.
       https://doi.org/10.1039/c4ob02057j.

(30)   Sella, E.; Shabat, D. Hydroquinone–Quinone Oxidation by Molecular Oxygen: A
       Simple Tool for Signal Amplification through Auto-Generation of Hydrogen
       Peroxide. *Org. Biomol. Chem.* **2013**, *11* (31), 5074.
       https://doi.org/10.1039/c3ob40962g.

(31)   Qiu, W. W.; Surendra, K.; Yin, L.; Corey, E. J. Selective Formation of Six-
       Membered Oxa- and Carbocycles by the In(III)-Activated Ring Closure of
       Acetylenic Substrates. *Org. Lett.* **2011**, *13* (21), 5893–5895.
       https://doi.org/10.1021/ol202621g.

(32)   Hans, R. H.; Guantai, E. M.; Lategan, C.; Smith, P. J.; Wan, B.; Franzblau, S. G.;
       Gut, J.; Rosenthal, P. J.; Chibale, K. Synthesis, Antimalarial and Antitubercular
       Activity of Acetylenic Chalcones. *Bioorganic Med. Chem. Lett.* **2010**, *20* (3), 942–
       944. https://doi.org/10.1016/j.bmcl.2009.12.062.

(33)   Sekiya, R.; Uemura, Y.; Murakami, H.; Haino, T. White-Light-Emitting Edge-
       Functionalized Graphene Quantum Dots. *Angew. Chemie - Int. Ed.* **2014**, *53* (22),
       5619–5623. https://doi.org/10.1002/anie.201311248.

(34)   Lucas, R.; Zerrouki, R.; Granet, R.; Krausz, P.; Champavier, Y. A Rapid Efficient
       Microwave-Assisted Synthesis of a 3′,5′-Pentathymidine by Copper(I)-Catalyzed
       [3+2] Cycloaddition. *Tetrahedron* **2008**, *64* (23), 5467–5471.

https://doi.org/10.1016/j.tet.2008.04.006.

(35) Pan, D.; Sun, J.; Jin, H.; Li, Y.; Li, L.; Wu, Y.; Zhang, L.; Yang, Z. Supramolecular Assemblies of Novel Aminonucleoside Phospholipids and Their Bonding to Nucleic Acids. *Chem. Commun.* **2015**, *51* (3), 469–472. https://doi.org/10.1039/C4CC07538B.

(36) Hyde, A. M.; Zultanski, S. L.; Waldman, J. H.; Zhong, Y. L.; Shevlin, M.; Peng, F. General Principles and Strategies for Salting-Out Informed by the Hofmeister Series. *Org. Process Res. Dev.* **2017**, *21* (9), 1355–1370. https://doi.org/10.1021/acs.oprd.7b00197.

(37) Himo, F.; Lovell, T.; Hilgraf, R.; Rostovtsev, V. V.; Noodleman, L.; Sharpless, K. B.; Fokin, V. V. Copper(I)-Catalyzed Synthesis of Azoles. DFT Study Predicts Unprecedented Reactivity and Intermediates. *J. Am. Chem. Soc.* **2005**, *127* (1), 210–216. https://doi.org/10.1021/ja0471525.

(38) Godeau, G.; Staedel, C.; Barthélémy, P. Lipid-Conjugated Oligonucleotides via "Click Chemistry" Efficiently Inhibit Hepatitis C Virus Translation. *J. Med. Chem.* **2008**, *51* (15), 4374–4376. https://doi.org/10.1021/jm800518u.

(39) Van Poecke, S.; Munier-Lehmann, H.; Helynck, O.; Froeyen, M.; Van Calenbergh, S. Synthesis and Inhibitory Activity of Thymidine Analogues Targeting Mycobacterium Tuberculosis Thymidine Monophosphate Kinase. *Bioorganic Med. Chem.* **2011**, *19* (24), 7603–7611. https://doi.org/10.1016/j.bmc.2011.10.021.

(40) Dai, C.; Cheng, Y.; Cui, J.; Wang, B. Click Reactions and Boronic Acids: Applications, Issues, and Potential Solutions. *Molecules* **2010**, *15* (8), 5768–5781. https://doi.org/10.3390/molecules15085768.

(41) Teichert, J. F.; Mazunin, D.; Bode, W. Chemical Sensing of Polyols with Shapeshifting Boronic Acids As a Self-Contained Sensor Array. *J. Am. Chem. Soc.* **2013**, *135*, 11314–11321. https://doi.org/10.1021/ja404981q.

(42) Chouhan, G.; James, K. CuAAC Macrocyclization: High Intramolecular Selectivity through the Use of Copper-Tris(Triazole) Ligand Complexes. *Org. Lett.* **2011**, *13* (10), 2754–2757. https://doi.org/10.1021/ol200861f.

(43) Haldón, E.; Nicasio, M. C.; Pérez, P. J. Copper-Catalysed Azide-Alkyne Cycloadditions (CuAAC): An Update. *Org. Biomol. Chem.* **2015**, *13* (37), 9528–9550. https://doi.org/10.1039/c5ob01457c.

(44) Chan, T. R.; Hilgraf, R.; Sharpless, K. B.; Fokin, V. V. Polytriazoles as Copper(I)-Stabilizing Ligands in Catalysis. *Org. Lett.* **2004**, *6* (17), 2853–2855. https://doi.org/10.1021/ol0493094.

(45) Hinkes, S. P. A.; Klein, C. D. P. Virtues of Volatility: A Facile Transesterification Approach to Boronic Acids. *Org. Lett.* **2019**, *21* (9), 3048–3052. https://doi.org/10.1021/acs.orglett.9b00584.

(46) Smith, P. A.; Koehler, M. F. T.; Girgis, H. S.; Yan, D.; Chen, Y.; Chen, Y.;

Crawford, J. J.; Durk, M. R.; Higuchi, R. I.; Kang, J.; et al. Optimized Arylomycins Are a New Class of Gram-Negative Antibiotics. *Nature* **2018**, *561* (7722), 189–194. https://doi.org/10.1038/s41586-018-0483-6.

(47) Dox, A. W. Acetamidine Hydrochloride. *Org. Synth.* **1928**, *8* (September), 1. https://doi.org/10.15227/orgsyn.008.0001.

(48) Bochkarev, M. N.; Balashova, T. V.; Maleev, A. A.; Fagin, A. A.; Fukin, G. K.; Baranov, E. V. Lanthanide Iodides as Promoters of Acetonitrile Amination. Molecular Structure of MeC(=NH)NHPri, MeC(=NH)NHBut and {Dy[MeC(=NH)NEt2]6}I3. *Inorganica Chim. Acta* **2007**, *360* (7), 2368–2378. https://doi.org/10.1016/j.ica.2006.12.009.

(49) Brown, H. A.; Thoden, J. B.; Tipton, P. A.; Holden, H. M. The Structure of Glucose-1-Phosphate Thymidylyltransferase from Mycobacterium Tuberculosis Reveals the Location of an Essential Magnesium Ion in the RmlA-Type Enzymes. *Protein Sci.* **2018**, *27* (2), 441–450. https://doi.org/10.1002/pro.3333.

(50) Dunetz, J. R.; Magano, J.; Weisenburger, G. A. Large-Scale Applications of Amide Coupling Reagents for the Synthesis of Pharmaceuticals. *Org. Process Res. Dev.* **2016**, *20* (2), 140–177. https://doi.org/10.1021/op500305s.

(51) Valeur, E.; Bradley, M. Amide Bond Formation: Beyond the Myth of Coupling Reagents. *Chem. Soc. Rev.* **2009**, *38* (2), 606–631. https://doi.org/10.1039/b701677h.

(52) Wang, W.; He, Y.; Xu, P.; You, Q.; Xiao, H.; Xiang, H. Synthesis and Biological Evaluation of Isoflavone Amide Derivatives with Antihyperlipidemic and Preadipocyte Antiproliferative Activities. *Bioorganic Med. Chem.* **2015**. https://doi.org/10.1016/j.bmc.2015.06.032.

(53) Kochetkova, S. V.; Fillipova, E. A.; Kolganova, N. A.; Timofeev, E. N.; Florentiev, V. L. Oligonucleotide Analogues Bearing an Acyclonucleoside Linked by an Internucleotide Amide Bond. *Russ. J. Bioorganic Chem.* **2008**, *34* (2), 207–214. https://doi.org/10.1007/s11171-008-2010-2.

(54) Loranger, M. W.; Forget, S. M.; McCormick, N. E.; Syvitski, R. T.; Jakeman, D. L. Synthesis and Evaluation of L-Rhamnose 1C-Phosphonates as Nucleotidylyltransferase Inhibitors. *J. Org. Chem.* **2013**, *78* (19), 9822–9833. https://doi.org/10.1021/jo401542s.

(55) Dalvit, C.; Fogliatto, G. P.; Stewart, A.; Veronesi, M.; Stockman, B. WaterLOGSY as a Method for Primary NMR Screening: Practical Aspects and Range of Applicability. *J. Biomol. NMR* **2001**, *21* (4), 349–359. https://doi.org/10.1023/A:1013302231549.

(56) Geist, L.; Mayer, M.; Cockcroft, X. L.; Wolkerstorfer, B.; Kessler, D.; Engelhardt, H.; McConnell, D. B.; Konrat, R. Direct NMR Probing of Hydration Shells of Protein Ligand Interfaces and Its Application to Drug Design. *J. Med. Chem.* **2017**, *60* (21), 8708–8715. https://doi.org/10.1021/acs.jmedchem.7b00845.

(57) Peng, J. W.; Lepre, C. A.; Fejzo, J.; Abdul-Manan, N.; Moore, J. M. Nuclear Magnetic Resonance-Based Approaches for Lead Generation in Drug Discovery. *Methods Enzymol.* **2001**, *338* (1999), 202–229. https://doi.org/10.1016/S0076-6879(02)38221-1.

(58) Timmons, S. C.; Mosher, R. H.; Knowles, S. A.; Jakeman, D. L. Exploiting Nucleotidylyltransferases to Prepare Sugar Nucleotides. *Org. Lett.* **2007**, *9* (5), 857–860. https://doi.org/10.1021/ol0630853.

(59) Forget, S. M.; Smithen, D. A.; Jee, A.; Jakeman, D. L. Mechanistic Evaluation of a Nucleoside Tetraphosphate with a Thymidylyltransferase. *Biochemistry* **2015**, *54* (8), 1703–1707. https://doi.org/10.1021/bi501438p.

(60) Furman, P. A.; Painter, G.; Wilson, J. E.; Cheng, N.; Hopkins, S. Substrate Inhibition of the Human Immunodeficiency Virus Type 1 Reverse Transcriptase. *Proc. Natl. Acad. Sci. U. S. A.* **1991**, *88* (14), 6013–6017. https://doi.org/10.1073/pnas.88.14.6013.

(61) Reed, M. C.; Lieb, A.; Nijhout, H. F. The Biological Significance of Substrate Inhibition: A Mechanism with Diverse Functions. *BioEssays*. 2010, pp 422–429. https://doi.org/10.1002/bies.200900167.

(62) Li, K.; Kelly, M. A.; Gao, J. Biocompatible Conjugation of Tris Base to 2-Acetyl and 2-Formyl Phenylboronic Acid. *Org. Biomol. Chem.* **2019**, *17* (24), 5908–5912. https://doi.org/10.1039/c9ob00726a.

(63) Chou, T. C.; Talalay, P. A Simple Generalized Equation for the Analysis of Multiple Inhibitions of Michaelis-Menten Kinetic Systems. *J. Biol. Chem.* **1977**, *252* (18), 6438–6442.

(64) Zhu, J. S.; Stiers, K. M.; Soleimani, E.; Groves, B. R.; Beamer, L. J.; Jakeman, D. L. Inhibitory Evaluation of ApMM/PGM from Pseudomonas Aeruginosa: Chemical Synthesis, Enzyme Kinetics, and Protein Crystallographic Study. *J. Org. Chem.* **2019**, *84* (15), 9627–9636. https://doi.org/10.1021/acs.joc.9b01305.

(65) Sculley, M. J.; Morrison, J. F.; Cleland, W. W. Slow-Binding Inhibition: The General Case. *Biochim. Biophys. Acta - Protein Struct. Mol. Enzymol.* **1996**, *1298* (1), 78–86. https://doi.org/10.1016/S0167-4838(96)00118-5.

(66) Stress, C. J.; Schmidt, P. J.; Gillingham, D. G. Comparison of Boron-Assisted Oxime and Hydrazone Formations Leads to the Discovery of a Fluorogenic Variant. *Org. Biomol. Chem.* **2016**, *14* (24), 5529–5533. https://doi.org/10.1039/C6OB00168H.

(67) Yang, W. R.; Choi, Y. S.; Jeong, J. H. Efficient Synthesis of Polymethoxyselenoflavones via Regioselective Direct C-H Arylation of Selenochromones. *Org. Biomol. Chem.* **2017**, *15* (14), 3074–3083. https://doi.org/10.1039/C7OB00118E.

(68) Wang, S.; Cheng, B. One-Pot Synthesis of Polypyrazoles by Click Reactions. *Sci. Rep.* **2017**, *7* (1), 1–9. https://doi.org/10.1038/s41598-017-12727-3.

(69)   Wang, W.; He, Y.; Xu, P.; You, Q.; Xiao, H.; Xiang, H. Synthesis and Biological Evaluation of Isoflavone Amide Derivatives with Antihyperlipidemic and Preadipocyte Antiproliferative Activities. *Bioorganic Med. Chem.* **2015**, *23* (15), 4428–4433. https://doi.org/10.1016/j.bmc.2015.06.032.

(70)   Madeira, F.; Park, Y. M.; Lee, J.; Buso, N.; Gur, T.; Madhusoodanan, N.; Basutkar, P.; Tivey, A. R. N.; Potter, S. C.; Finn, R. D.; et al. The EMBL-EBI Search and Sequence Analysis Tools APIs in 2019. *Nucleic Acids Res.* **2019**, *47* (W1), W636–W641. https://doi.org/10.1093/nar/gkz268.

(71)   RCSB PDB - 6B5E: Mycobacterium tuberculosis RmlA in complex with dTDP-glucose https://www.rcsb.org/structure/6b5e (accessed Jun 6, 2020).

(72)   Excel Solver: Which Solving Method Should I Choose? | EngineerExcel https://www.engineerexcel.com/excel-solver-solving-method-choose/ (accessed May 25, 2020).

APPENDIX A: Identity Matrix Comparing Peptide Sequences From Various RmlA Homologues

Percent Identity Matrix - created by Clustal2.1

Number	GenBank no.	% identity (1)	% identity (2)	% identity (3)	% identity (4)
1.	CRH14180.1	100.00	58.68	58.33	61.11
2.	ADR74236.1	58.68	100.00	66.44	63.45
3.	AVN85499.1	58.33	66.44	100.00	67.13
4.	ARU35951.1	61.11	63.45	67.13	100.00

Legend: 1: RmlA from *Mycobacterium tuberculosis*; 2: RmlA from *Escherichia coli*; 3: Cps2L from *Streptococcus pneumoniae*; 4: RmlA from *Pseudomonas aeruginosa*.

APPENDIX B: Characterization Data for Final Compounds and Certain Synthesized Intermediates
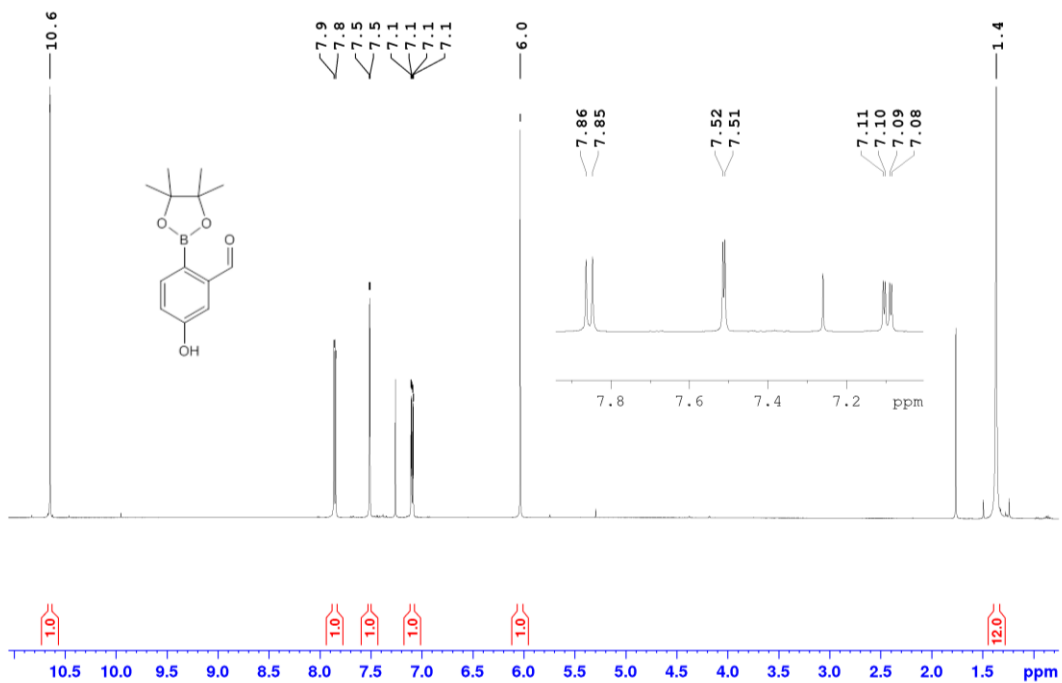
^{1}H NMR spectrum (500 MHz, CDCl$_3$) of 2-formyl-4-hydroxyphenylboronic acid pinacol ester (**2a**)
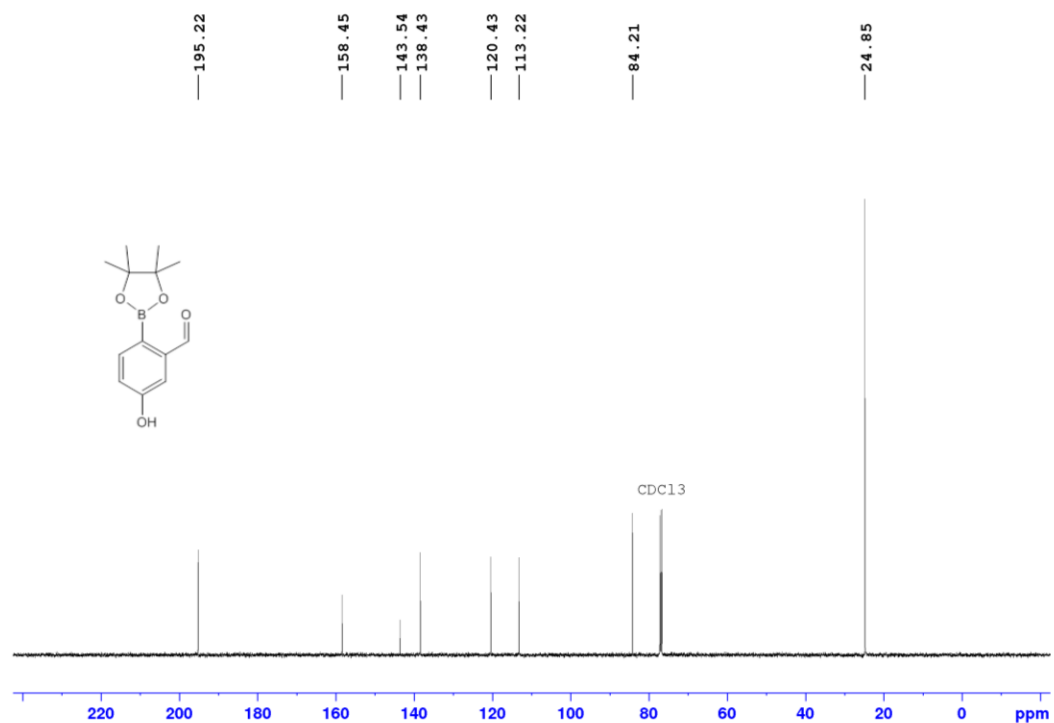
^{13}C NMR spectrum (126 MHz, CDCl$_3$) of 2-formyl-4-hydroxyphenylboronic acid pinacol ester (**2a**)
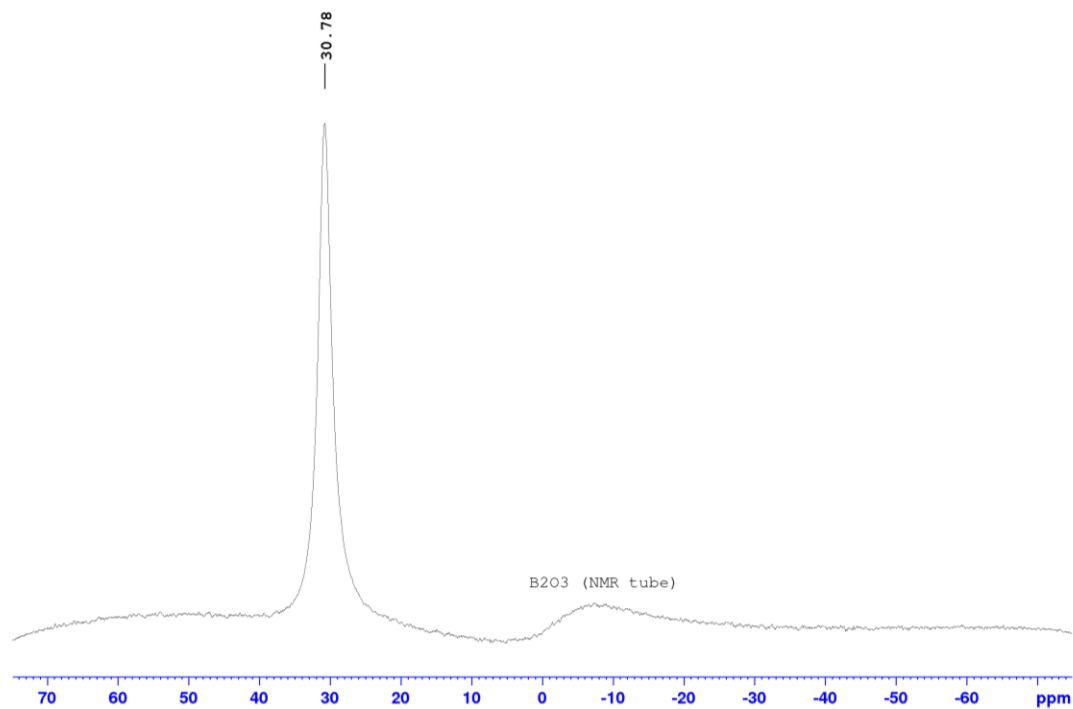
^{11}B NMR spectrum (160 MHz, CDCl$_3$) of 2-formyl-4-hydroxyphenylboronic acid pinacol ester (**2a**).
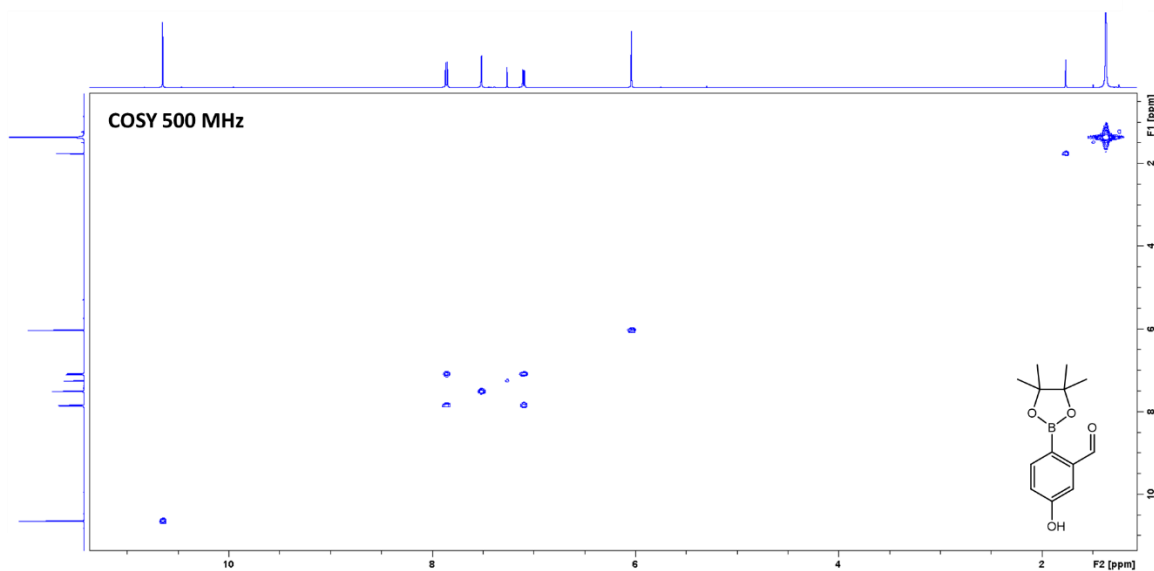
COSY NMR spectrum (500 MHz, CDCl$_3$) of 2-formyl-4-hydroxyphenylboronic acid pinacol ester (**2a**).
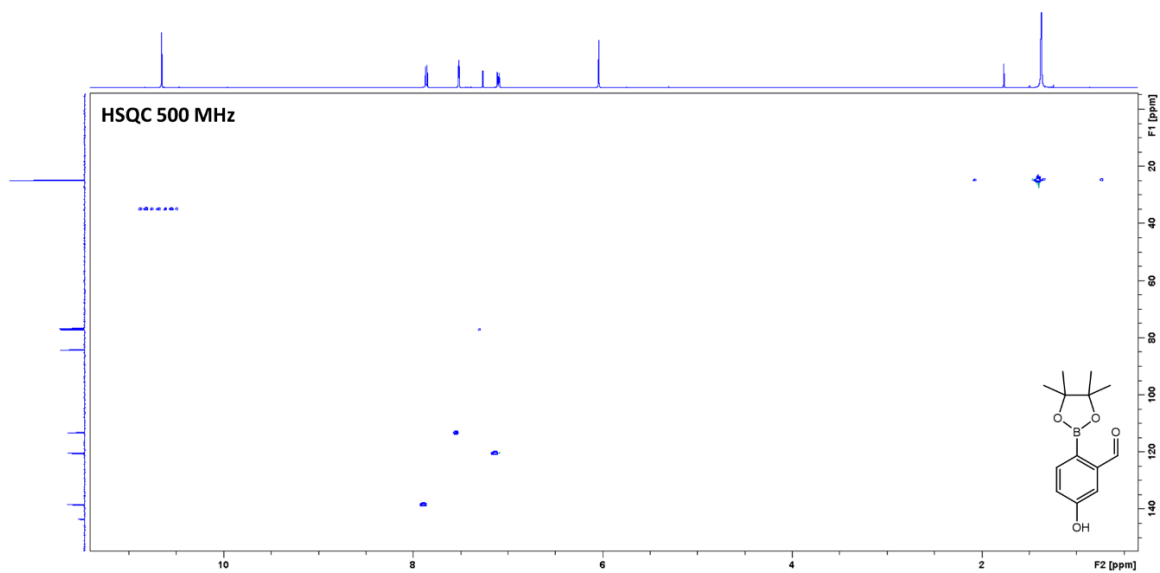
HSQC NMR spectrum (500 MHz, CDCl₃) of 2-formyl-4-hydroxyphenylboronic acid pinacol ester (**2a**).
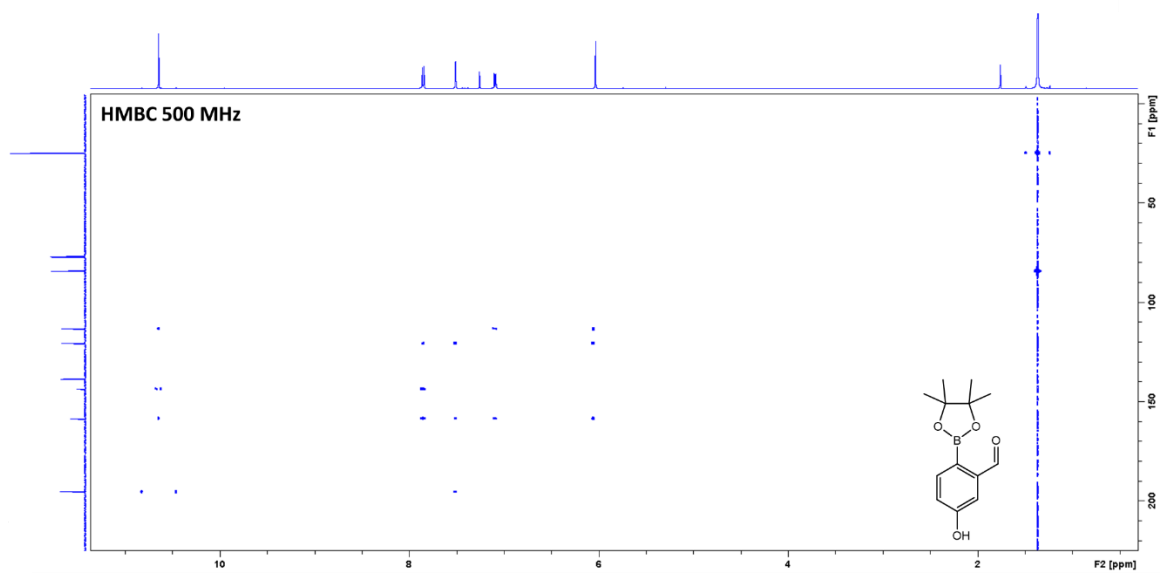
HMBC NMR spectrum (500 MHz, CDCl₃) of 2-formyl-4-hydroxyphenylboronic acid pinacol ester (**2a**).
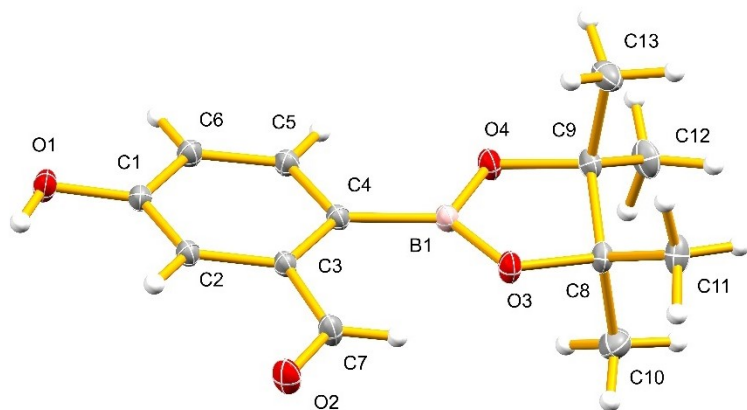
ORTEP diagram of of 2-formyl-4-hydroxyphenylboronic acid pinacol ester (**2a**).
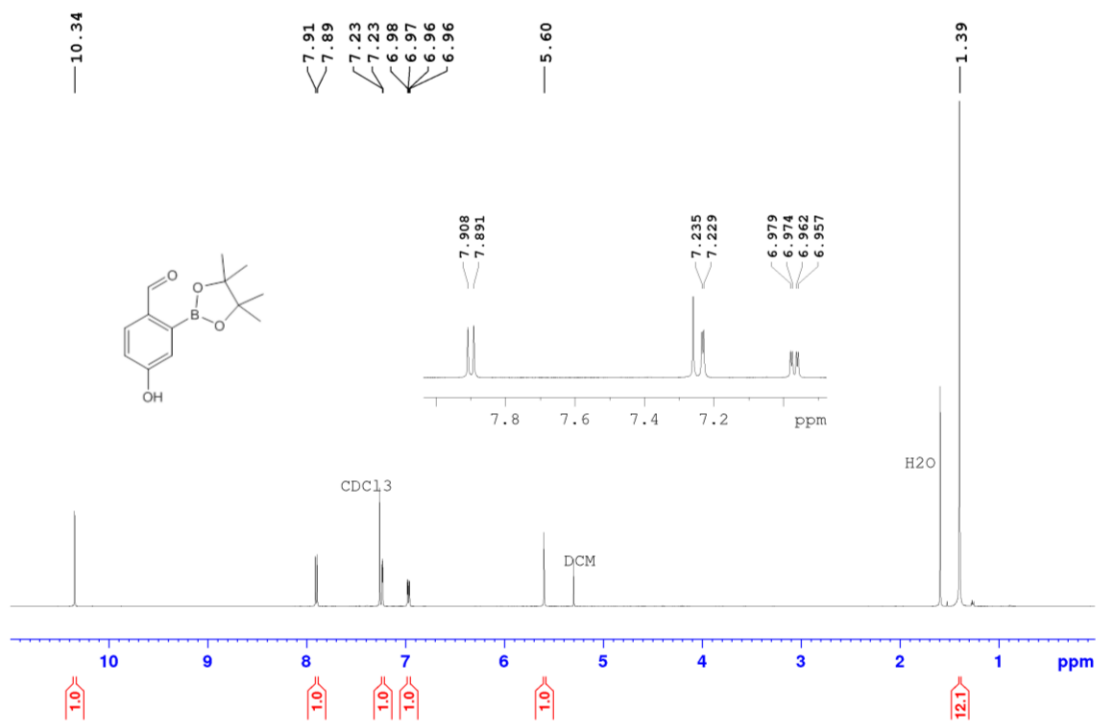
^{1}H NMR spectrum (500 MHz, CDCl3) of 2-formyl-5-hydroxyphenylboronic acid pinacol ester (**2b**).
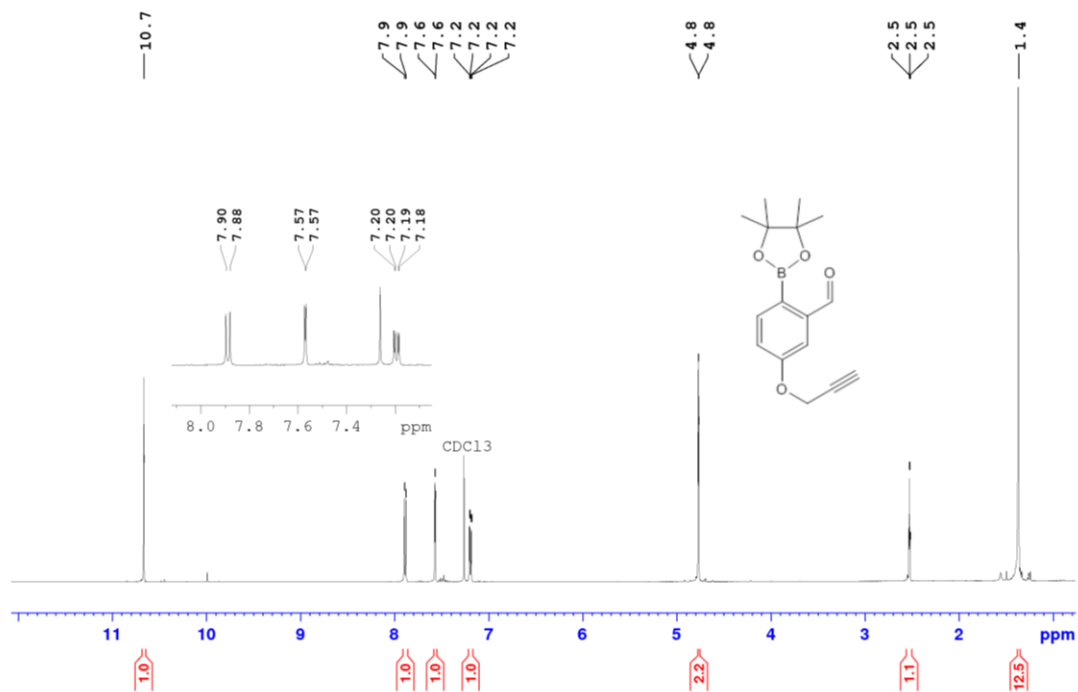
¹H NMR spectrum (500 MHz, CDCl₃) of 2-formyl-4-(2-propyn-1-yloxy)phenylboronic acid pinacol ester (**3a**).
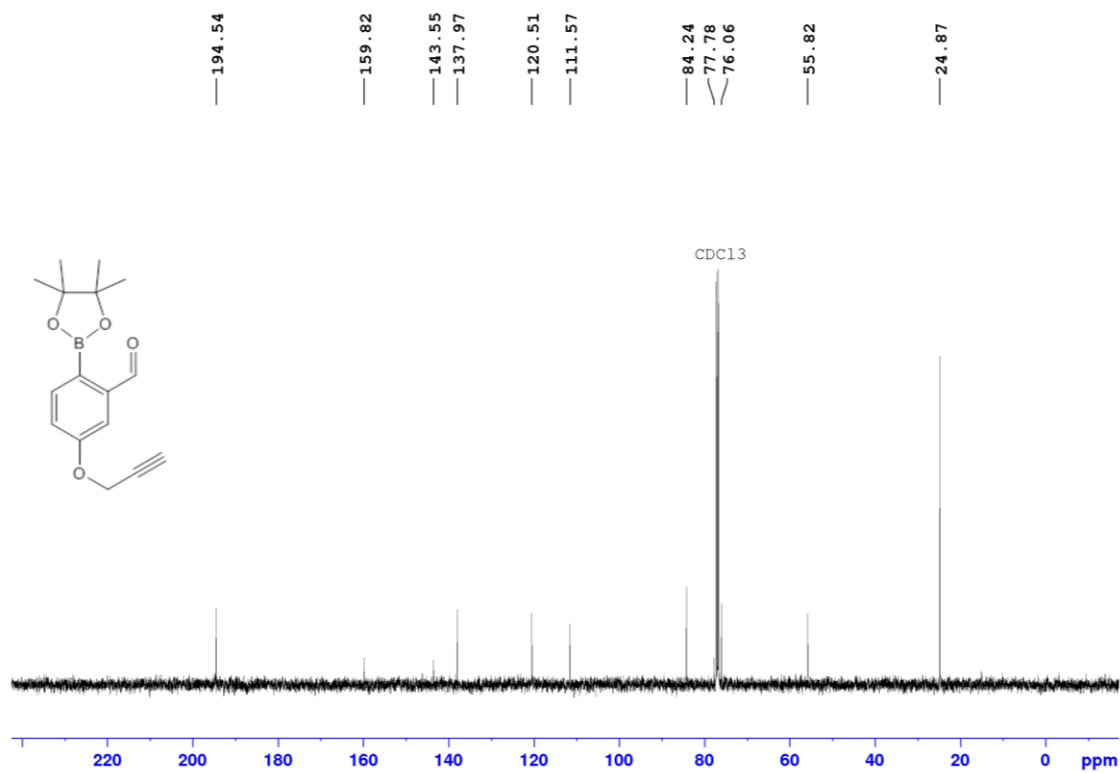
¹³C NMR spectrum (126 MHz, CDCl₃) of 2-formyl-4-(2-propyn-1-yloxy)phenylboronic acid pinacol ester (**3a**).
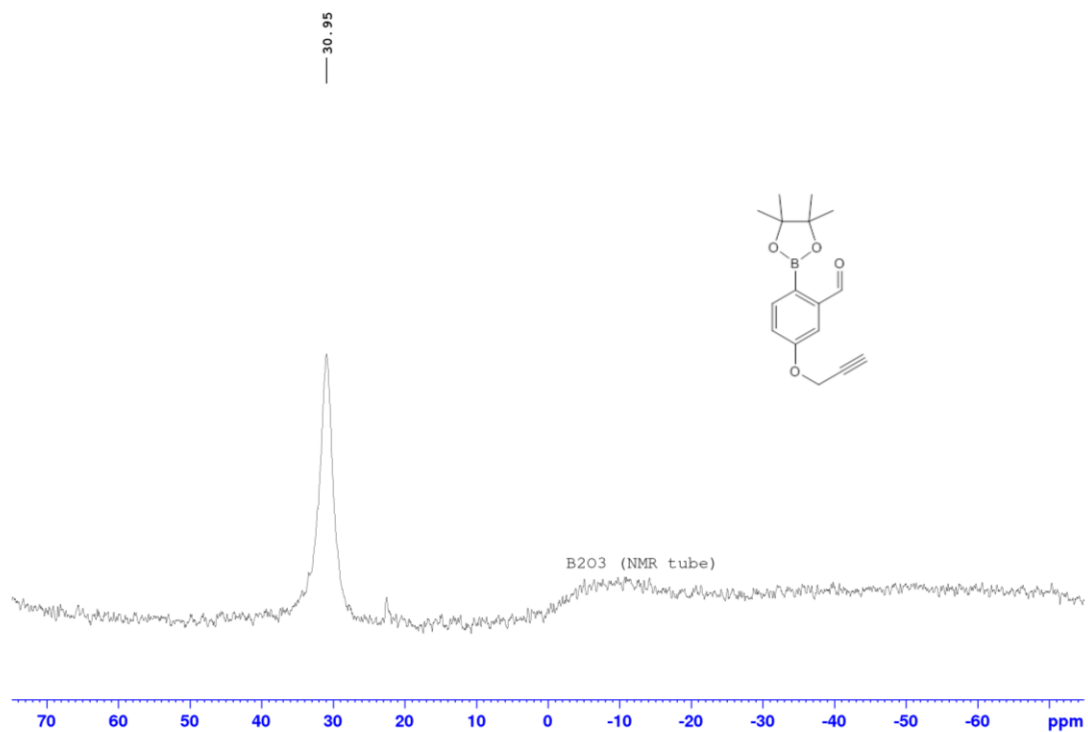
^{11}B NMR spectrum (160 MHz, CDCl$_3$) of 2-formyl-4-(2-propyn-1-yloxy)phenylboronic acid pinacol ester (**3a**).
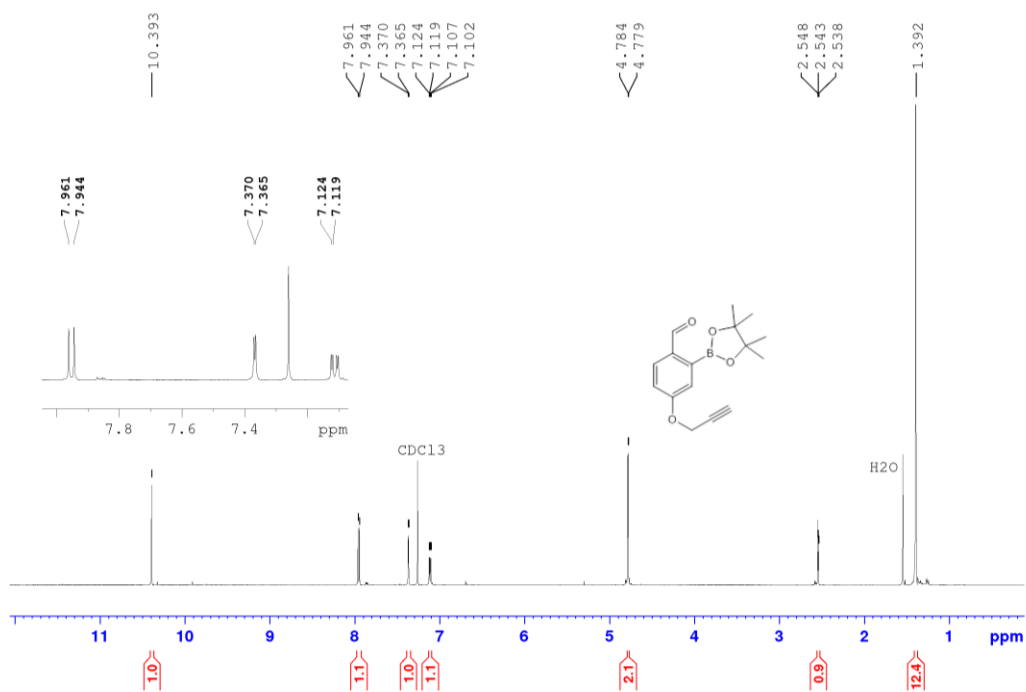
^{1}H NMR spectrum (500 MHz, CDCl$_3$) of 2-formyl-5-(2-propyn-1-yloxy)phenylboronic acid pinacol ester (**3b**).
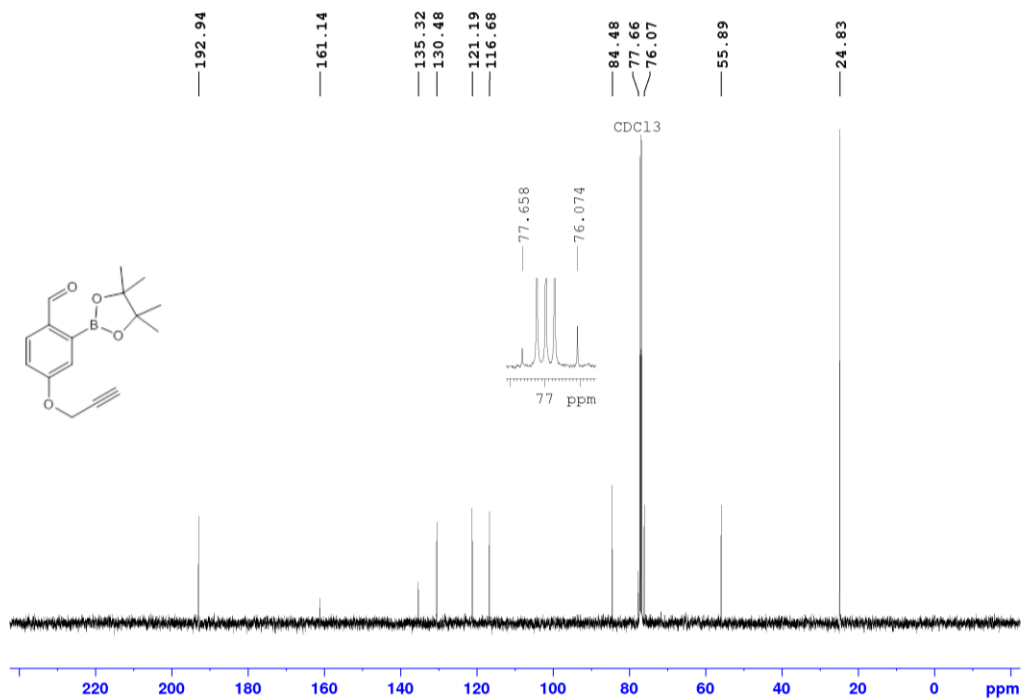
^{13}C NMR spectrum (126 MHz, CDCl$_3$) of 2-formyl-5-(2-propyn-1-yloxy)phenylboronic acid pinacol ester (**3b**).
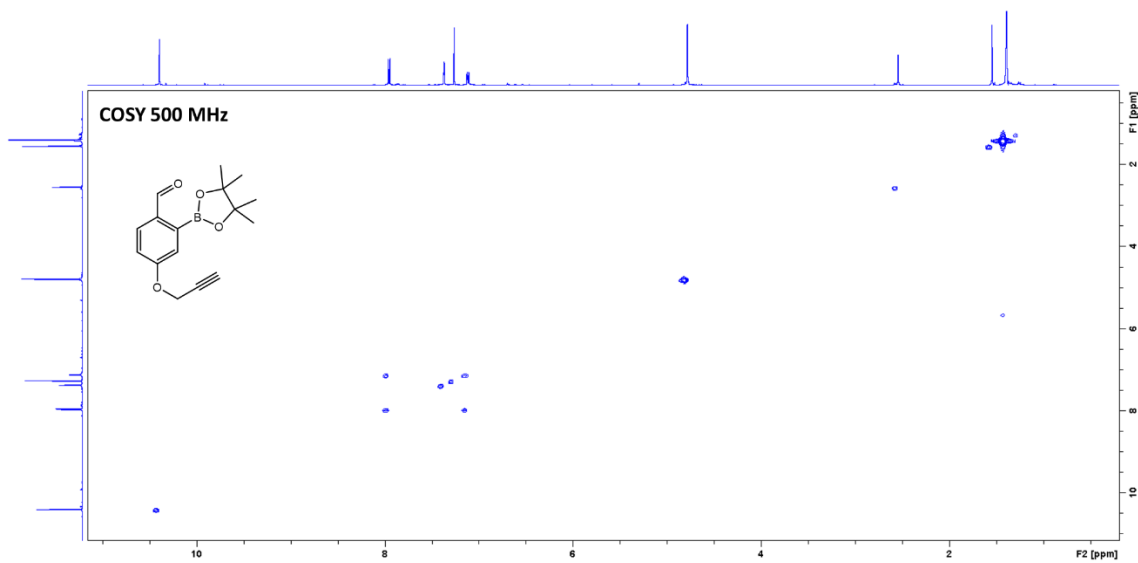
COSY NMR spectrum (500 MHz, CDCl$_3$) of 2-formyl-5-(2-propyn-1-yloxy)phenylboronic acid pinacol ester (**3b**).
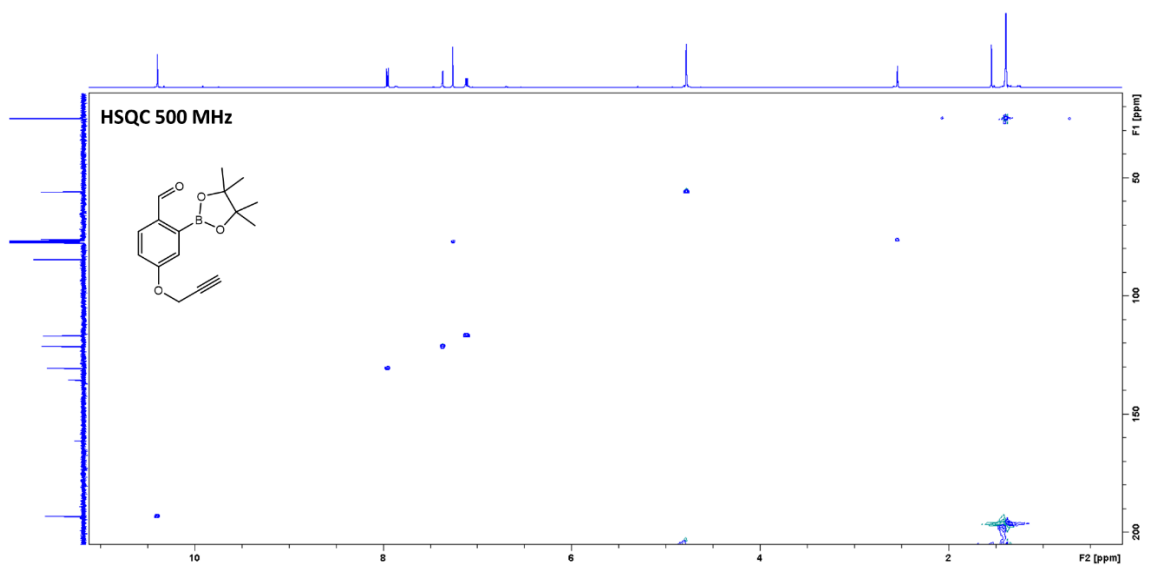
HSQC NMR spectrum (500 MHz, CDCl₃) of 2-formyl-5-(2-propyn-1-yloxy)phenylboronic acid pinacol ester (**3b**).
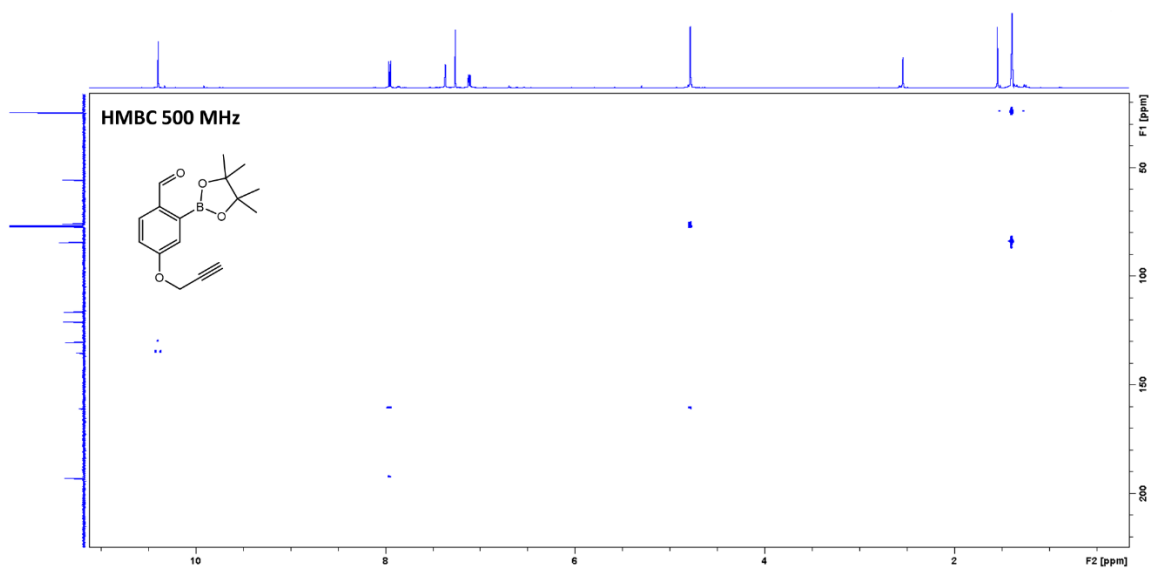
HMBC NMR spectrum (500 MHz, CDCl₃) of 2-formyl-5-(2-propyn-1-yloxy)phenylboronic acid pinacol ester (**3b**).

^{11}B NMR spectrum not acquired for this compound.
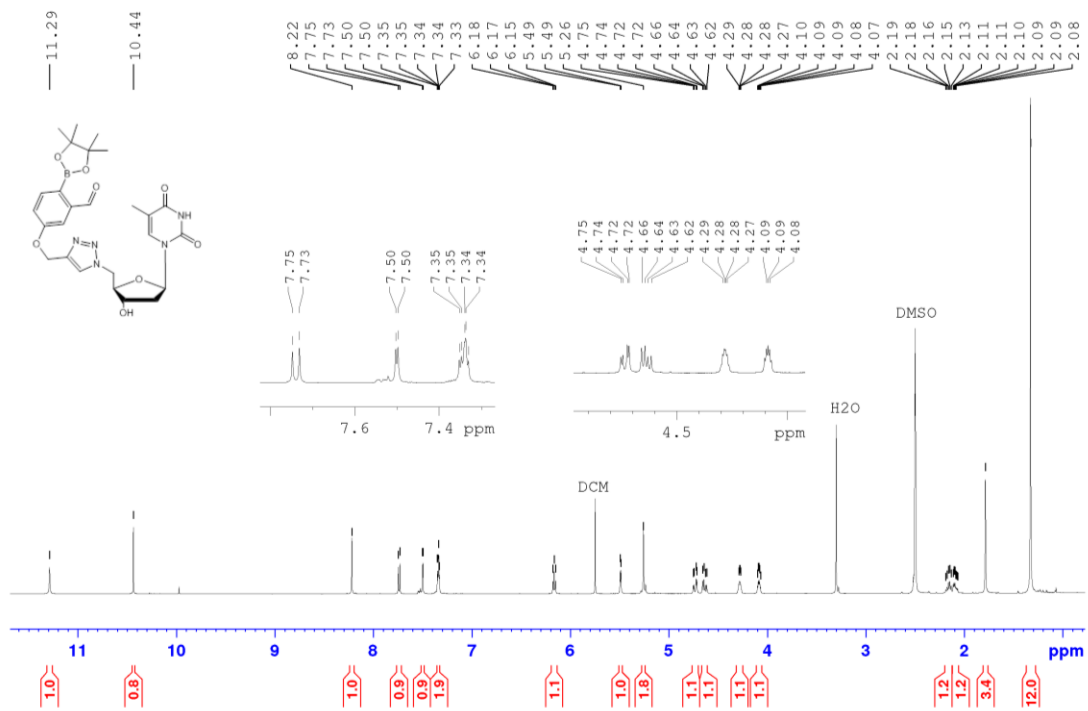
^{1}H NMR spectrum (500 MHz, d_6-DMSO) of **4a**.
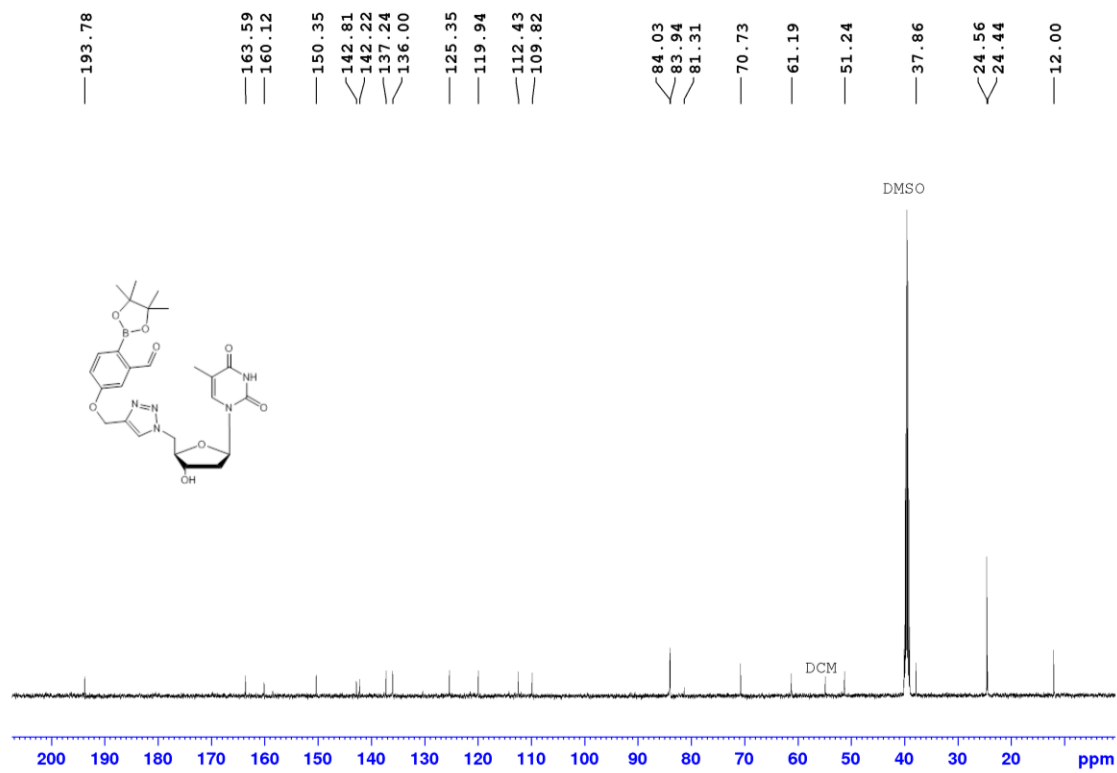
^{13}C NMR spectrum (126 MHz, d_6-DMSO) of **4a**.
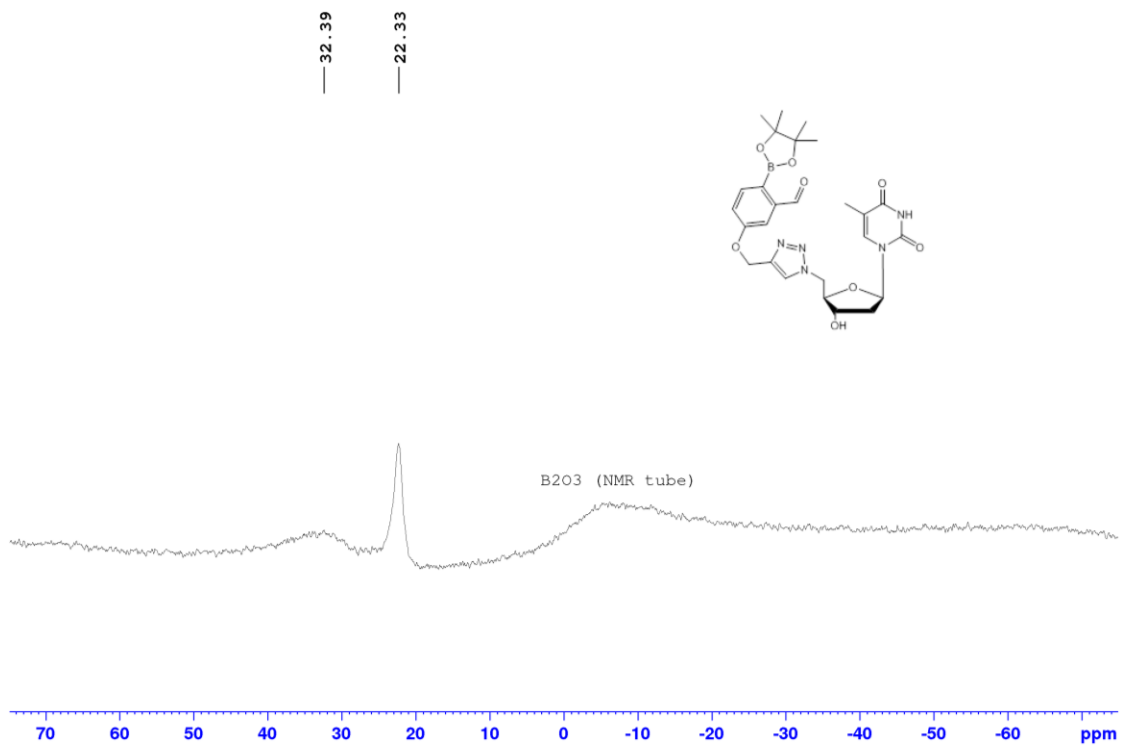
^{11}B NMR spectrum (160 MHz, d_6-DMSO) of **4a**.
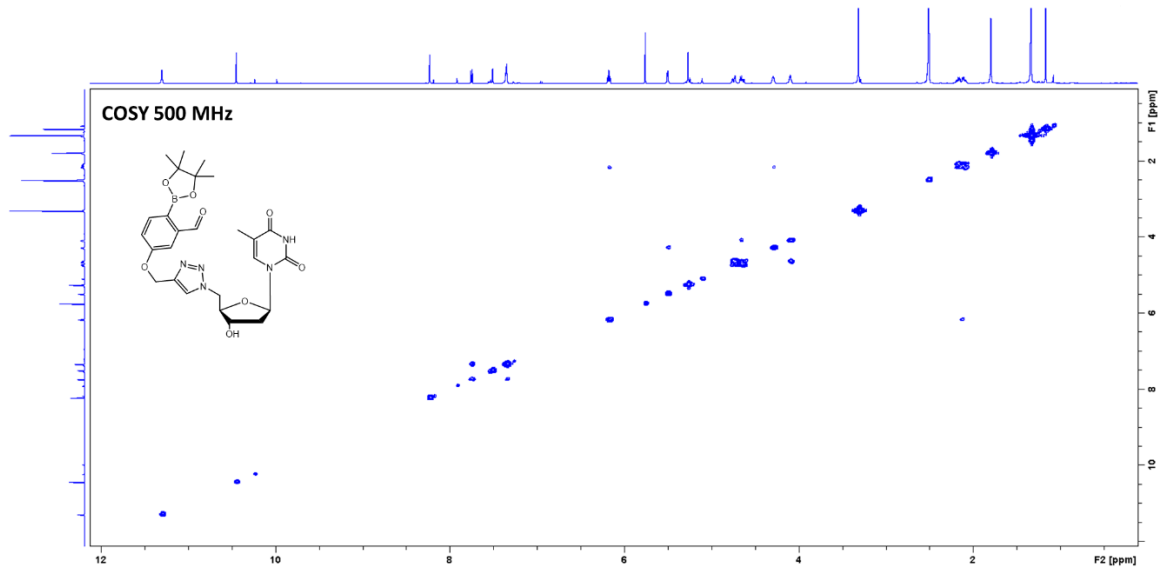
COSY NMR spectrum (500 MHz, d_6-DMSO) of **4a**.
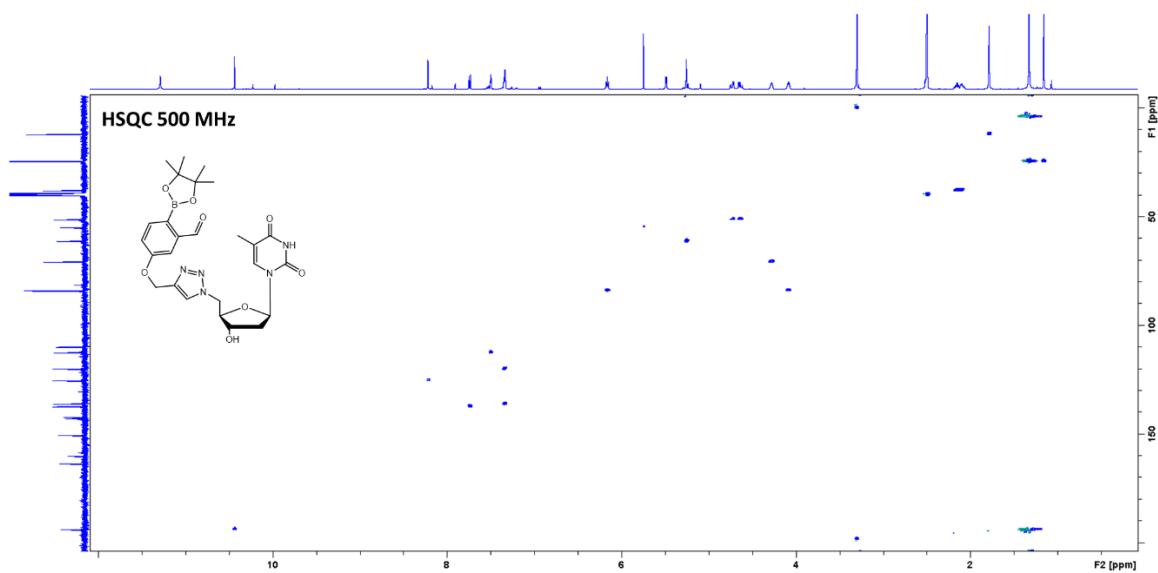
HSQC NMR spectrum (500 MHz, d_6-DMSO) of **4a**.

HMBC NMR spectrum ((500 MHz, d_6-DMSO) of **4a.**

¹H NMR spectrum (500 MHz, d_6-DMSO) of **4b**.

¹¹B NMR spectrum (160 MHz, d_6-DMSO) of **4b**.

¹³C NMR, COSY, HSQC and HMBC not acquired for **4b** due to shimming error and global pandemic.

^{1}H NMR spectrum (500 MHz, CDCl$_3$) of 2-(propyn-1-yloxy)benzene (**3c**).
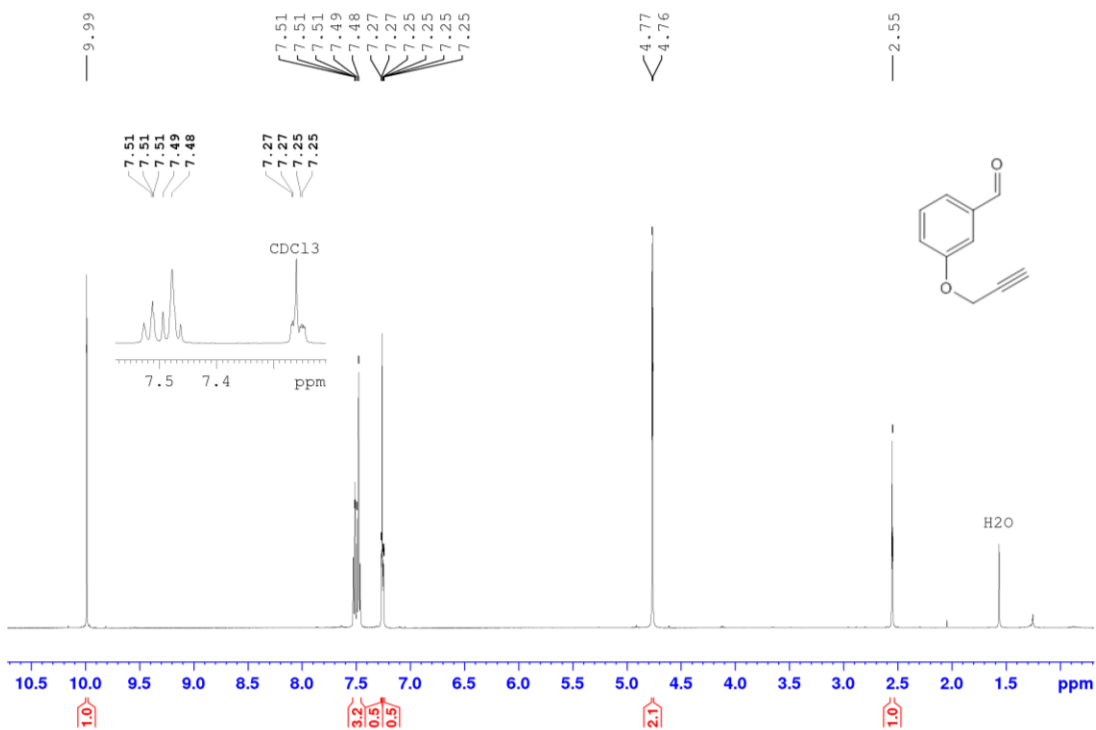
^{1}H NMR spectrum (500 MHz, CDCl$_3$) of 3-(2-propyn-1-yloxy)benzaldehyde (**3d**).
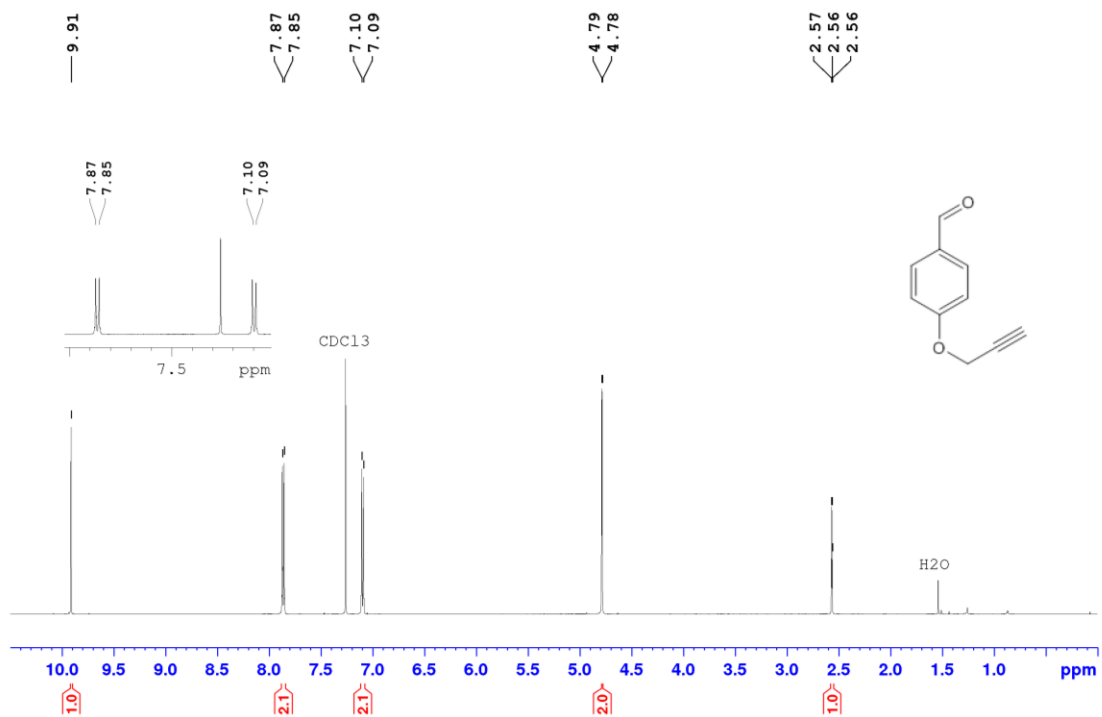
^{1}H NMR spectrum (500 MHz, CDCl$_3$) of 4-(2-propyn-1-yloxy)benzaldehyde (**3e**).
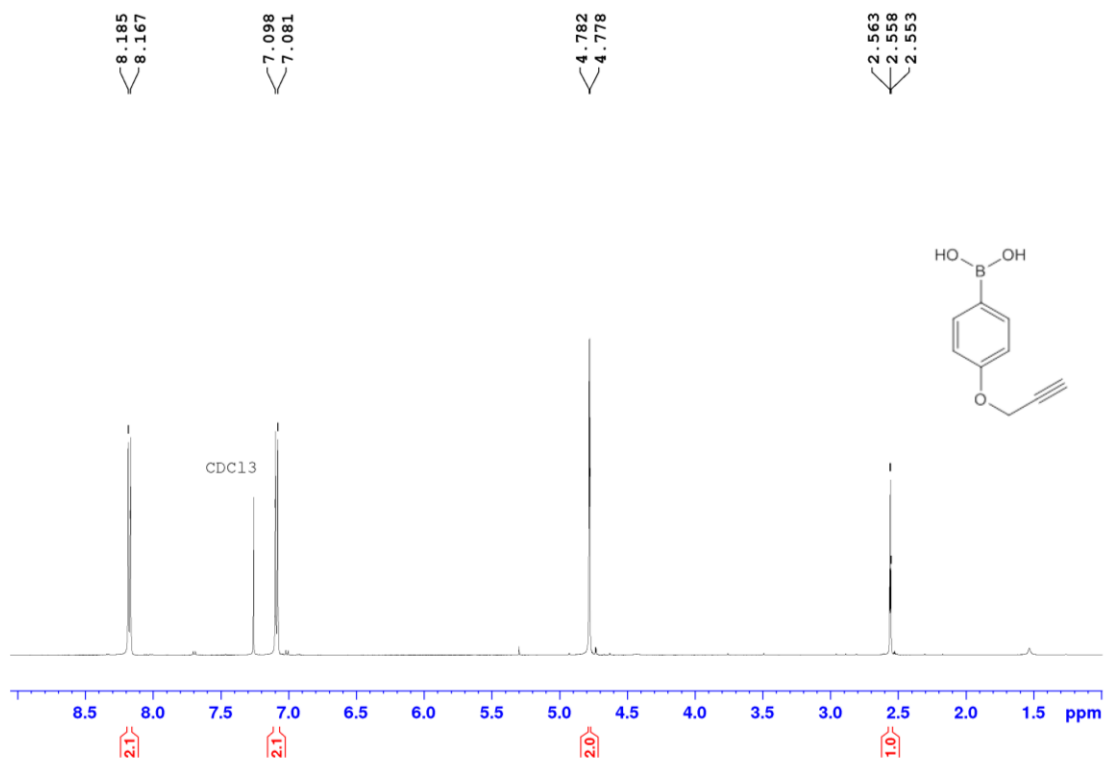
^{1}H NMR spectrum (500 MHz, CDCl$_3$) of 4-(2-propyn-1-yloxy)phenylboronic acid (**3f**).
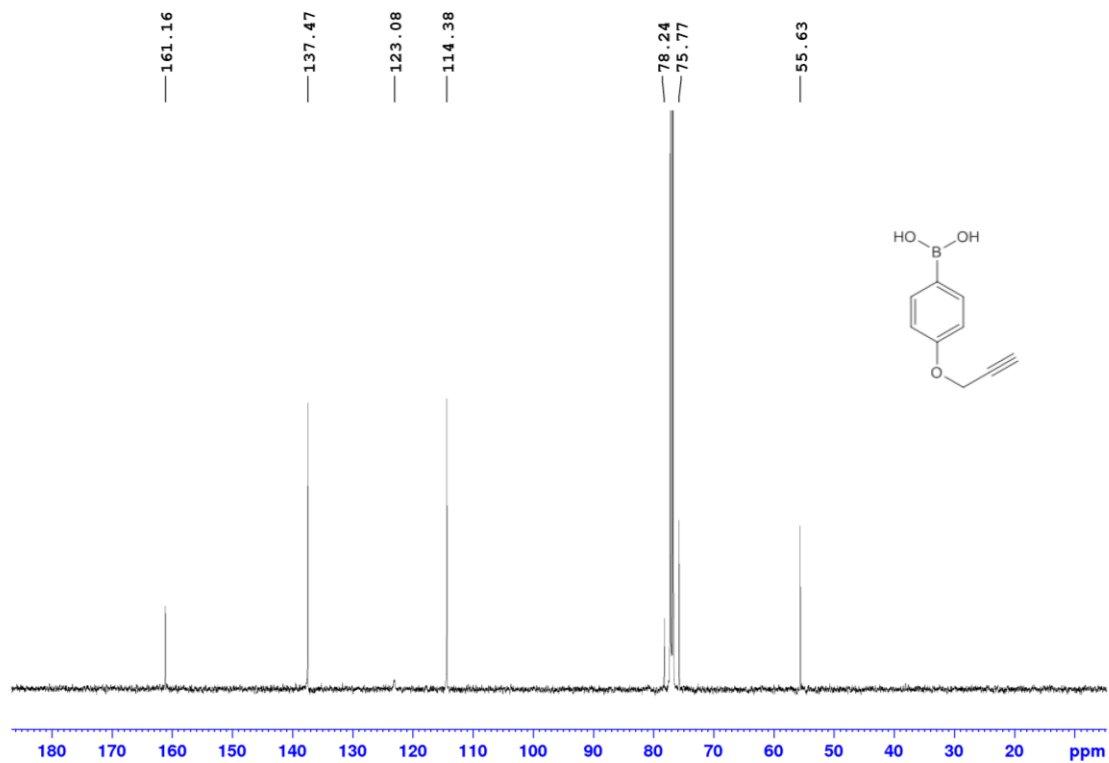
^{13}C NMR spectrum (126 MHz, CDCl$_3$) of 4-(2-propyn-1-yloxy)phenylboronic acid (**3f**).
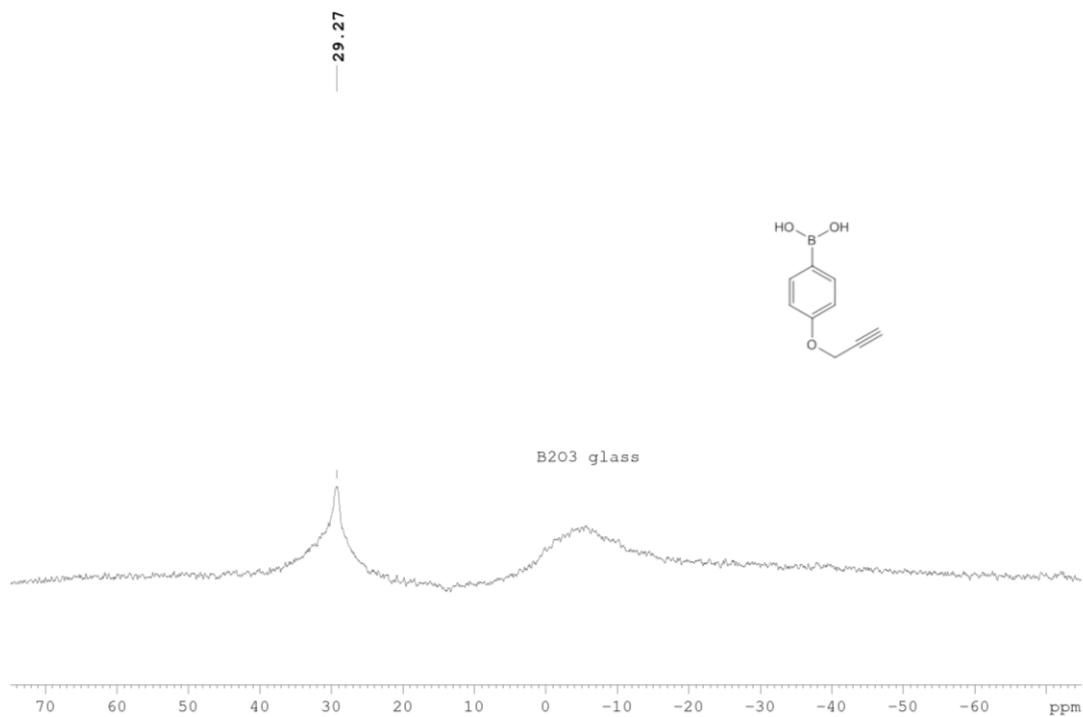
^{11}B NMR spectrum (160 MHz, CDCl$_3$) of 4-(2-propyn-1-yloxy)phenylboronic acid (**3f**).
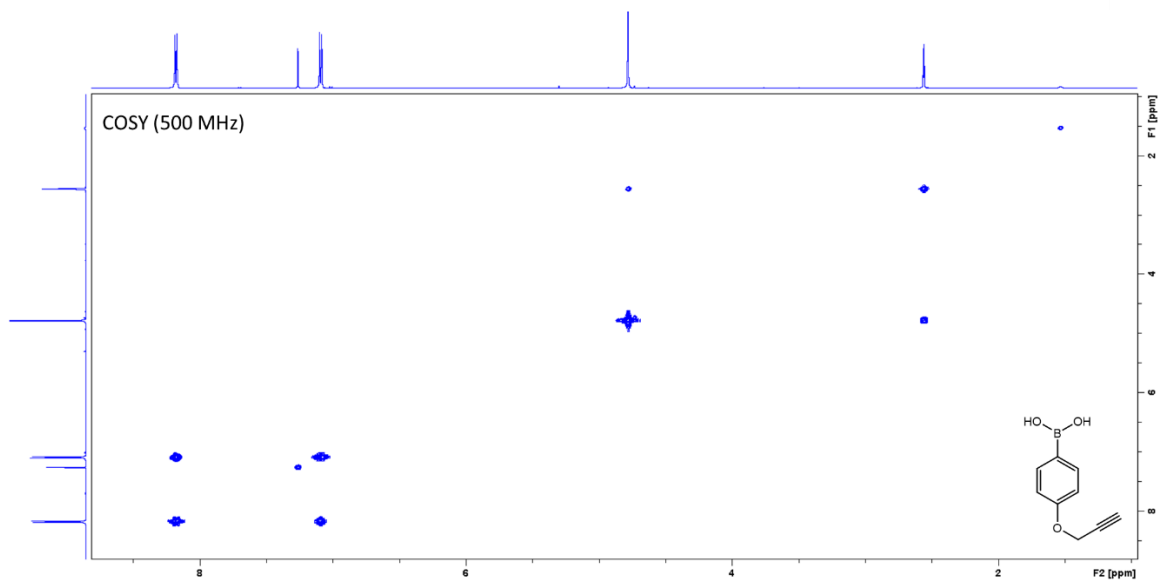
COSY NMR spectrum (500 MHz, CDCl$_3$) of 4-(2-propyn-1-yloxy)phenylboronic acid (**3f**).
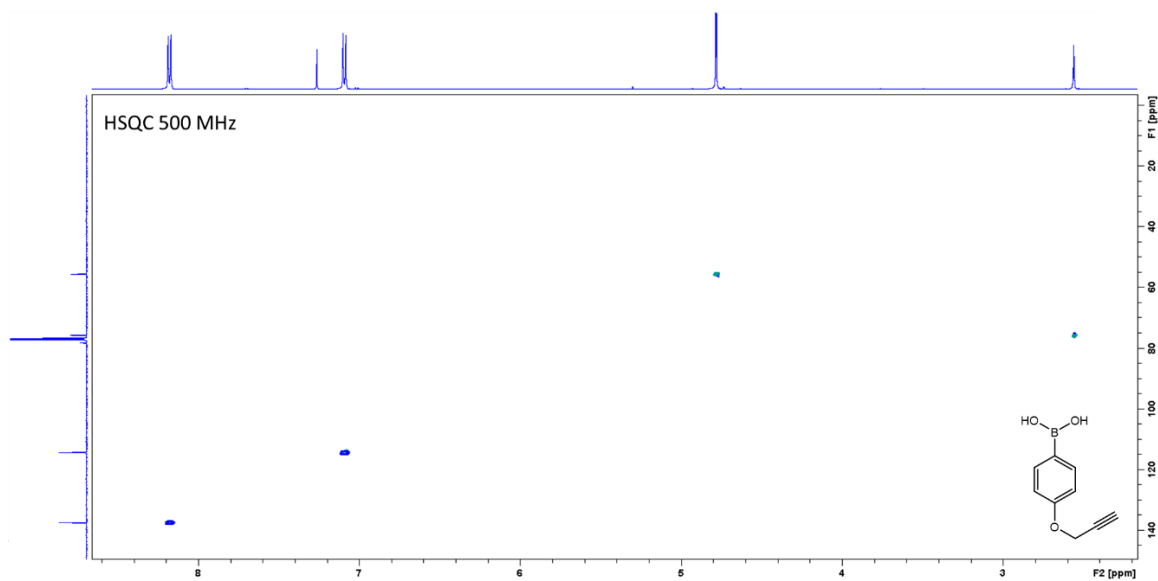
HSQC NMR spectrum (500 MHz, CDCl$_3$) of 4-(2-propyn-1-yloxy)phenylboronic acid (**3f**).
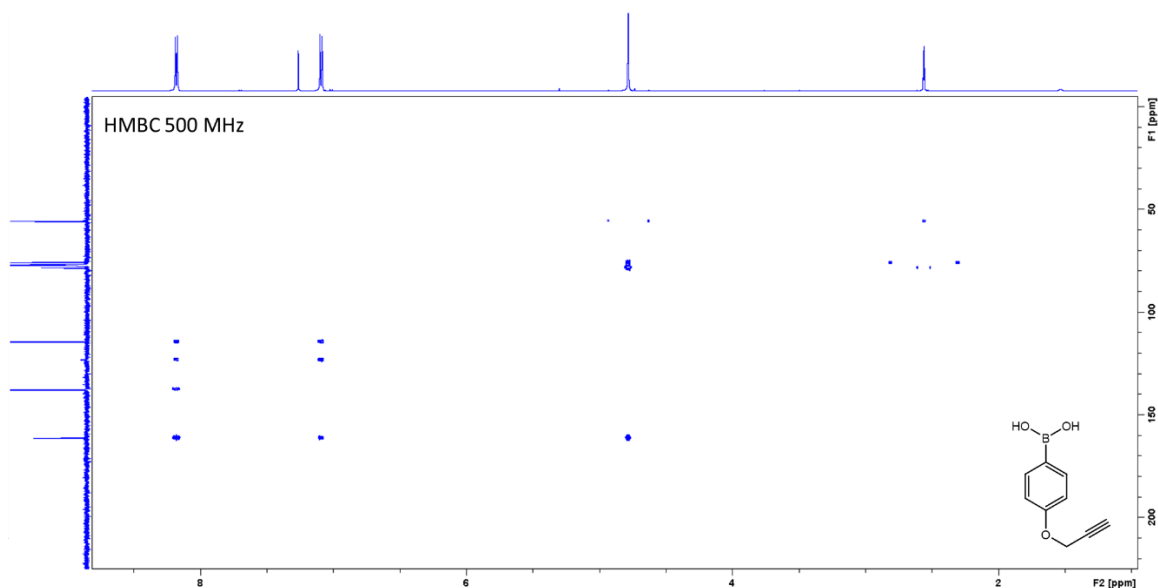
HMBC NMR spectrum (500 MHz, CDCl₃) of 4-(2-propyn-1-yloxy)phenylboronic acid (**3f**).
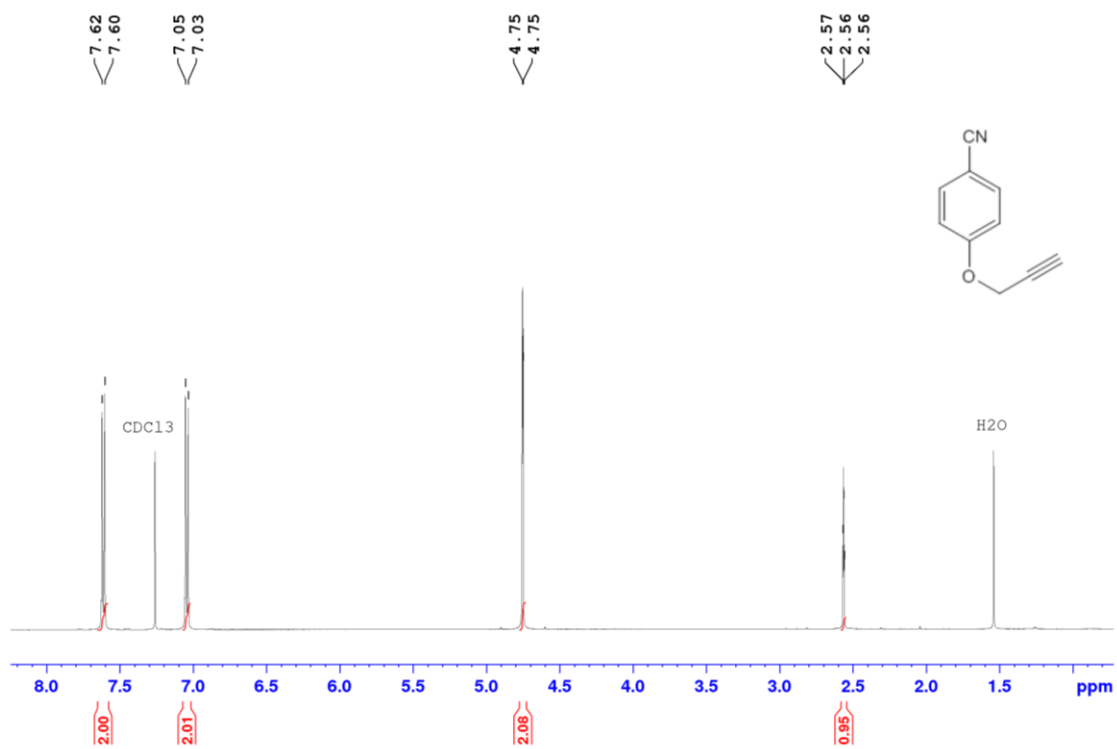
¹H NMR spectrum (500 MHz, CDCl₃) of 4-(2-propyn-1-yloxy)benzonitrile (**3g**).
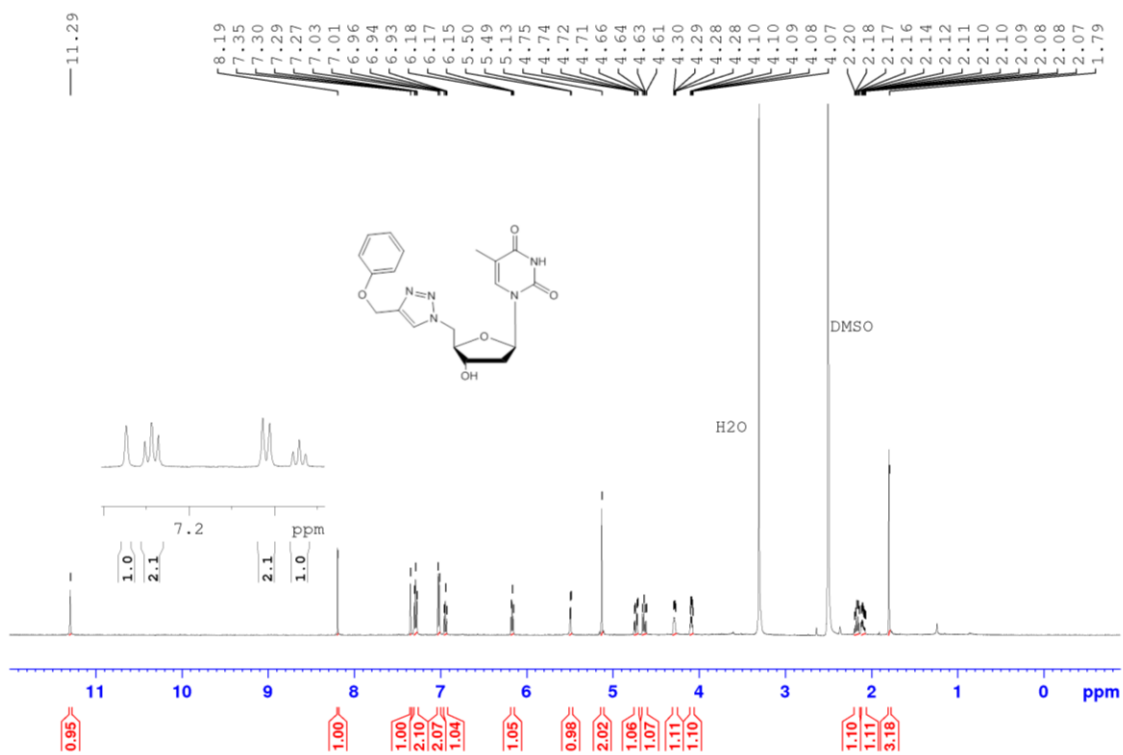
^{1}H NMR spectrum (500 MHz, d_6-DMSO) of **4c**.
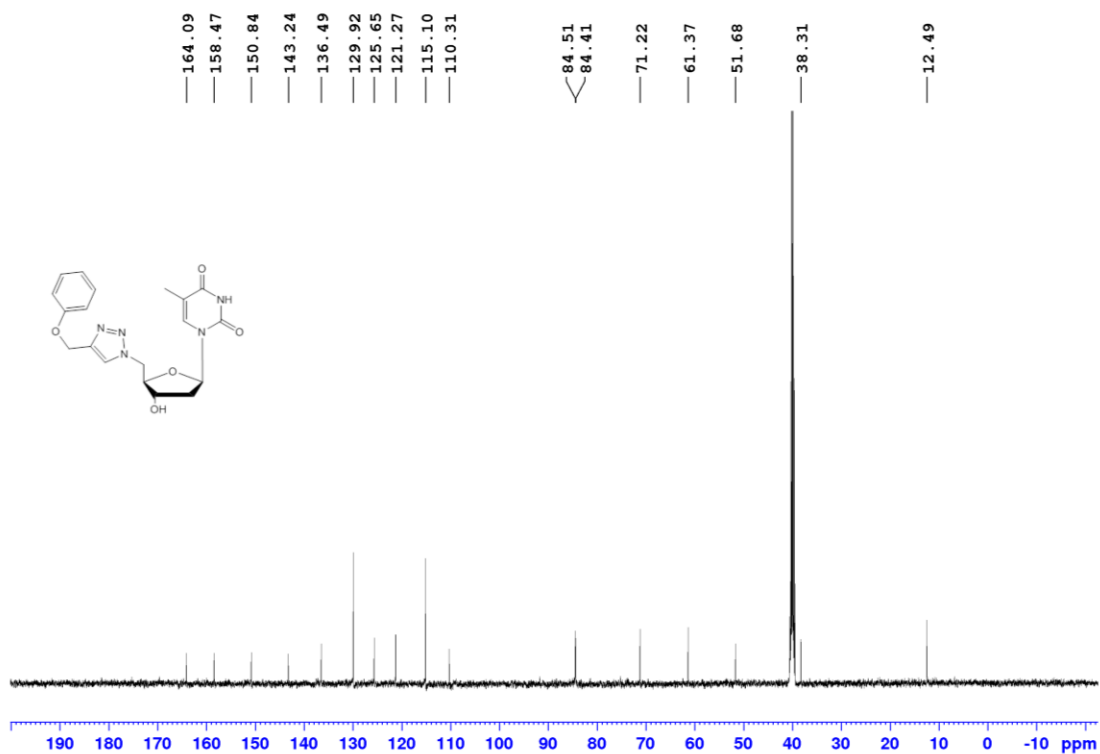
¹³C NMR spectrum (126 MHz, *d₆*-DMSO) of **4c**.
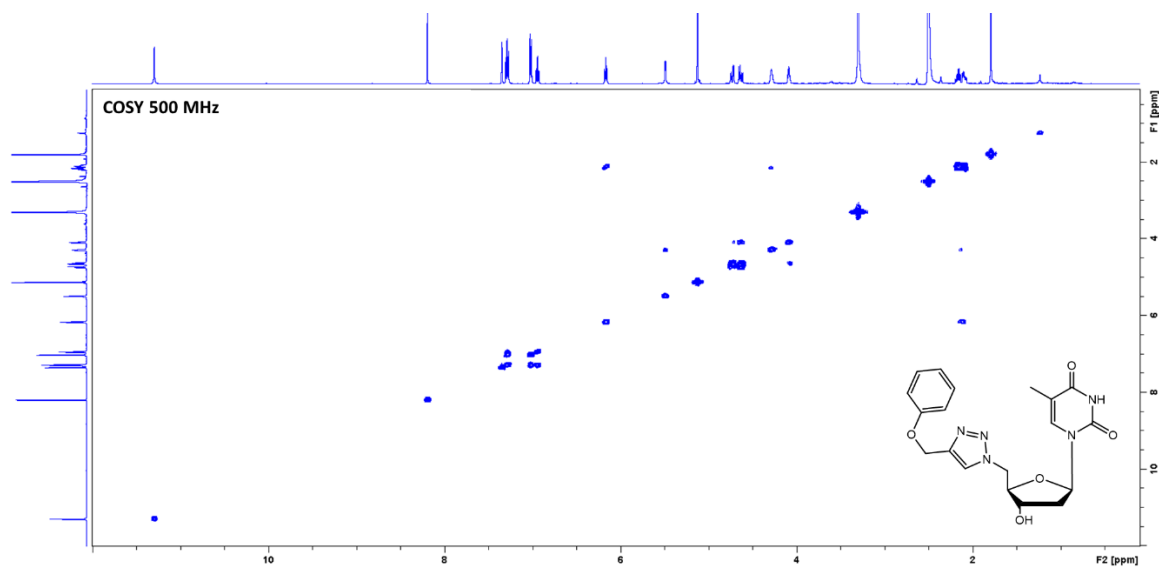
COSY NMR spectrum (500 MHz, *d₆*-DMSO) of **4c**.
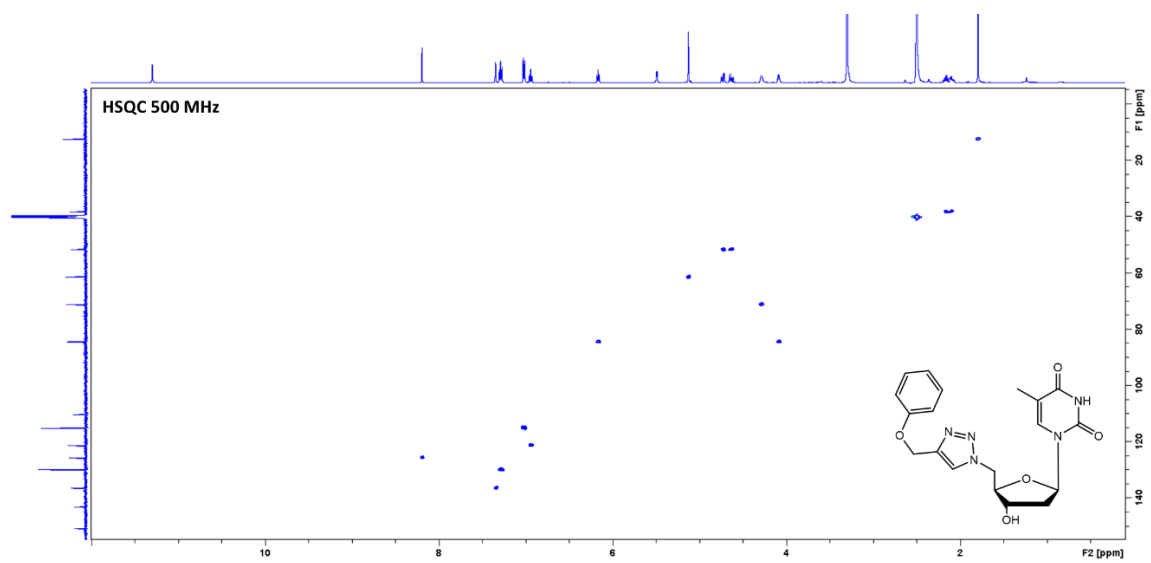
HSQC NMR spectrum (500 MHz, *d₆*-DMSO) of **4c**.
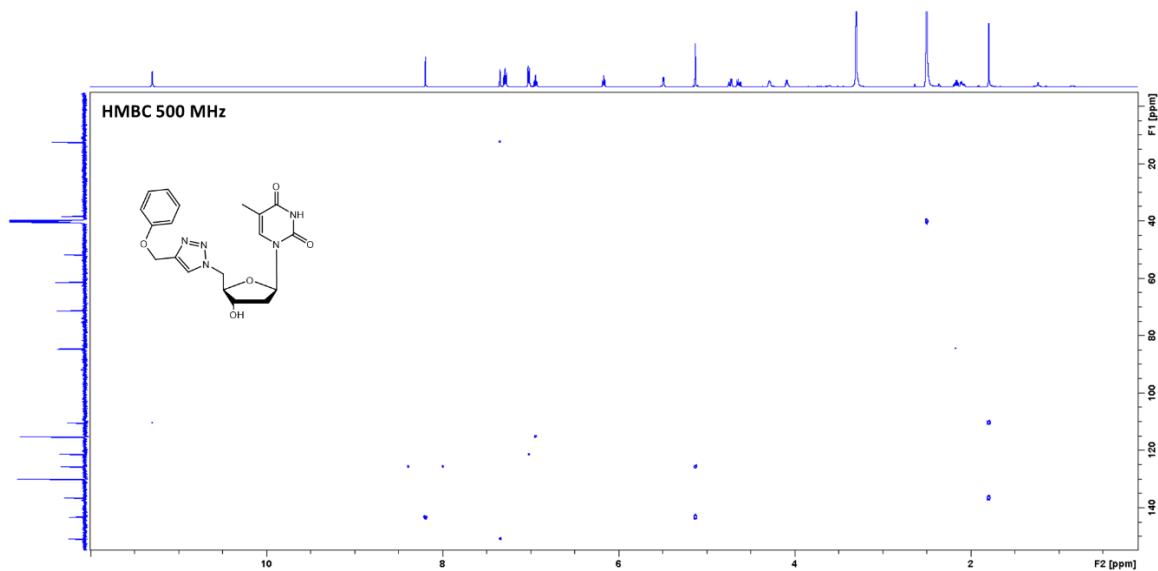
HMBC NMR spectrum (500 MHz, d_6-DMSO) of **4c**.
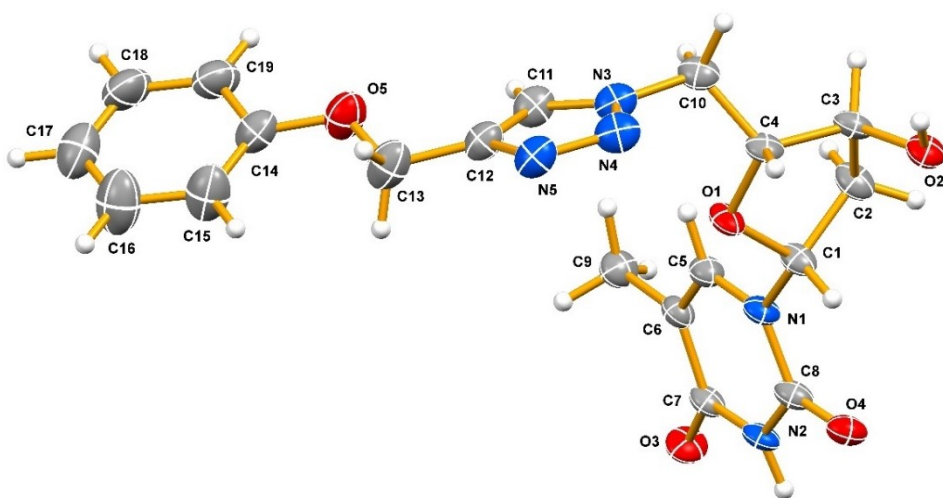
ORTEP diagram of **4c**.
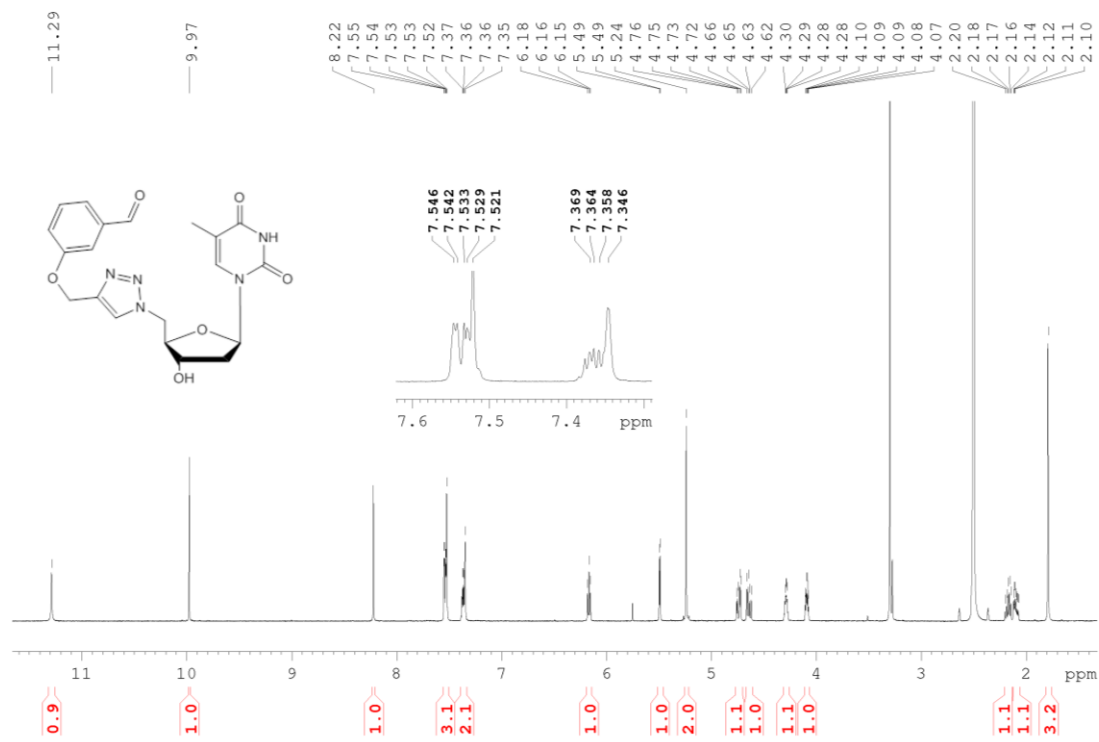
^{1}H NMR spectrum (500 MHz, d_6-DMSO) of **4d**.
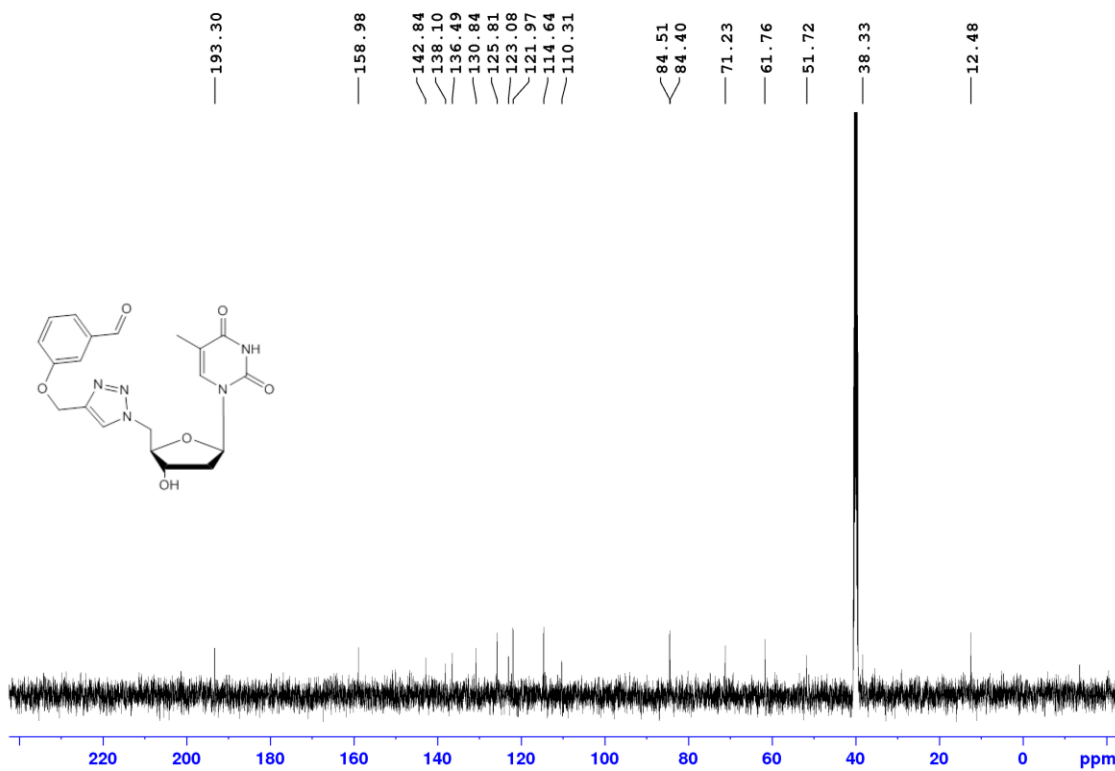
^{13}C NMR spectrum (126 MHz, d_6-DMSO) of **4d**.
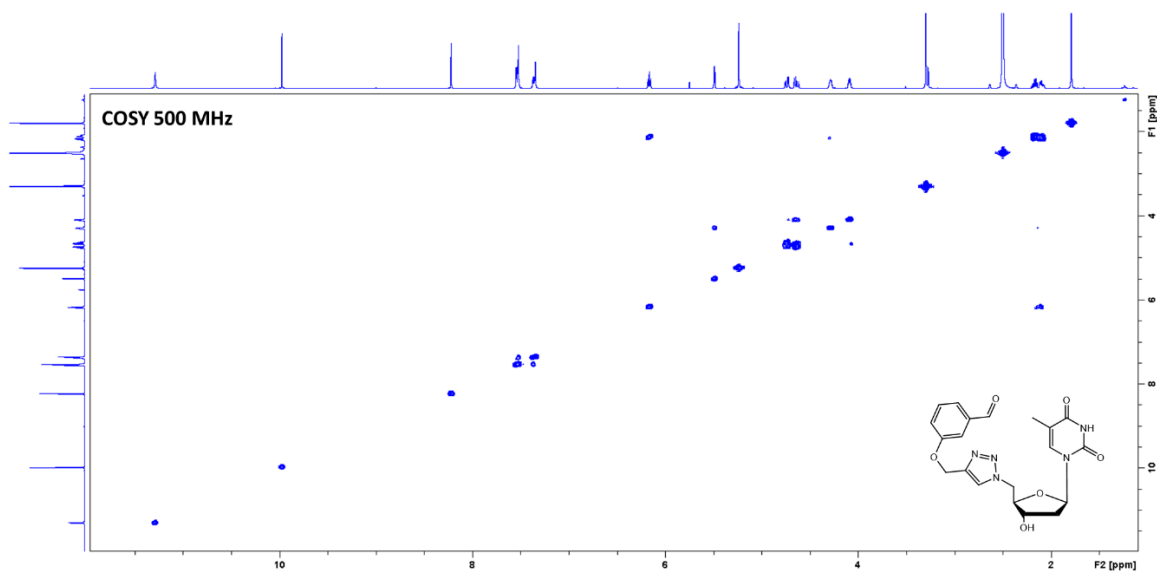
COSY NMR spectrum (500 MHz, d_6-DMSO) of **4d**.
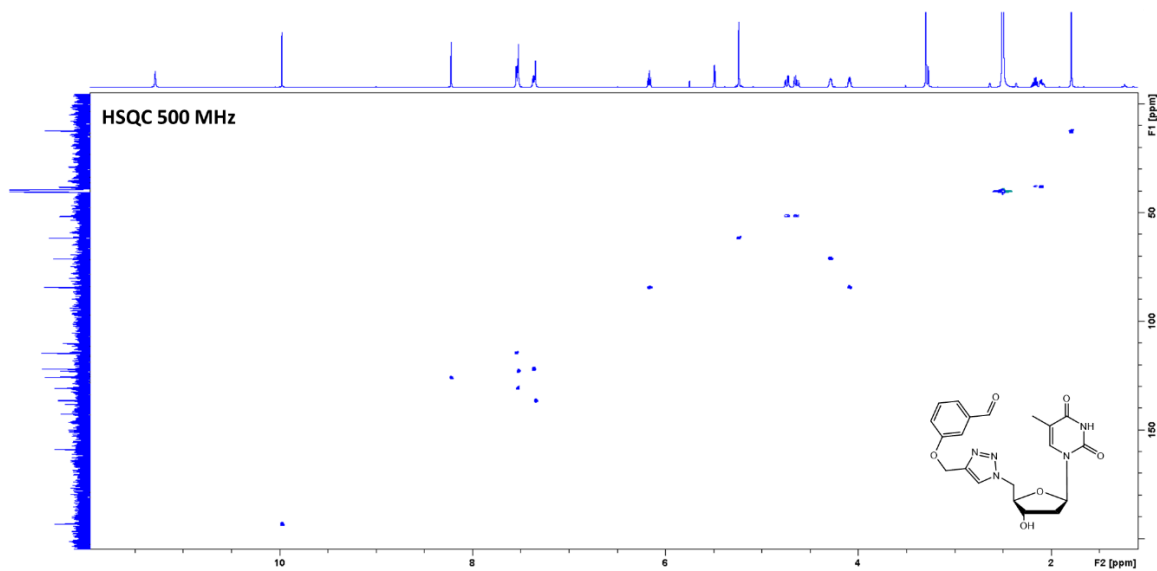
HSQC NMR spectrum (500 MHz, d_6-DMSO) of **4d**.
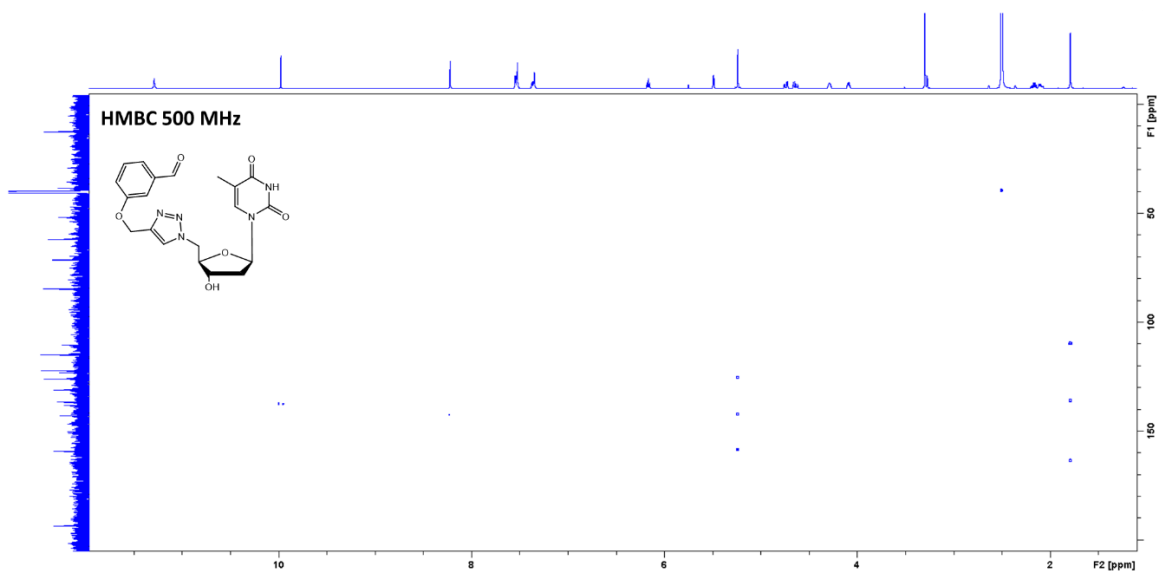
HMBC NMR spectrum (500 MHz, d_6-DMSO) of **4d**.
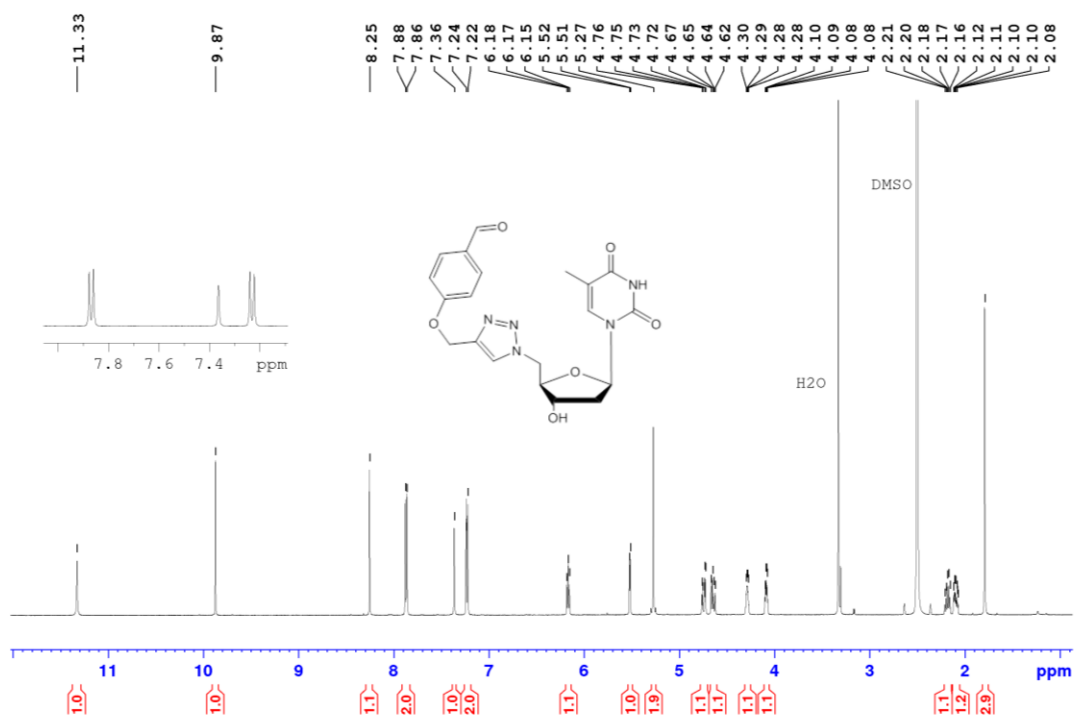
^{1}H NMR spectrum (500 MHz, d_6-DMSO) of **4e**.
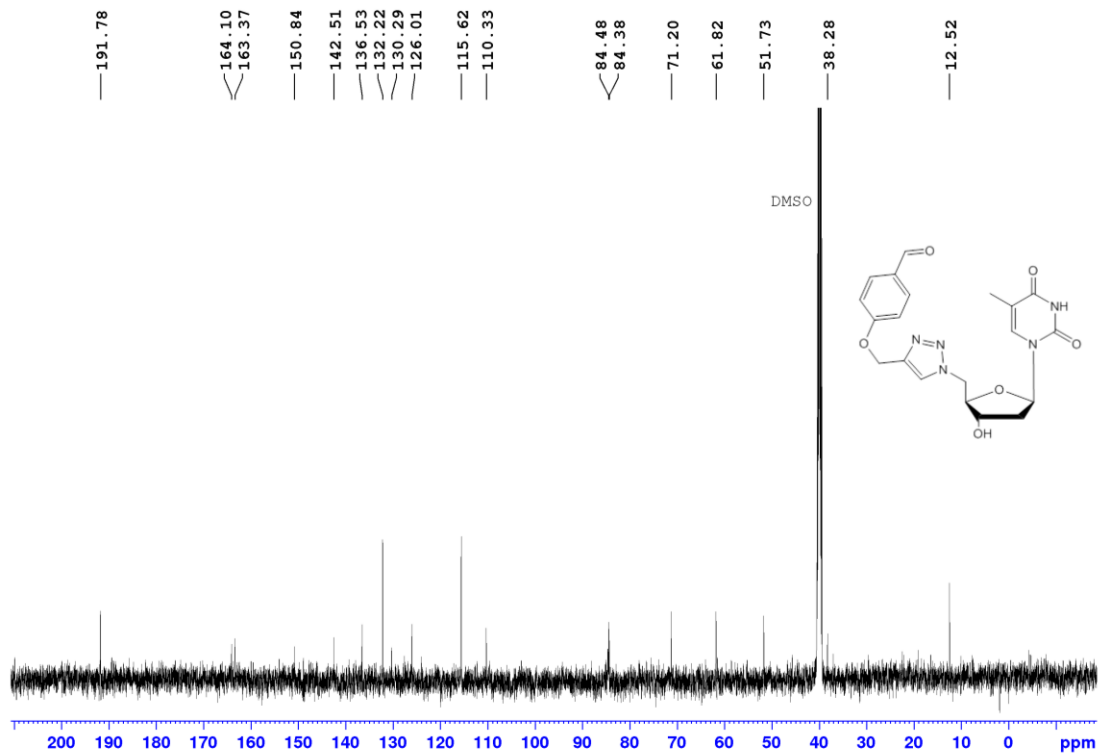
^{13}C NMR spectrum (126 MHz, d_6-DMSO) of **4e**.
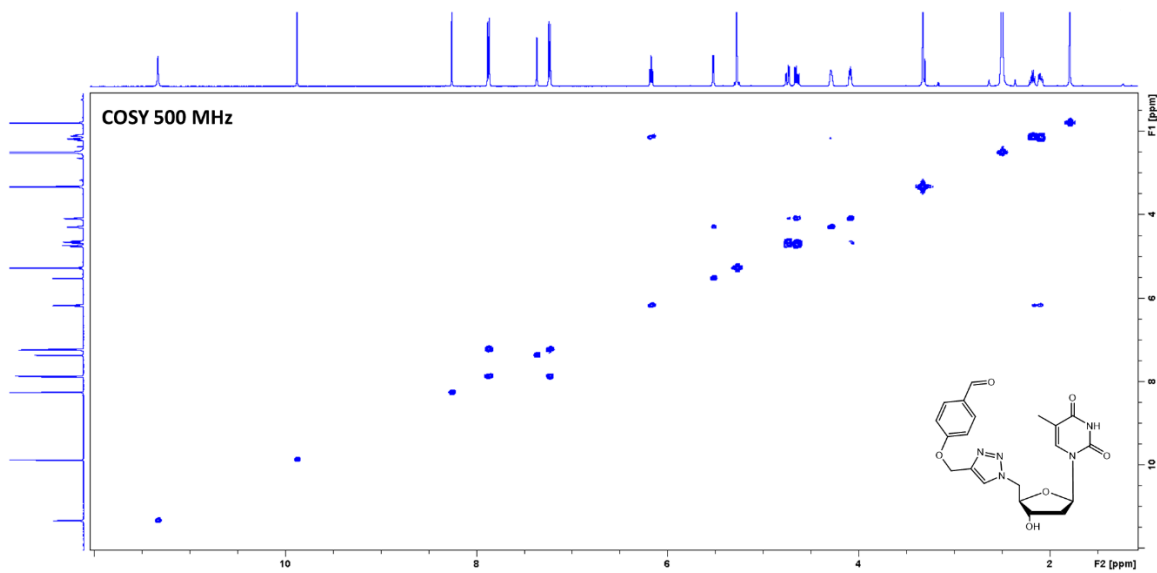
COSY NMR spectrum (500 MHz, d_6-DMSO) of **4e**.
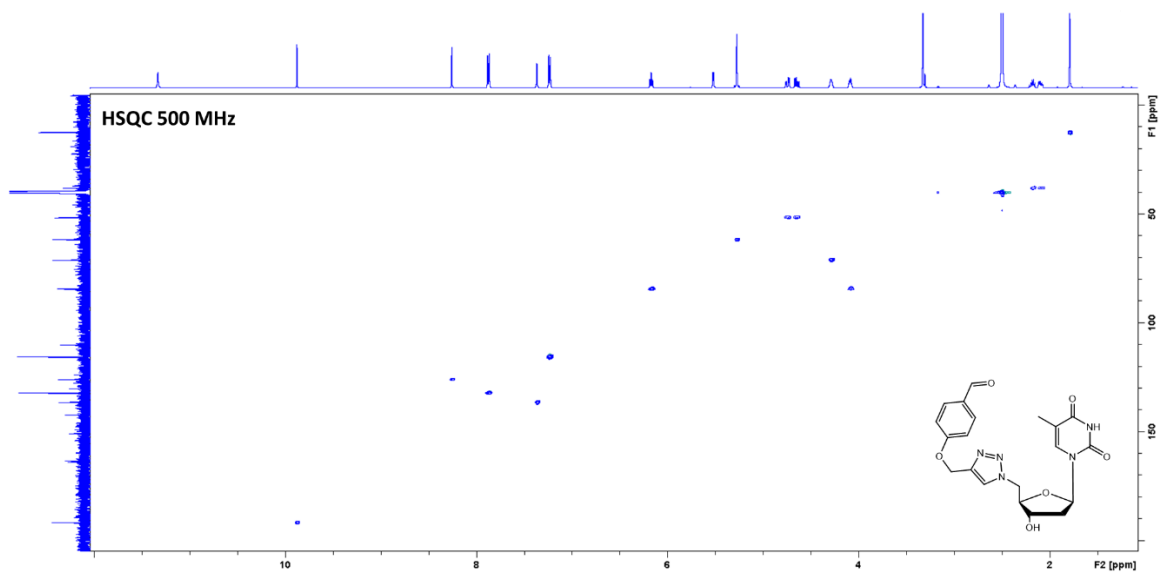
HSQC NMR spectrum (500 MHz, d_6-DMSO) of **4e**.
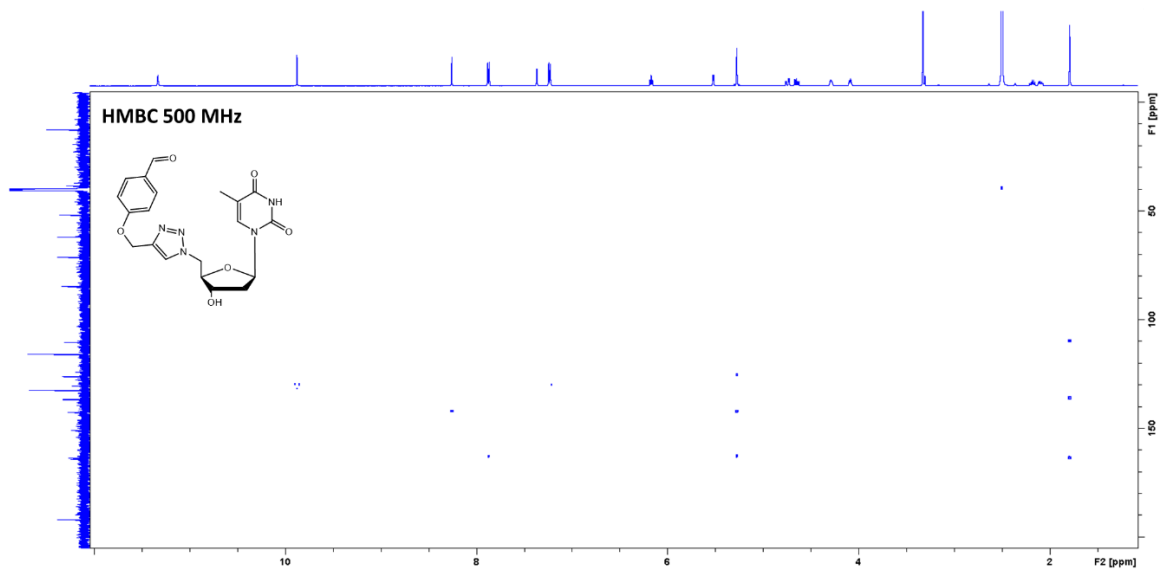
HMBC NMR spectrum (500 MHz, d_6-DMSO) of **4e**.
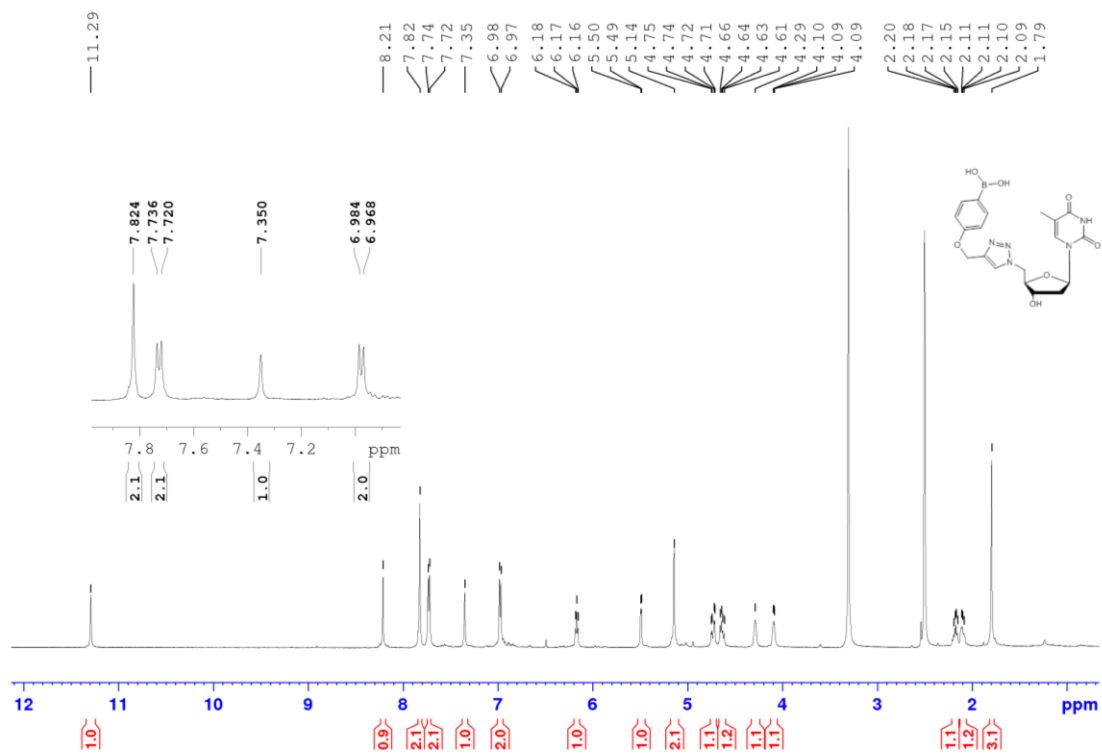
^{1}H NMR spectrum (500 MHz, d_6-DMSO) of **4f**.
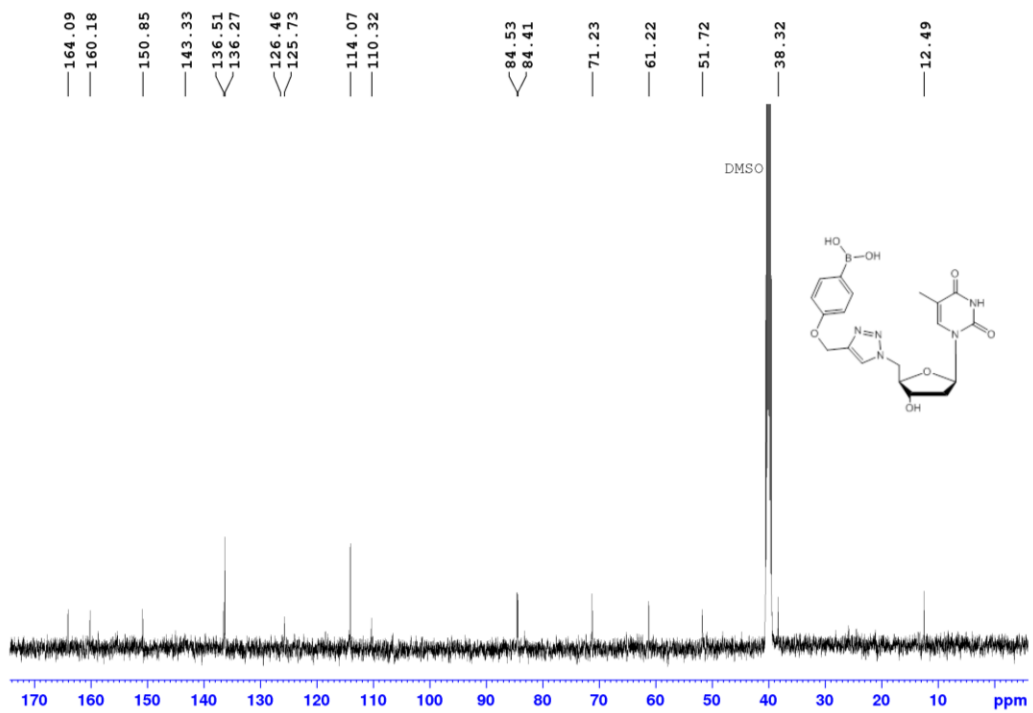
^{13}C NMR spectrum (126 MHz, d_6-DMSO) of **4f**.
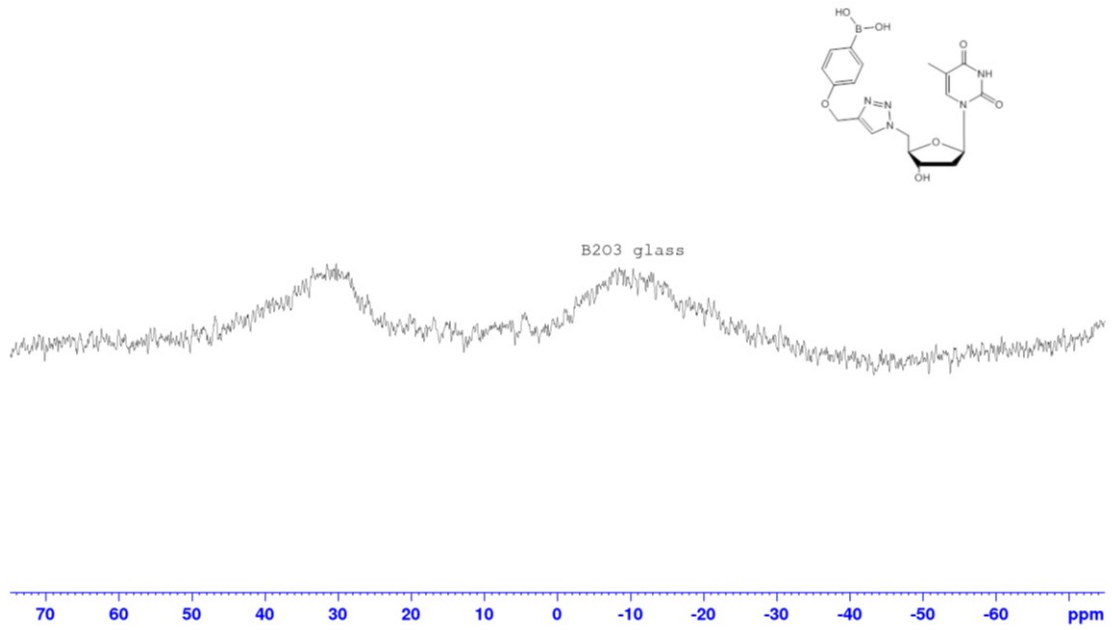
^{11}B NMR spectrum (160 MHz, d_6-DMSO) of **4f**.
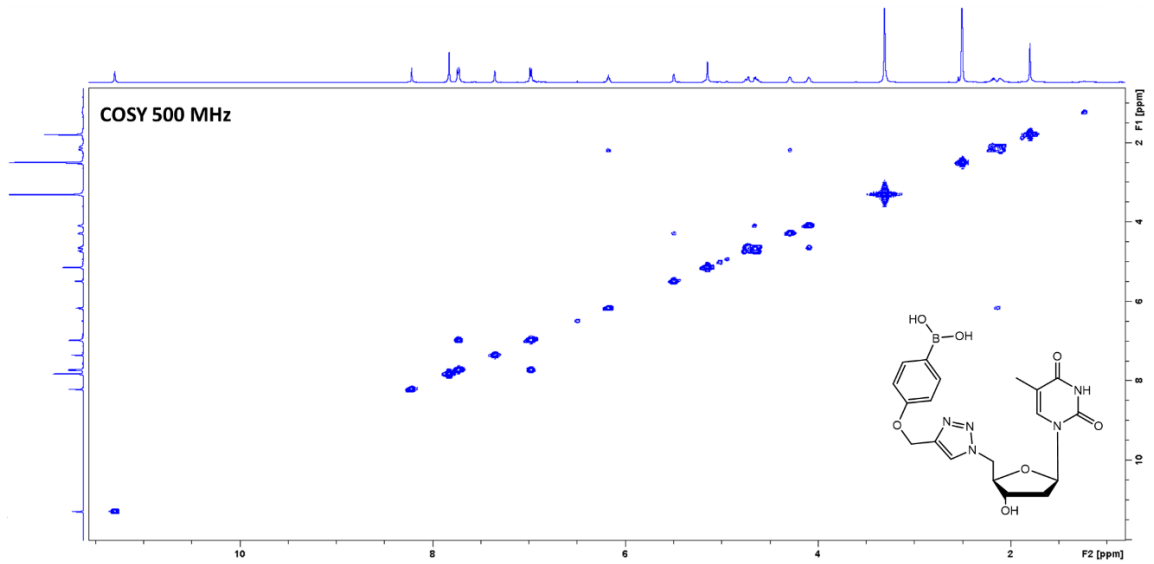
COSY NMR spectrum (500 MHz, d_6-DMSO) of **4f**.
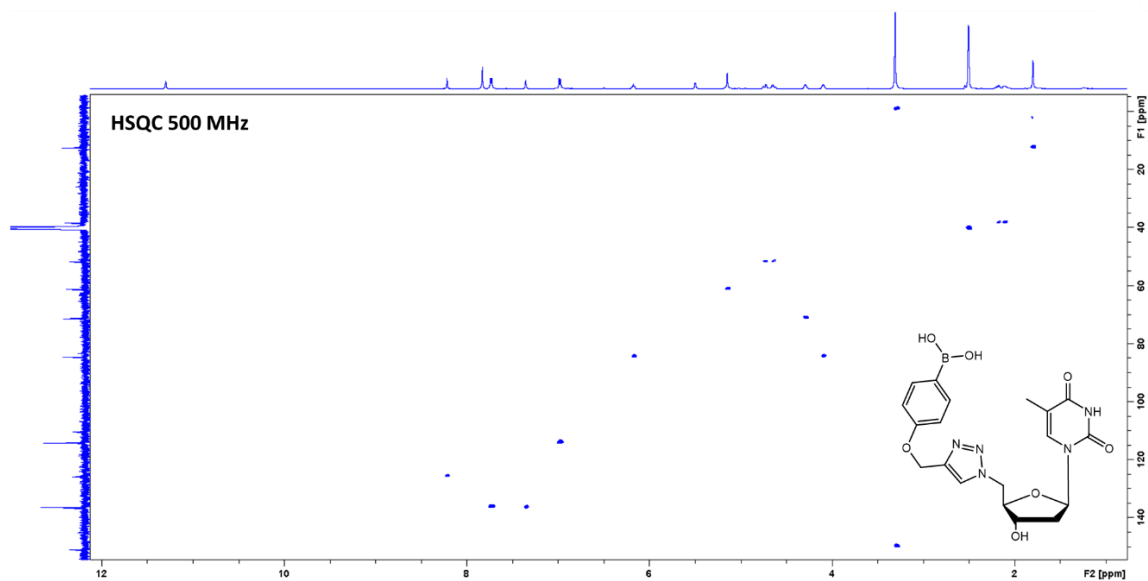
HSQC NMR spectrum (500 MHz, d_6-DMSO) of **4f**.
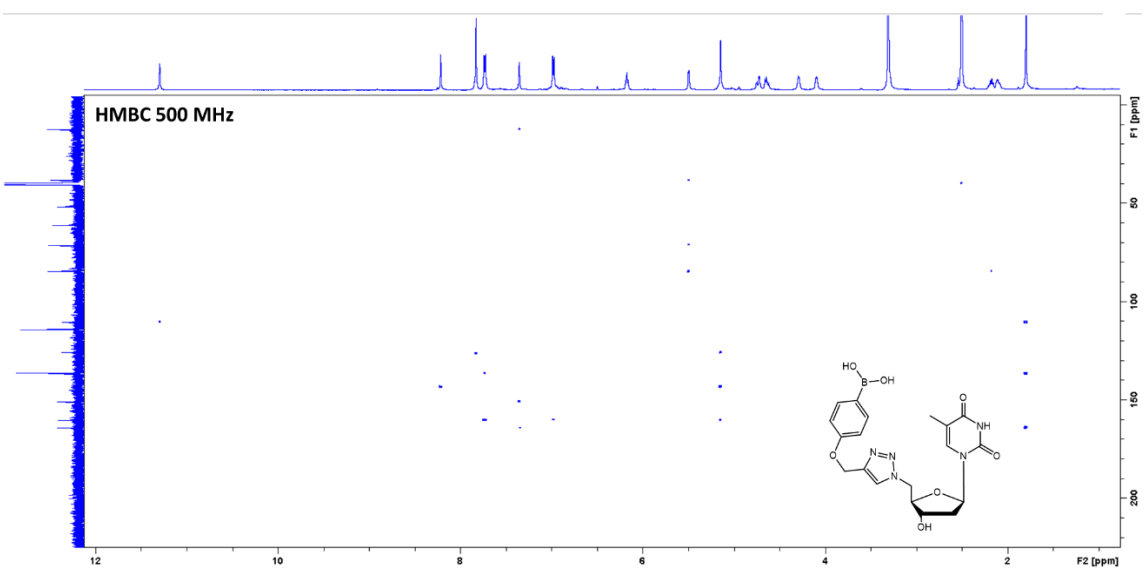
HMBC NMR spectrum (500 MHz, d_6-DMSO) of **4f**.
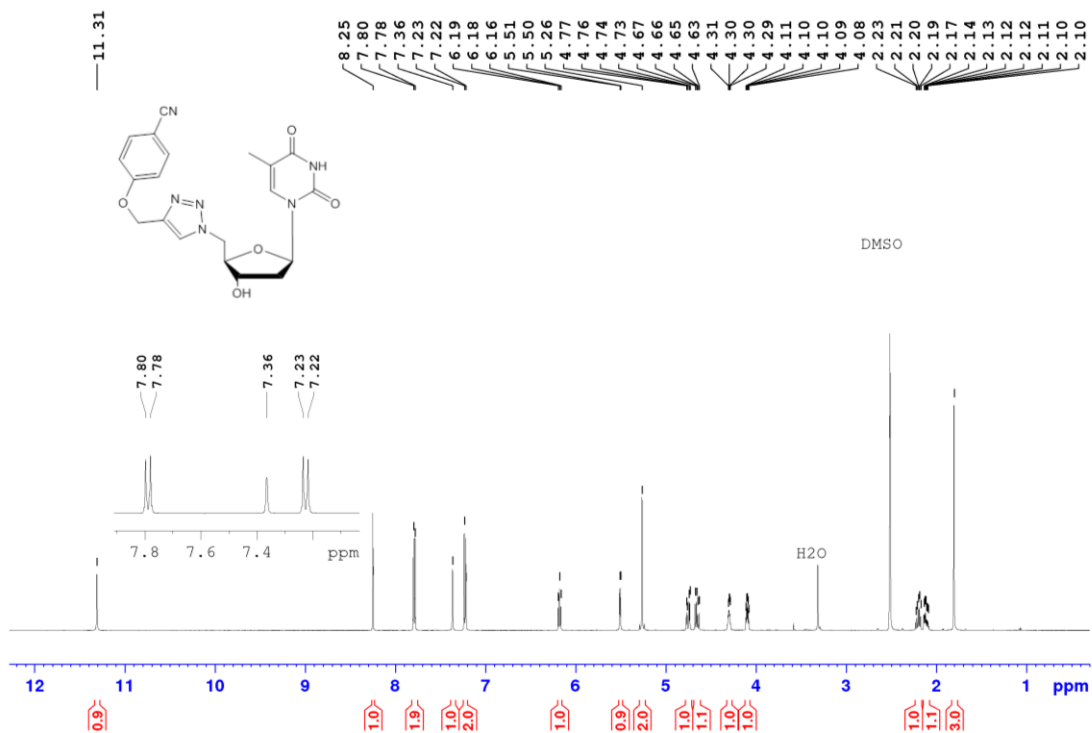
^{1}H NMR spectrum (500 MHz, d_6-DMSO) of **4g**.
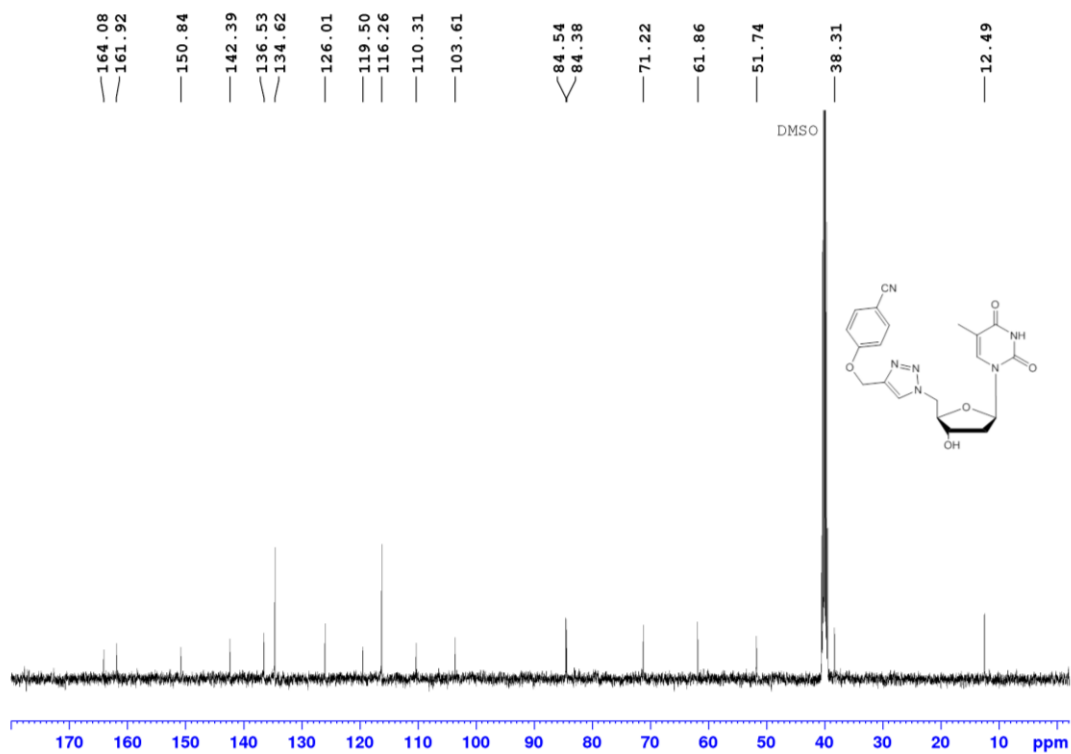
^{13}C NMR spectrum (126 MHz, d_6-DMSO) of **4g**.
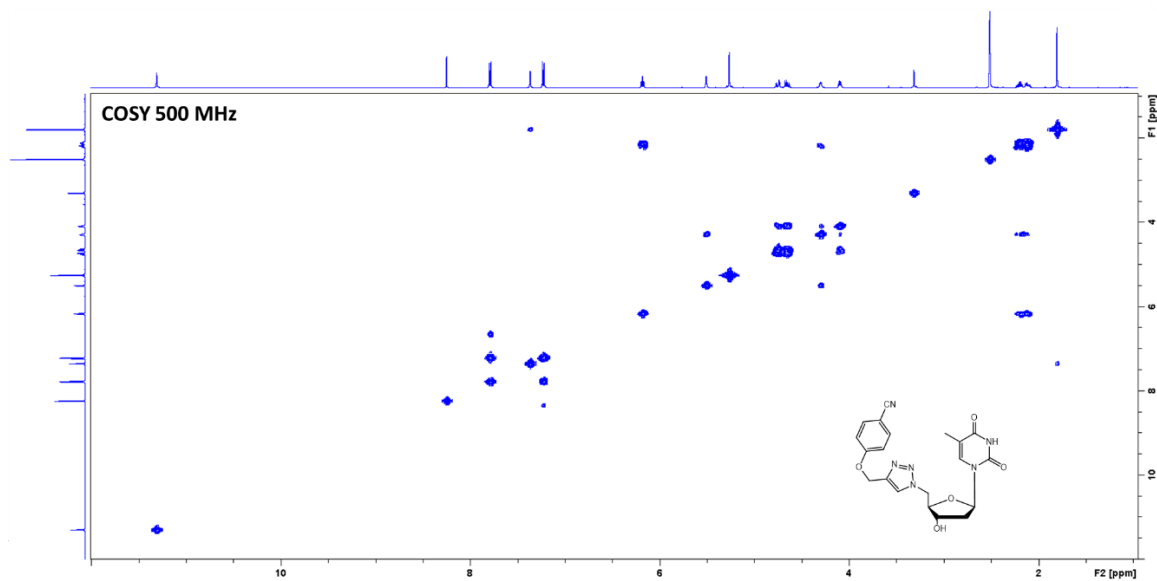
COSY NMR spectrum (500 MHz, *d₆*-DMSO) of **4g**.
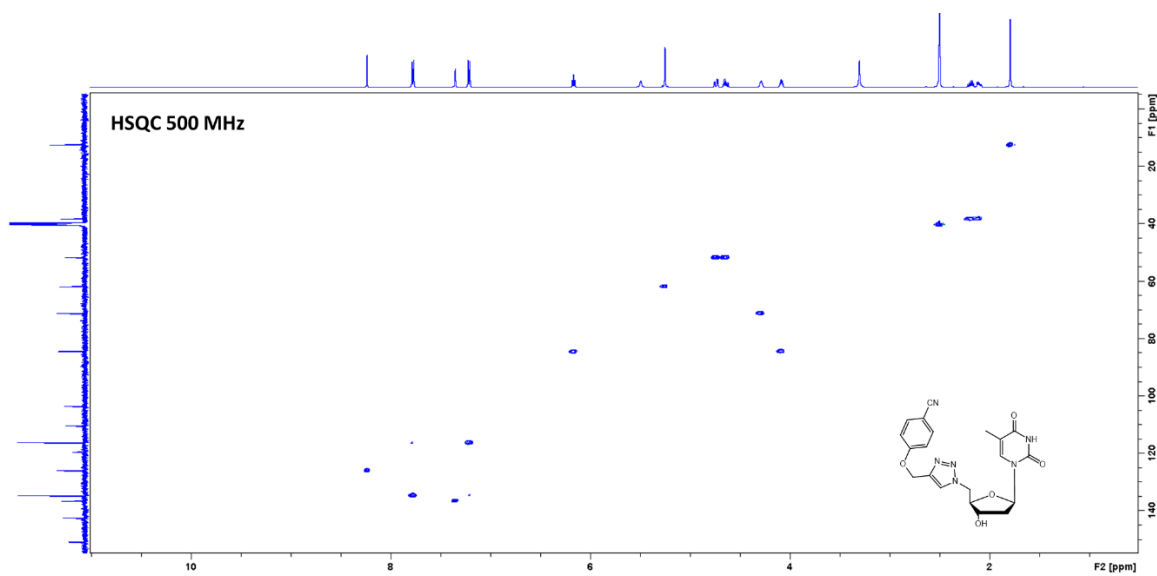
HSQC NMR spectrum (500 MHz, *d₆*-DMSO) of **4g**.
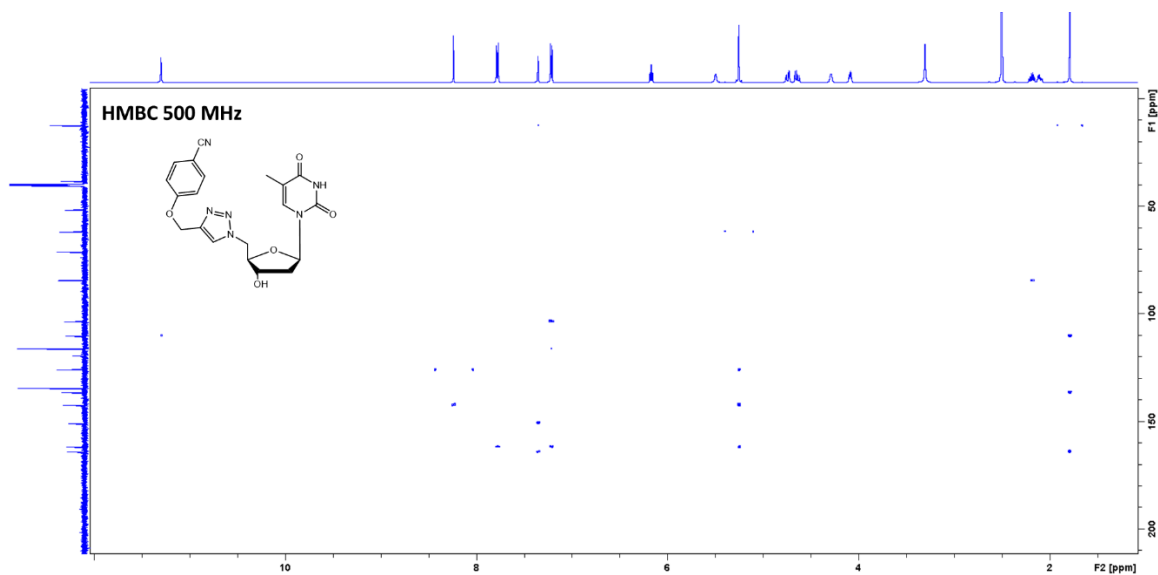
HMBC NMR spectrum (500 MHz, d_6-DMSO) of **4g**.
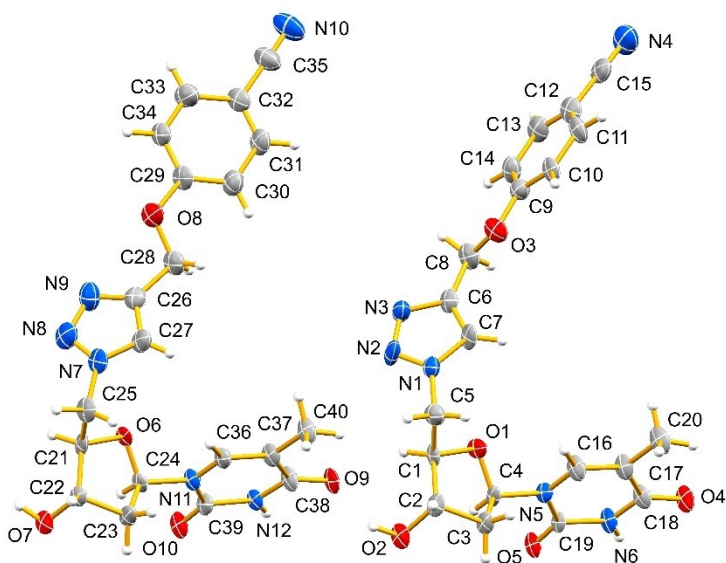
ORTEP diagram of **4g**.
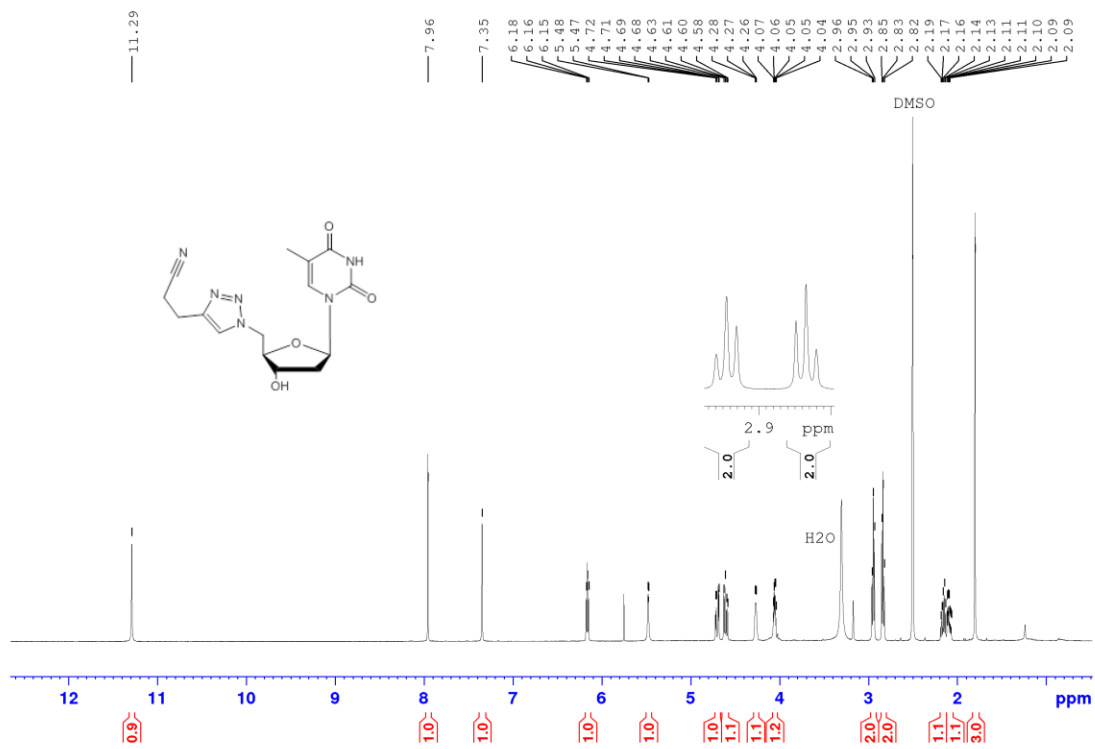
^{1}H NMR spectrum (500 MHz, d_6-DMSO) of **7**.
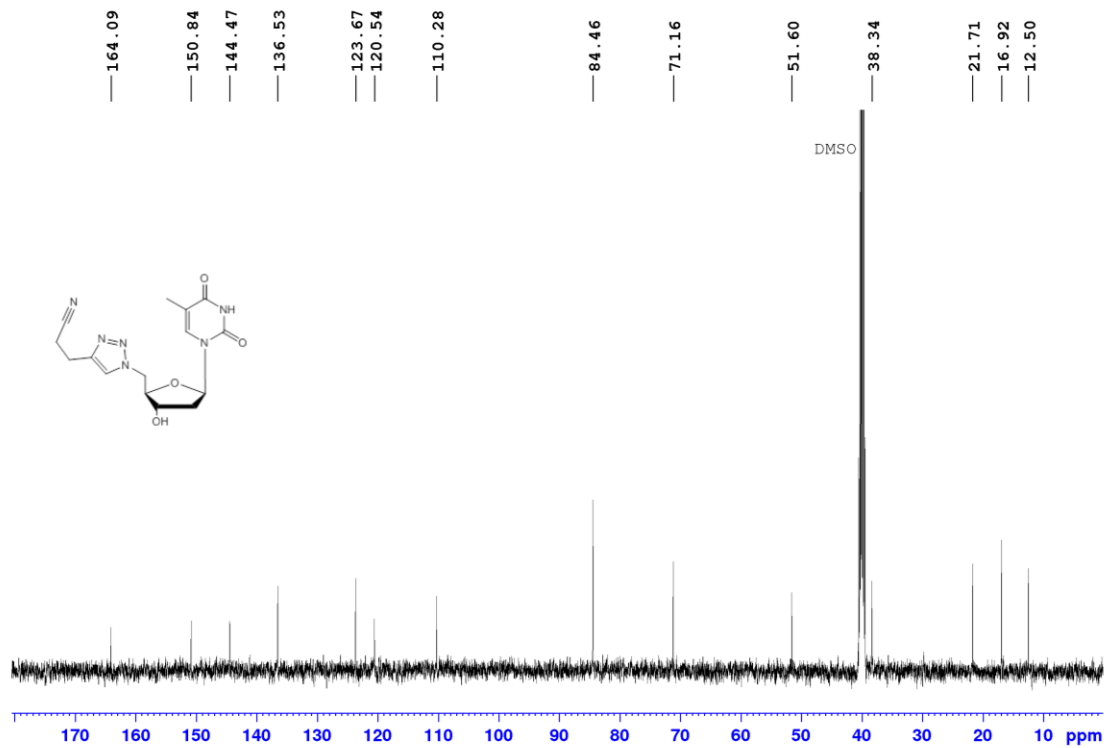
^{13}C NMR spectrum (126 MHz, d_6-DMSO) of **7**.
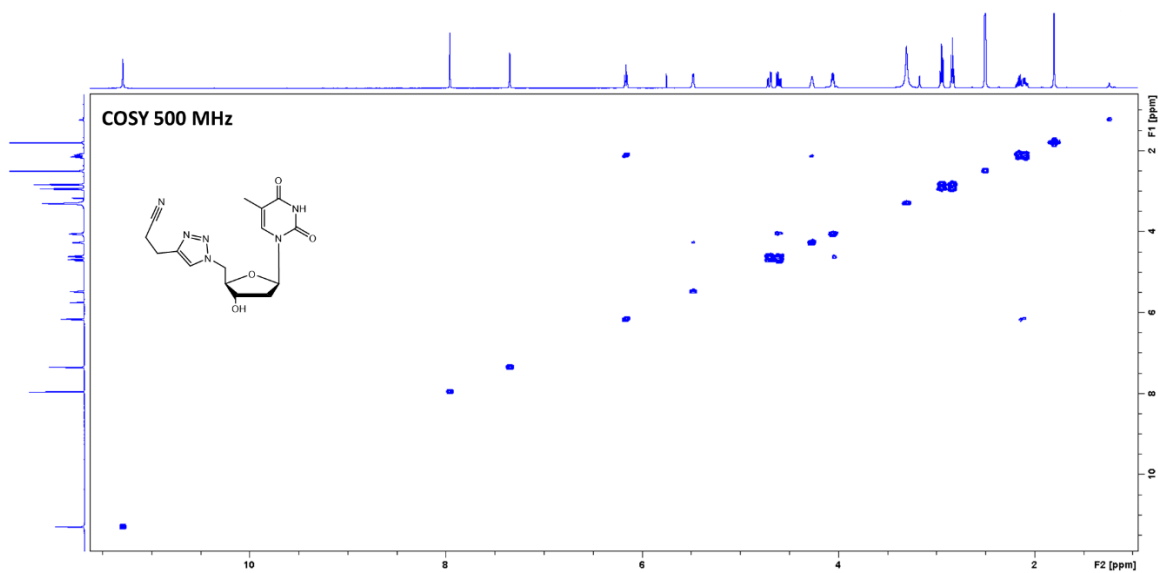
COSY NMR spectrum (500 MHz, d_6-DMSO) of **7**.
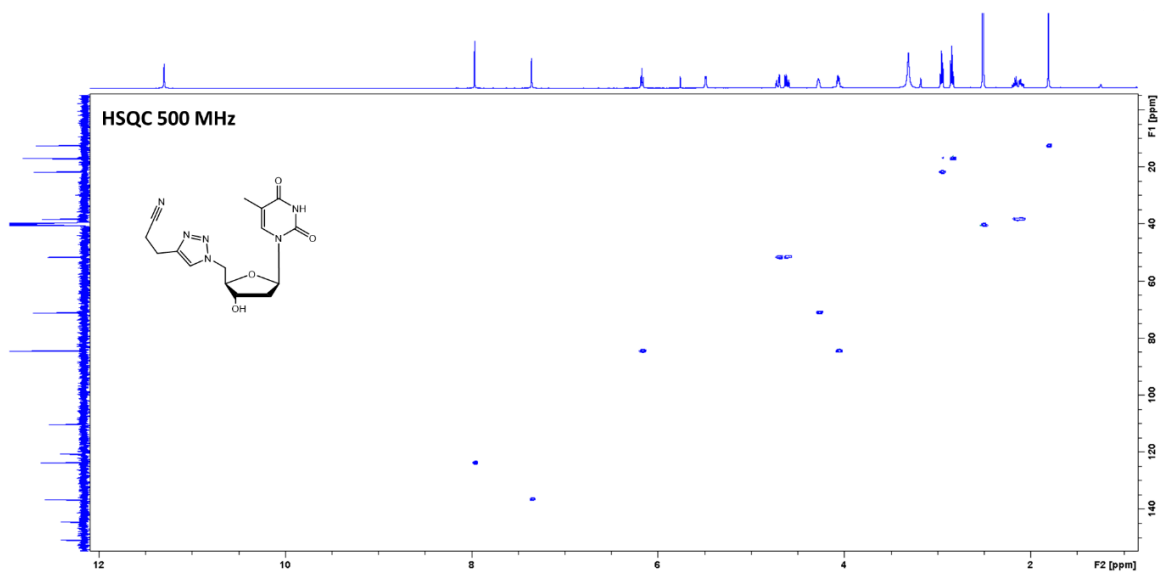
HSQC NMR spectrum (500 MHz, d_6-DMSO) of **7**.
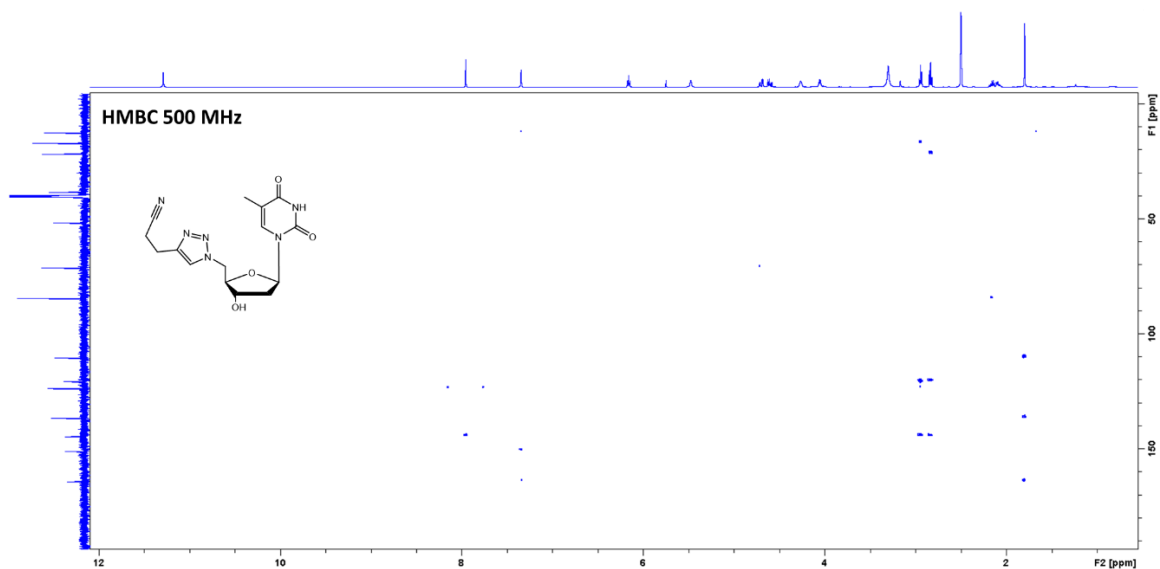
HMBC NMR spectrum (500 MHz, d_6-DMSO) of **7**.
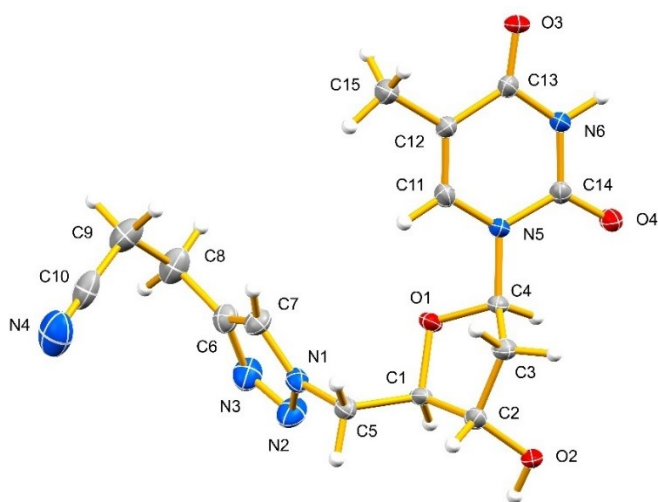
ORTEP diagram of **7**.
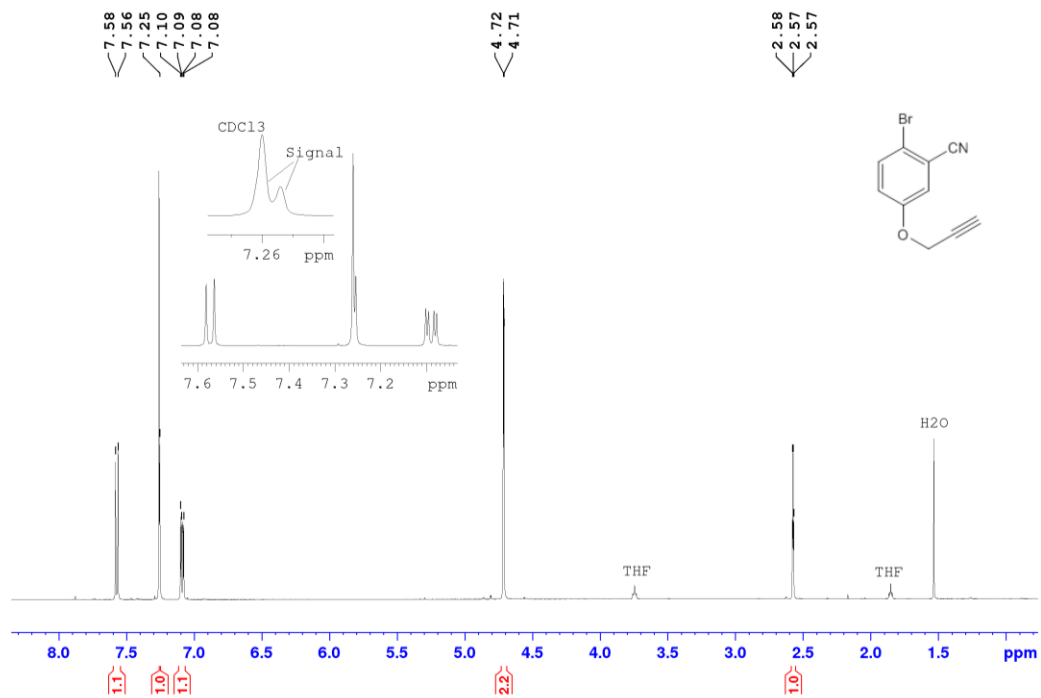
^{1}H NMR spectrum (500 MHz, CDCl$_3$) of 2-bromo-5-(2-propyn-1-yloxy)benzonitrile (**3h**).
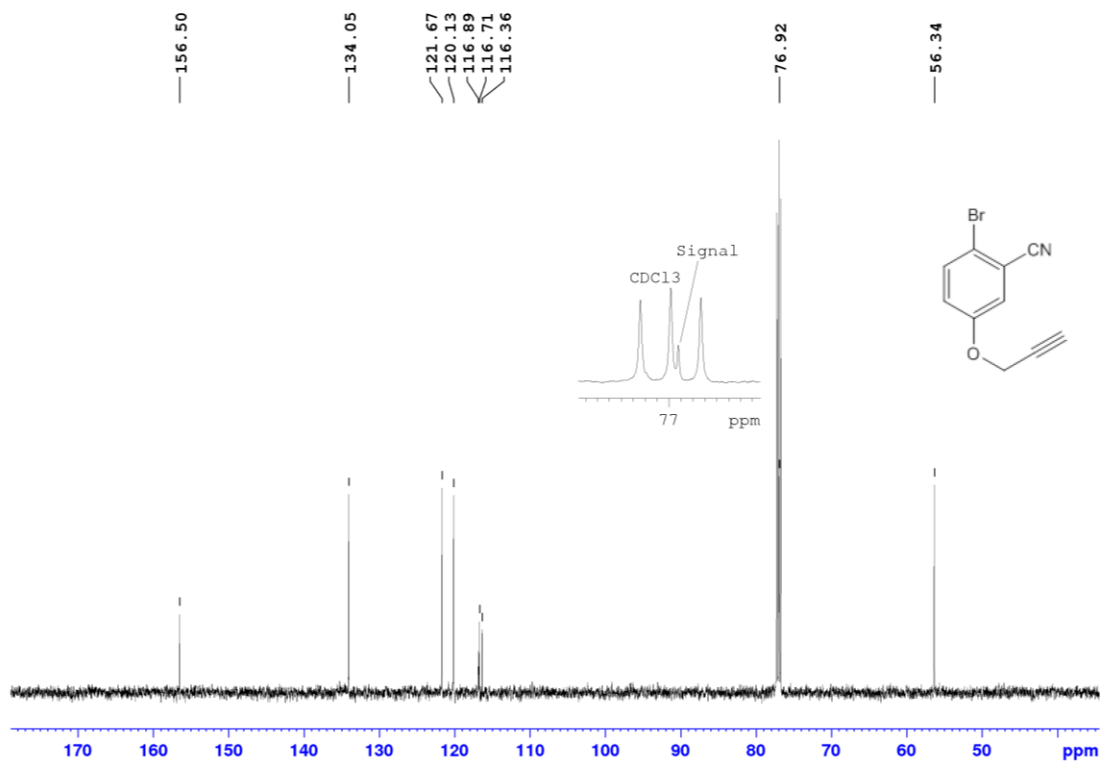
^{13}C NMR spectrum (126 MHz, CDCl$_3$) of 2-bromo-5-(2-propyn-1-yloxy)benzonitrile (**3h**).
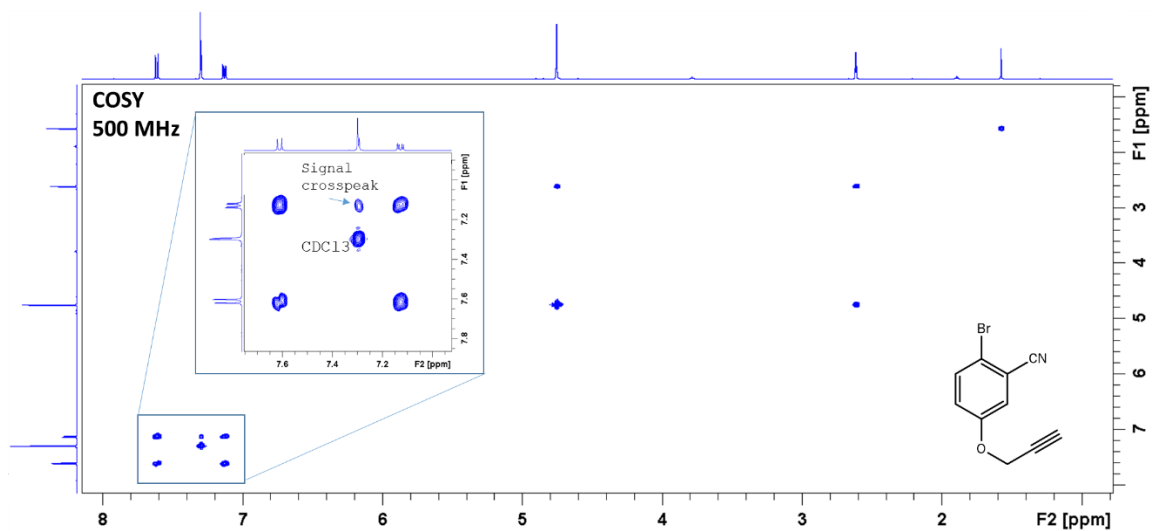
COSY NMR spectrum (500 MHz, CDCl₃) of 2-bromo-5-(2-propyn-1-yloxy)benzonitrile (**3h**).

HSQC NMR spectrum (500 MHz, CDCl₃) of 2-bromo-5-(2-propyn-1-yloxy)benzonitrile (**3h**).

HMBC NMR spectrum (500 MHz, CDCl₃) of 2-bromo-5-(2-propyn-1-yloxy)benzonitrile (**3h**).

¹H NMR spectrum (500 MHz, d_6-DMSO) of **4h**.
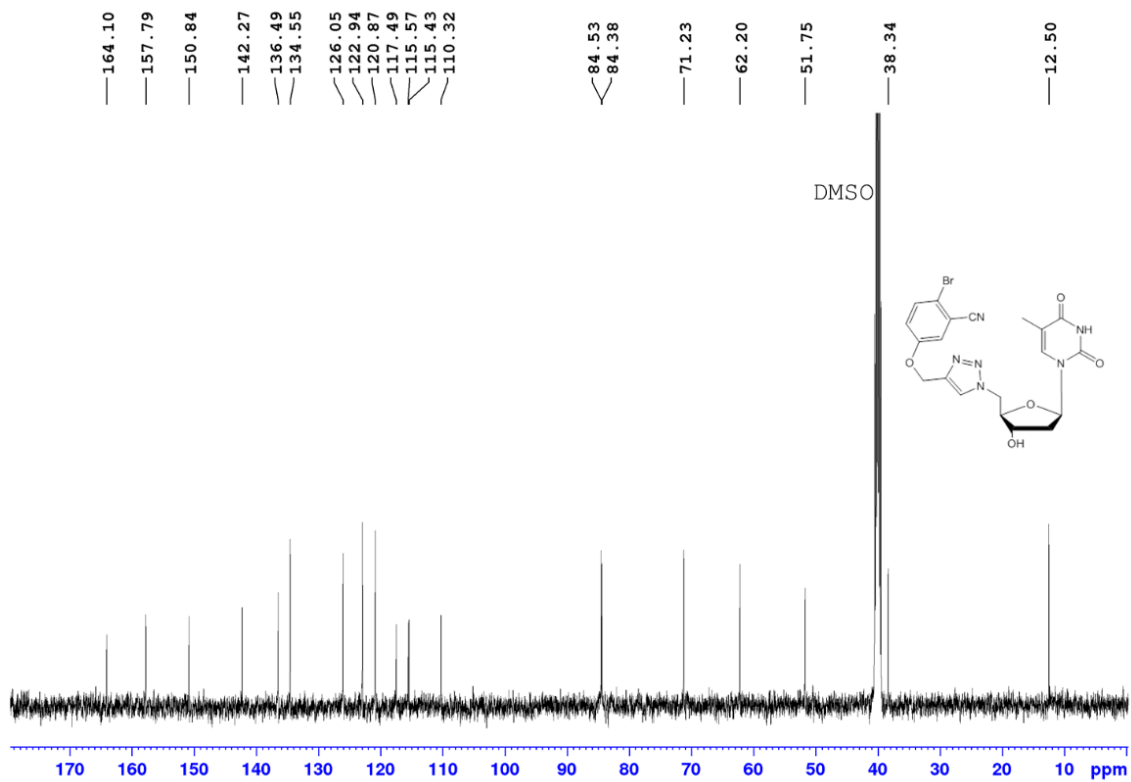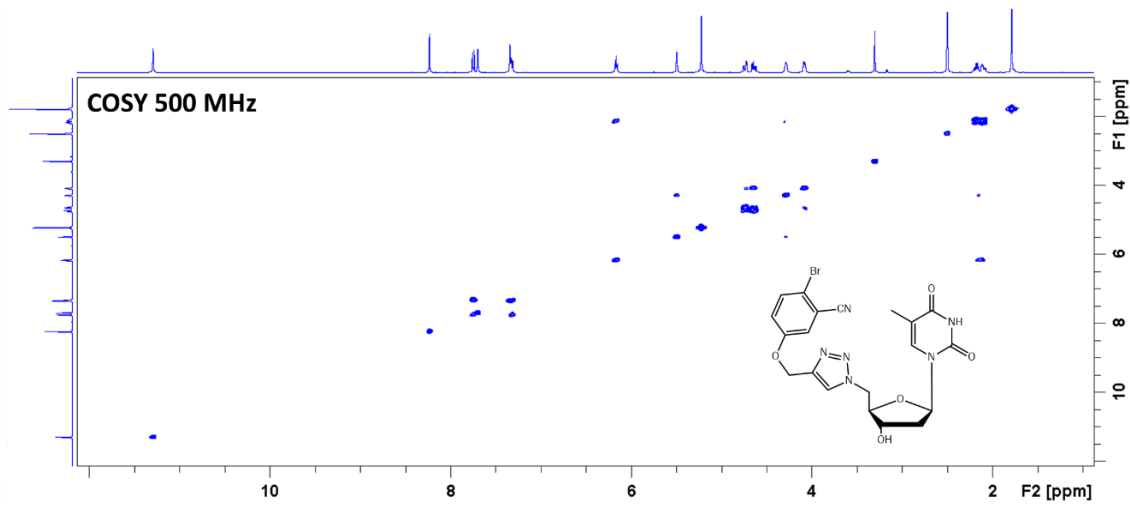
^{13}C NMR spectrum (126 MHz, d_6-DMSO) of **4h**.

COSY NMR spectrum (500 MHz, d_6-DMSO) of **4h**.

HSQC NMR spectrum (500 MHz, *d₆*-DMSO) of **4h**.

HSQC NMR spectrum (500 MHz, *d₆*-DMSO) of **4h**.

^{1}H NMR spectrum (500 MHz, d_6-DMSO) of **8**.

^{13}C NMR spectrum (126 MHz, d_6-DMSO) of **8**.
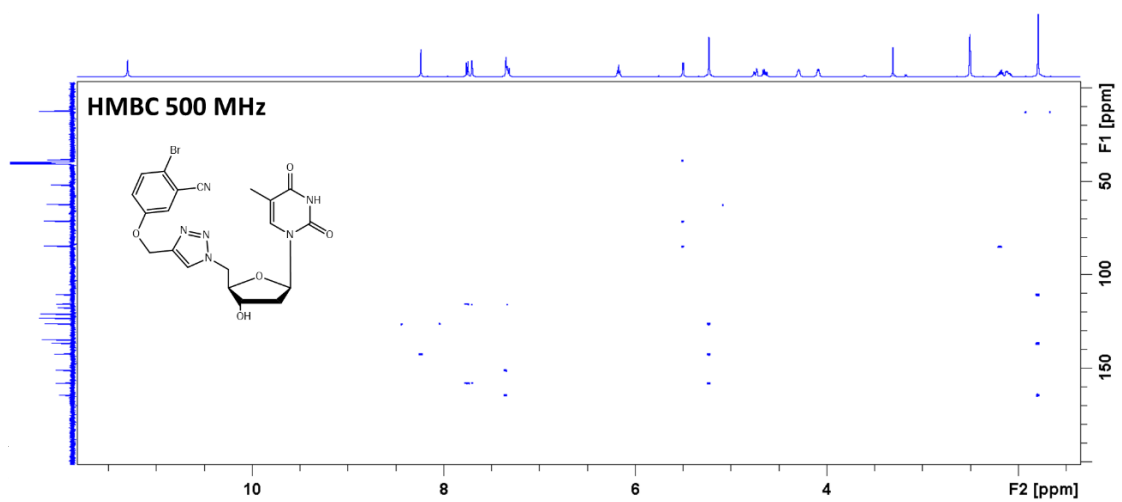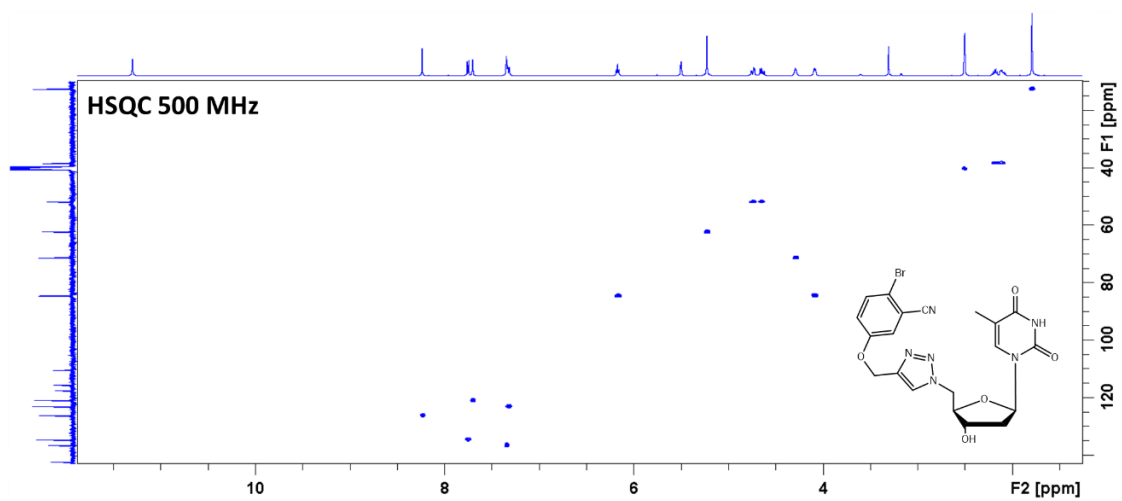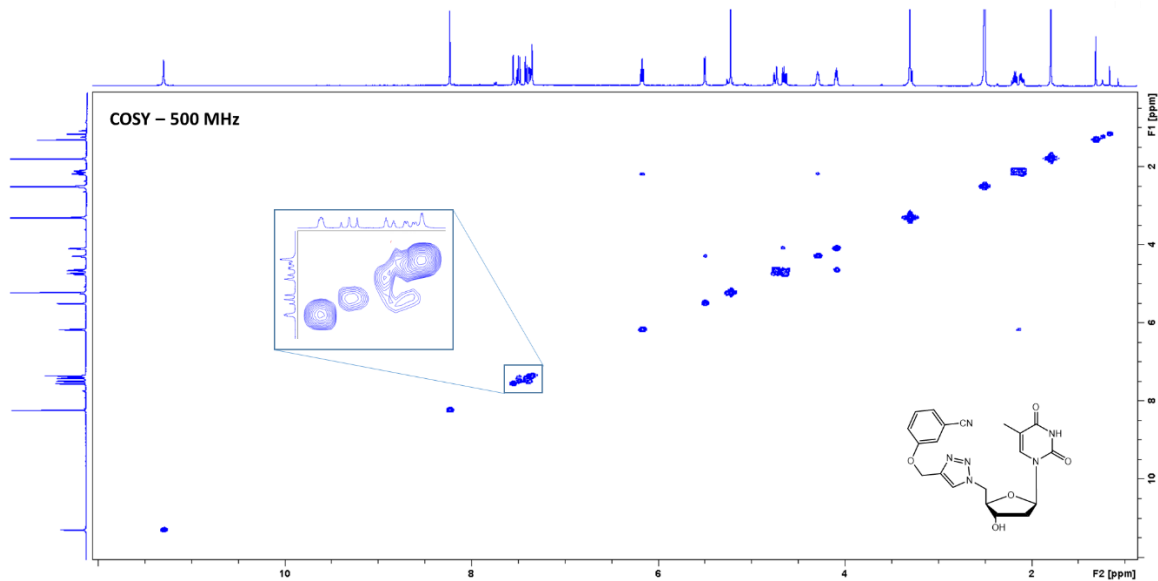
COSY NMR spectrum (500 MHz, d_6-DMSO) of **8**.
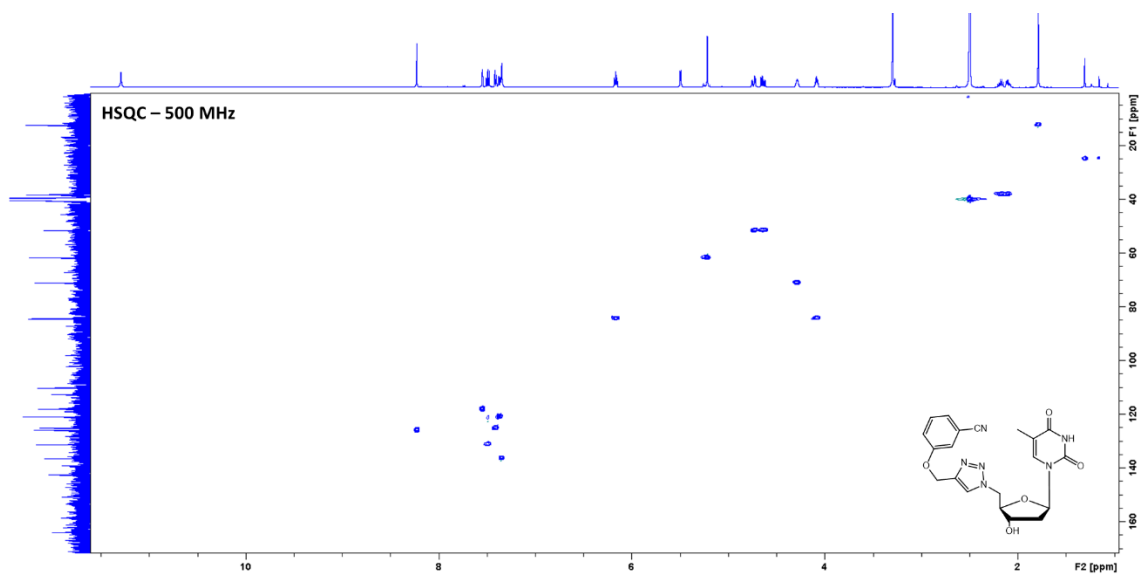
HSQC NMR spectrum (500 MHz, d_6-DMSO) of **8**.
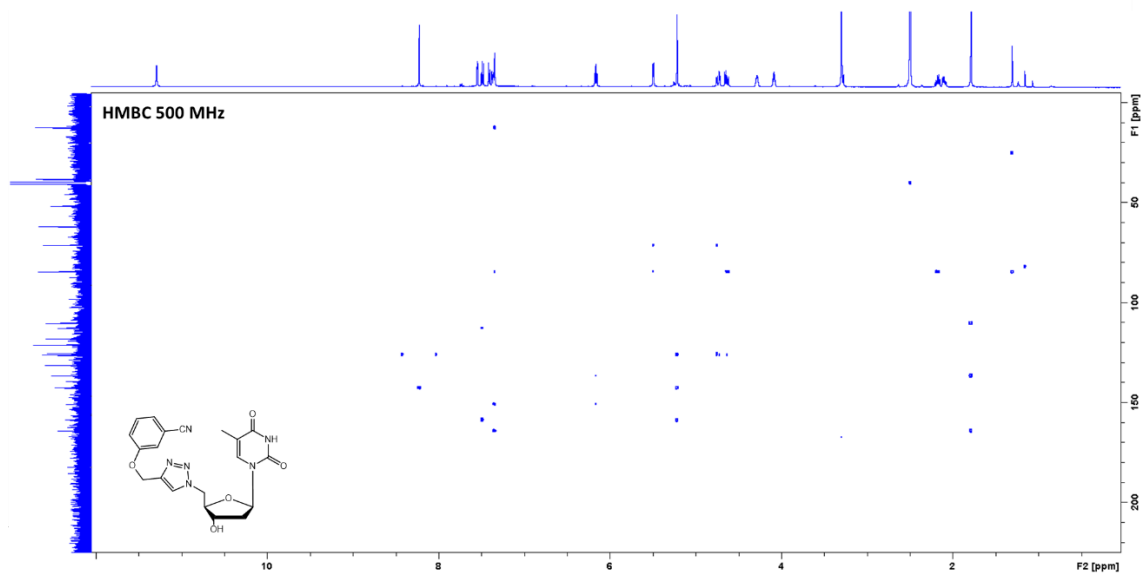
HMBC NMR spectrum (500 MHz, d_6-DMSO) of **8**.
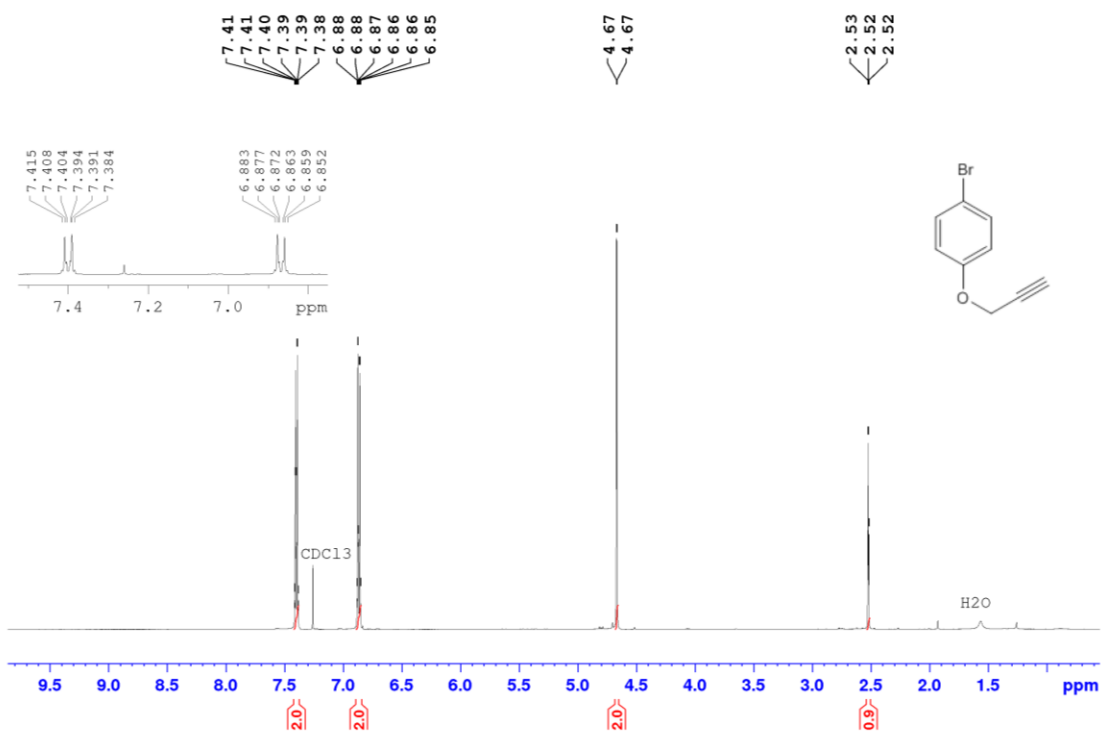
^{1}H NMR spectrum (500 MHz, CDCl$_3$) of 1-bromo-4-(2-propyn-1-yloxy)benzene (**3i**).
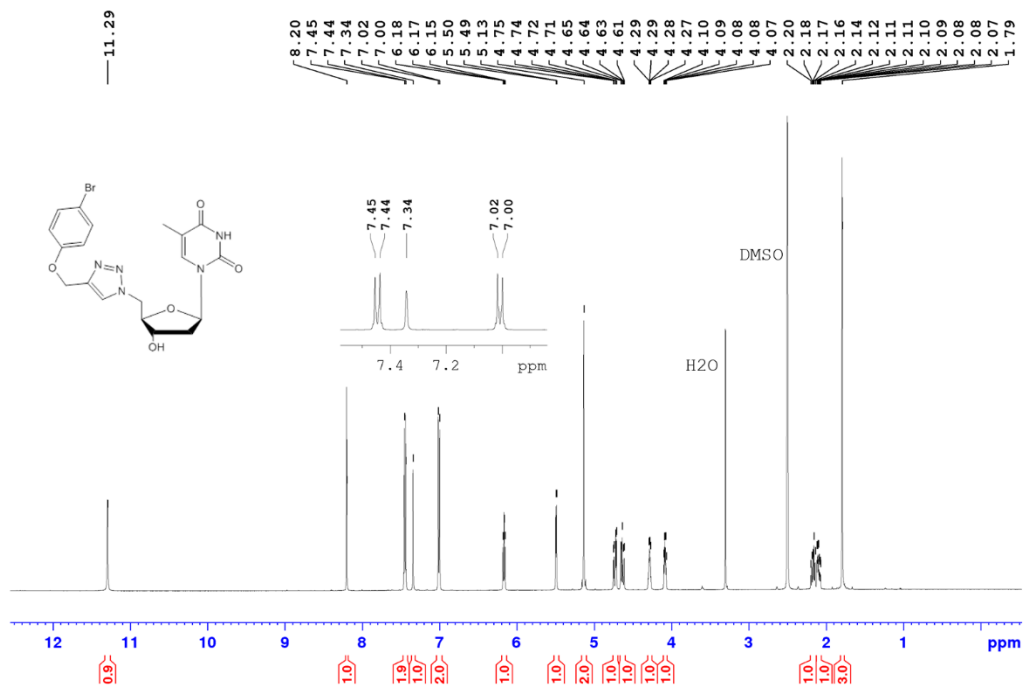
^{1}H NMR spectrum (500 MHz, d_6-DMSO) of **4i**.
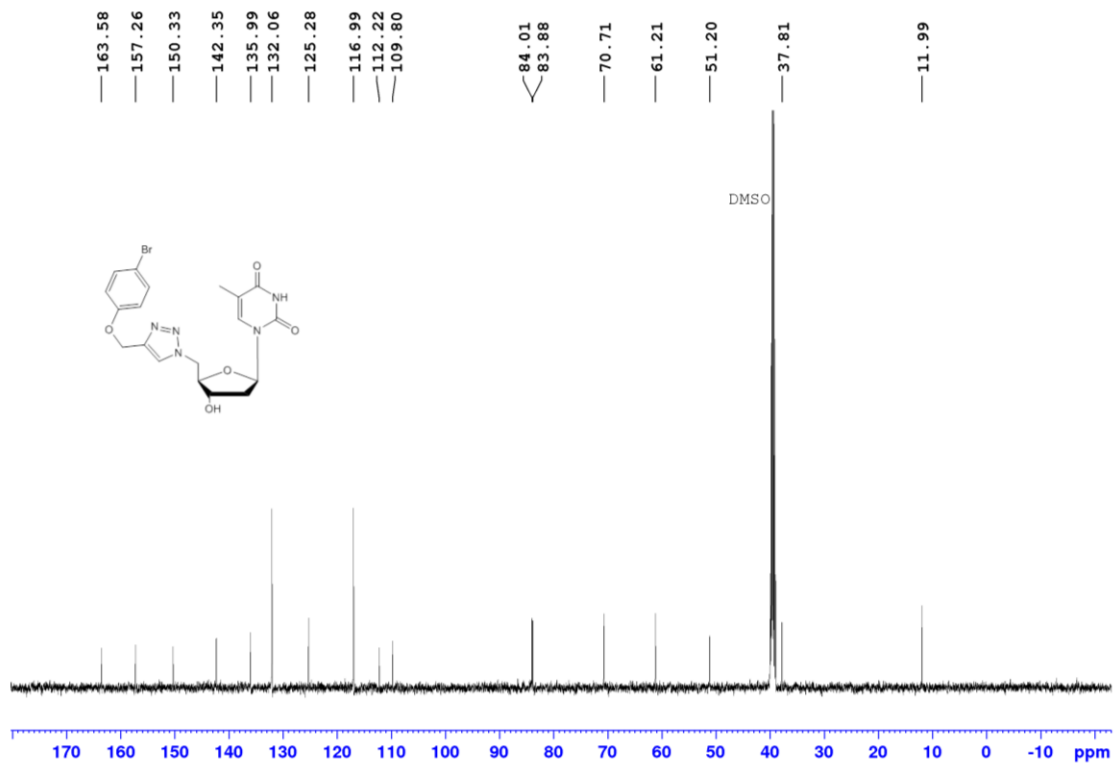
^{13}C NMR spectrum (126 MHz, d_6-DMSO) of **4i**.

128
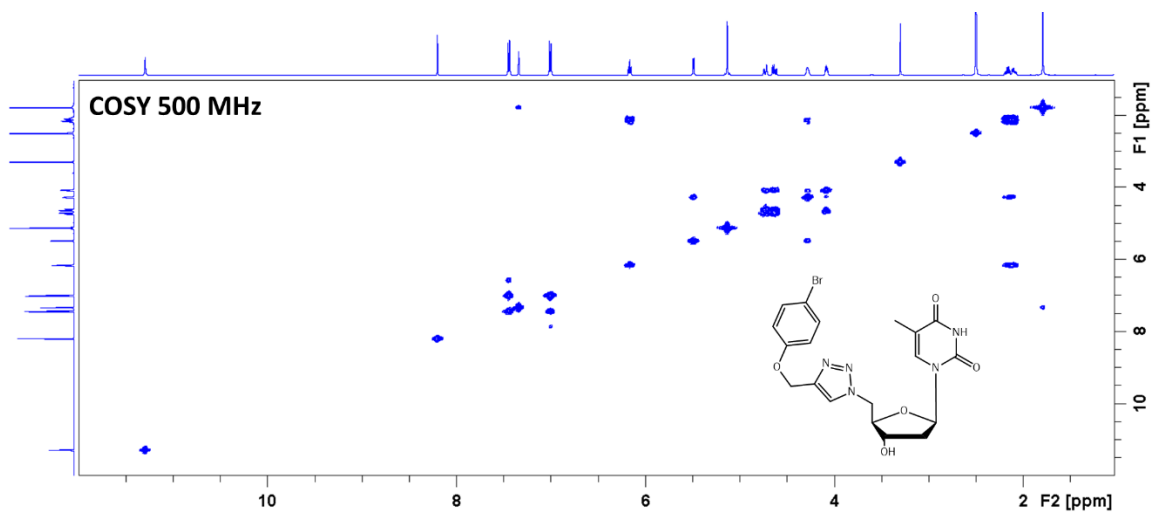
COSY NMR spectrum (500 MHz, d_6-DMSO) of **4i**.
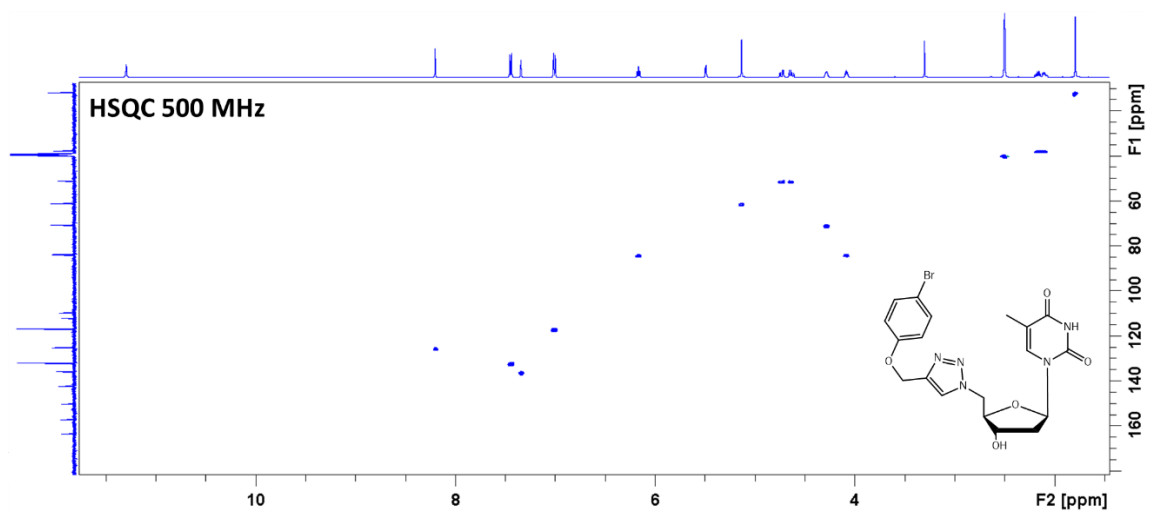
HSQC NMR spectrum (500 MHz, d_6-DMSO) of **4i**.
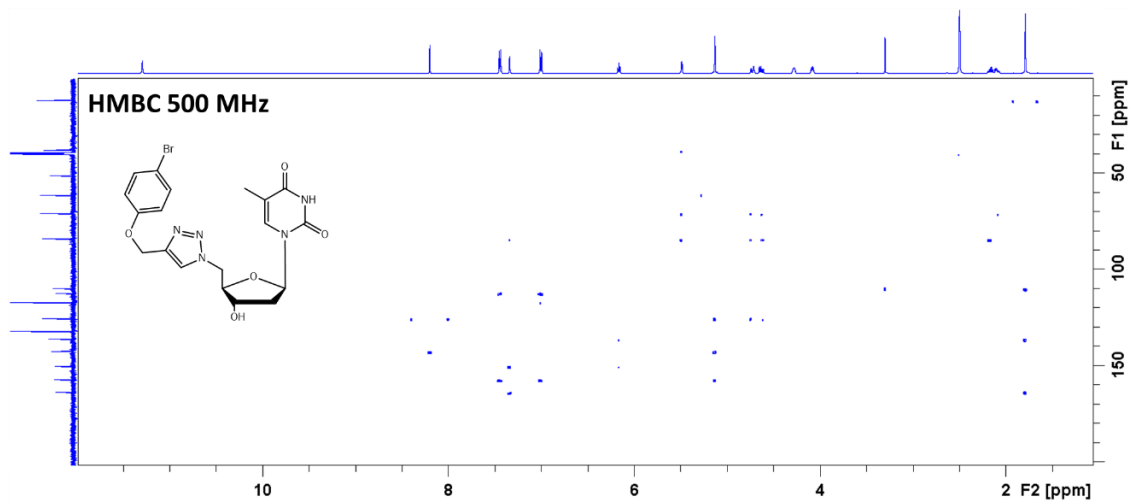
HMBC NMR spectrum (500 MHz, d_6-DMSO) of **4i**.
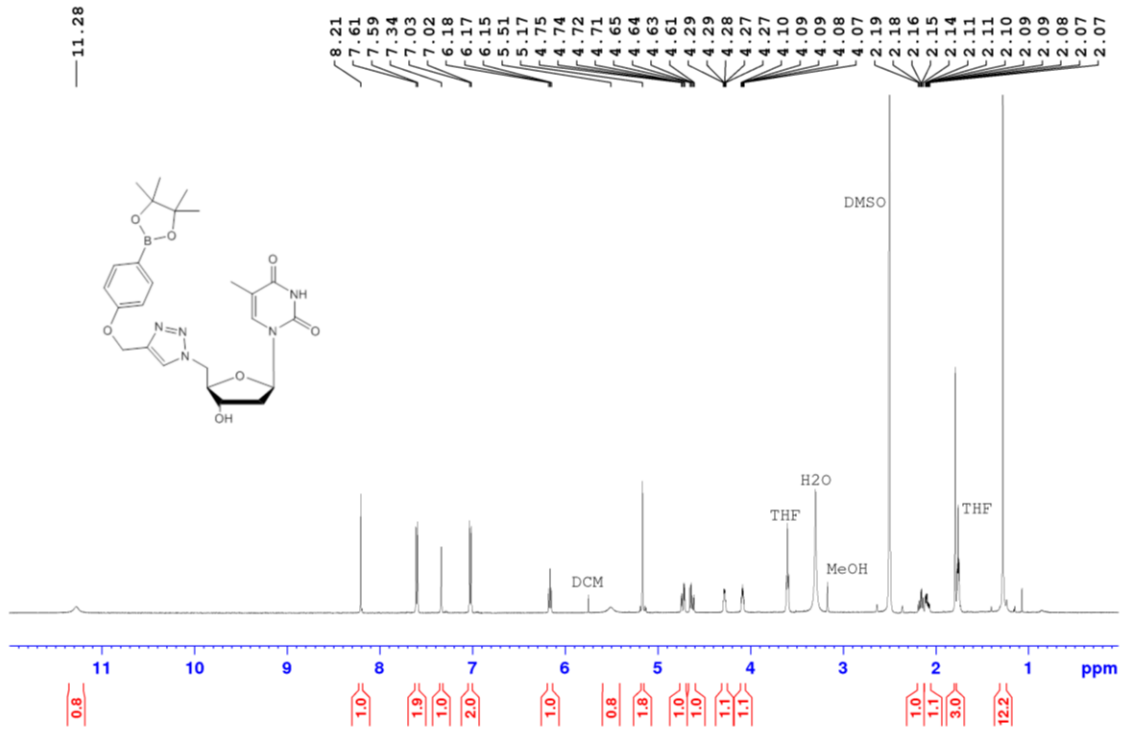
^{1}H NMR spectrum (500 MHz, d_6-DMSO) of **9**.
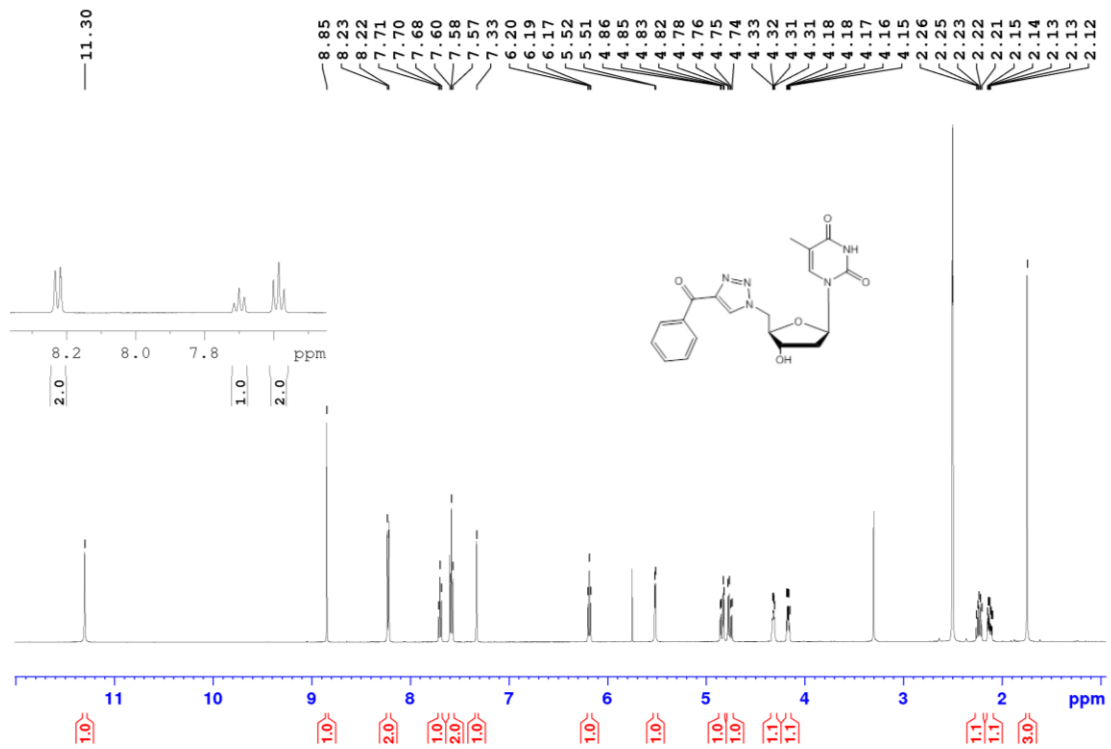
¹H NMR spectrum (500 MHz, *d₆*-DMSO) of **10a**.
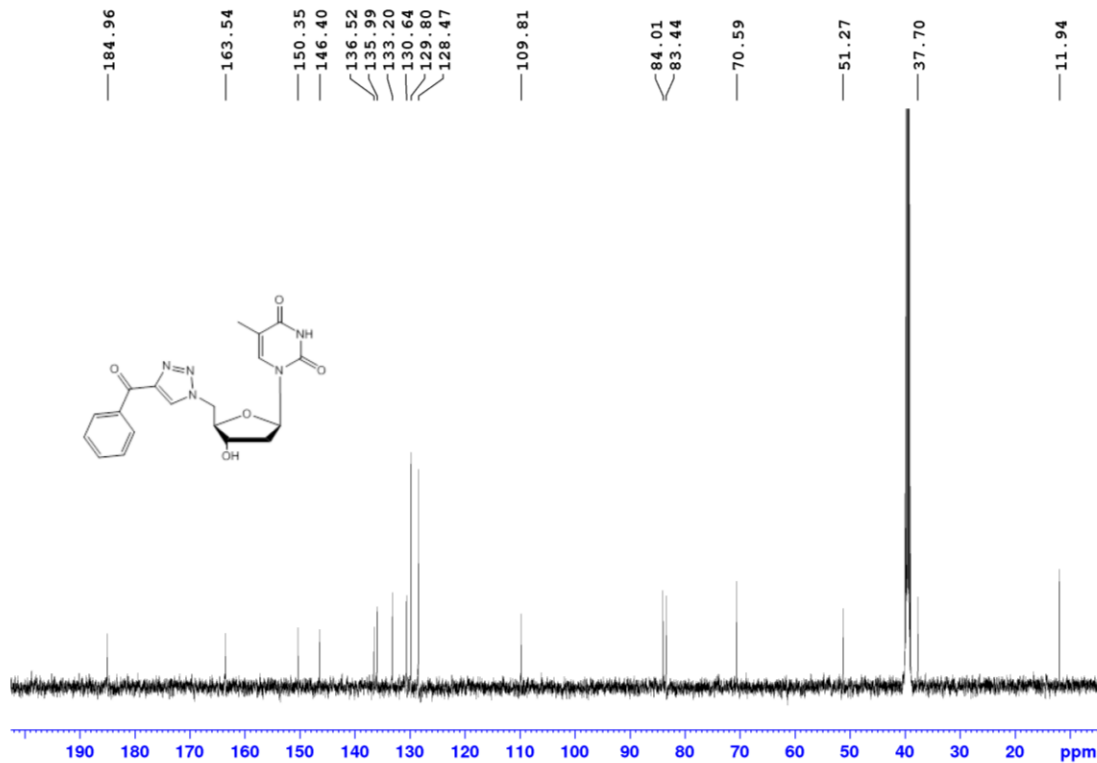
¹³C NMR spectrum (126 MHz, *d₆*-DMSO) of **10a**.
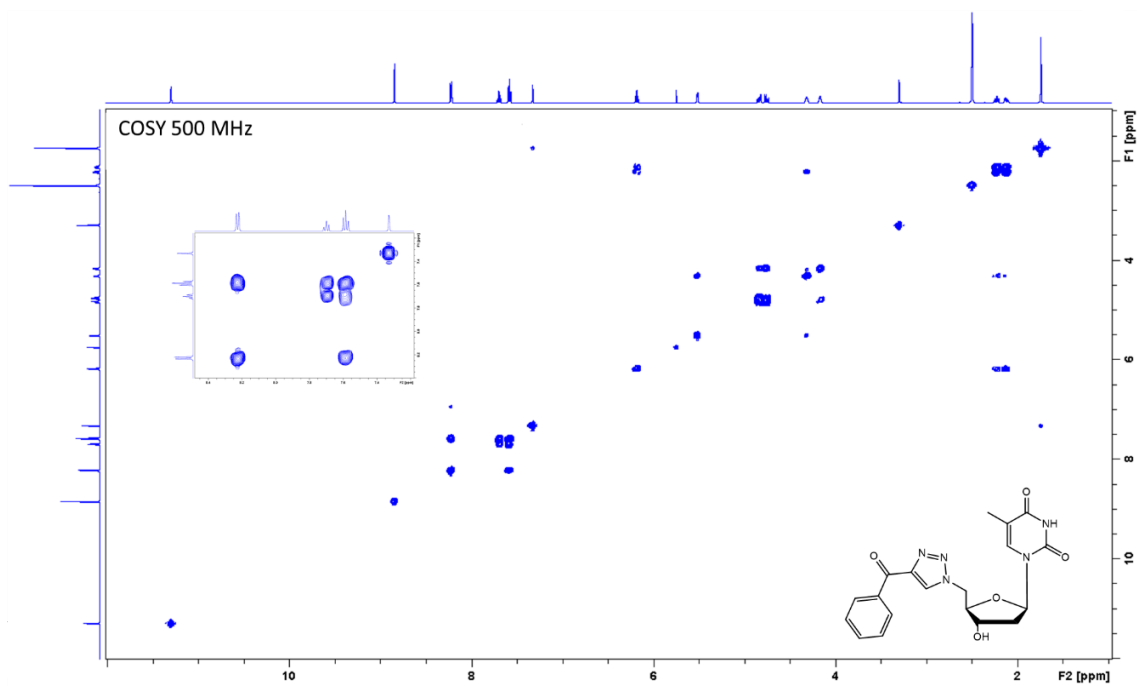
COSY NMR spectrum (500 MHz, *d₆*-DMSO) of **10a**.
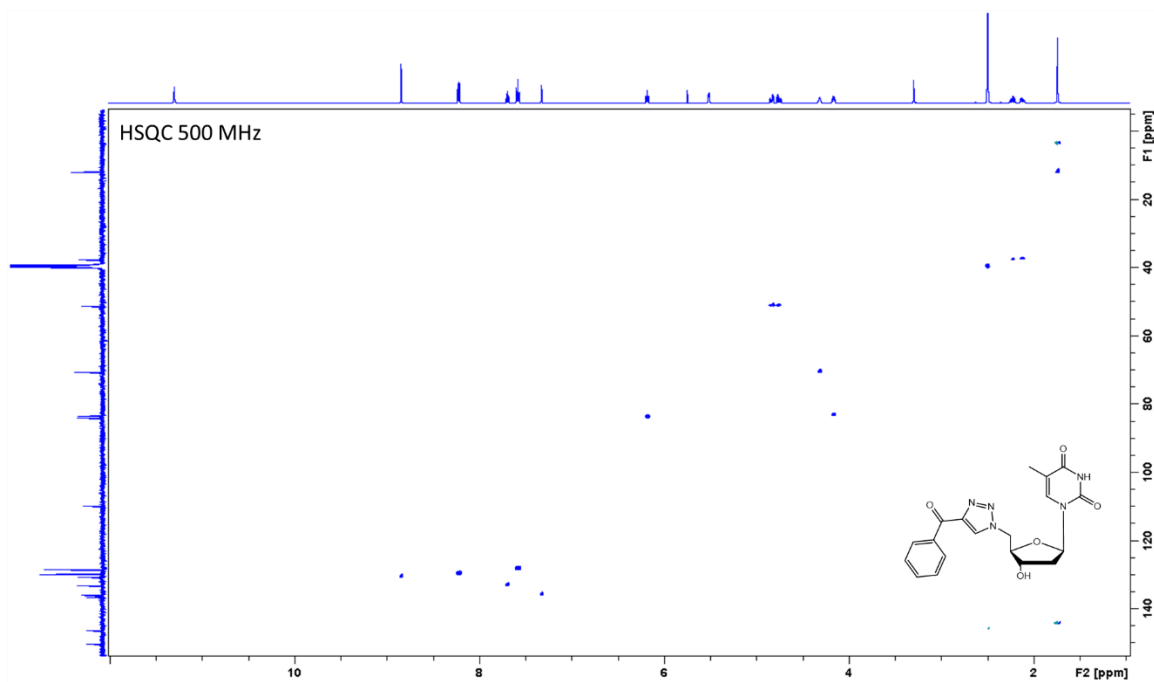
HSQC NMR spectrum (500 MHz, d_6-DMSO) of **10a**.
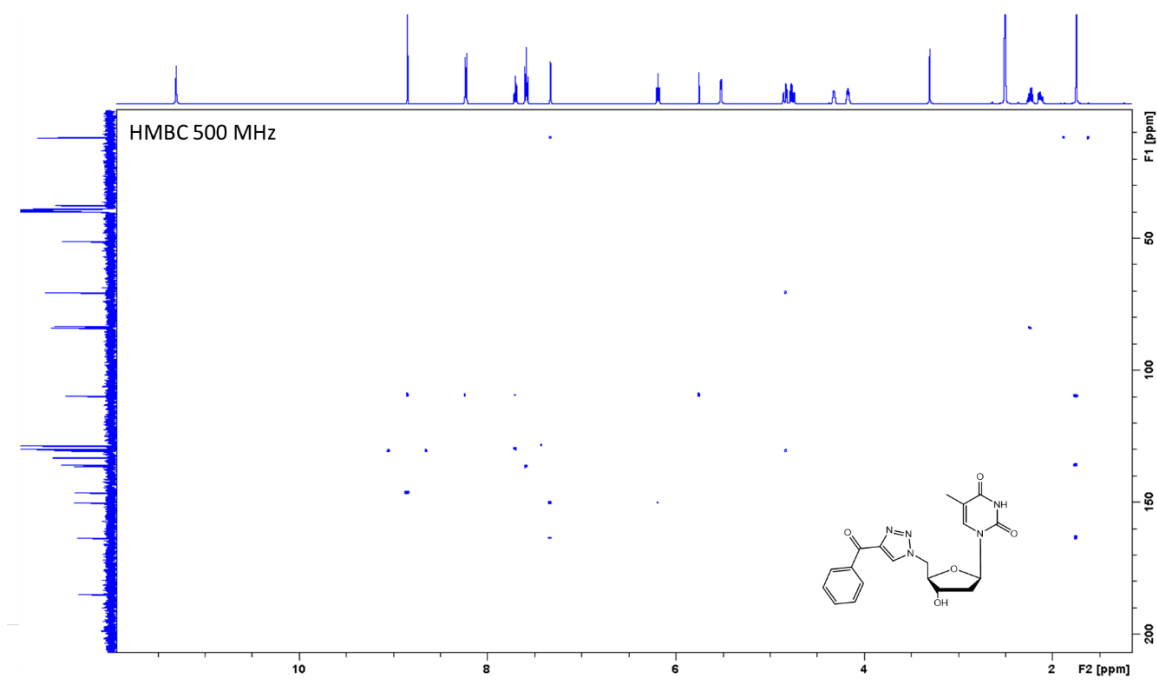
HMBC NMR spectrum (500 MHz, d_6-DMSO) of **10a**.
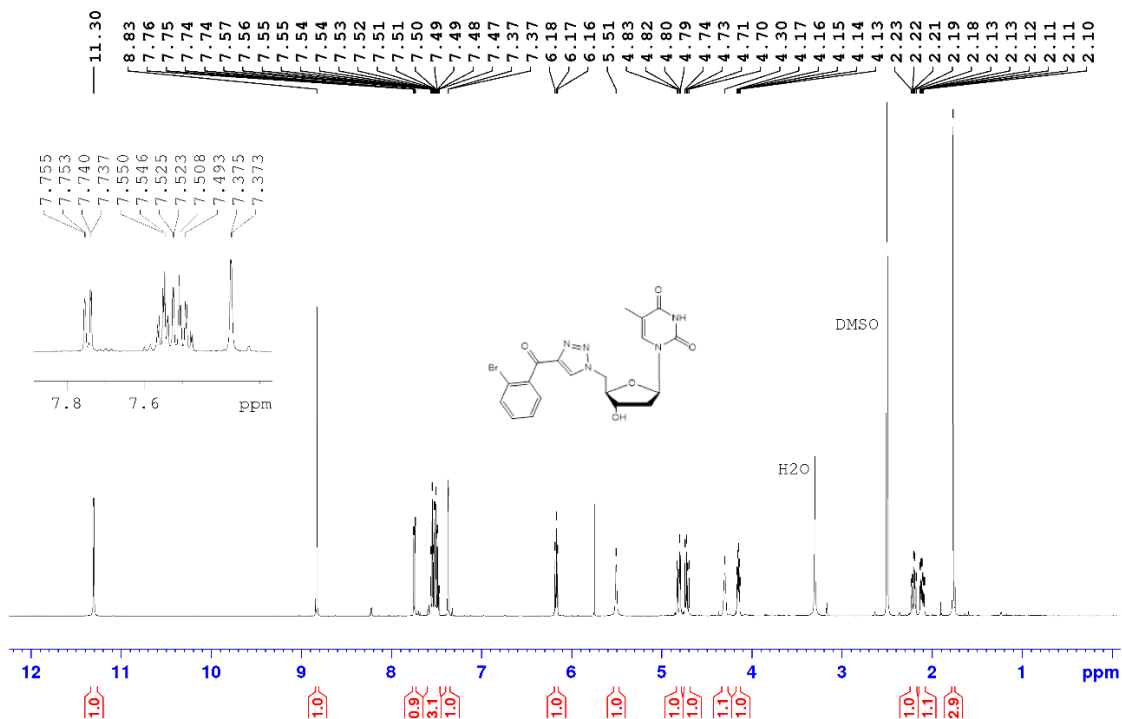
^{1}H NMR spectrum (500 MHz, d_6-DMSO) of **13**.
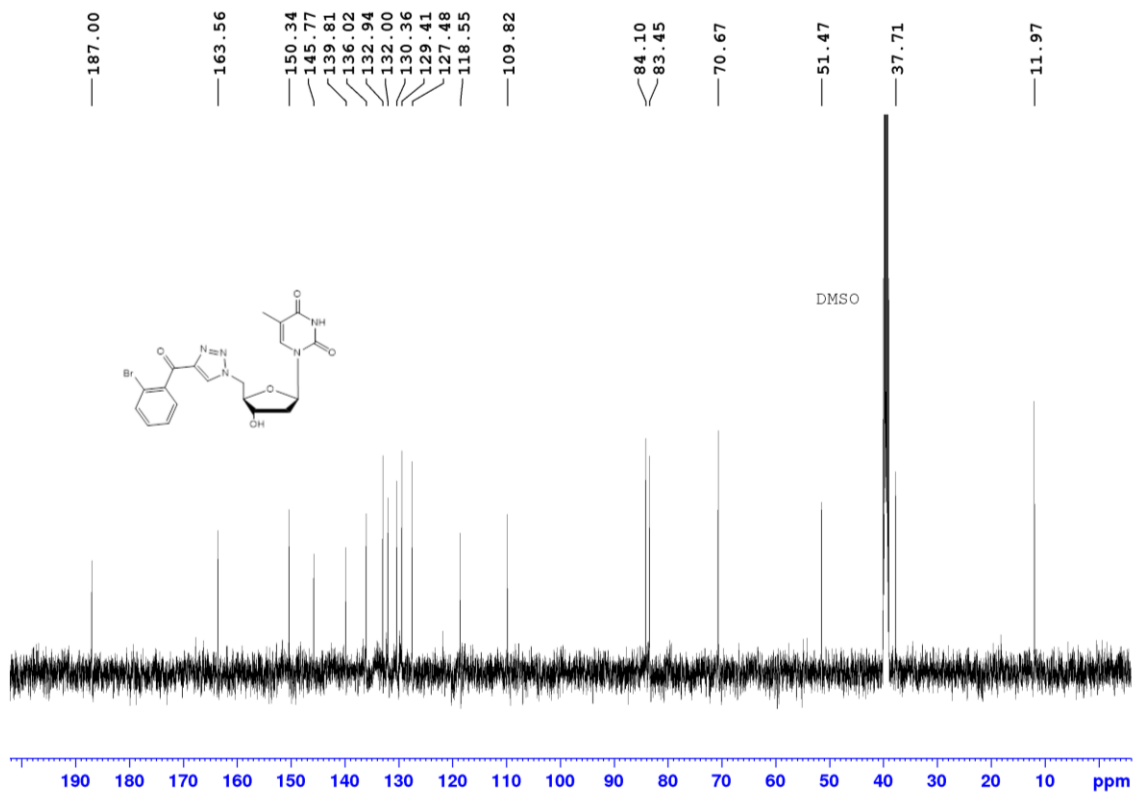
¹³C NMR spectrum (126 MHz, *d₆*-DMSO) of **13**.
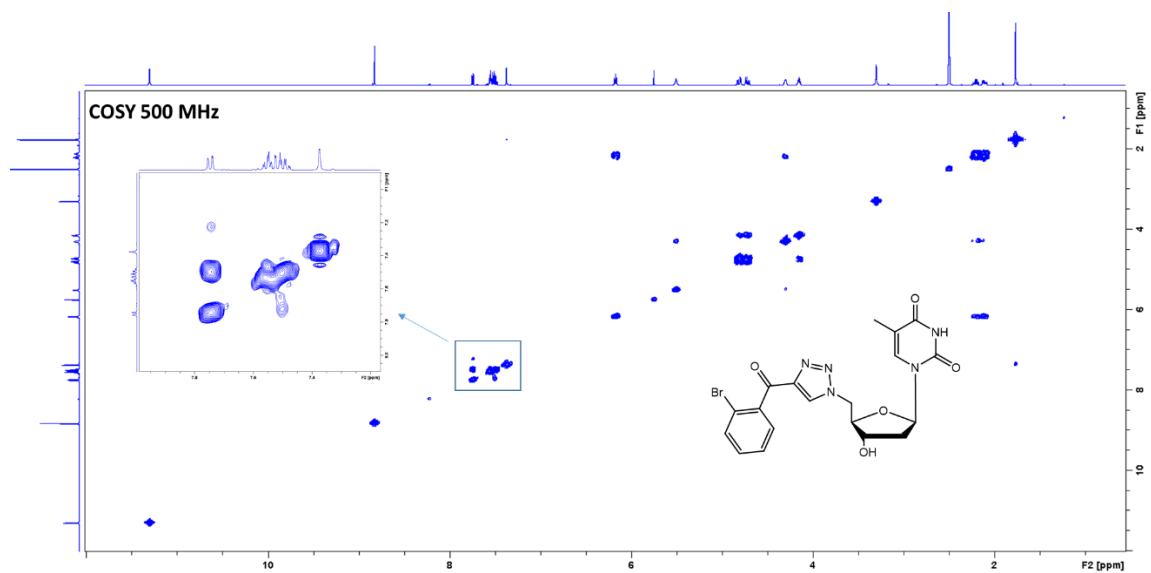
COSY NMR spectrum (500 MHz, *d₆*-DMSO) of **13**.
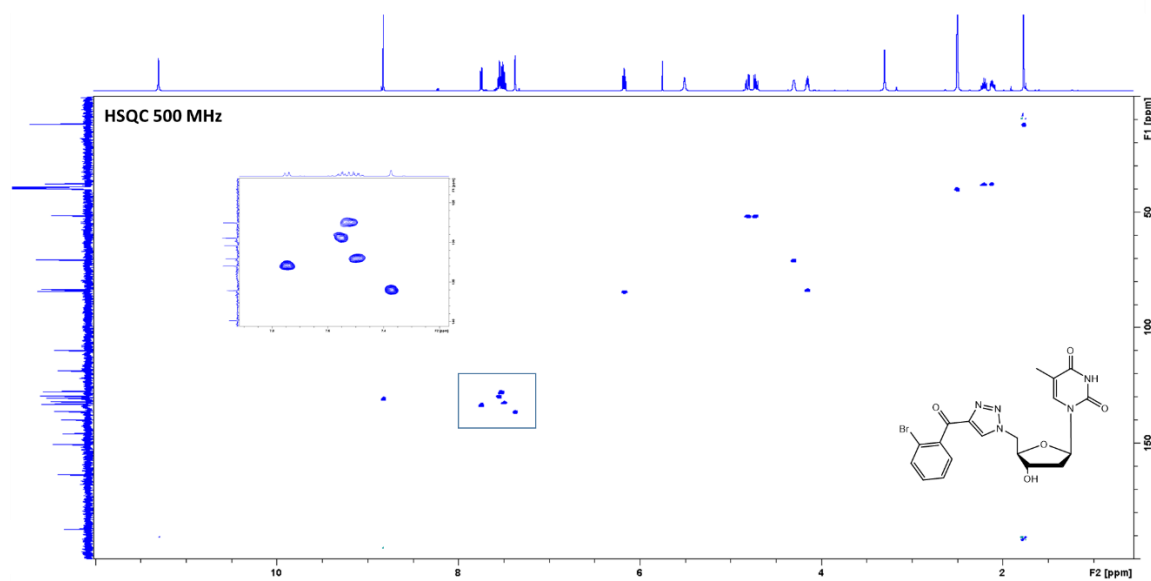
HSQC NMR spectrum (500 MHz, *d₆*-DMSO) of **13**.
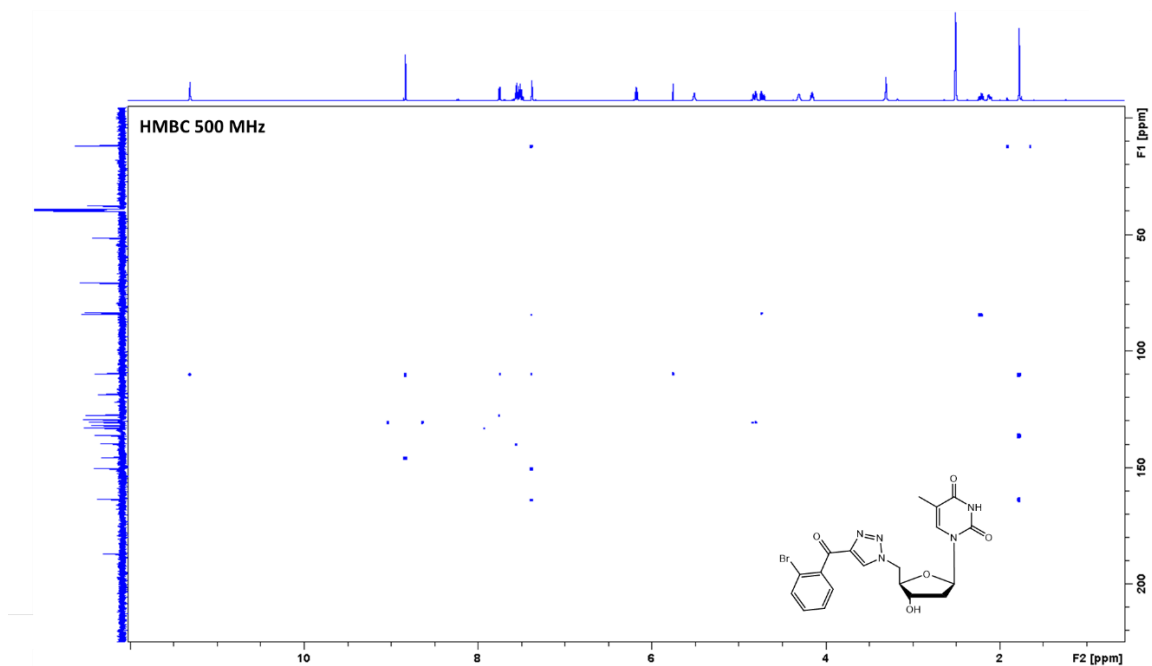
HMBC NMR spectrum (500 MHz, d_6-DMSO) of **13**.
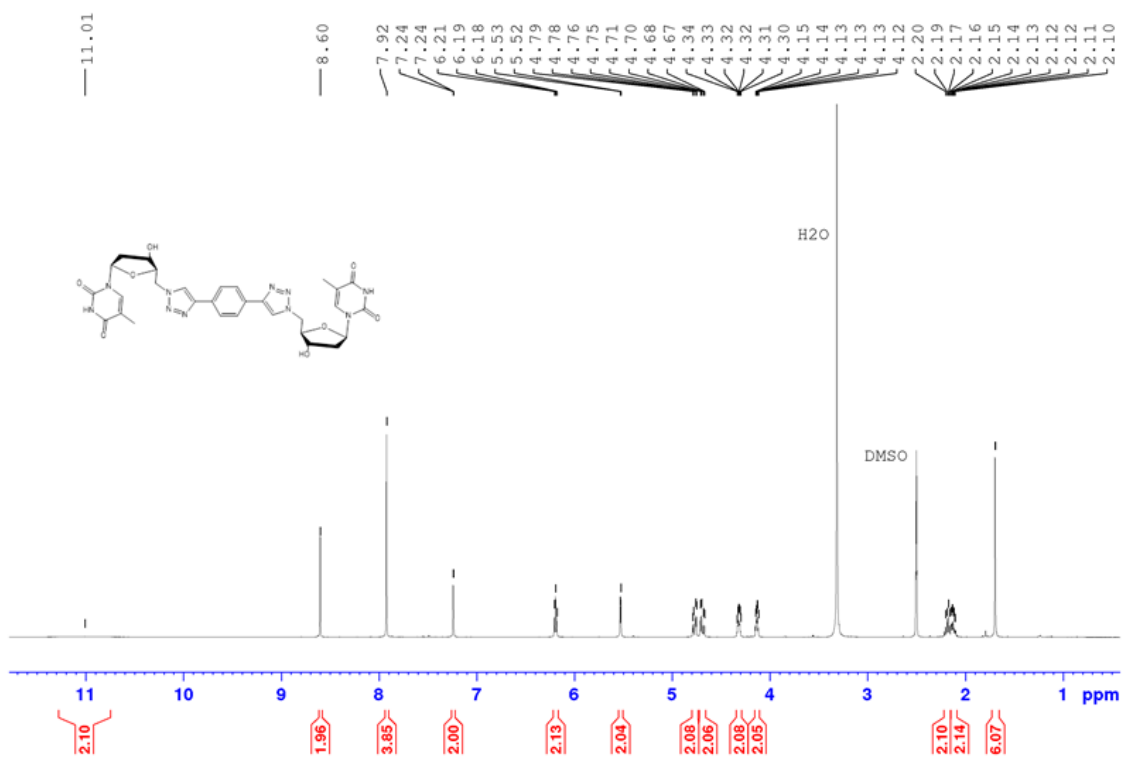
^{1}H NMR spectrum (500 MHz, d_6-DMSO) of **14a**.
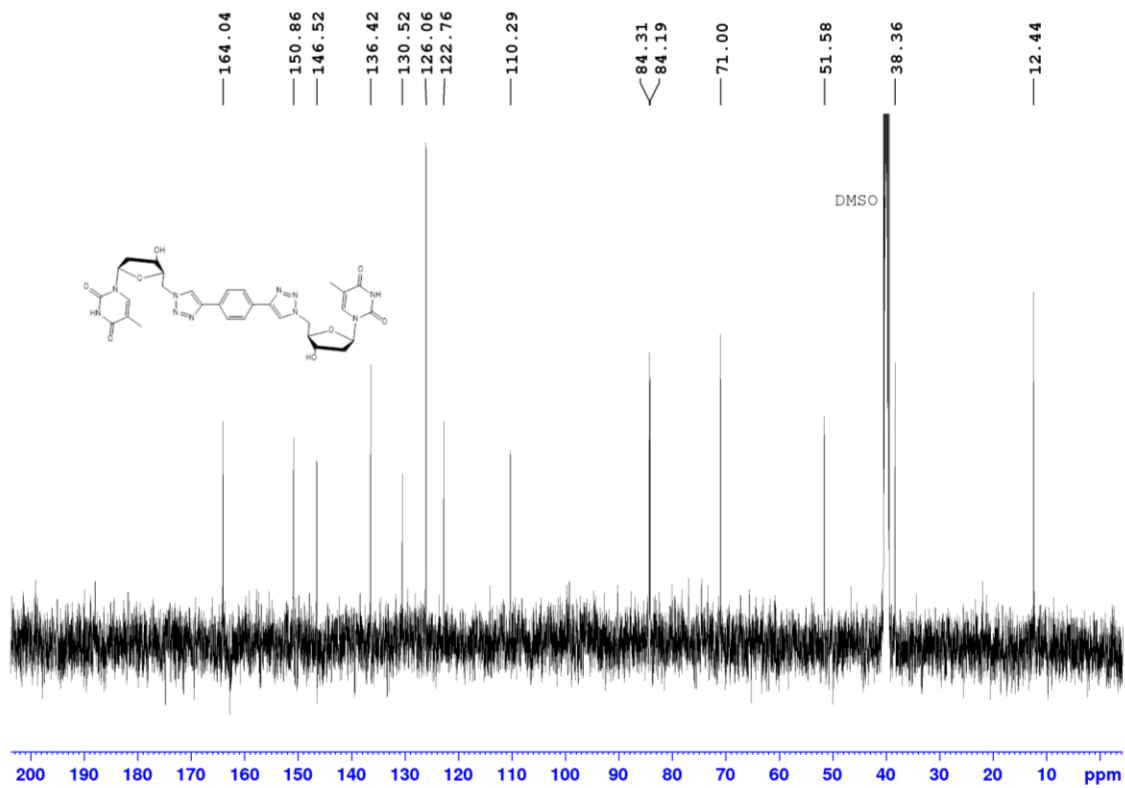
^{13}C NMR spectrum (126 MHz, d_6-DMSO) of **14a**.
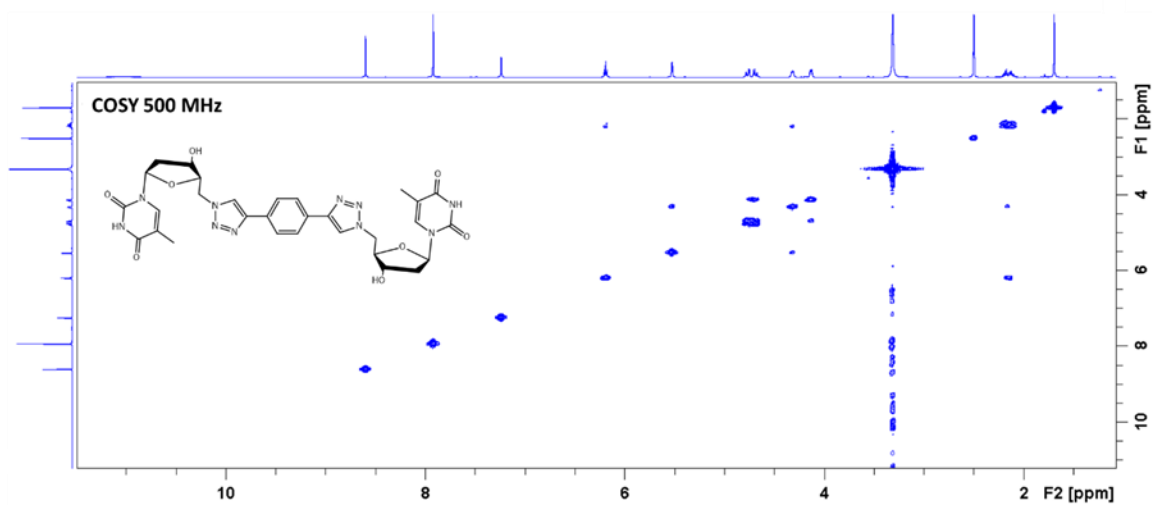
COSY NMR spectrum (500 MHz, d_6-DMSO) of **14a**.
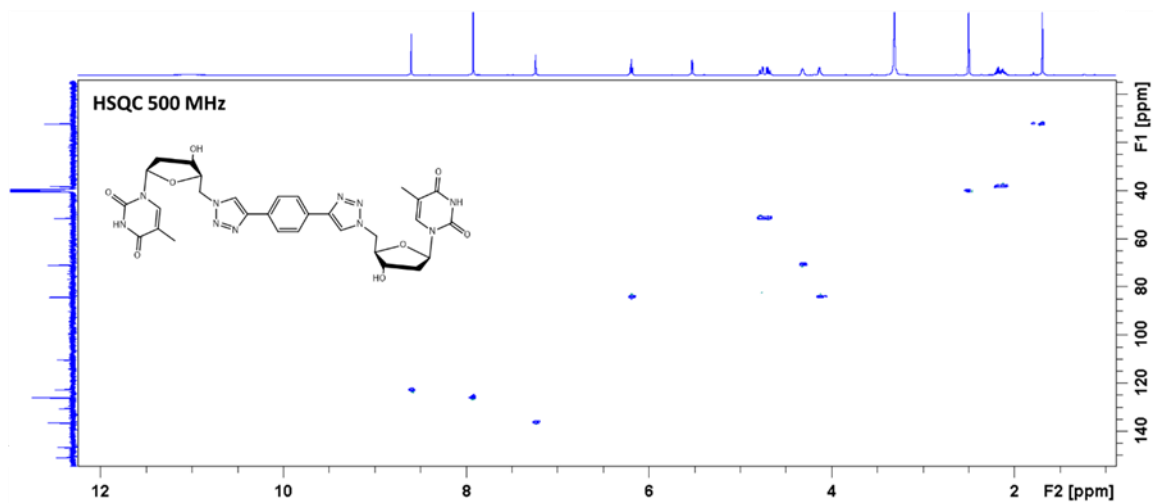
HSQC NMR spectrum (500 MHz, d_6-DMSO) of **14a**.
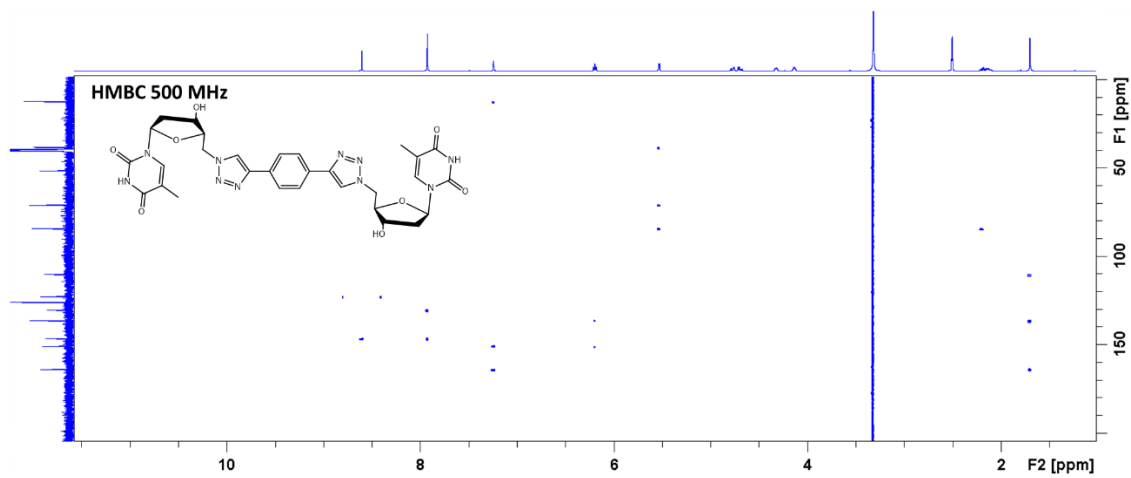
HMBC NMR spectrum (500 MHz, d_6-DMSO) of **14a**.
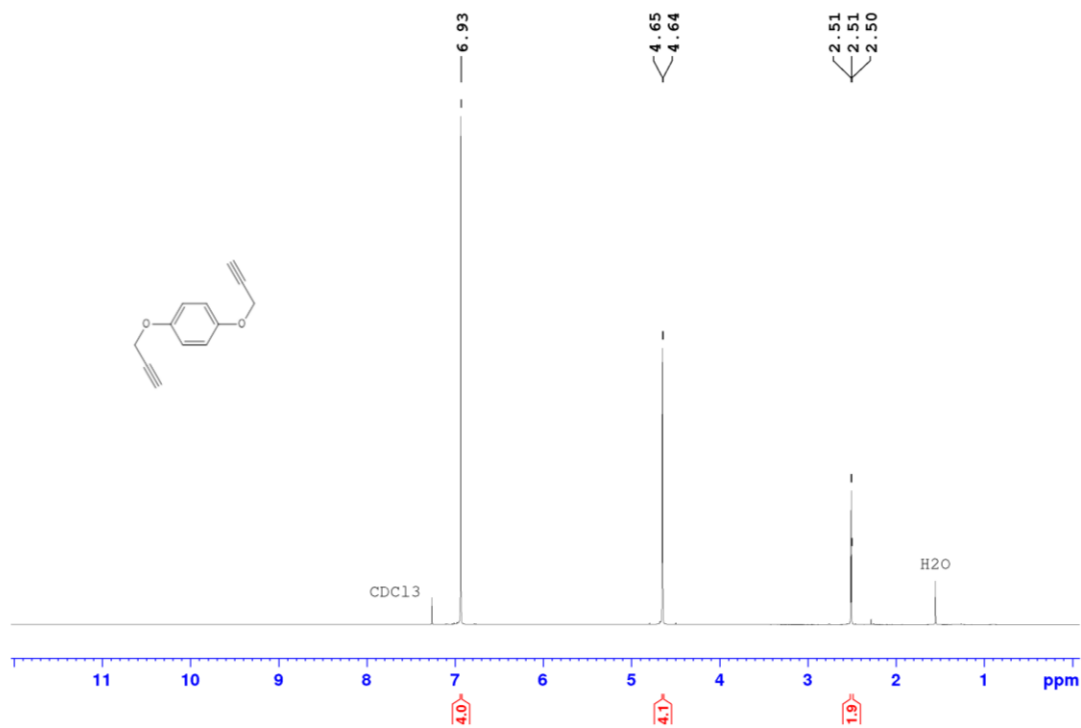
^{1}H NMR spectrum (500 MHz, d_6-DMSO) of 1,4-bis(2-propyn-1-yloxy)benzene (**3j**).
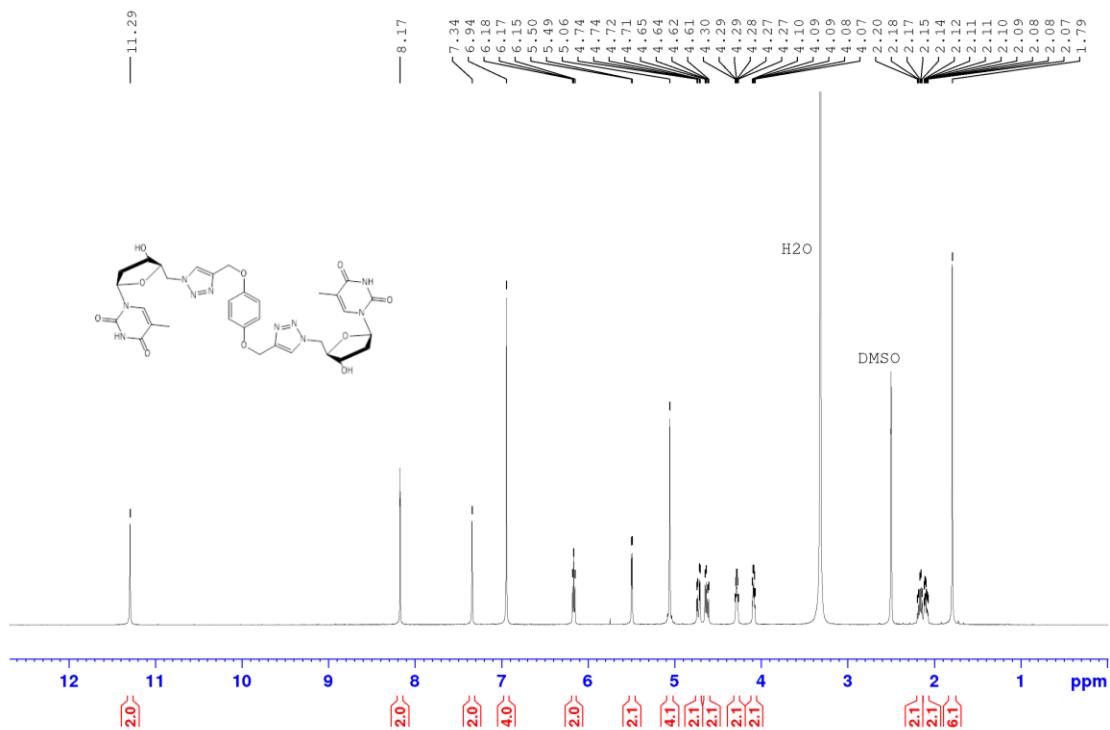
^{1}H NMR spectrum (500 MHz, d_6-DMSO) of **14b**.
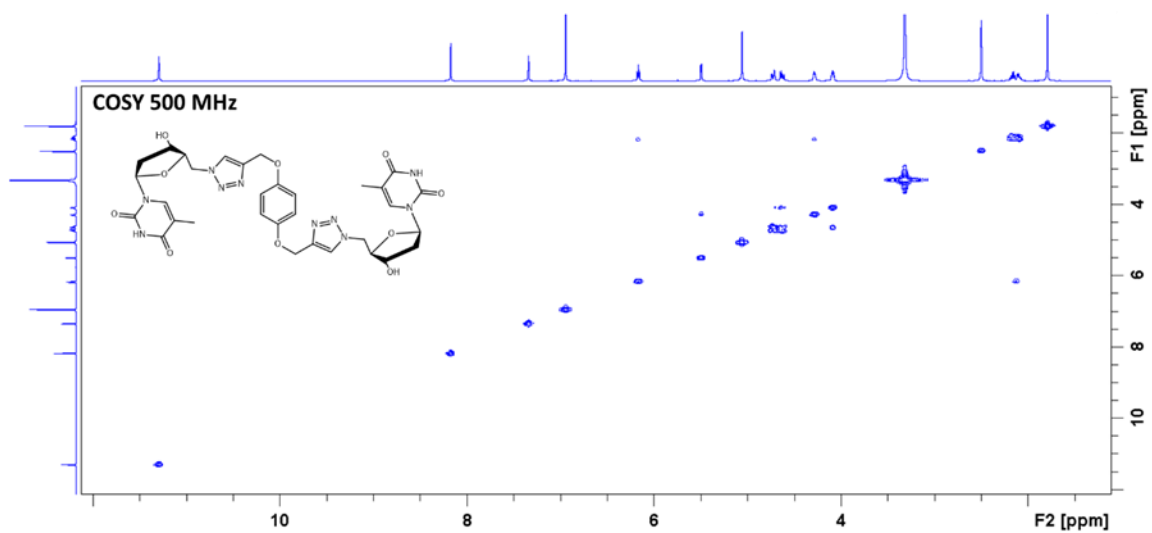
COSY NMR spectrum (500 MHz, d_6-DMSO) of **14b**.

^{13}C, HSQC, HMBC not available for **14b**.
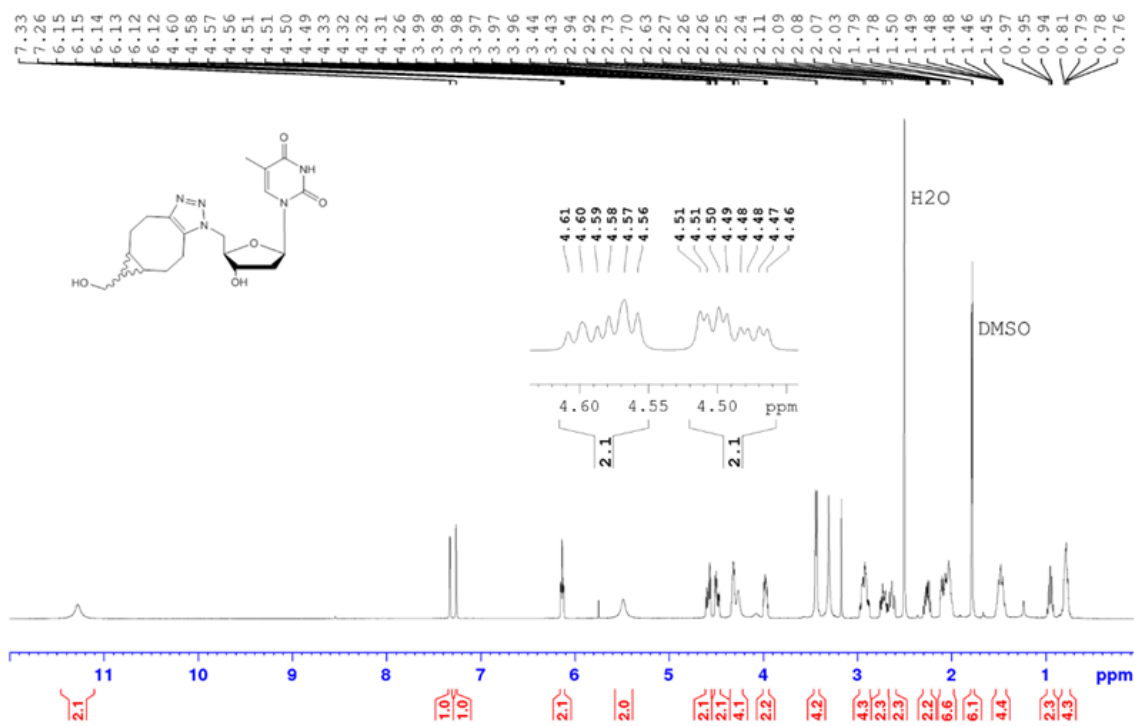
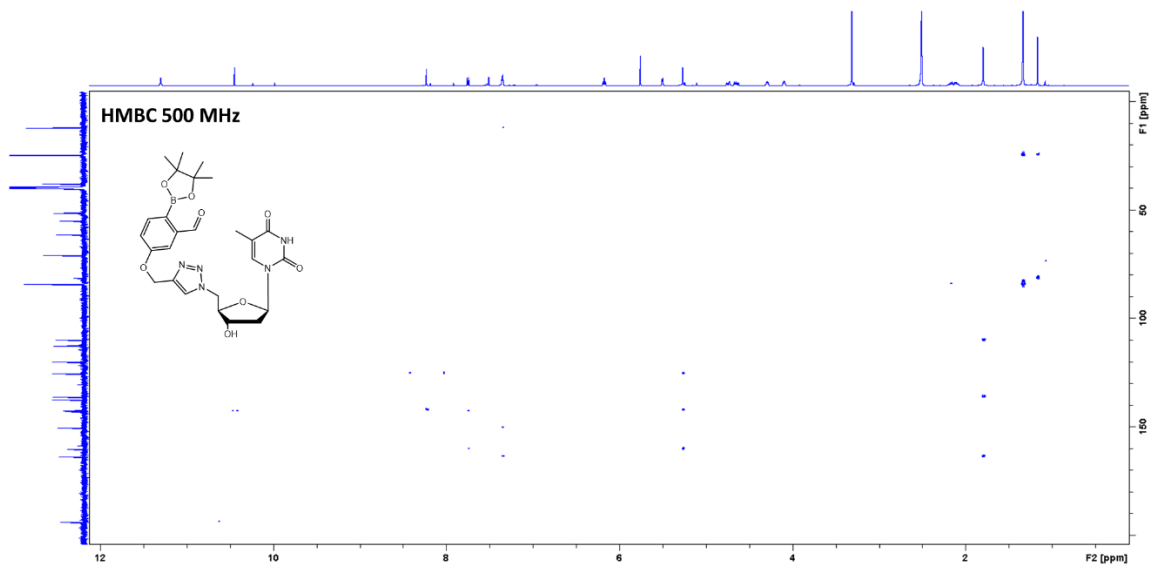^{1}H NMR spectrum (500 MHz, d_6-DMSO) of **15**.
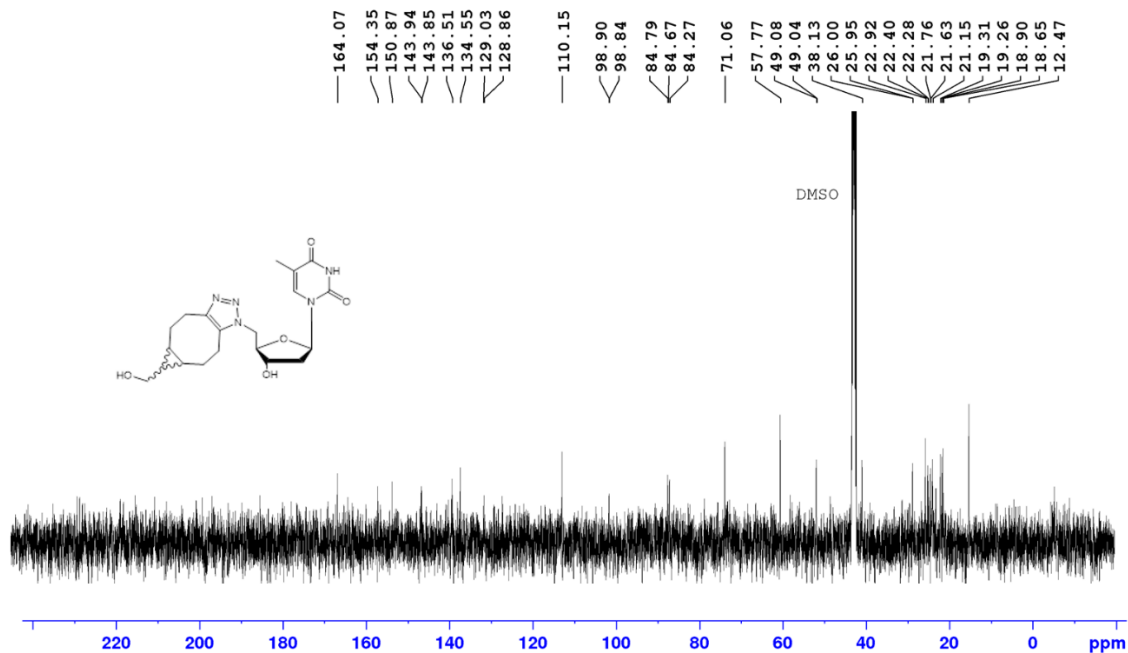
^{13}C NMR spectrum (126 MHz, d_6-DMSO) of **15**.
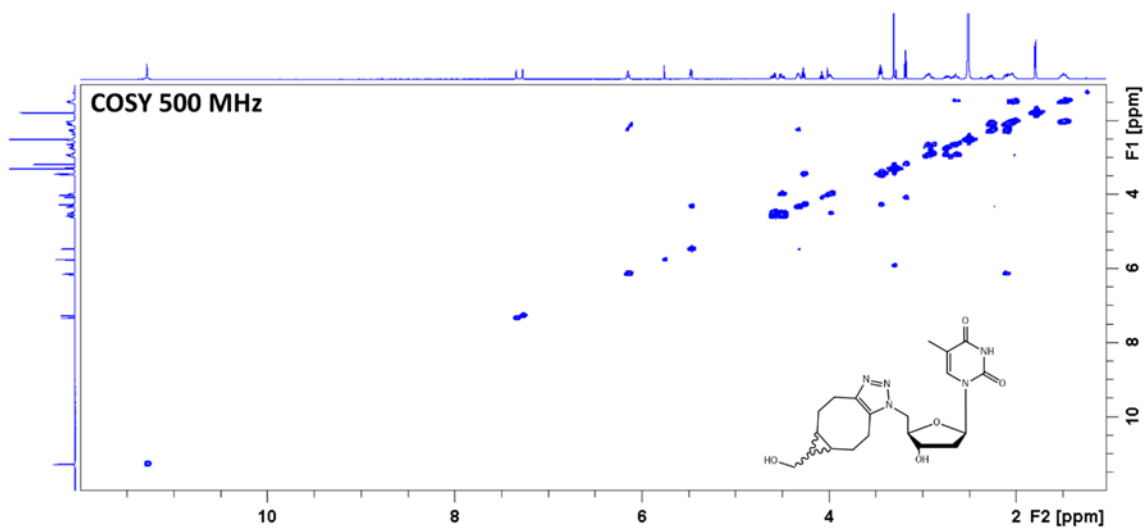
COSY NMR spectrum (500 MHz, d_6-DMSO) of **15**.
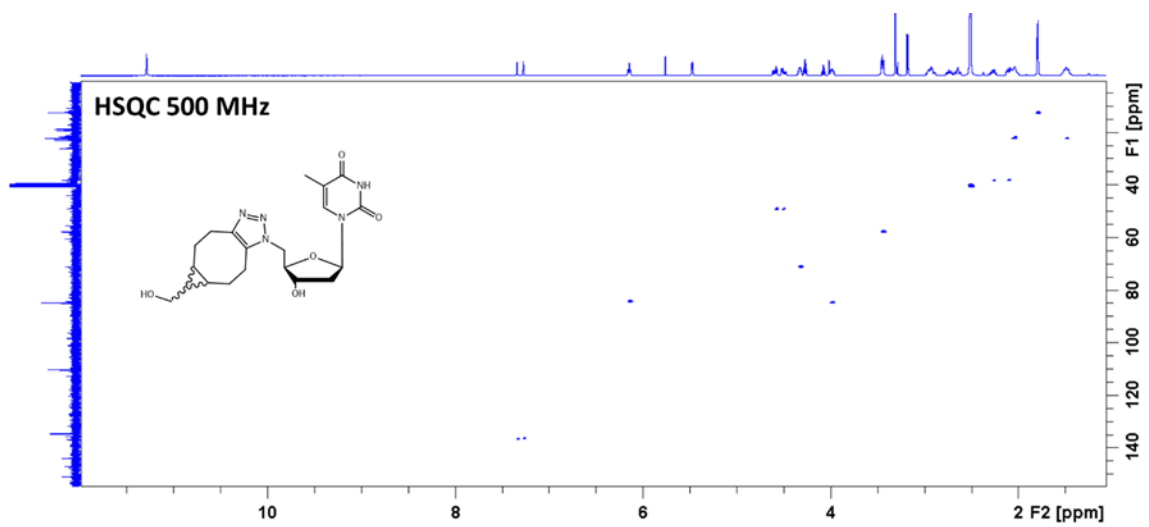
HSQC NMR spectrum (500 MHz, d_6-DMSO) of **15**.
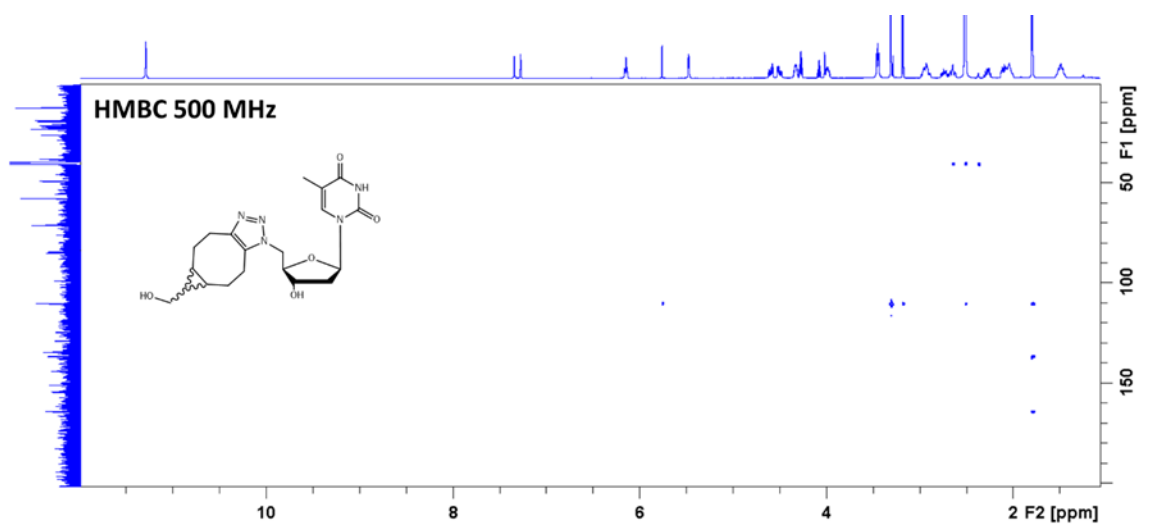
HMBC NMR spectrum (500 MHz, d_6-DMSO) of **15**.
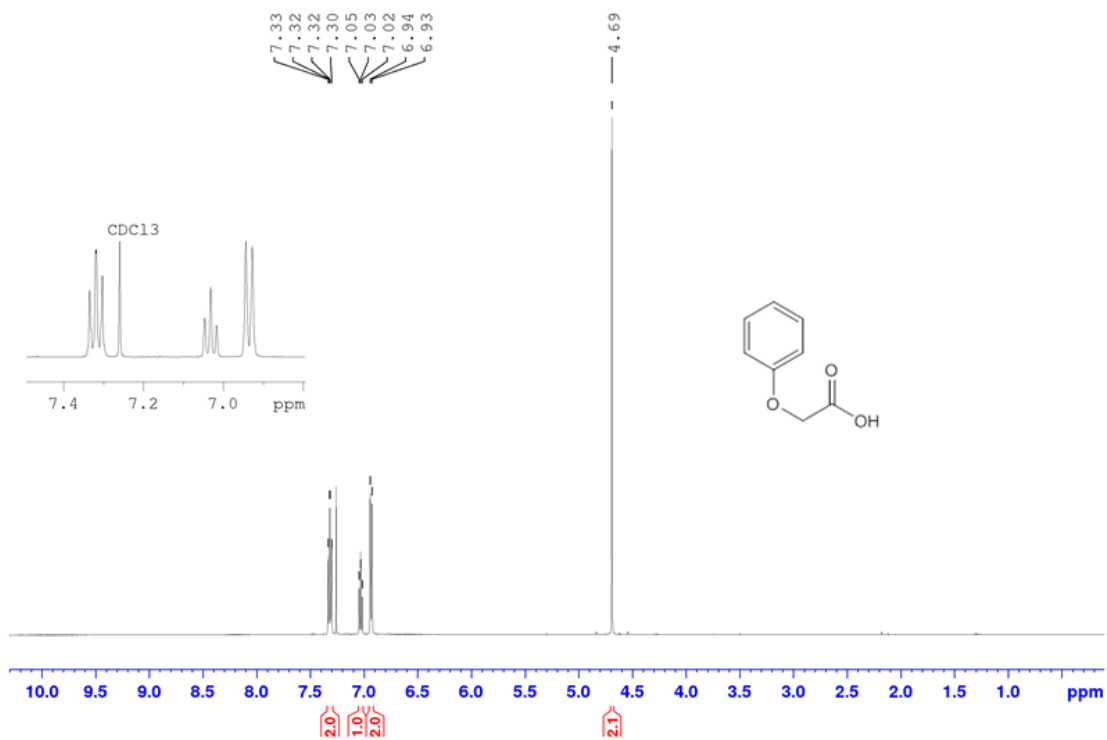
^{1}H NMR spectrum (500 MHz, CDCl$_3$) of phenoxyacetic acid (**16**).
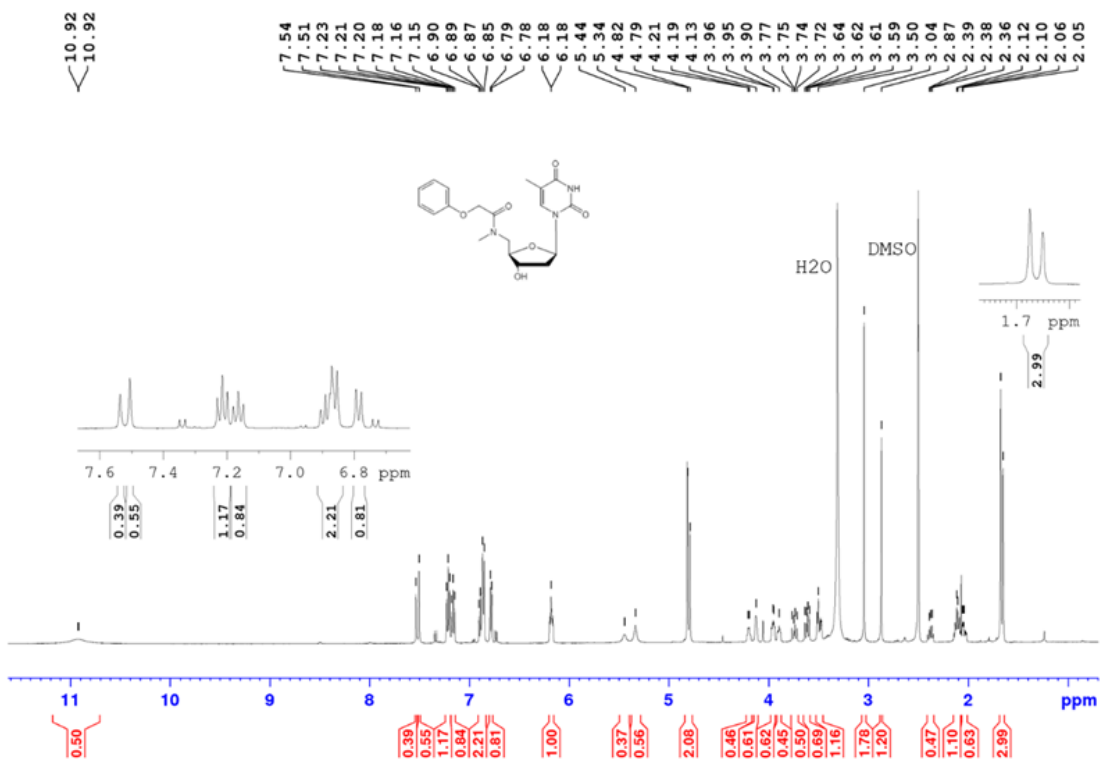
^{1}H NMR spectrum (500 MHz, d_6-DMSO) of **18**.

142
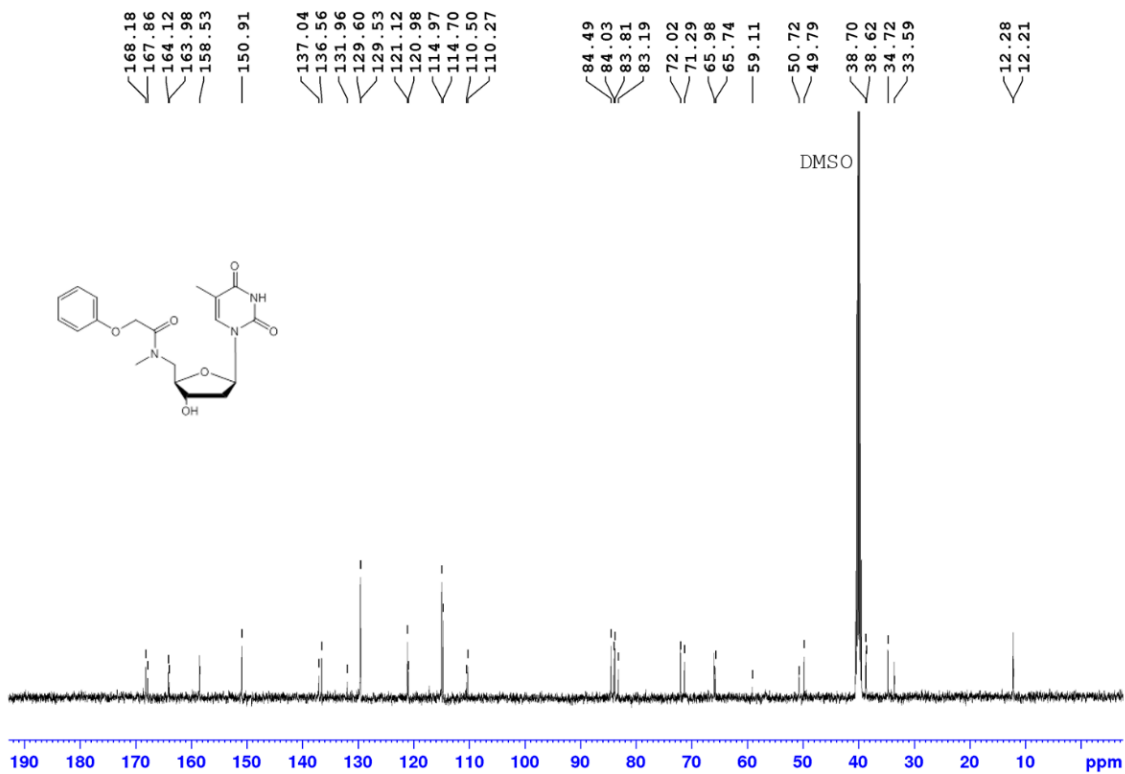
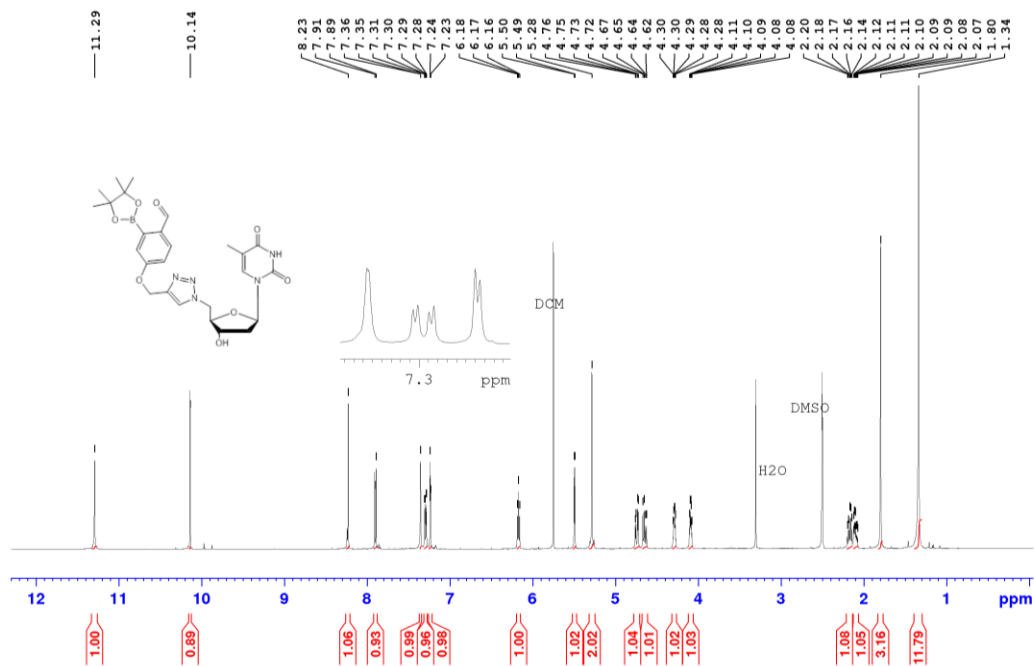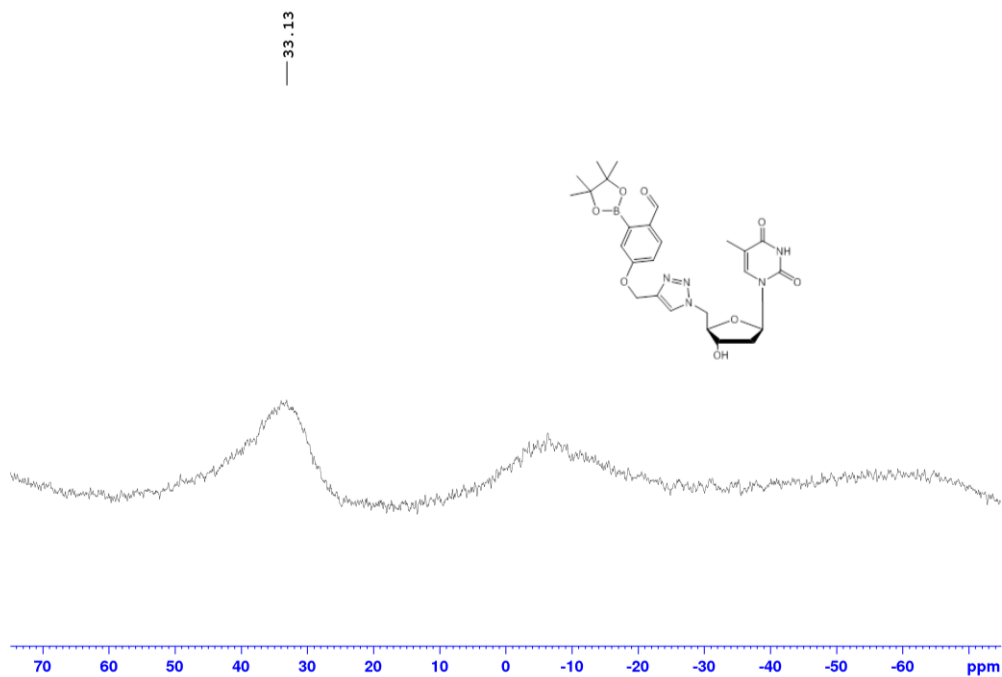^{13}C NMR spectrum (126 MHz, d_6-DMSO) of **18**.
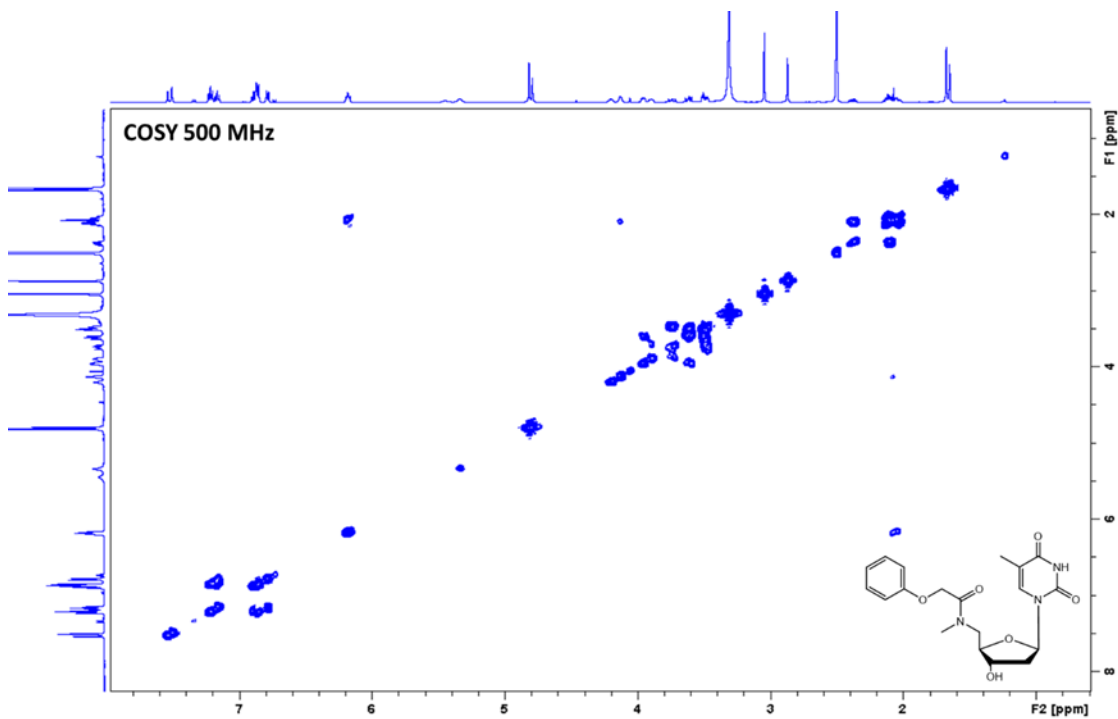
COSY NMR spectrum (500 MHz, d_6-DMSO) of **18**.
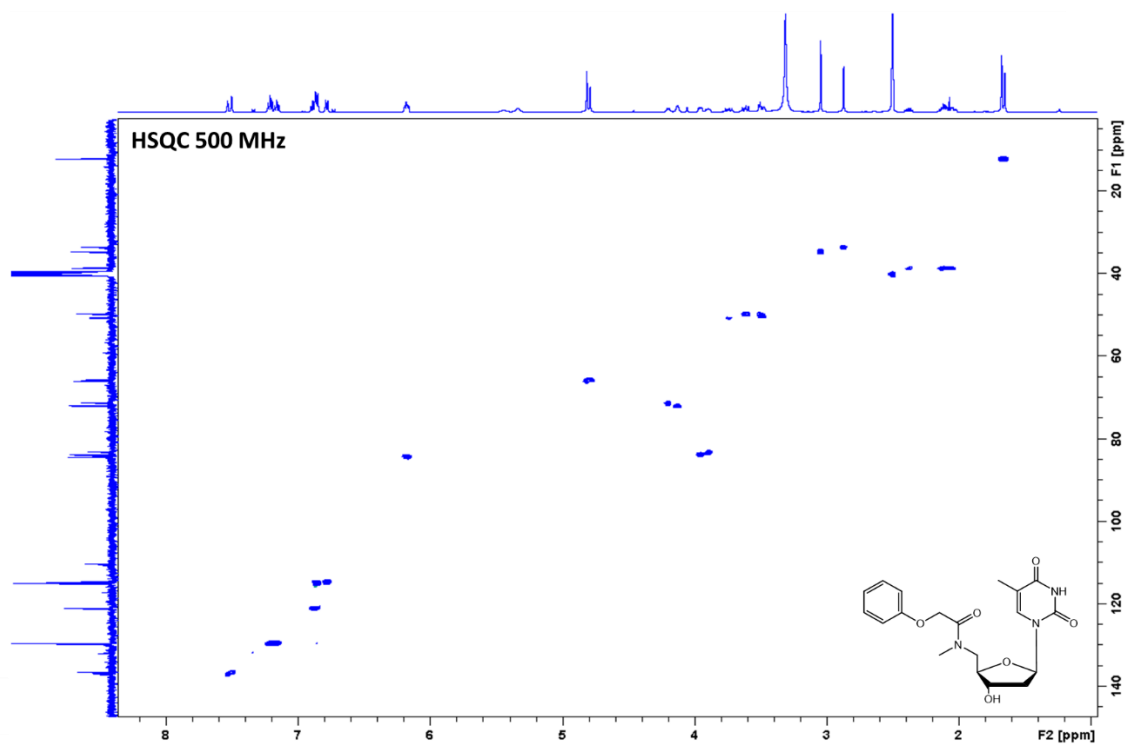
HSQC NMR spectrum (500 MHz, d_6-DMSO) of **18**.
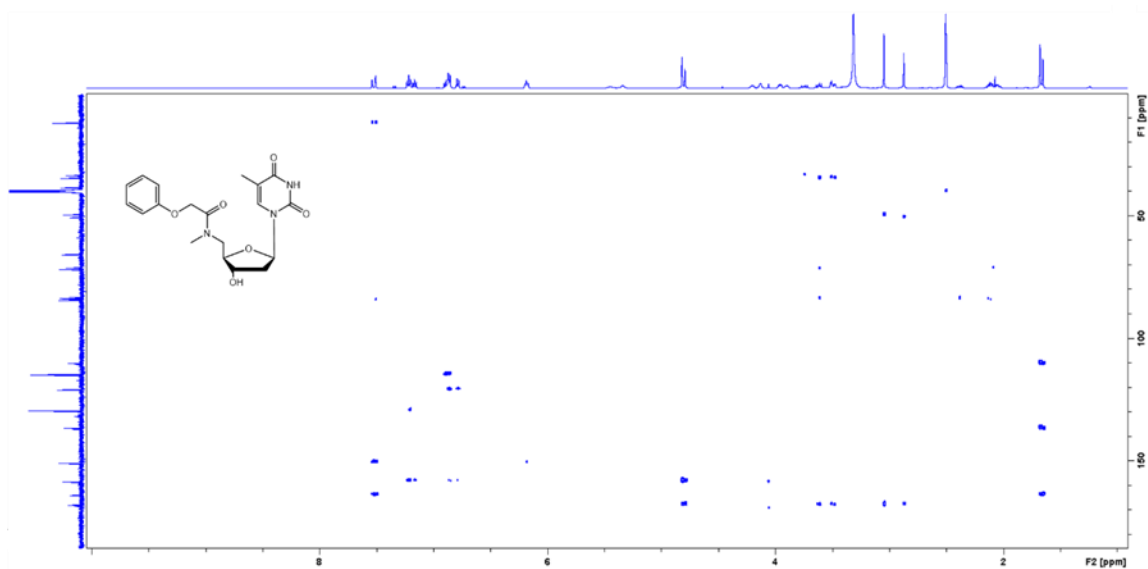
HMBC NMR spectrum (500 MHz, d_6-DMSO) of **18**.
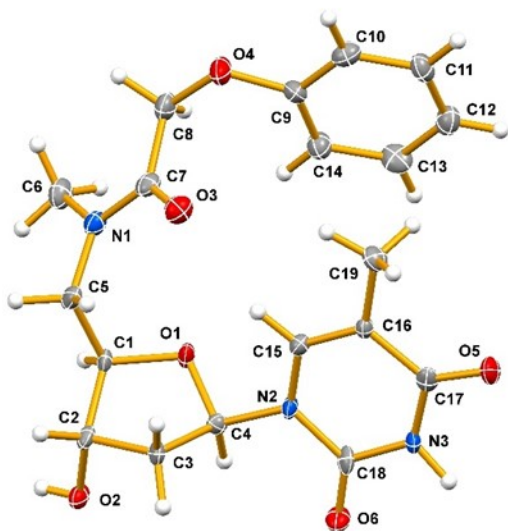
ORTEP diagram of **18**.

APPENDIX C: Solver Tutorial

The Solver add-in is available via the pathway in Excel: File → Options → Add-ins → Manage Excel Add-ins (click "Go…"). Check Solver Add-in, and click OK.

The Solver tool is accessible under the Data tab in Excel.

- In order to use Solver you will need:
    - A dataset (e.g. rate data)
    - An equation which should model the data (e.g. the modified Michaelis-Menten equation)
        - I like to write the equation for myself in the equation editor to keep track

	A	B	C	D	E	F	G	H
1								
2								
3								
4								
5		[S]	Rate data					
6		20	11.59394					
7		40	18.15758					
8		60	20.48485					
9		80	22.82424					
10		100	24.48485					
11		200	27.60606					
12		300	27.10303					
13		350	23.5697					
14								
15								
16								

$$v = \frac{V_{max}[S]}{K_M + [S](1 + \frac{[S]}{K_S})}$$

- Variables to be optimized (in this case, V_{max}, K_M and K_S) are allotted their own cells. I usually colour code them next to their labels so I can keep track:

- Estimates should be provided for each variable. To do this, I like to plot the data and guess based on the shape of the curve
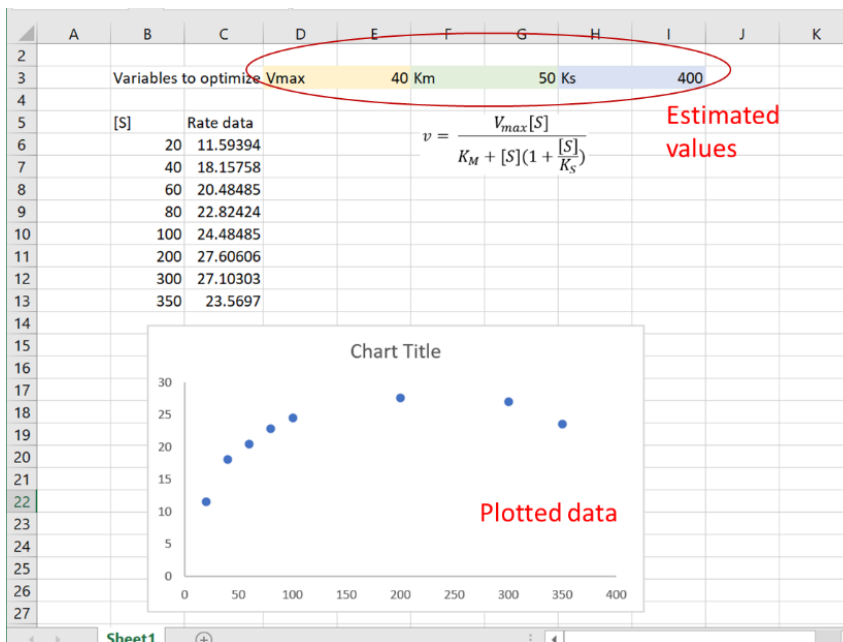
- In the column next to your data, type your equation into the top cell, referring to the cells containing your variables (by first typing "=", you will be allowed to refer to other cells by clicking on the cells or typing in the cell identity (e.g. E3)
  - Note that this equation both depends on the independent variable (in this case, [S]) and the variables to be optimized. Since each calculated point will refer to a different [S] but will otherwise contain the same values, the cells

containing (in this case, V_{max}, K_M, and K_S) can be "locked" by typing "$" in front of the column (alpha) and row (numeric) components of the cell identity (e.g. E3 → $E$3). This can also be accomplished by clicking the cell of interest, and then pressing f4. This will prevent the reference cells from changing as the equation is copied down the column. Of course, the value for [S] should change, and if your sheet is set up as in the graphics, the reference cell for [S] will be adjusted as the equation is copied.

| File | Home | Insert | Page Layout | Formulas | Data | Review | View | Help | | Share |

SUM   fx   =$E$3*B6/($G$3+B6*(1+B6/$I$3))

	A	B	C	D	E	F	G	H	I	J	K
2											
3		Variables to optimize	Vmax		40	Km		50	Ks	400	
4											
5		[S]	Rate data	Calculated							
6		20	11.59394	$I$3))							
7		40	18.15758								
8		60	20.48485								
9		80	22.82424								
10		100	24.48485								
11		200	27.60606								
12		300	27.10303								
13		350	23.5697								

$$v = \frac{V_{max}[S]}{K_M + [S](1 + \frac{[S]}{K_S})}$$

Chart Title
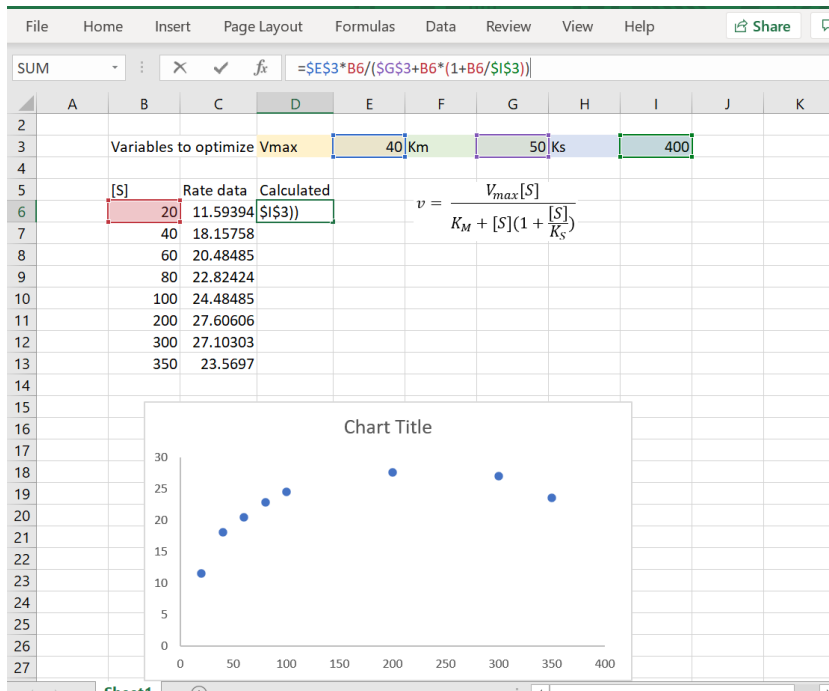
- Copy the equation down the column by selecting the top cell and double clicking on the green square in the corner. You can then plot your calculated points against the data by clicking the plot and then dragging the blue rectangle encapsulating the datapoints over one column. The calculated values will appear on the graph (orange in the figure below).

148

	A	B	C	D	E	F	G	H	I	J
2										
3		Variables to optimize	Vmax		40	Km		50	Ks	400	
4										
5		[S]	Rate data	Calculated						
6		20	11.59394	11.26761						
7		40	18.15758	17.02128						
8		60	20.48485	20.16807						
9		80	22.82424	21.91781						
10		100	24.48485	22.85714						
11		200	27.60606	22.85714						
12		300	27.10303	20.86957						
13		350	23.5697	19.82301						

$$v = \frac{V_{max}[S]}{K_M + [S](1 + \frac{[S]}{K_S})}$$

Chart Title
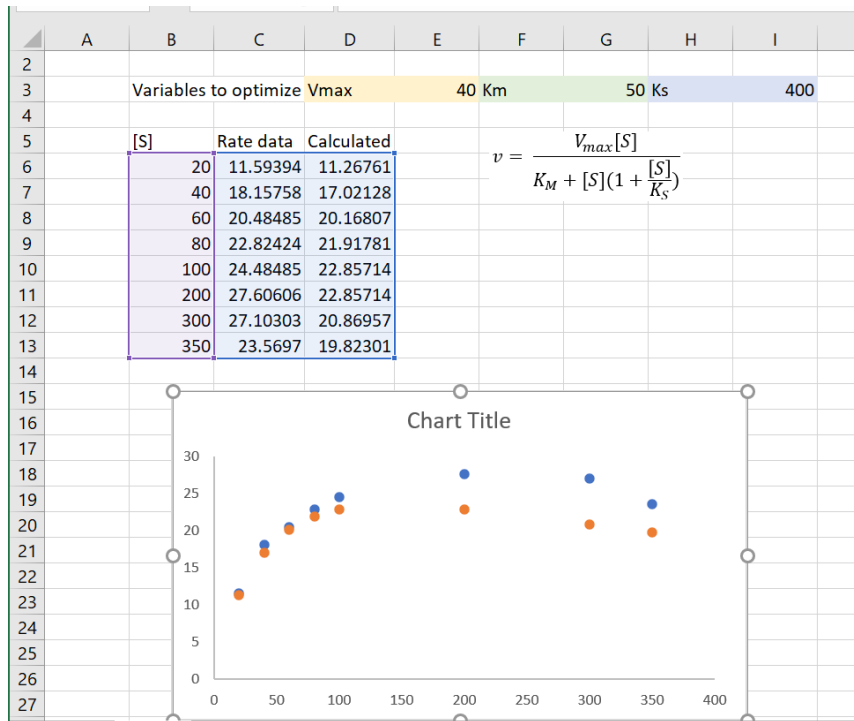
- If your fit is completely off from the data, you can manually adjust the variable values. The estimates must be close enough that the algorithm has a reasonable starting point, otherwise the fit may fail to converge.

- Next to the "calculated values" column, calculate the absolute difference between the calculated and data values. (type "=abs([cell a] – [cell b])"). Copy the equation down.

  - Note that instead of absolute difference, squared difference is often used, which is why this method is usually referred to as a "least squares" algorithm. Either method will work: the most important thing is that all the differences are positive integers.

SUM | =ABS(C13-D13)

	A	B	C	D	E	F	G	H	I	J
1										
2										
3			Variables to optimize	Vmax		40 Km		50 Ks		400
4										
5		[S]	Rate data	Calculated	Abs diff					
6		20	11.59394	11.26761	0.326333					
7		40	18.15758	17.02128	1.136299					
8		60	20.48485	20.16807	0.316781					
9		80	22.82424	21.91781	0.906434					
10		100	24.48485	22.85714	1.627705					
11		200	27.60606	22.85714	4.748918					
12		300	27.10303	20.86957	6.233465					
13		350	23.5697	19.82301	C13-D13)					

$$v = \frac{V_{max}[S]}{K_M + [S](1 + \frac{[S]}{K_S})}$$

Chart Title

- Sum the absolute differences (I usually do this in the cell next to or underneath the column of absolute differences to keep track)

F13 | =SUM(E6:E13)

	A	B	C	D	E	F	G	H	I
2									
3			Variables to optimize	Vmax		40 Km		50 Ks	400
4									
5		[S]	Rate data	Calculated	Abs diff				
6		20	11.59394	11.26761	0.326333				
7		40	18.15758	17.02128	1.136299				
8		60	20.48485	20.16807	0.316781				
9		80	22.82424	21.91781	0.906434				
10		100	24.48485	22.85714	1.627705				
11		200	27.60606	22.85714	4.748918				
12		300	27.10303	20.86957	6.233465				
13		350	23.5697	19.82301	3.746688	19.04262			

$$v = \frac{V_{max}[S]}{K_M + [S](1 + \frac{[S]}{K_S})}$$

Chart Title

Sheet1

150

- Open Solver (Data → Solver).
  - Next to "set objective", click the up arrow, then click your cell containing the sum of absolute differences. Click the down arrow on the popup box to return to Solver.
  - Next to "To:" click "minimum".
  - Under "By changing variable cells", click the up arrow, then, holding **Ctrl**, select each of the cells containing the variables you intend to optimize.
  - Under "select a solving method", I usually use the default GRG Nonlinear method.[d]
  - Click "solve". After a moment, a popup box should appear, telling you whether the algorithm has converged. Click OK.

---
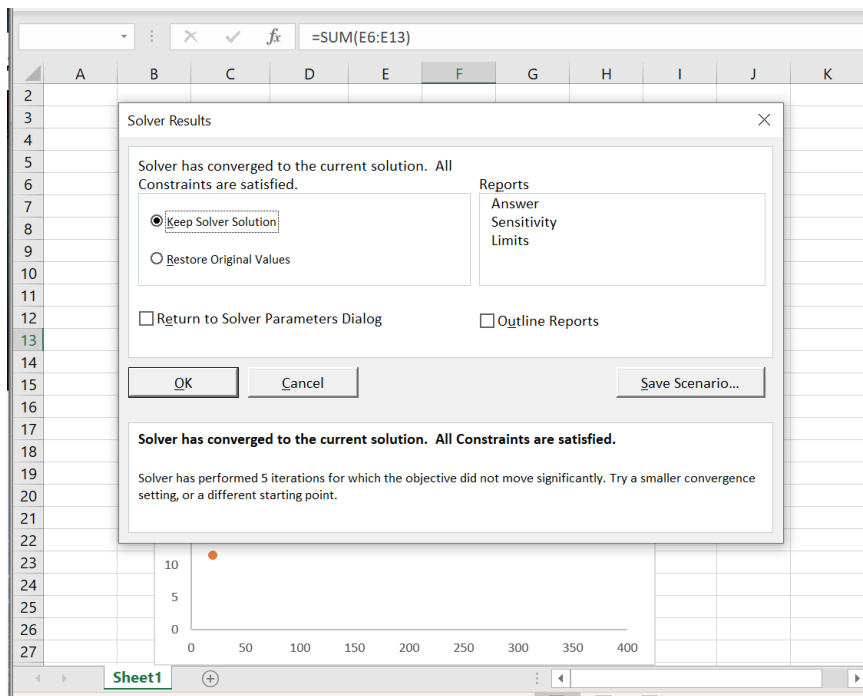
[d] [a]The GRG Nonlinear method finds the minimum value of the "target" cell by varying the values (of the variables you have told the method to consider) until the partial derivative of the function you have set up equals zero (indicating a local minimum).[72] Note that this may not find the global minimum value, which is why selecting appropriate starting estimates is important.

	A	B	C	D	E	F	G	H	I	J	K
3		Variables to optimize	Vmax		36.82019	Km		43.23083	Ks	1399.095	
4											
5		[S]	Rate data	Calculated	Abs diff						
6		20	11.59394	11.59386	8.3E-05						
7		40	18.15758	17.45562	0.70196						
8		60	20.48485	20.88024	0.395393						
9		80	22.82424	23.04769	0.223449						
10		100	24.48485	24.48504	0.000192						
11		200	27.60606	27.09152	0.514538						
12		300	27.10303	27.10302	8.74E-06						
13		350	23.5697	26.80408	3.234386	5.07001					

$$v = \frac{V_{max}[S]}{K_M + [S](1 + \frac{[S]}{K_S})}$$

Optimized values

Minimized SAD

Chart Title

- That's it! Note, however, that the fit is more accurate the fewer parameters you're adjusting at the same time. With 3 parameters, there's greater room for error and inconsistency. You may therefore choose to optimize each parameter separately. Sometimes experimentation is the best way to get the optimal fit, which is quantified by the SAD value.

APPENDIX D: Derivations of Equations 2 and 7-10.

Derivation of Equation 2

Derivation of Equation for substrate inhibition

Reaction scheme:

$$E + S \underset{K_M}{\rightleftharpoons} E \cdot S \xrightarrow{k_{cat}} E + P$$
$$+$$
$$S$$
$$\updownarrow K_S$$
$$E \cdot S \cdot S$$

Equations / Definitions

$$\cdot K_M = \frac{[E][S]}{[ES]} \qquad \cdot V = k_{cat}[ES]$$

$$\cdot K_S = \frac{[ES][S]}{[ESS]} \qquad \cdot V_{max} = k_{cat}[E]_{TOT}$$

Define $[E]_{TOT}$:

$$[E]_{TOT} = [E] + [ES] + [ESS]$$

→ substitute in equilibrium expressions

$$= [E] + \frac{[E][S]}{K_M} + \frac{[ES][S]}{K_S}$$

– eliminate $[ES]$

$$= [E] + \frac{[E][S]}{K_M} + \frac{[E][S][S]}{K_M \cdot K_S}$$

– factor out $[E]$

$$= [E]\left(1 + \frac{[S]}{K_M} + \frac{[S]^2}{K_M \cdot K_S}\right)$$

– solve for $[E]$

$$[E] = \frac{[E]_{TOT}}{1 + \frac{[S]}{K_M} + \frac{[S]^2}{K_M \cdot K_S}}$$

– substitute in $V = k_{cat}[ES]$
↳ $V = k_{cat}\frac{[E][S]}{K_M}$

$$V = \frac{k_{cat}[E]_{TOT}[S]}{K_M\left(1 + \frac{[S]}{K_M} + \frac{[S]^2}{K_M \cdot K_S}\right)}$$

– substitute in $V_{max} = k_{cat}[E]_{TOT}$
– Multiply through K_M

$$V = \frac{V_{max}[S]}{K_M + [S] + \frac{[S]^2}{K_S}}$$

– factor denominator

$$V = \frac{V_{max}[S]}{K_M + [S]\left(1 + \frac{[S]}{K_S}\right)}$$

– final Equation

Derivation of Equation 7

Derivation of equation for Substrate + Competitive Inhibition

Reaction Scheme:

$$E + S \xrightleftharpoons{K_M} E \cdot S \xrightarrow{k_{cat}} E + P$$

$$+ \qquad +$$

$$I \qquad S$$

$$\updownarrow K_I \qquad \updownarrow K$$
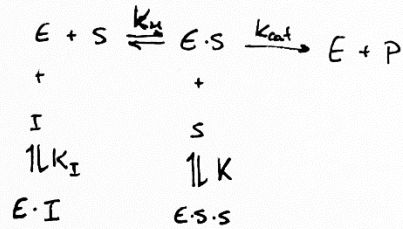
$$E \cdot I \qquad E \cdot S \cdot S$$

Equations/Definitions

$$\cdot K_M = \frac{[E][S]}{[ES]} \qquad \cdot K_S = \frac{[ES][S]}{[ESS]}$$

$$\cdot K_I = \frac{[E][I]}{[EI]} \qquad \cdot v = k_{cat}[ES]$$

$$\qquad\qquad\qquad \cdot V_{max} = k_{cat}[E]_{TOT}$$

Define $[E]_{TOT}$:

$$[E]_{TOT} = [E] + [ES] + [EI] + [ESS]$$

- Substitute in equilibrium expressions
- write all terms in terms of $[E]$

$$= [E] + \frac{[E][S]}{K_M} + \frac{[E][I]}{K_I} + \frac{[ES][S]}{K_S}$$

$$= [E] + \frac{[E][S]}{K_M} + \frac{[E][I]}{K_I} + \frac{[E][S][S]}{K_M \cdot K_S}$$

- factor out $[E]$

$$[E]_{TOT} = [E]\left(1 + \frac{[S]}{K_M} + \frac{[I]}{K_I} + \frac{[S]^2}{K_M \cdot K_S}\right)$$

- solve for $[E]$

$$[E] = \frac{[E]_{TOT}}{1 + \frac{[S]}{K_M} + \frac{[I]}{K_I} + \frac{[S]^2}{K_M \cdot K_S}}$$

- substitute into $v = k_{cat}[ES]$
$$\hookrightarrow v = \frac{k_{cat}[E][S]}{K_M}$$

$$v = \frac{k_{cat} \cdot [E]_{TOT} \cdot [S]}{K_M\left(1 + \frac{[S]}{K_M} + \frac{[I]}{K_I} + \frac{[S]^2}{K_M \cdot K_S}\right)}$$

- Substitute in $V_{max} = k_{cat}[E]_{TOT}$
- Multiply through K_M

$$v = \frac{V_{max}[S]}{K_M + [S] + \frac{K_M[I]}{K_I} + \frac{[S]^2}{K_S}}$$

- factor denominator

$$v = \frac{V_{max}[S]}{K_M\left(1 + \frac{[I]}{K_I}\right) + [S]\left(1 + \frac{[S]}{K_S}\right)}$$

- final Equation

Derivation of Equation 8

Derivation of Equation for Uncompetitive + Substrate Inhibition

Reaction Scheme:

$$E \cdot S \cdot S$$

$$\Updownarrow K_S$$

$$S$$

$$+$$

$$E + S \underset{}{\overset{K_M}{\rightleftharpoons}} E \cdot S \xrightarrow{k_{cat}} E + P$$

$$+$$

$$I$$

$$\Updownarrow K_I$$

$$E \cdot S \cdot I$$
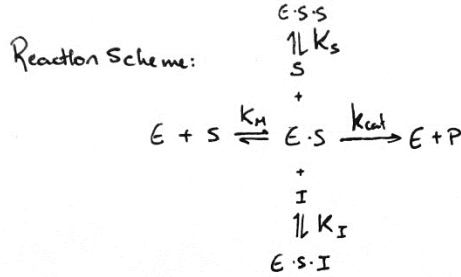
Equations / Definitions:

$$\cdot \; K_M = \frac{[E][S]}{[ES]} \qquad \cdot \; K_S = \frac{[ES][S]}{[ESS]}$$

$$\cdot \; K_I = \frac{[ES][I]}{[ESI]} \qquad \cdot \; v = k_{cat}[ES]$$

$$\cdot \; V_{max} = k_{cat}[E]_{TOT}$$

Define $[E]_{TOT}$:

$$[E]_{TOT} = [E] + [ES] + [ESI] + [ESS]$$

— Substitute in Equilibrium Expressions

$$= [E] + \frac{[E][S]}{K_M} + \frac{[ES][I]}{K_I} + \frac{[ES][S]}{K_S}$$

— sub in K_M expression to eliminate $[ES]$

$$= [E] + \frac{[E][S]}{K_M} + \frac{[E][S][I]}{K_M \cdot K_I} + \frac{[E][S][S]}{K_M \cdot K_S}$$

— factor out $[E]$

$$[E]_{TOT} = [E]\left(1 + \frac{[S]}{K_M} + \frac{[S][I]}{K_M \cdot K_I} + \frac{[S]^2}{K_M \cdot K_S}\right)$$

— Solve for $[E]$

$$[E] = \frac{[E]_{TOT}}{1 + \frac{[S]}{K_M} + \frac{[S][I]}{K_M \cdot K_I} + \frac{[S]^2}{K_M \cdot K_S}}$$

— Sub into $v = k_{cat}[ES]$

$$\hookrightarrow \; v = k_{cat}\frac{[E][S]}{K_M}$$

$$v = \frac{k_{cat}[E]_{TOT}[S]}{K_M\left(1 + \frac{[S]}{K_M} + \frac{[S][I]}{K_M \cdot K_I} + \frac{[S]^2}{K_M \cdot K_S}\right)}$$

— substitute in $V_{max} = k_{cat}[E]_{TOT}$

— Multiply K_M through denominator

$$v = \frac{V_{max} \cdot [S]}{K_M + [S] + \frac{[S][I]}{K_I} + \frac{[S]^2}{K_S}}$$

— factor denominator

$$v = \frac{V_{max}[S]}{K_M + [S]\left(1 + \frac{[I]}{K_I} + \frac{[S]}{K_S}\right)}$$

— final Equation

155

Derivation of Equation 9

Derivation of equation for Substrate + Noncompetitive Inhibition

Reaction Scheme:

$$E \cdot S \cdot S$$
$$\updownarrow K_S$$
$$S$$
$$+$$
$$E + S \underset{\xleftarrow{\hspace{0.5cm}}}{\overset{K_M}{\rightleftharpoons}} ES \xrightarrow{k_{cat}} E + P$$
$$+ \qquad\qquad +$$
$$I \qquad\qquad I$$
$$\updownarrow K_I \qquad \updownarrow K_I$$
$$E \cdot I \qquad E \cdot S \cdot I$$
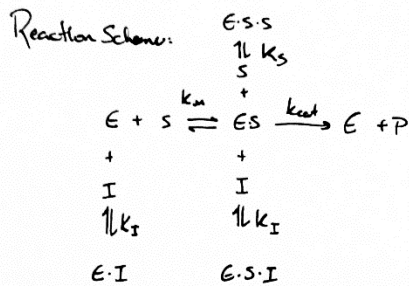
Equations / Definitions:

$$\cdot\ K_M = \frac{[E][S]}{[ES]} \qquad\qquad \cdot\ K_S = \frac{[ES][S]}{[ESS]}$$

$$\cdot\ K_I = \frac{[E][I]}{[EI]} = \frac{[ES][I]}{[ESI]} \qquad \cdot\ v = k_{cat}[ES]$$

$$\qquad\qquad\qquad\qquad\qquad\qquad \cdot\ V_{max} = k_{cat}[E]_{TOT}$$

Define $[E]_{TOT}$:

$$[E]_{TOT} = [E] + [ES] + [EI] + [ESI] + [ESS]$$

— Substitute in equilibrium expressions

$$= [E] + \frac{[E][S]}{K_M} + \frac{[E][I]}{K_I} + \frac{[ES][I]}{K_I} + \frac{[ES][S]}{K_S}$$

— Eliminate [ES]

$$= [E] + \frac{[E][S]}{K_M} + \frac{[E][I]}{K_I} + \frac{[E][S][I]}{K_M \cdot K_I} + \frac{[E][S][S]}{K_I \cdot K_S}$$

— Factor out [E]

$$= [E]\left(1 + \frac{[S]}{K_M} + \frac{[I]}{K_I} + \frac{[S][I]}{K_M \cdot K_I} + \frac{[S]^2}{K_I \cdot K_S} \right)$$

— solve for [E]

$$[E] = \frac{[E]_{TOT}}{1 + \frac{[S]}{K_M} + \frac{[I]}{K_I} + \frac{[S][I]}{K_M \cdot K_I} + \frac{[S]^2}{K_I \cdot K_S}}$$

— sub into $v = k_{cat}[ES]$
    ↳ $v = \dfrac{k_{cat}[E][S]}{K_M}$

$$v = \frac{k_{cat}[E]_{TOT}[S]}{K_M\left(1 + \frac{[S]}{K_M} + \frac{[I]}{K_I} + \frac{[S][I]}{K_M \cdot K_I} + \frac{[S]^2}{K_I \cdot K_S} \right)}$$

— Substitute in $V_{max} = k_{cat}[E]_{TOT}$
— Multiply K_M through

$$v = \frac{V_{max}[S]}{K_M + [S] + \frac{K_M[I]}{K_I} + \frac{[S][I]}{K_I} + \frac{[S]^2}{K_I \cdot K_S}}$$

— Factor denominator

$$v = \frac{V_{max}[S]}{K_M\left(1 + \frac{[I]}{K_I} \right) + [S]\left(1 + \frac{[I]}{K_I} + \frac{[S]}{K_S} \right)}$$

— Final Equation

Derivation of Equation 10

Derivation of equation for substrate + Mixed Inhibition

Reaction Scheme:

$$E \cdot S \cdot S$$
$$\updownarrow K_S$$
$$S$$
$$+$$
$$E + S \underset{K_M}{\rightleftharpoons} E \cdot S \xrightarrow{k_{cat}} E + P$$
$$+ \qquad\qquad +$$
$$I \qquad\qquad I$$
$$\updownarrow K_{IC} \qquad \updownarrow K_{IU}$$
$$E \cdot I \qquad E \cdot S \cdot I$$
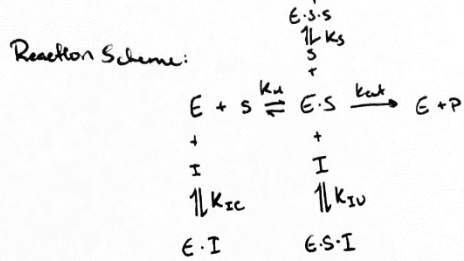
Equations / Definitions:

$$\cdot K_M = \frac{[E][S]}{[ES]} \qquad \cdot K_{IC} = \frac{[E][I]}{[EI]}$$

$$\cdot K_S = \frac{[ES][S]}{[ESS]} \qquad K_{IU} = \frac{[ES][I]}{[ESI]}$$

$$\cdot v = k_{cat}[ES] \qquad \cdot V_{max} = k_{cat}[E]_{TOT}$$

Define $[E]_{TOT}$:

$$[E]_{TOT} = [E] + [ES] + [EI] + [ESS] + [ESI]$$

- substitute in equilibrium expressions

$$= [E] + \frac{[E][S]}{K_M} + \frac{[E][I]}{K_{IC}} + \frac{[ES][S]}{K_S} + \frac{[ES][I]}{K_{IU}}$$

- eliminate $[ES]$

$$= [E] + \frac{[E][S]}{K_M} + \frac{[E][I]}{K_{IC}} + \frac{[E][S][S]}{K_M \cdot K_S} + \frac{[E][S][I]}{K_M \cdot K_{IU}}$$

- factor out $[E]$

$$= [E] \left(1 + \frac{[S]}{K_M} + \frac{[I]}{K_{IC}} + \frac{[S]^2}{K_M \cdot K_S} + \frac{[S][I]}{K_M \cdot K_{IU}} \right)$$

- solve for $[E]$

$$[E] = \frac{[E]_{TOT}}{1 + \frac{[S]}{K_M} + \frac{[I]}{K_{IC}} + \frac{[S]^2}{K_M \cdot K_S} + \frac{[S][I]}{K_M \cdot K_{IU}}}$$

- substitute into $v = k_{cat}[ES]$
$$\hookrightarrow v = k_{cat} \frac{[E][S]}{K_M}$$

$$v = \frac{k_{cat}[E]_{TOT}[S]}{K_M \left(1 + \frac{[S]}{K_M} + \frac{[I]}{K_{IC}} + \frac{[S]^2}{K_M \cdot K_S} + \frac{[S][I]}{K_M \cdot K_{IU}} \right)}$$

- Substitute in $V_{max} = k_{cat}[E]_{TOT}$
- Multiply through K_M

$$v = \frac{V_{max}[S]}{K_M + [S] + \frac{[I]K_M}{K_{IC}} + \frac{[S]^2}{K_S} + \frac{[S][I]}{K_{IU}}}$$

- Factor denominator

$$v = \frac{V_{max}[S]}{K_M \left(1 + \frac{[I]}{K_{IC}} \right) + [S] \left(1 + \frac{[S]}{K_S} + \frac{[I]}{K_{IU}} \right)}$$

- final Equation

APPENDIX E: Lineweaver-Burk Plots of Kinetic Data
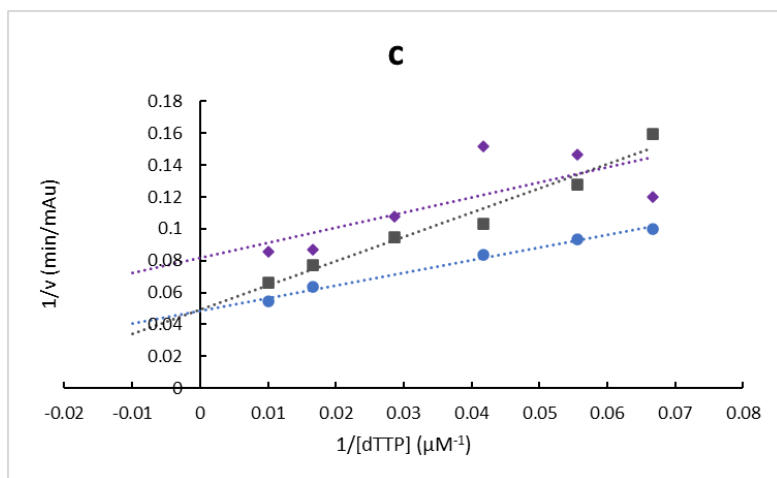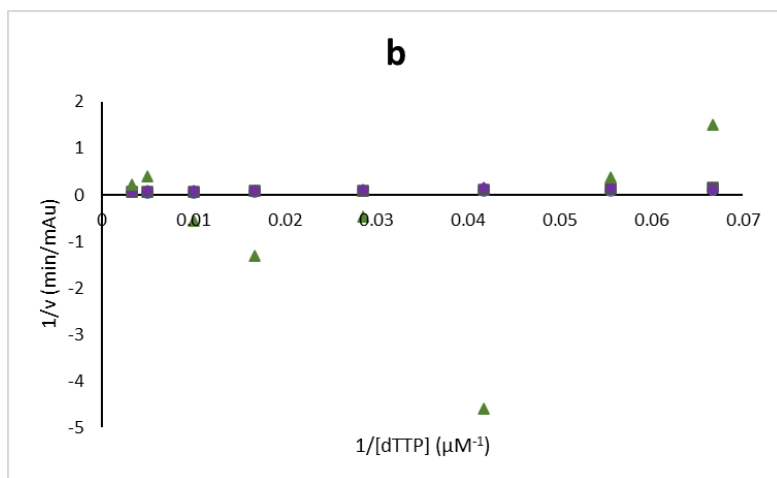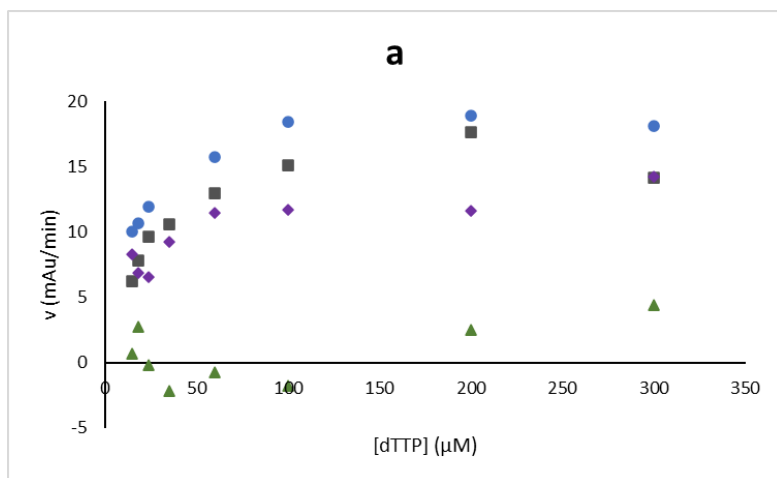
Inhibition of Cps2L by **4a** at 0 (●), 200 (■), 400 (◆) and 800 (▲) μM inhibitor. a) Michaelis-Menten plot of data; b) Lineweaver-Burk plot of all data; c) Lineweaver-Burk plot of data, with nonlinear datapoints removed, and trendlines superimposed. 800 μM dataset removed for clarity.
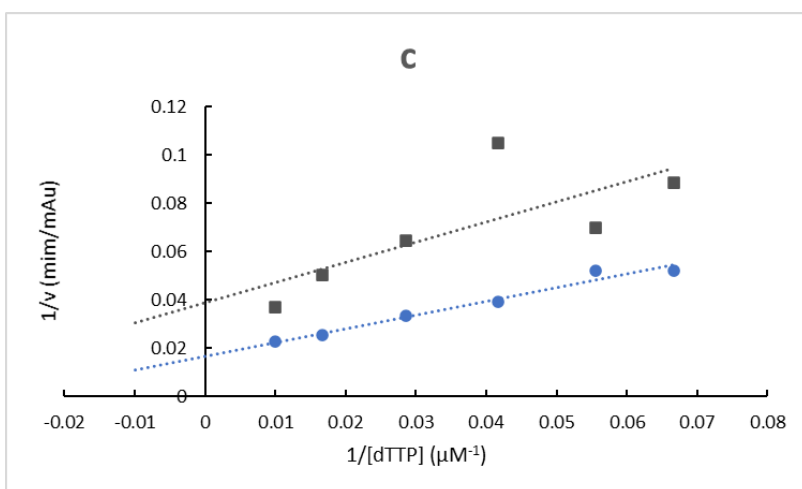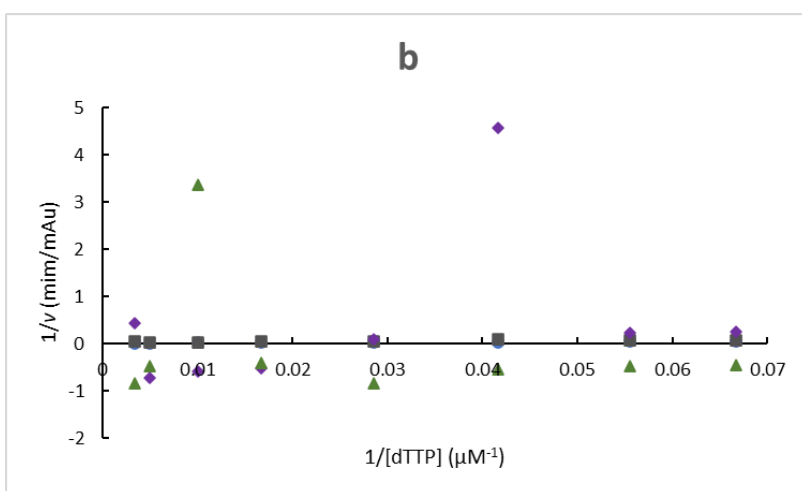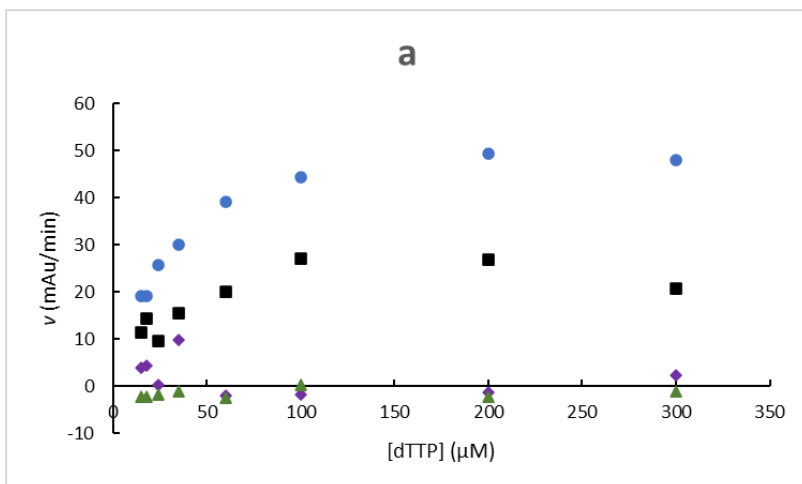
Inhibition of Cps2L by **4b** at 0 (●), 200 (■), 400 (♦) and 800 (▲) μM inhibitor. a) Michaelis-Menten plot of data; b) Lineweaver-Burk plot of all data; c) Lineweaver-Burk plot of data, with nonlinear datapoints removed, and trendlines superimposed. 400 and 800 μM datasets removed for clarity.
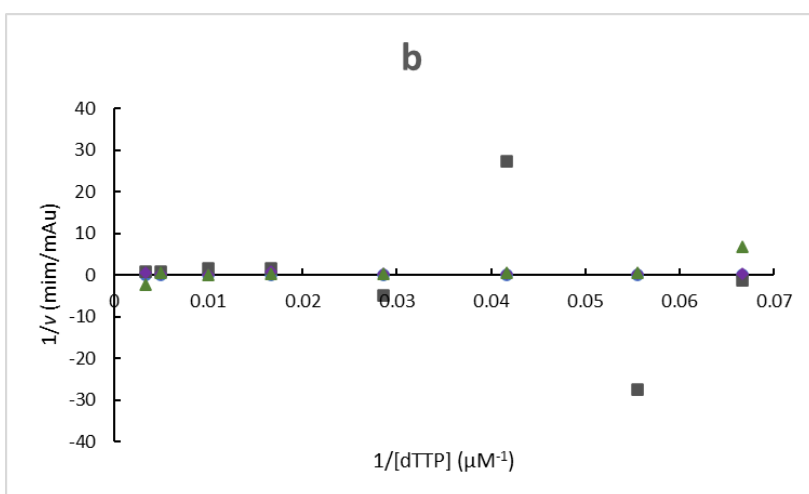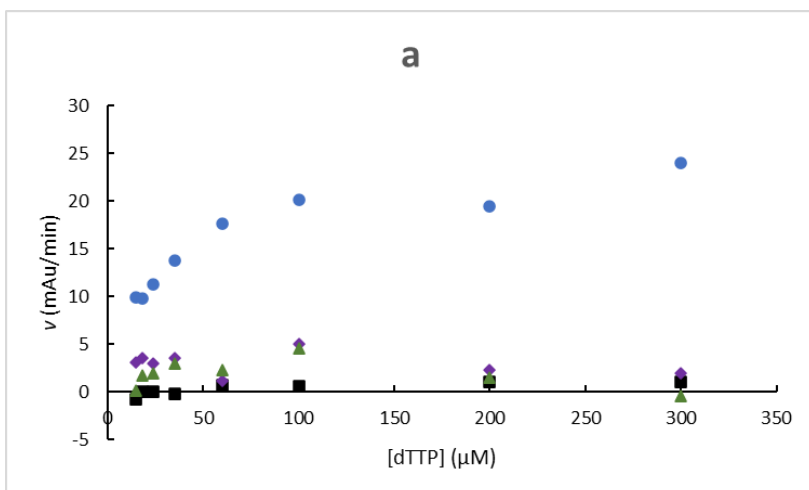
Inhibition of Cps2L by **4d** at 0 (●), 25 (■), 50 (♦) and 100 (▲) µM inhibitor. a) Michaelis-Menten plot of data; b) Lineweaver-Burk plot of all data. None of the inhibition data gave linear correlations in the Lineweaver-Burk plot.
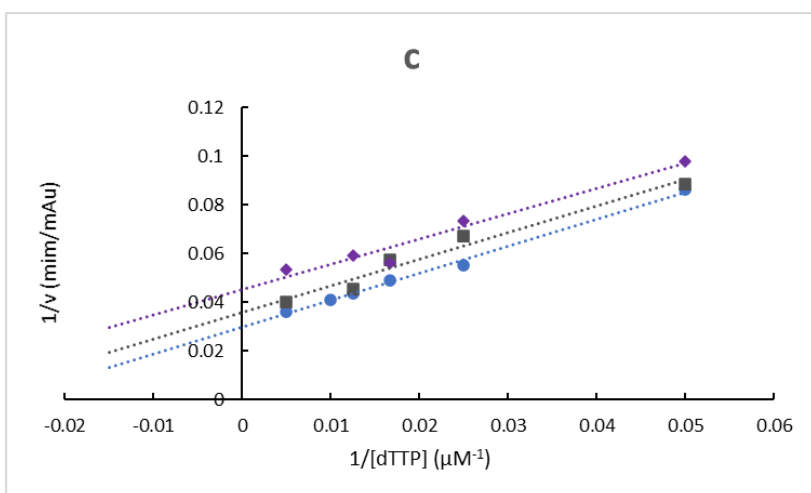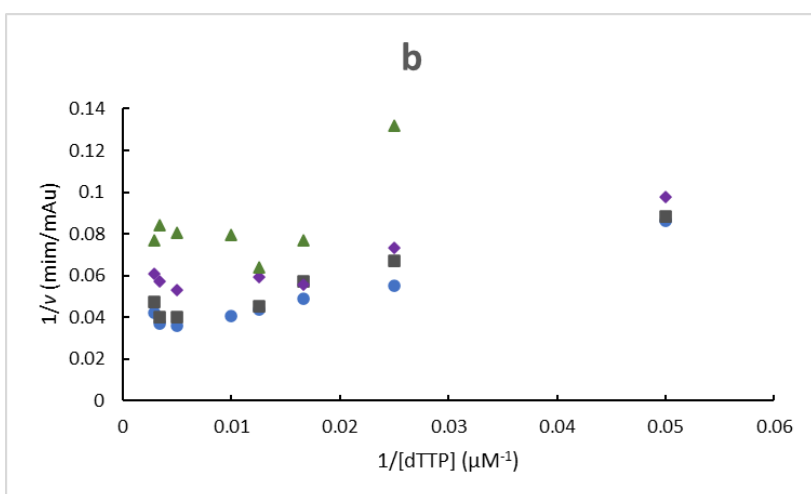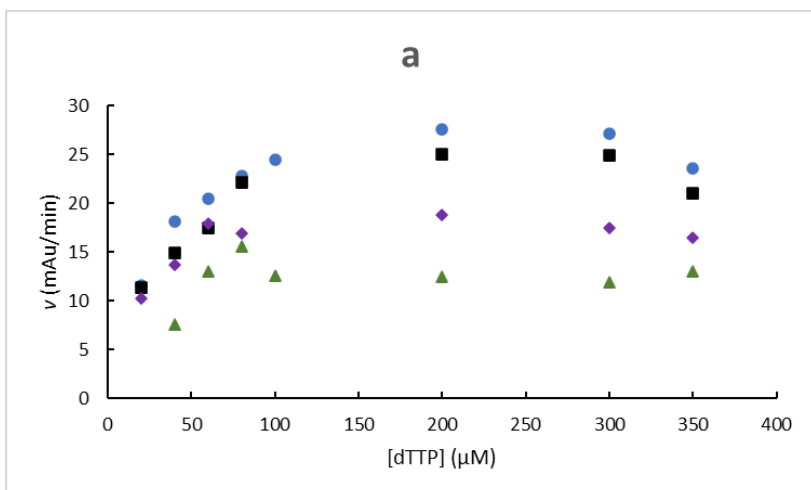
Inhibition of Cps2L by **4e** at 0 (●), 100 (■), 200 (♦) and 300 (▲) μM inhibitor. a) Michaelis-Menten plot of data; b) Lineweaver-Burk plot of all data; c) Lineweaver-Burk plot of data, with nonlinear points removed, and trendlines superimposed. 300 μM dataset removed for clarity.

161
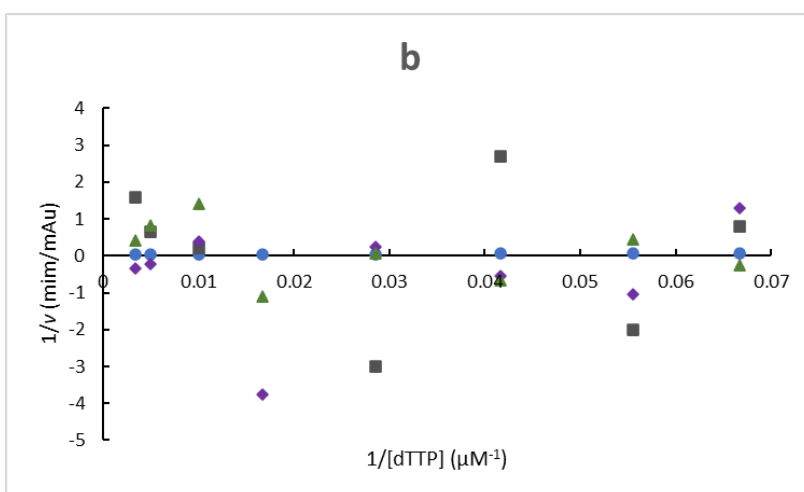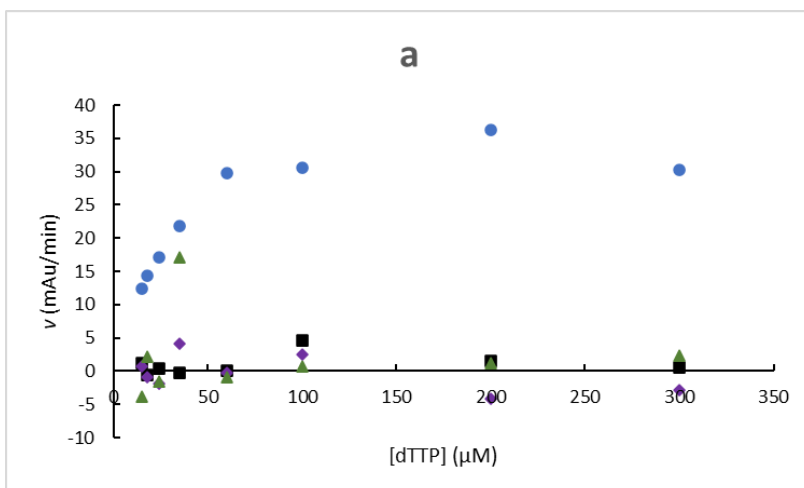
Inhibition of Cps2L by **4f** at 0 (●), 200 (■), 400 (◆) and 800 (▲) μM inhibitor. a) Michaelis-Menten plot of data; b) Lineweaver-Burk plot of all data. None of the inhibition data gave linear correlations in the Lineweaver-Burk plot.
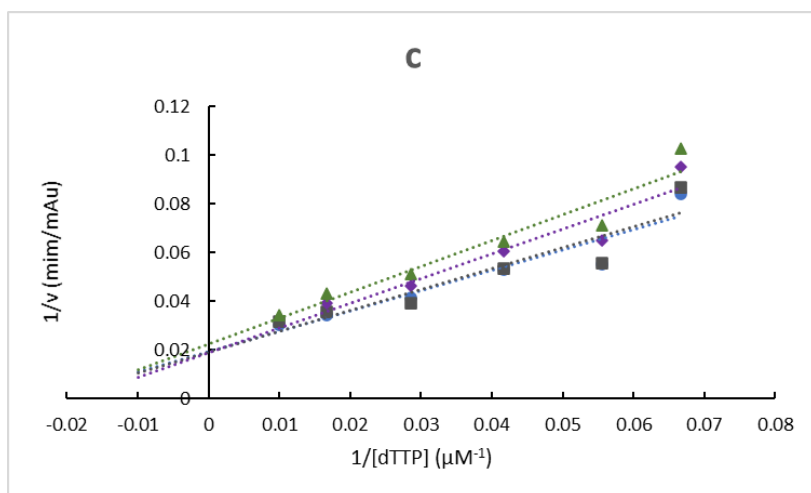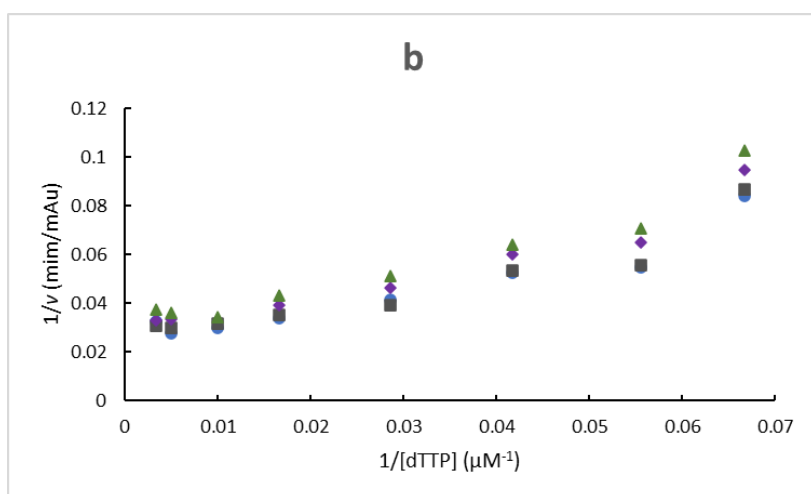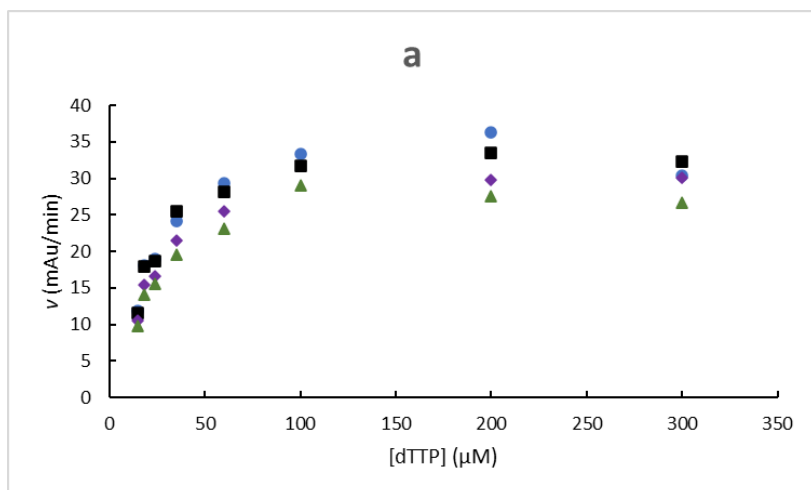
Inhibition of Cps2L by **4g** at 0 (●), 200 (■), 400 (♦) and 800 (▲) μM inhibitor. a)
Michaelis-Menten plot of data; b) Lineweaver-Burk plot of all data; c) Lineweaver-Burk
plot of data, with nonlinear datapoints removed, and trendlines superimposed.
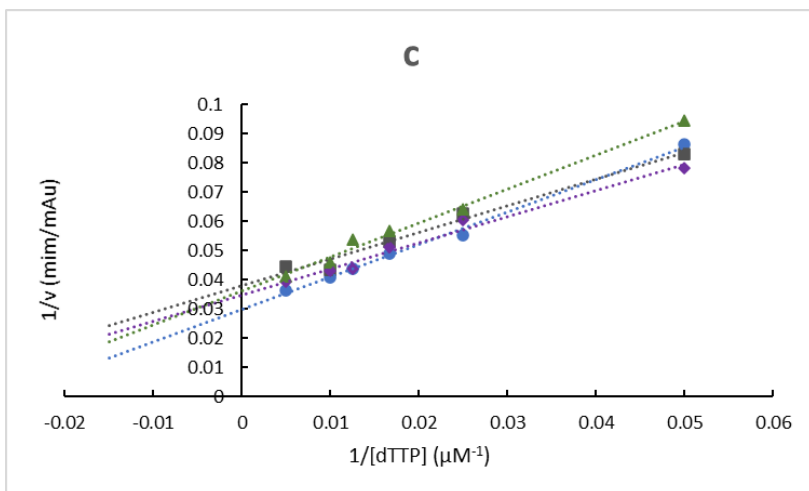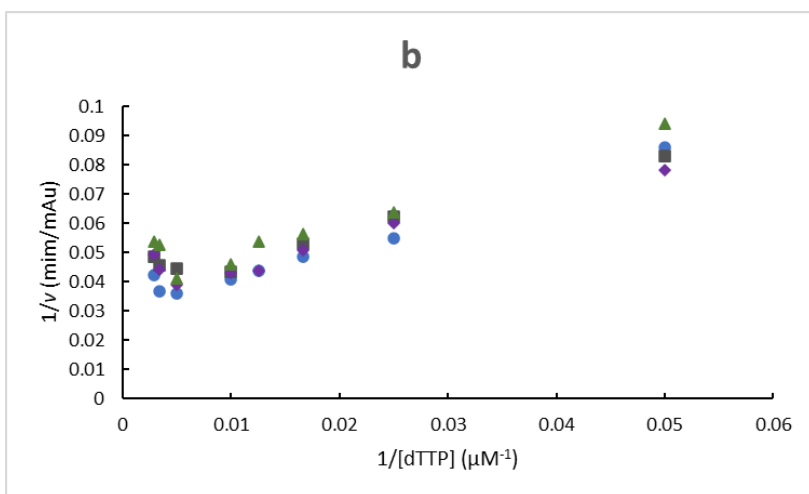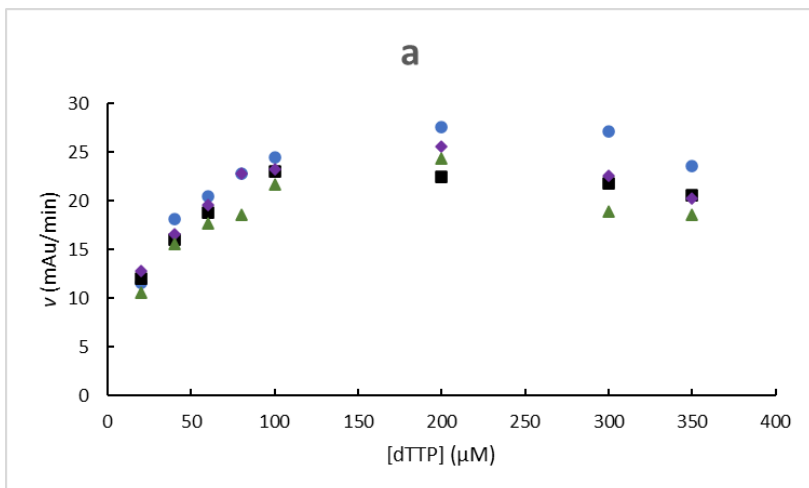
Inhibition of Cps2L by **7** at 0 (●), 200 (■), 400 (◆) and 800 (▲) μM inhibitor. a) Michaelis-Menten plot of data; b) Lineweaver-Burk plot of all data; c) Lineweaver-Burk plot of data, with nonlinear datapoints removed, and trendlines superimposed.
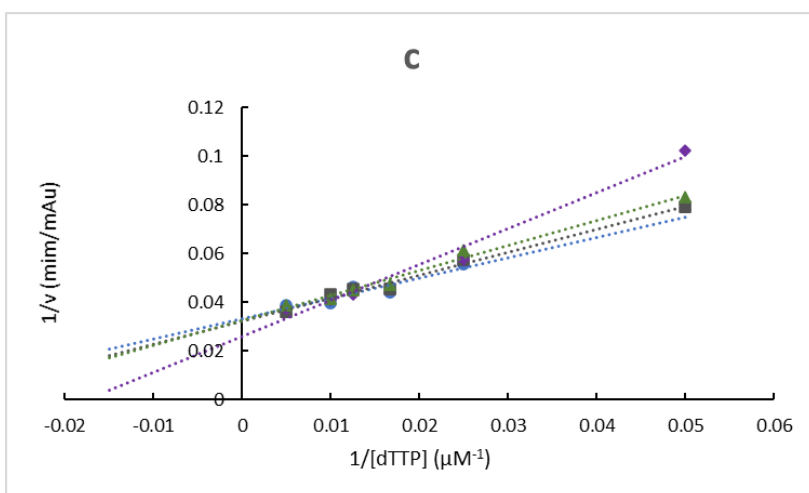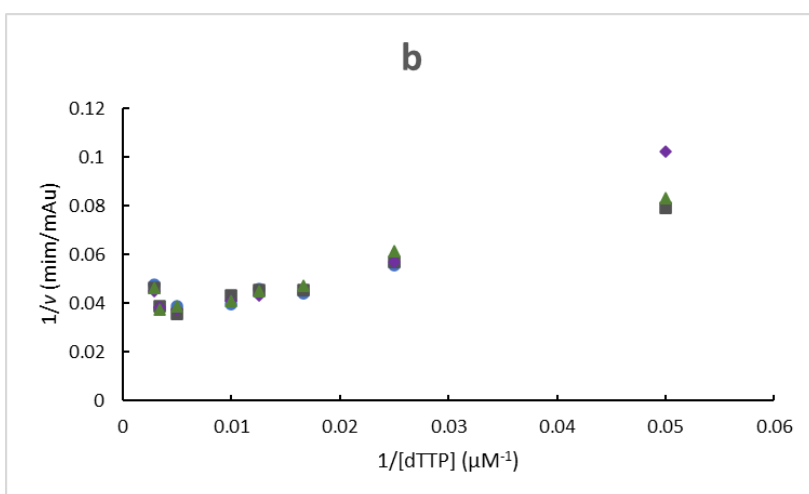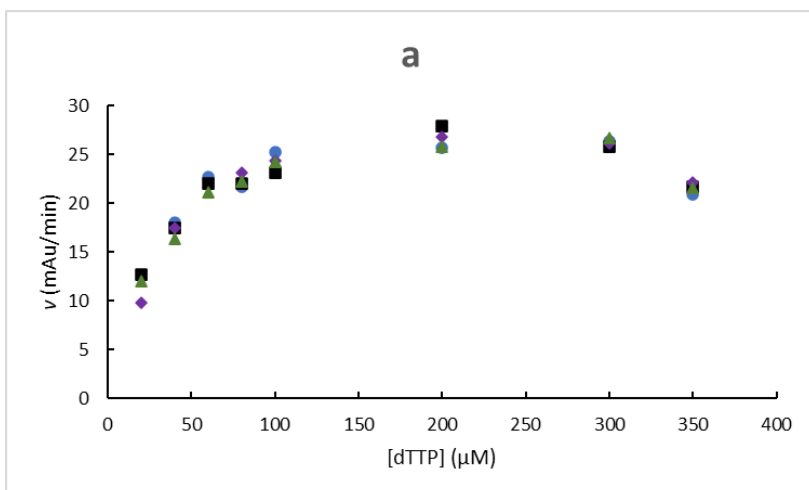
Inhibition of Cps2L by **8** at 0 (●), 200 (■), 400 (◆) and 800 (▲) µM inhibitor. a) Michaelis-Menten plot of data; b) Lineweaver-Burk plot of all data; c) Lineweaver-Burk plot of data, with nonlinear datapoints removed, and trendlines superimposed.
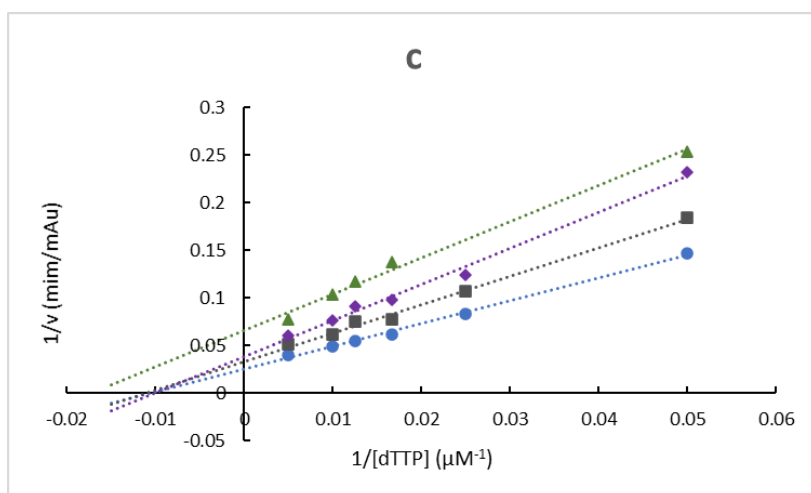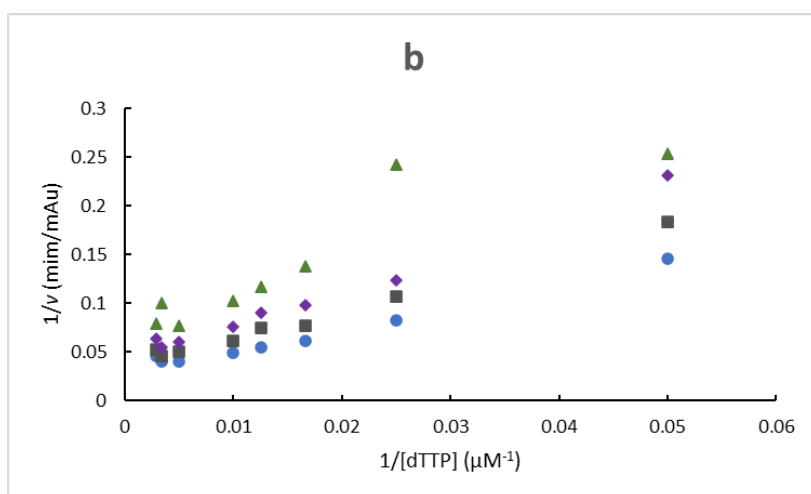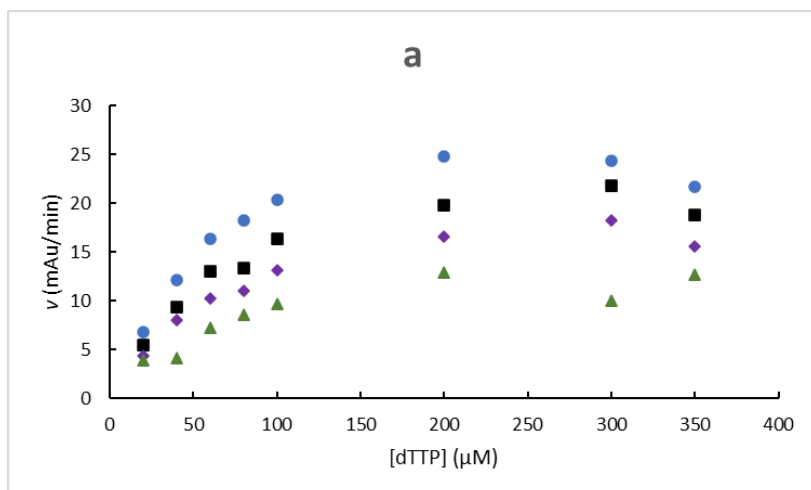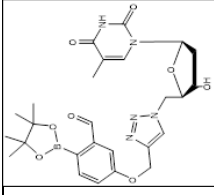
Inhibition of Cps2L by **10a** at 0 (●), 200 (■), 400 (◆) and 800 (▲) μM inhibitor. a) Michaelis-Menten plot of data; b) Lineweaver-Burk plot of all data; c) Lineweaver-Burk plot of data, with nonlinear datapoints removed, and trendlines superimposed.

APPENDIX F: Kinetic Inhibition Data

Appendix E1. Left: rate inhibition data (solid shapes) and mathematical model (lines / open shapes) for inhibition of Cps2L by **4a** according to a) competitive, b) uncompetitive, c) noncompetitive, and d) mixed inhibition, with substrate inhibition. Calculated parameters: V_{max} = 56.4 mAu/min; K_M = 46.3 µM; K_{IS} (substrate) = 428.8 µM. Below: Summary of calculated inhibition constants and error (SAD) for each model.
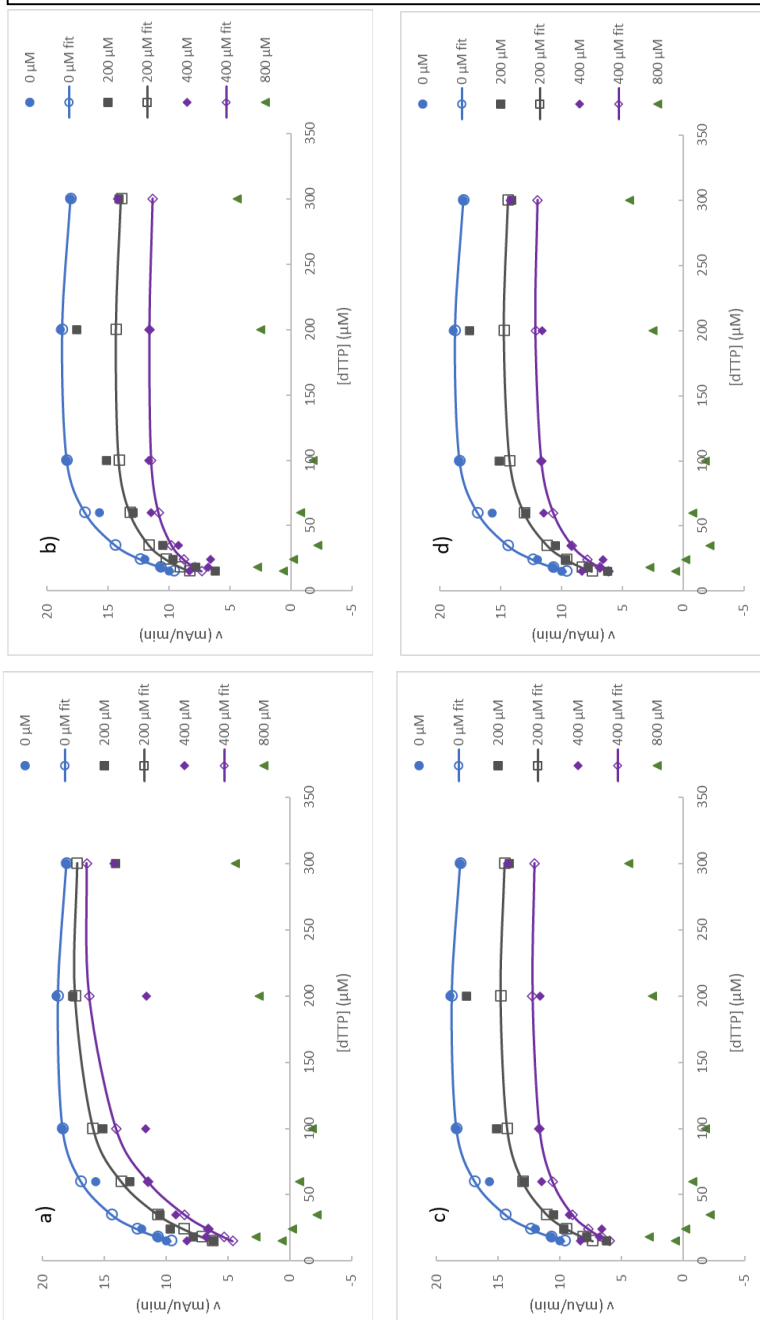
Note: Optimization of the fit did not consider the 800 µM dataset due to poor quality.
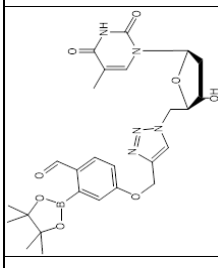
Mode of inhibition	K_{IC} (µM)	K_{IU} (µM)	Sum of absolute differences (SAD) (mAu/min)
Competitive (a)	219.9	-	21.8
Uncompetitive (b)	-	503.3	17.5
Noncompetitive (c)	645.5		28.3
Mixed (d)	786.5	620.6	28.0

Structure	
4a	

Appendix E2.
Left: rate inhibition data (solid shapes) and mathematical model (lines / open shapes) for inhibition of Cps2L by **4b** according to a) competitive, b) uncompetitive, c) noncompetitive, and d) mixed inhibition, with substrate inhibition. Calculated parameters: $V_{max} = 62.8$ mAu/min; $K_M = 34.3$ μM; K_{IS} (substrate) = 1544 μM. Below: Summary of calculated inhibition constants and error (SAD) for each model.
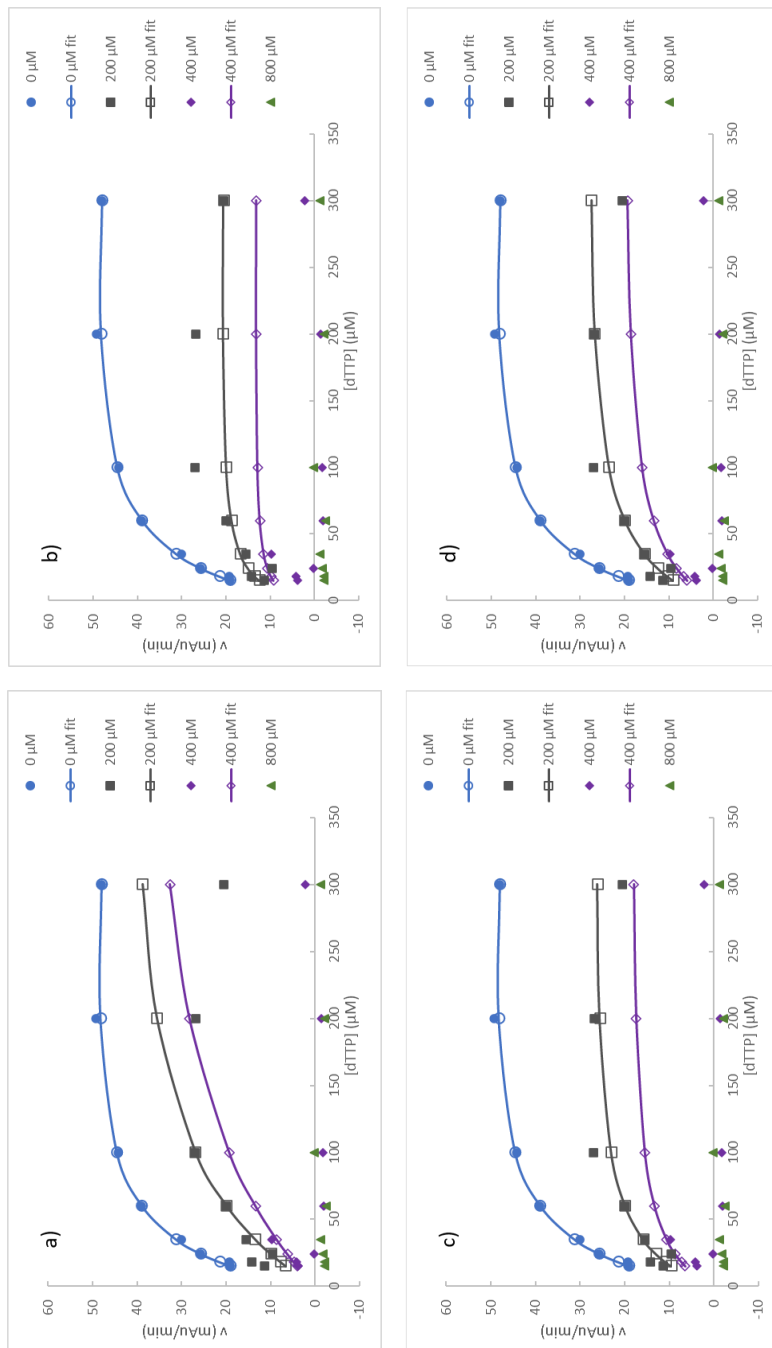
Note: Optimization of the fit did not consider the 800 μM or last 5 400 μM datapoints due to poor quality.

Structure	Mode of inhibition	K_{IC} (μM)	K_{IU} (μM)	Sum of absolute differences (SAD) (mAu/min)
	Competitive (a)	74.4	-	45.6
	Uncompetitive (b)	-	115.1	38.6
	Noncompetitive (c)	204.2		31.3
4b	Mixed (d)	162.0	240.0	30.0
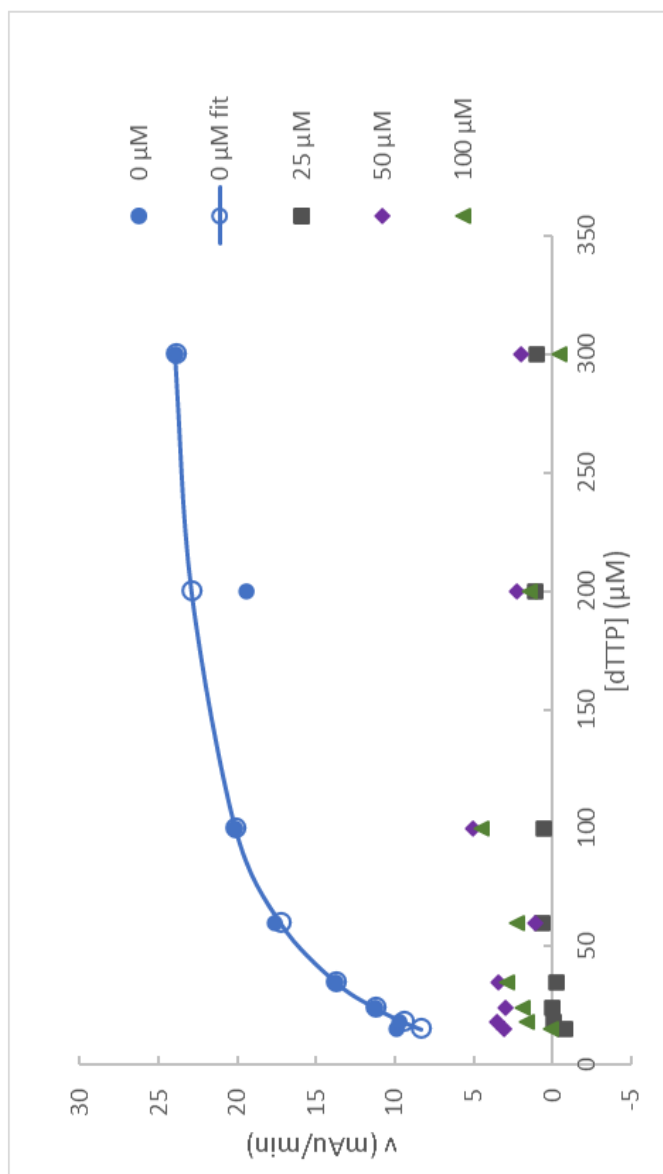
Appendix E3.

Rate inhibition data (solid shapes) for inhibition of Cps2L by **4d**. The fitting algorithm failed to converge for each model attempted (competitive, noncompetitive, uncompetitive, and mixed inhibition). Qualitative observation of the data suggests that this compound completely inactivates Cps2L at the concentrations tested. Calculated parameters (from 0 μM inhibitor): $V_{max} = 26.9$ mAu/min; $K_M = 33.3$ μM; K_{IS} (substrate) $= 21900$ μM.
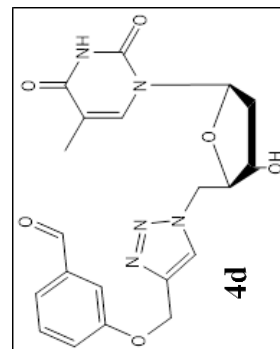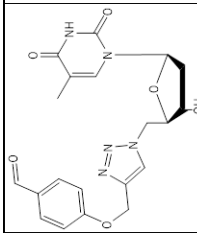
Appendix E4.
Left: rate inhibition data (solid shapes) and mathematical model (lines / open shapes) for inhibition of Cps2L by **4e** according to a) competitive, b) uncompetitive, c) noncompetitive, and d) mixed inhibition, with substrate inhibition. Calculated parameters: $V_{max} = 39.2$ mAu/min; $K_M = 50.0$ µM; K_{IS} (substrate) = 1000 µM. Below: Summary of calculated inhibition constants and error (SAD) for each model.

a), b), c), d) rate inhibition plots of v (mAu/min) versus [dTTP] (µM), with data series for 0 µM, 100 µM, 200 µM, 300 µM and corresponding fits.
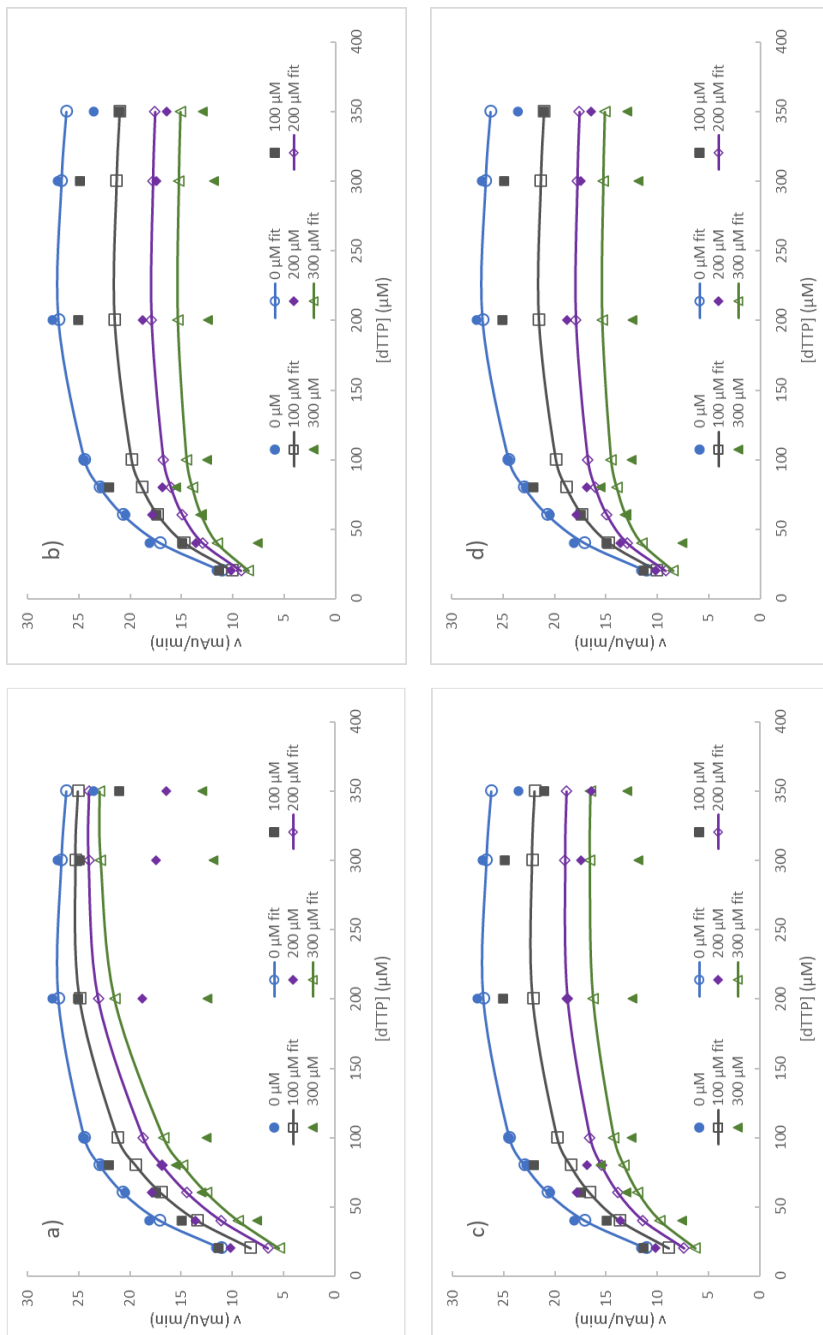
Structure	Mode of inhibition	K_{IC} (µM)	K_{IU} (µM)	Sum of absolute differences (SAD) (mAu/min)
	Competitive (a)	201.8	-	80.9
	Uncompetitive (b)	-	272.3	48.4
	Noncompetitive (c)	393.2		57.9
4e	Mixed (d)	538453	272.2	48.4
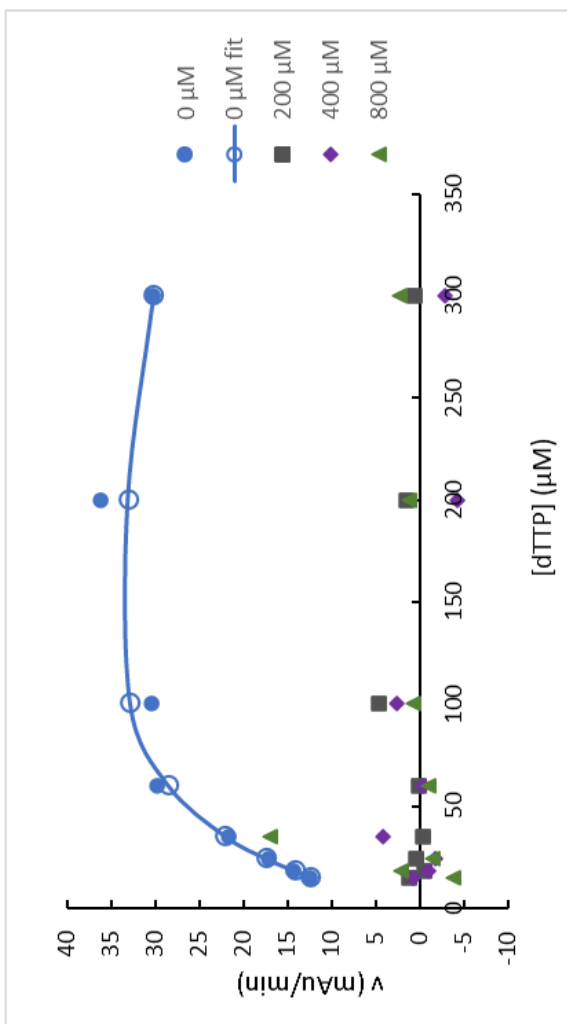
Appendix E5.

Rate inhibition data (solid shapes) for inhibition of Cps2L by **4f**. The fitting algorithm failed to converge for each model attempted (competitive, noncompetitive, uncompetitive, and mixed inhibition). Qualitative observation of the data suggests that this compound completely inactivates Cps2L at the concentrations tested. Calculated parameters (from 0 µM inhibitor): V_{max} = 61.2 mAu/min; K_M = 58.4 µM; K_{IS} (substrate) = 361.4 µM.
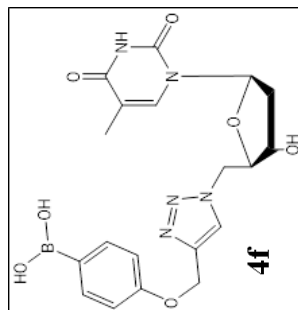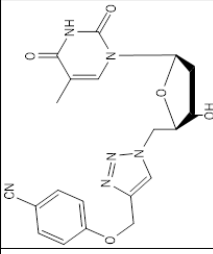
Appendix E6.
Left: rate inhibition data (solid shapes) and mathematical model (lines / open shapes) for inhibition of Cps2L by **4g** according to a) competitive, b) uncompetitive, c) noncompetitive, and d) mixed inhibition, with substrate inhibition. Calculated parameters: V_{max} = 56.4 mAu/min; K_M = 46.3 µM; K_{IS} (substrate) = 428.8 µM. Below: Summary of calculated inhibition constants and error (SAD) for each model.
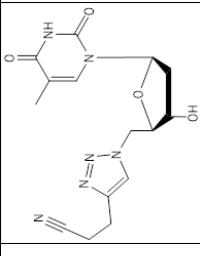
Mode of inhibition	K_{IC} (µM)	K_{IU} (µM)	Sum of absolute differences (SAD) (mAu/min)
Competitive (a)	1660	-	41.9
Uncompetitive (b)	-	2314	35.0
Noncompetitive (c)	3492		34.1
Mixed (d)	3739	3457	33.9

Structure
4g

Appendix E7.
Left: rate inhibition data (solid shapes) and mathematical model (lines / open shapes) for inhibition of Cps2L by **7** according to a) competitive, b) uncompetitive, c) noncompetitive, and d) mixed inhibition, with substrate inhibition. Calculated parameters: V_{max} = 34.4 mAu/min; K_M = 60.6 μM; K_{IS} (substrate) = 600.4 μM. Below: Summary of calculated inhibition constants and error (SAD) for each model.

a)

b)

c)

d)
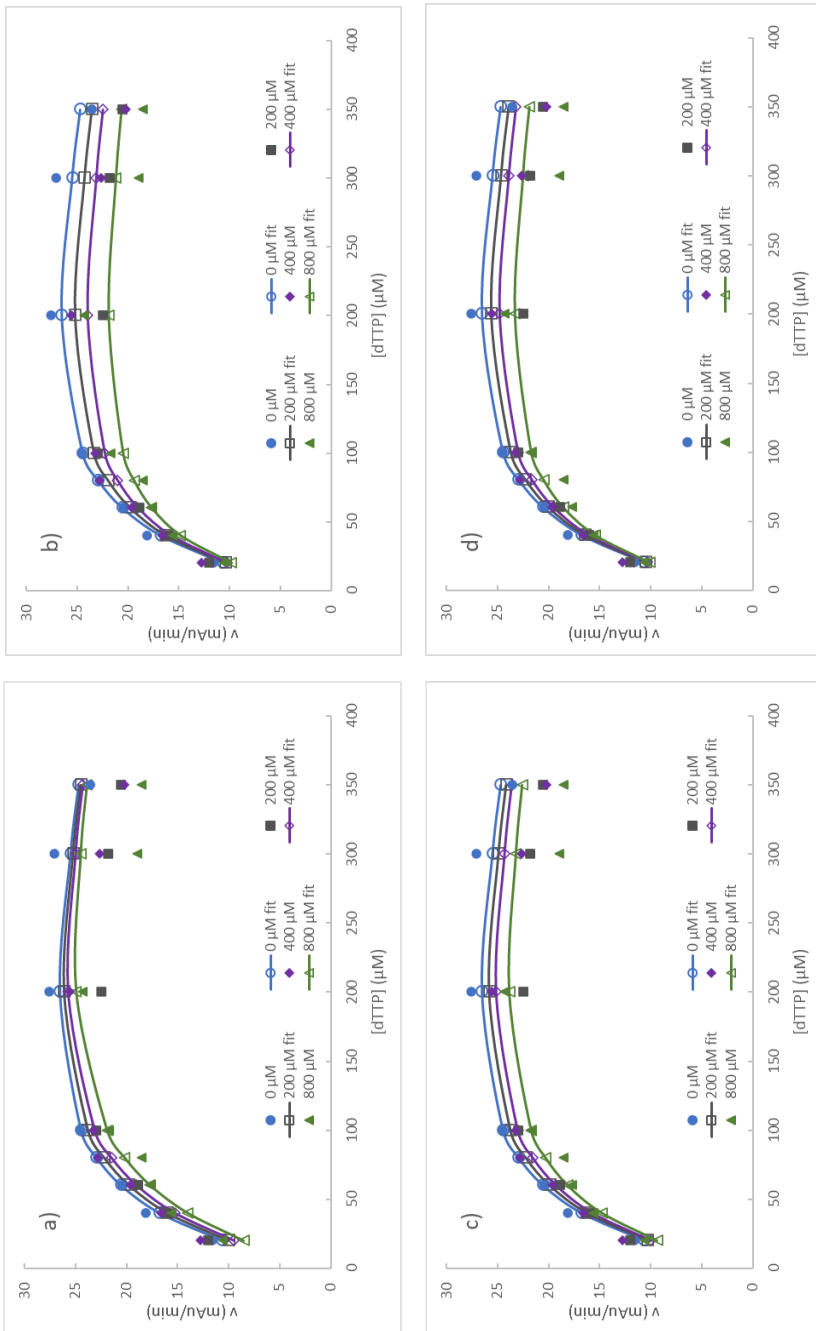
Structure	Mode of inhibition	K_{IC} (μM)	K_{IU} (μM)	Sum of absolute differences (SAD) (mAu/min)
	Competitive (a)	2344	-	47.6
	Uncompetitive (b)	-	2319	36.8
	Noncompetitive (c)	5627		40.8
7	Mixed (d)	5326034	3504	37.5
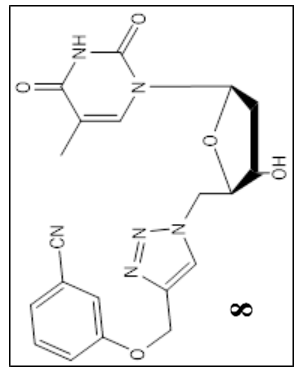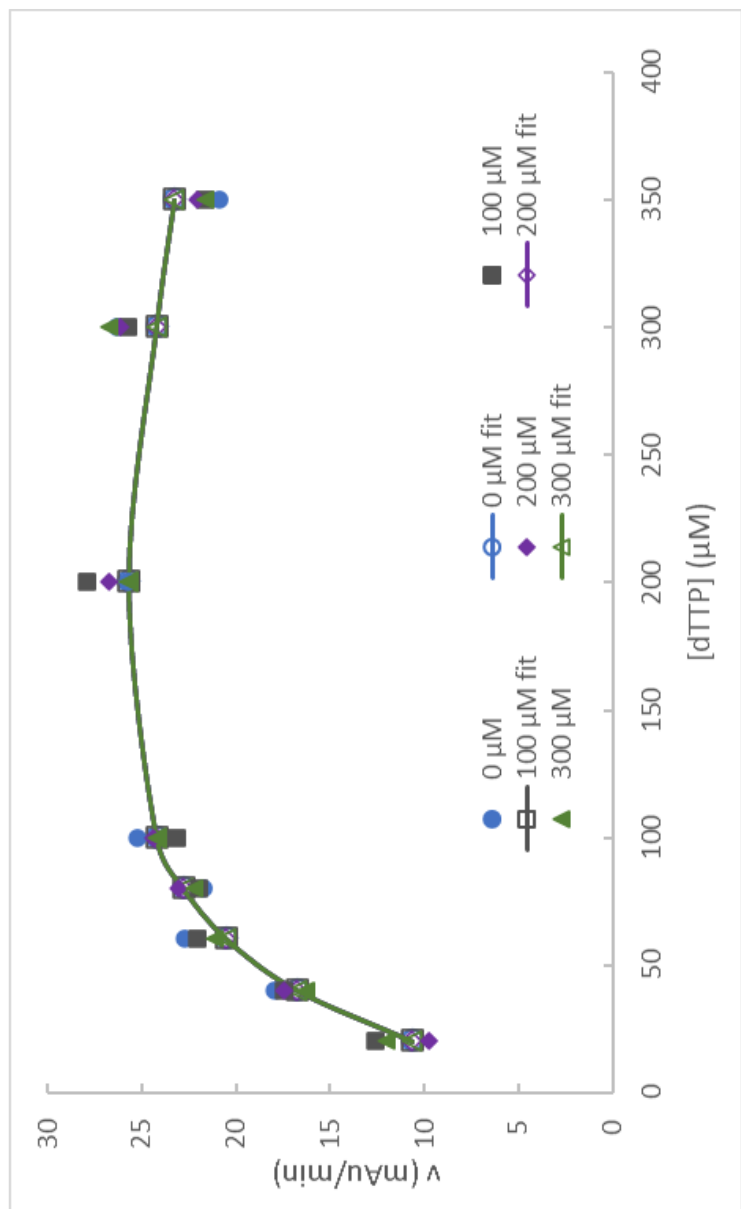
Appendix E8.
Rate inhibition data (solid shapes) and mathematical model (lines / open shapes) for inhibition of Cps2L by **8**. The fitting algorithm failed to converge for each model attempted (competitive, noncompetitive, uncompetitive, and mixed inhibition). Qualitative observation of the data suggests that this compound fails to inhibit Cps2L at the concentrations tested. Calculated parameters: V_{max} = 44.6 mAu/min; K_M = 62.9 μM; K_{IS} (substrate) = 475.6 μM.

174
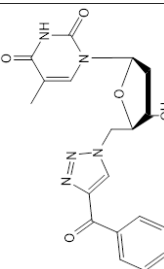
Appendix E9.
Left: rate inhibition data (solid shapes) and mathematical model (lines / open shapes) for inhibition of Cps2L by **10a** according to a) competitive, b) uncompetitive, c) noncompetitive, and d) mixed inhibition, with substrate inhibition.
Calculated parameters:
$V_{max} = 43.7$ mAu/min;
$K_M = 98.9$ μM; K_{IS} (substrate) $= 616.5$ μM.
Below: Summary of calculated inhibition constants and error (SAD) for each model.

Structure	Mode of inhibition	K_{IC} (μM)	K_{IU} (μM)	Sum of absolute differences (SAD) (mAu/min)
	Competitive (a)	332.3	-	34.3
	Uncompetitive (b)	-	339.9	37.7
	Noncompetitive (c)	668.5		19.9
10a	Mixed (d)	556.2	858.6	19.2

APPENDIX G: Kinetic Data From Excel Sheets

G.1: Compound 4a

Raw data

AR2-169	4a			
	0 µM	200 µM	400 µM	800 µM
15	10	6.254545	8.315152	0.660606
18	10.69697	7.842424	6.830303	2.733333
24	11.97576	9.672727	6.575758	-0.218182
35		10.55152	9.266667	-2.169697
60	15.73939	12.94546	11.48485	-0.757576
100	18.4303	15.13939	11.67273	-1.793939
200	18.90303	17.60606	11.61212	2.490909
300	18.10909	14.13939	14.26061	4.393939
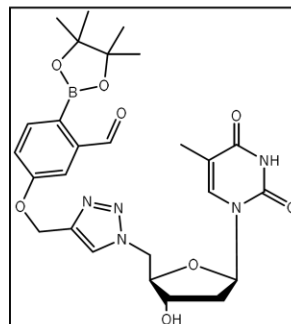
$$v = \frac{Vmax\,[S]}{Km + [S](1 + \frac{[S]}{K_I})}$$

Zero inhibitor

	Vmax	24.12346	Km	22.31487	Kis	1164.886
	0 µM	calc	SAD			
15	10	9.647318	0.352682			
18	10.69697	10.69697	6.75E-08			
24	11.97576	12.36853	0.392777			
35		14.46585				
60	15.73939	16.94751	1.208118			
100	18.4303	18.429	0.001299			
200	18.90303	18.7985	0.104531			
300	18.10909	18.11181	0.002715			
			2.062121			

0 inhibitor

(scatter plot with Series1 data points and Series2 fit line; x-axis 0 to 400, y-axis 0 to 20)
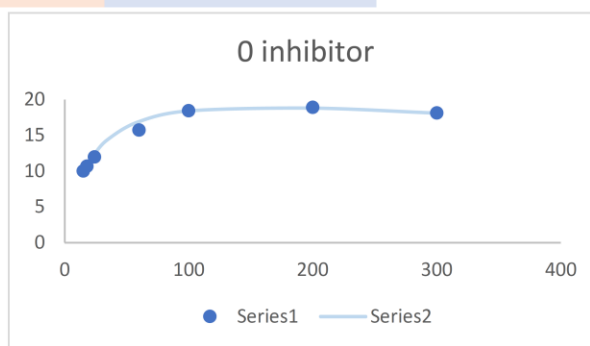
$$v = \frac{Vmax\,[S]}{Km(1 + \frac{[I]}{K_I}) + [S](1 + \frac{[S]}{K_{IS}})}$$

Substrate + competitive inhibition

	Vmax	24.12346	Km	22.31487	Ki	219.9153	Kis	1164.886
		0		200		400		
	0 µM	0 µM fit	200 µM	200 µM fit	400 µM	400 µM fit	800 µM	
15	10	9.647318	6.254545	6.260187	8.315152	4.633416	0.660606	
18	10.69697	10.69697	7.842424	7.1316	6.830303	5.348808	2.733333	
24	11.97576	12.36853	9.672727	8.627923	6.575758	6.624483	-0.21818	
35		14.46585	10.55152	10.73373	9.266667	8.532408	-2.1697	
60	15.73939	16.94751	12.94546	13.69362	11.484848	11.48796	-0.75758	
100	18.4303	18.429	15.13939	15.95536	11.672727	14.06718	-1.79394	
200	18.90303	18.7985	17.60606	17.42099	11.612121	16.23157	2.490909	
300	18.10909	18.11181	14.13939	17.23639	14.260606	16.44169	4.393939	
	SAD 0		SAD 200		SAD 400		SAD 800	
15	0.352682		0.005642		3.681736485		0.660606	
18	6.75E-08		0.710824		1.48149527		2.733333	
24	0.392777		1.044804		0.048725159		0.218182	

		0.182216	0.73425852	2.169697
35		0.182216	0.73425852	2.169697
60	1.208118	0.74817	0.00311252	0.757576
100	0.001299	0.815963	2.394452292	1.793939
200	0.104531	0.185073	4.619453531	2.490909
300	0.002715	3.096993	2.18108539	4.393939
	2.062121	6.789685	12.96323378	21.81504

$$v = \frac{Vmax\,[S]}{Km + [S](1 + \frac{[I]}{K_I} + \frac{[S]}{K_{IS}})}$$

Substrate + uncompetitive inhibition

Vmax	24.12346	Km	22.31487	Ki		503.3327	Kis	1164.886

	0		200		400		800
	0 µM	0 µM fit	200 µM	200 µM fit	400 µM	400 µM fit	800 µM
15	10	9.647318	6.254545	8.3245	8.315152	7.320703	0.660606
18	10.69697	10.69697	7.842424	9.094547	6.830303	7.909667	2.733333
24	11.97576	12.36853	9.672727	10.27518	6.575758	8.787849	-0.21818
35		14.46585	10.55152	11.68226	9.266667	9.797057	-2.1697
60	15.73939	16.94751	12.94546	13.24902	11.484848	10.87561	-0.75758
100	18.4303	18.429	15.13939	14.1375	11.672727	11.46717	-1.79394
200	18.90303	18.7985	17.60606	14.35393	11.612121	11.60916	2.490909
300	18.10909	18.11181	14.13939	13.95008	14.260606	11.34356	4.393939
	SAD 0		SAD 200		SAD 400		SAD 800
15	0.352682		2.069955		0.994449366		0.660606
18	6.75E-08		1.252123		1.079363593		2.733333
24	0.392777		0.602452		2.212091402		0.218182
35			1.130744		0.530390196		2.169697
60	1.208118		0.303563		0.609239172		0.757576
100	0.001299		1.001896		0.205554515		1.793939
200	0.104531		3.252128		0.002963979		2.490909
300	0.002715		0.189316		2.917048796		4.393939
	2.062121		9.802177		5.634052225		17.49835

$$v = \frac{Vmax\,[S]}{Km(1 + \frac{[I]}{K_I}) + [S](1 + \frac{[I]}{K_I} + \frac{[S]}{K_{IS}})}$$

Substrate + nonncompetitive inhibition

Vmax	24.12346	Km	22.31487	Ki		645.4881	Kis	1164.886

	0		200		400		800
	0 µM	0 µM fit	200 µM	200 µM fit	400 µM	400 µM fit	800 µM
15	10	9.647318	6.254545	7.37423	8.315152	5.968047	0.660606
18	10.69697	10.69697	7.842424	8.179862	6.830303	6.621706	2.733333
24	11.97576	12.36853	9.672727	9.466415	6.575758	7.667365	-0.21818
35		14.46585	10.55152	11.09123	9.266667	8.993264	-2.1697
60	15.73939	16.94751	12.94546	13.05029	11.484848	10.61035	-0.75758
100	18.4303	18.429	15.13939	14.29133	11.672727	11.67097	-1.79394
200	18.90303	18.7985	17.60606	14.82077	11.612121	12.23242	2.490909
300	18.10909	18.11181	14.13939	14.49022	14.260606	12.07562	4.393939
	SAD 0		SAD 200		SAD 400		SAD 800

15	0.352682		1.119685		2.347104759	0.660606
18			0.337438		0.208596654	2.733333
24	0.392777		0.206312		1.091607481	0.218182
35	14.46585		0.539716		0.273402983	2.169697
60	1.208118		0.104833		0.874499501	0.757576
100	0.001299		0.848062		0.001756603	1.793939
200	0.104531		2.785287		0.620296949	2.490909
300	0.002715		0.350831		2.184985216	4.393939
	16.52798		6.292165		5.417264931	28.23741

$$v = \frac{Vmax\,[S]}{Km(1 + \frac{[I]}{K_{IC}}) + [S](1 + \frac{[I]}{K_{IU}} + \frac{[S]}{K_{IS}})}$$

Substrate + mixed inhibition					Kic		786.5276		
Vmax	24.12346	Km	22.31487	Kiu		620.6017	Kis	1164.886	
	0		200			400		800	
	0 µM	0 µM fit	200 µM	200 µM fit	400 µM	400 µM fit	SAD 800		
15	10	9.647318	6.254545	7.536018	8.315152	6.182901	0.660606		
18	10.69697	10.69697	7.842424	8.339505	6.830303	6.833496	2.733333		
24	11.97576	12.36853	9.672727	9.614443	6.575758	7.863487	0.218182		
35		14.46585	10.55152	11.20977	9.266667	9.150172	2.169697		
60	15.73939	16.94751	12.94546	13.10872	11.484848	10.68781	0.757576		
100	18.4303	18.429	15.13939	14.29111	11.672727	11.67067	1.793939		
200	18.90303	18.7985	17.60606	14.7643	11.612121	12.15567	2.490909		
300	18.10909	18.11181	14.13939	14.41841	14.260606	11.9762	4.393939		
	SAD 0		SAD 200		SAD 400		SAD 800		
15	0.352682		1.281473		2.132251427		0.660606		
18			0.497081		0.003192721		2.733333		
24	0.392777		0.058284		1.287728574		0.218182		
35	14.46585		0.658251		0.116494699		2.169697		
60	1.208118		0.163261		0.797037734		0.757576		
100	0.001299		0.848286		0.00205558		1.793939		
200	0.104531		2.841759		0.543549197		2.490909		
300	0.002715		0.279016		2.284406576		4.393939		
	16.52798		6.627411		4.882309933		28.0377		

G.2. Compound 4b

Template

Raw data

AR2-167	4b	MOPS		
	0 µM	200 µM	400 µM	800 µM
15	19.15152	11.30909	3.854545	-2.2
18	19.20606	14.27879	4.230303	-2.169697
24	25.65455	9.515152	0.218182	-1.848485
35	29.98788	15.55758	9.787879	-1.218182
60	39.07273	19.92727	-1.95758	-2.551515
100	44.24242	27.07273	-1.73939	0.29697
200	49.23636	26.76364	-1.38788	-2.187879
300	47.98182	20.61212	2.236364	-1.187879
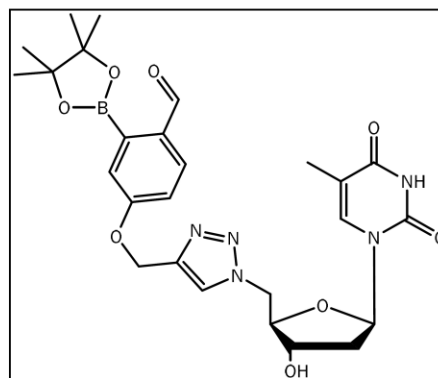
$$v = \frac{Vmax\,[S]}{Km + [S](1 + \frac{[S]}{K_I})}$$

Zero inhibitor

	Vmax	62.8011	Km	34.3597	Ki	1543.848
		calc	SAD			
15	19.15152	19.02854	0.122971			
18	19.20606	21.50331				
24	25.65455	25.66243	0.007886			
35	29.98788	31.33199	1.344109			
60	39.07273	38.96997	0.102762			
100	44.24242	44.59133	0.348903			
200	49.23636	48.25861	0.977755			
300	47.98182	47.98182	4.44E-07			
			2.904387			

0 inhibitor
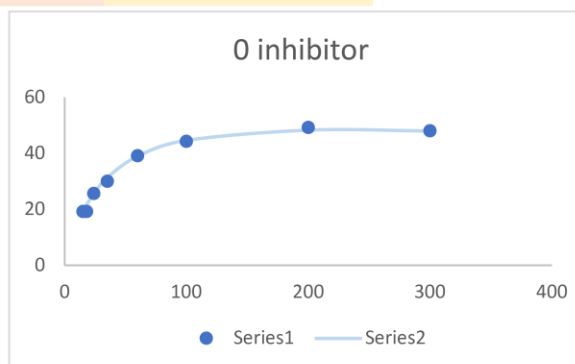
$$v = \frac{Vmax\,[S]}{Km(1 + \frac{[I]}{K_I}) + [S](1 + \frac{[S]}{K_{IS}})}$$

Substrate + competitive inhibition

	Vmax	62.8011	Km	34.3597	Ki		74.37217	Kis	1543.848
		0		200			400		800
	0 µM	0 µM fit	200 µM	200 µM fit	400 µM		400 µM fit	800 µM	800 µM fit
15	19.15152	19.02854	11.30909	6.638369	3.854545		4.020486	-2.2	
18	19.20606	21.50331	14.27879	7.79767	4.230303		4.762303	-2.1697	
24	25.65455	25.66243	9.515152	9.972903	0.218182		6.18904	-1.84849	
35	29.98788	31.33199	15.55758	13.52202	9.787879		8.621385	-1.21818	
60	39.07273	38.96997	19.92727	19.92727	-1.957576		13.38613	-2.55152	
100	44.24242	44.59133	27.07273	26.92594	-1.739394		19.28569	0.29697	
200	49.23636	48.25861	26.76364	35.61482	-1.387879		28.22092	-2.18788	
300	47.98182	47.98182	20.61212	38.84164	2.236364		32.62653	-1.18788	
	SAD 0		SAD 200		SAD 400			SAD 800	
15	0.122971		4.670722		0.165940571			2.2	
18			6.481118		0.532000399			2.169697	

24	0.007886	0.457751		1.848485
35	1.344109	2.035557	1.166493761	1.218182
60	0.102762	2.64E-09		2.551515
100	0.348903	0.146783		0.29697
200	0.977755	8.851184		2.187879
300	4.44E-07	18.22952		1.187879
	2.904387	40.87263	1.864434731	45.64145

$$v = \frac{Vmax\,[S]}{Km + [S](1 + \frac{[I]}{K_I} + \frac{[S]}{K_{IS}})}$$

Substrate + uncompetitive inhibition

	Vmax	62.8011	Km	34.3597	Ki		115.078	Kis	1543.848
		0		200		400		800	
	0 µM	0 µM fit	200 µM	200 µM fit	400 µM		400 µM fit	800 µM	
15	19.15152	19.02854	11.30909	12.4647	3.854545		9.267801	-2.2	
18	19.20606	21.50331	14.27879	13.48102	4.230303		9.818139	-2.1697	
24	25.65455	25.66243	9.515152	15.00569	0.218182		10.60273	-1.84849	
35	29.98788	31.33199	15.55758	16.78129	9.787879		11.45947	-1.21818	
60	39.07273	38.96997	19.92727	18.74952	-1.957576		12.34437	-2.55152	
100	44.24242	44.59133	27.07273	19.96016	-1.739394		12.85781	0.29697	
200	49.23636	48.25861	26.76364	20.66303	-1.387879		13.14587	-2.18788	
300	47.98182	47.98182	20.61212	20.61212	2.236364		13.12524	-1.18788	
	SAD 0		SAD 200		SAD 400			SAD 800	
15	0.122971		1.155611		5.413256165			2.2	
18			0.797771		5.587835987			2.169697	
24	0.007886		5.490539					1.848485	
35	1.344109		1.223713		1.671587934			1.218182	
60	0.102762		1.177754					2.551515	
100	0.348903		7.112568					0.29697	
200	0.977755		6.100603					2.187879	
300	4.44E-07		7.25E-09					1.187879	
	2.904387		23.05856		12.67268009			38.63563	

$$v = \frac{Vmax\,[S]}{Km(1 + \frac{[I]}{K_I}) + [S](1 + \frac{[I]}{K_I} + \frac{[S]}{K_{IS}})}$$

Substrate + nonncompetitive inhibition

	Vmax	62.8011	Km	34.3597	Ki		204.2429	Kis	1543.848
		0		200		400		800	
	0 µM	0 µM fit	200 µM	200 µM fit	400 µM		400 µM fit	800 µM	
15	19.15152	19.02854	11.30909	9.628157	3.854545		6.444485	-2.2	
18	19.20606	21.50331	14.27879	10.88601	4.230303		7.287692	-2.1697	
24	25.65455	25.66243	9.515152	13.00677	0.218182		8.710907	-1.84849	
35	29.98788	31.33199	15.55758	15.91951	9.787879		10.67056	-1.21818	
60	39.07273	38.96997	19.92727	19.92726	-1.957576		13.38612	-2.55152	
100	44.24242	44.59133	27.07273	23.05427	-1.739394		15.54582	0.29697	
200	49.23636	48.25861	26.76364	25.64566	-1.387879		17.46291	-2.18788	

300	47.98182	47.98182	20.61212	26.1646	2.236364	17.98628	-1.18788
	SAD 0		SAD 200		SAD 400		SAD 800
15	0.122971		1.680934		2.589939647		2.2
18	2.29725		3.392782		3.057389395		2.169697
24	0.007886		3.491618				1.848485
35	1.344109		0.361932		0.88268525		1.218182
60	0.102762		1.33E-05				2.551515
100	0.348903		4.018462				0.29697
200	0.977755		1.11798				2.187879
300	4.44E-07		5.552483				1.187879
	5.201637		19.61621		6.530014292		31.34786

$$v = \frac{Vmax\,[S]}{Km(1 + \frac{[I]}{K_I}) + [S](1 + \frac{[I]}{K_I} + \frac{[S]}{K_{IS}})}$$

Substrate + mixed inhibition					Kic		162.0224		
Vmax	62.8011	Km		34.3597	Kiu		240.068	Kis	1543.848
		0		200		400			800
	0 µM	0 µM fit	200 µM	200 µM fit	400 µM	400 µM fit	800 µM		
15	19.15152	19.02854	11.30909	9.021814	3.854545	5.912532	-2.2		
18	19.20606	21.50331	14.27879	10.27852	4.230303	6.753286	-2.1697		
24	25.65455	25.66243	9.515152	12.44195	0.218182	8.211597	-1.84849		
35	29.98788	31.33199	15.55758	15.50917	9.787879	10.30506	-1.21818		
60	39.07273	38.96997	19.92727	19.92727	-1.957576	13.38613	-2.55152		
100	44.24242	44.59133	27.07273	23.55981	-1.739394	16.00911	0.29697		
200	49.23636	48.25861	26.76364	26.76362	-1.387879	18.51625	-2.18788		
300	47.98182	47.98182	20.61212	27.5042	2.236364	19.27713	-1.18788		
	SAD 0		SAD 200		SAD 400		SAD 800		
15	0.122971		2.287277		2.057986531		2.2		
18	2.29725		4.000267		2.522982816		2.169697		
24	0.007886		2.926801				1.848485		
35	1.344109		0.048408		0.517179979		1.218182		
60	0.102762		9.67E-08				2.551515		
100	0.348903		3.512915				0.29697		
200	0.977755		1.56E-05				2.187879		
300	4.44E-07		6.892078				1.187879		
	5.201637		19.66776		5.098149327		29.96755		

G.3. Compound 4d

Template

Raw data

MB1-5	4d	MOPS		
	0 µM	25 µM	50 µM	100 µM
15	9.860606	-0.77576	3.109091	0.145455
18	9.757576	-0.03636	3.509091	1.660606
24	11.27879	0.036364	2.963636	1.933333
35	13.73939	-0.21212	3.472727	2.933333
60	17.6303	0.642424	1.090909	2.284848
100	20.14546	0.575758	5.024242	4.533333
200	19.4	1.066667	2.29697	1.436364
300	23.95152	1	1.975758	-0.430303
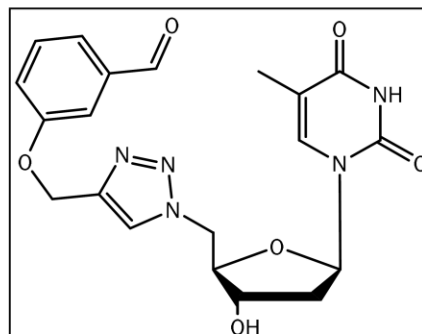
$$v = \frac{Vmax\,[S]}{Km + [S](1 + \frac{[S]}{K_I})}$$

Zero inhibitor

	Vmax	26.9351	Km	33.26064	Ki	21899.76
		calc	SAD			
15	9.860606	8.369978	1.490628			
18	9.757576	9.45544				
24	11.27879	11.28429	0.0055			
35	13.73939	13.79941	0.060016			
60	17.6303	17.29843	0.331877			
100	20.14546	20.14332	0.002134			
200	19.4	22.91499	3.51499			
300	23.95152	23.95151	9.61E-09			
			5.405145			
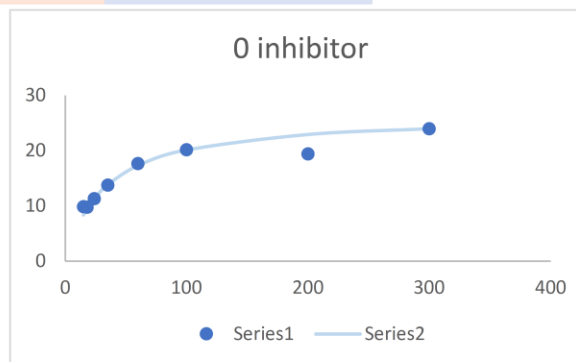
$$v = \frac{Vmax\,[S]}{Km(1 + \frac{[I]}{K_I}) + [S](1 + \frac{[S]}{K_{IS}})}$$

Substrate + competitive inhibition

	Vmax	26.9351	Km	33.26064	Ki	1	Kis	21899.76
		0		25		50		100
	0 µM	0 µM fit	25 µM	25 µM fit	50 µM	50 µM fit	100 µM	100 µM fit
15	9.860606	8.369978	-0.77576	0.459232	3.109091	0.236093	0.145455	0.119735
18	9.757576	9.45544	-0.03636	0.549203	3.509091	0.282815	1.660606	0.143554
24	11.27879	11.28429	0.036364	0.727318	2.963636	0.375769	1.933333	0.191066
35	13.73939	13.79941	-0.21212	1.047671	3.472727	0.544505	2.933333	0.277732
60	17.6303	17.29843	0.642424	1.747253	1.090909	0.920094	2.284848	0.472616
100	20.14546	20.14332	0.575758	2.790527	5.024242	1.499102	4.533333	0.77852
200	19.4	22.91499	1.066667	5.050632	2.29697	2.838083	1.436364	1.512719
300	23.95152	23.95151	1	6.913016	1.975758	4.039452	-0.4303	2.205725
	SAD 0		SAD 25		SAD 50		SAD 100	
15	1.490628		1.23499		2.872998088		0.02572	

18		0.585567	3.226276042	1.517052	
24	0.0055	0.690954	2.587867086	1.742267	
35	0.060016	1.259792	2.928221704	2.655601	
60	0.331877	1.104829	0.170814786	1.812232	
100	0.002134	2.214769	3.525140285	3.754813	
200	3.51499	3.983965	0.541113061	0.076355	
300	9.61E-09	5.913016	2.063694345	2.636028	
	5.405145	16.98788	15.85243105	14.22007	52.46553

$$v = \frac{Vmax\,[S]}{Km + [S](1 + \frac{[I]}{K_I} + \frac{[S]}{K_{IS}})}$$

Substrate + uncompetitive inhibition

	Vmax	26.9351	Km	33.26064	Ki		1	Kis	21899.76
		0		25			50		100
	0 µM	0 µM fit	25 µM	25 µM fit	50 µM	50 µM fit	100 µM	100 µM fit	
15	9.860606	8.369978	-0.77576	0.954534	3.109091	0.506127	0.145455	0.260953	
18	9.757576	9.45544	-0.03636	0.967196	3.509091	0.509665	1.660606	0.261891	
24	11.27879	11.28429	0.036364	0.983501	2.963636	0.514157	1.933333	0.263072	
35	13.73939	13.79941	-0.21212	0.999376	3.472727	0.518462	2.933333	0.264194	
60	17.6303	17.29843	0.642424	1.014234	1.090909	0.522433	2.284848	0.265221	
100	20.14546	20.14332	0.575758	1.022703	5.024242	0.52467	4.533333	0.265797	
200	19.4	22.91499	1.066667	1.029022	2.29697	0.526329	1.436364	0.266222	
300	23.95152	23.95151	1	1.031026	1.975758	0.526852	-0.4303	0.266356	
	SAD 0		SAD 200		SAD 400		SAD 800		
15	1.490628		1.730292		2.602964008		0.115498		
18			1.00356		2.999426049		1.398715		
24	0.0055		0.947137		2.449479439		1.670261		
35	0.060016		1.211497		2.954264809		2.669139		
60	0.331877		0.37181		0.568476483		2.019627		
100	0.002134		0.446945		4.499571559		4.267536		
200	3.51499		0.037645		1.770641369		1.170142		
300	9.61E-09		0.031026		1.44890568		0.696659		
	5.405145		5.779912		17.84482372		14.00758	43.03746	

$$v = \frac{Vmax\,[S]}{Km(1 + \frac{[I]}{K_I}) + [S](1 + \frac{[I]}{K_I} + \frac{[S]}{K_{IS}})}$$

Substrate + nonncompetitive inhibition

	Vmax	26.9351	Km	33.26064	Ki		5	Kis	21899.76
		0		25			50		100
	0 µM	0 µM fit	25 µM	25 µM fit	50 µM	50 µM fit	100 µM	100 µM fit	
15	9.860606	8.369978	-0.77576	1.395244	3.109091	0.761054	0.145455	0.398651	
18	9.757576	9.45544	-0.03636	1.576286	3.509091	0.859811	1.660606	0.450383	
24	11.27879	11.28429	0.036364	1.881435	2.963636	1.026273	1.933333	0.537582	
35	13.73939	13.79941	-0.21212	2.301472	3.472727	1.255426	2.933333	0.657628	
60	17.6303	17.29843	0.642424	2.887305	1.090909	1.575104	2.284848	0.825117	
100	20.14546	20.14332	0.575758	3.366801	5.024242	1.836914	4.533333	0.962335	

| 200 | 19.4 | 22.91499 | 1.066667 | 3.844054 | 2.29697 | 2.097999 | 1.436364 | 1.099324 |
| 300 | 23.95152 | 23.95151 | 1 | 4.032857 | 1.975758 | 2.201793 | -0.4303 | 1.153935 |

	SAD 0	SAD 200	SAD 400	SAD 800	
15	1.490628	2.171002	2.348036672	0.253196	
18		1.61265	2.649280058	1.210223	
24	0.0055	1.845071	1.937363271	1.395751	
35	0.060016	2.513593	2.217300729	2.275705	
60	0.331877	2.244881	0.484194673	1.459731	
100	0.002134	2.791043	3.187328488	3.570998	
200	3.51499	2.777387	0.19897062	0.33704	
300	9.61E-09	3.032857	0.226035059	1.584238	
	5.405145	18.98848	13.02247451	12.08688	49.50298

G.4. Compound 4e

Raw data

AR-78	4e			
	0 μM	100 μM	200 μM	300 μM
20	11.59394	11.32121	10.21212	
40	18.15758	14.92121	13.64242	7.587879
60	20.48485	17.43636	17.90909	12.98788
80	22.82424	22.09091	16.85455	15.56364
100	24.48485			12.53939
200	27.60606	25.02424	18.78182	12.40606
300	27.10303	24.85455	17.48485	11.87879
350	23.5697	21.06061	16.41212	12.97576
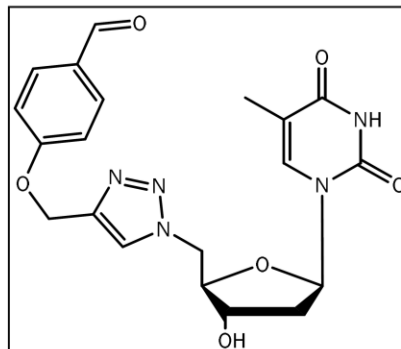
$$v = \frac{Vmax\,[S]}{Km + [S](1 + \frac{[S]}{K_I})}$$

Zero inhibitor

	Vmax	39.17574	Km	49.99992	Ki	999.9998
		calc	SAD			
20	11.59394	11.12948	0.464456			
40	18.15758	17.10732	1.050252			
60	20.48485	20.69142	0.206577			
80	22.82424	22.97699	0.152743			
100	24.48485	24.48485	2.67E-10			
200	27.60606	27.01776	0.588304			
300	27.10303	26.71073	0.392295			
350	23.5697	26.24212	2.672427			
			5.527055			

0 inhibitor
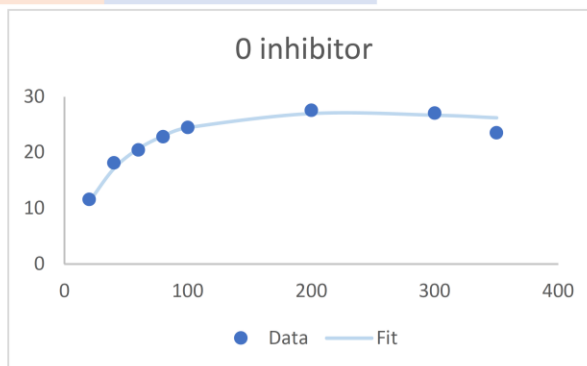
$$v = \frac{Vmax\,[S]}{Km(1 + \frac{[I]}{K_I}) + [S](1 + \frac{[S]}{K_{IS}})}$$

Substrate + competitive inhibition

	Vmax	39.17574	Km	49.99992	Ki	201.8263	Kis	999.9998
		0		100		200		300
	0 μM	0 μM fit	100 μM	100 μM fit	200 μM	200 μM fit	300 μM	300 μM fit
20	11.59394	11.12948	11.32121	8.232474	10.212121	6.532152		5.413961
40	18.15758	17.10732	14.92121	13.4655	13.642424	11.10208	7.587879	9.444423
60	20.48485	20.69142	17.43636	16.98693	17.909091	14.40749	12.98788	12.50814
80	22.82424	22.97699	22.09091	19.44523	16.854545	16.85455	15.56364	14.87302
100	24.48485	24.48485		21.20201		18.69541	12.53939	16.71882
200	27.60606	27.01776	25.02424	24.89137	18.781818	23.07527	12.40606	21.50616
300	27.10303	26.71073	24.85455	25.28698	17.484848	24.00732	11.87879	22.85094
350	23.5697	26.24212	21.06061	25.05421	16.412121	23.96918	12.97576	22.97423
	SAD 0		SAD 100		SAD 200		SAD 300	
20	0.464456		3.088738		3.679968771		5.413961	

40	1.050252	1.455713	2.540346465	1.856544
60	0.206577	0.449431	3.501603684	0.479738
80	0.152743	2.645679	8.02641E-09	0.690621
100	2.67E-10			4.179428
200	0.588304	0.132873	4.293449917	9.100095
300	0.392295	0.432432	6.522471552	10.97215
350	2.672427	3.993601	7.55706	9.998474
	5.527055	12.19847	20.5378404	42.69101	80.95437

$$v = \frac{Vmax\,[S]}{Km + [S](1 + \frac{[I]}{K_I} + \frac{[S]}{K_{IS}})}$$

Substrate + uncompetitive inhibition

Vmax	39.17574	Km	49.99992	Ki	272.2674	Kis	999.9998
	0		100		200		300
	0 µM	0 µM fit	100 µM	100 µM fit	200 µM	200 µM fit	300 µM	300 µM fit
20	11.59394	11.12948	11.32121	10.07793	10.212121	9.207923		8.476195
40	18.15758	17.10732	14.92121	14.74277	13.642424	12.9525	7.587879	11.54994
60	20.48485	20.69142	17.43636	17.32966	17.909091	14.9076	12.98788	13.07955
80	22.82424	22.97699	22.09091	18.90461	16.854545	16.05845	15.56364	13.95715
100	24.48485	24.48485		19.9136		16.7807	12.53939	14.49956
200	27.60606	27.01776	25.02424	21.55728	18.781818	17.93292	12.40606	15.35185
300	27.10303	26.71073	24.85455	21.36137	17.484848	17.79714	11.87879	15.25223
350	23.5697	26.24212	21.06061	21.06061	16.412121	17.58787	12.97576	15.09828

SAD 0		SAD 200		SAD 400		SAD 800	
20	0.464456		1.243287		1.004197501		8.476195
40	1.050252		0.178438		0.689925934		3.962062
60	0.206577		0.106706		3.001492673		0.091671
80	0.152743		3.1863		0.796091536		1.606481
100	2.67E-10						1.960165
200	0.588304		3.46696		0.848902731		2.94579
300	0.392295		3.493174		0.312287122		3.373447
350	2.672427		1.16E-08		1.175752129		2.122524
	5.527055		11.67487		6.652897498		24.53834	48.39315

$$v = \frac{Vmax\,[S]}{Km(1 + \frac{[I]}{K_I}) + [S](1 + \frac{[I]}{K_I} + \frac{[S]}{K_{IS}})}$$

Substrate + nonncompetitive inhibition

Vmax	39.17574	Km	49.99992	Ki	393.1846	Kis	999.9998
	0		100		200		300
	0 µM	0 µM fit	100 µM	100 µM fit	200 µM	200 µM fit	300 µM	300 µM fit
20	11.59394	11.12948	11.32121	8.88306	10.212121	7.391191		6.32837
40	18.15758	17.10732	14.92121	13.68705	13.642424	11.40654	7.587879	9.777441
60	20.48485	20.69142	17.43636	16.60263	17.909091	13.86316	12.98788	11.89969
80	22.82424	22.97699	22.09091	18.49403	16.854545	15.4748	15.56364	13.30303
100	24.48485	24.48485		19.77076		16.57882	12.53939	14.27428

200	27.60606	27.01776	25.02424	22.15927	18.781818	18.78182	12.40606	16.29776
300	27.10303	26.71073	24.85455	22.21617	17.484848	19.01632	11.87879	16.62219
350	23.5697	26.24212	21.06061	21.96536	16.412121	18.88724	12.97576	16.56579

	SAD 0	SAD 200	SAD 400	SAD 800	
20	0.464456	2.438152	2.820930446	6.32837	
40	1.050252	1.234159	2.235883321	2.189562	
60	0.206577	0.83373	4.045928192	1.088191	
80	0.152743	3.596876	1.379741974	2.260609	
100	2.67E-10			1.734881	
200	0.588304	2.864971	2.1457E-09	3.891699	
300	0.392295	2.638379	1.531475142	4.743404	
350	2.672427	0.904752	2.47512103	3.590036	
	5.527055	14.51102	12.01395908	25.82675	57.87878

$$v = \frac{Vmax\,[S]}{Km(1+\frac{[I]}{K_{IC}}) + [S](1+\frac{[I]}{K_{IU}}+\frac{[S]}{K_{IS}})}$$

| Substrate + mixed inhibition				Kic	538453.5		
Vmax	39.17574	Km	49.99992	Kiu	272.2869	Kis	999.9998

	0		100		200		300	
	0 µM	0 µM fit	100 µM	100 µM fit	200 µM	200 µM fit	300 µM	300 µM fit
20	11.59394	11.12948	11.32121	10.07679	10.212121	9.206028		8.473787
40	18.15758	17.10732	14.92121	14.74163	13.642424	12.95074	7.587879	11.54784
60	20.48485	20.69142	17.43636	17.32867	17.909091	14.90614	12.98788	13.07787
80	22.82424	22.97699	22.09091	18.90379	16.854545	16.05727	15.56364	13.95582
100	24.48485	24.48485		19.91293		16.77974	12.53939	14.49849
200	27.60606	27.01776	25.02424	21.55704	18.781818	17.93259	12.40606	15.35149
300	27.10303	26.71073	24.85455	21.36132	17.484848	17.79706	11.87879	15.25215
350	23.5697	26.24212	21.06061	21.0606	16.412121	17.58787	12.97576	15.09828

	SAD 0	SAD 200	SAD 400	SAD 800	
20	0.464456	1.244422	1.006092653	8.473787	
40	1.050252	0.17958	0.691688139	3.95996	
60	0.206577	0.10769	3.002949245	0.089989	
80	0.152743	3.187118	0.797272393	1.607819	
100	2.67E-10			1.959094	
200	0.588304	3.467198	0.849232059	2.945428	
300	0.392295	3.493228	0.312213011	3.373365	
350	2.672427	1.84E-06	1.17574958	2.122521	
	5.527055	11.67924	6.6594475	24.53196	48.39771

G.5. Compound 4f

Raw data

MB1-8	4f			
	0 µM	200 µM	400 µM	800 µM
15	12.47879	1.248485	0.763636	-3.781818
18	14.4303	-0.49697	-0.9697	2.206061
24	17.13333	0.369697	-1.82424	-1.509091
35	21.7697	-0.33333	4.133333	17.08485
60	29.79394	0.060606	-0.26667	-0.909091
100	30.52121	4.660606	2.569697	0.70303
200	36.29091	1.521212	-4.2303	1.218182
300	30.23636	0.630303	-2.88485	2.393939
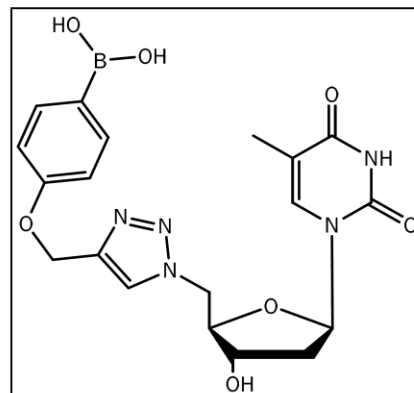
$$v = \frac{Vmax\,[S]}{Km + [S](1 + \frac{[S]}{K_I})}$$

Zero inhibitor

	Vmax	61.21975	Km	58.38922	Ki	361.4128
		calc	SAD			
15	12.47879	12.40743	0.071355			
18	14.4303	14.2582	0.172098			
24	17.13333	17.4949	0.36157			
35	21.7697	22.14011	0.370413			
60	29.79394	28.61847	1.175467			
100	30.52121	32.90351	2.382296			
200	36.29091	33.1755	3.115407			
300	30.23636	30.23636	7.16E-06			
			7.648614			

0 inhibitor

$$v = \frac{Vmax\,[S]}{Km(1 + \frac{[I]}{K_I}) + [S](1 + \frac{[S]}{K_{IS}})}$$

Substrate + competitive inhibition

	Vmax	61.21975	Km	58.38922	Ki		1	Kis	361.4128
			0		200		400		800
	0 µM	0 µM fit	200 µM	200 µM fit	400 µM	400 µM fit	800 µM	800 µM fit
15	12.47879	12.40743	1.248485	0.078141	0.763636	0.039194	-3.78182	0.019628
18	14.4303	14.2582	-0.49697	0.093743	-0.969697	0.047026	2.206061	0.023552
24	17.13333	17.4949	0.369697	0.124919	-1.824242	0.062683	-1.50909	0.031398
35	21.7697	22.14011	-0.33333	0.181975	4.133333	0.091363	17.08485	0.045776
60	29.79394	28.61847	0.060606	0.311124	-0.266667	0.156412	-0.90909	0.07842
100	30.52121	32.90351	4.660606	0.516017	2.569697	0.260048	0.70303	0.13054
200	36.29091	33.1755	1.521212	1.016356	-4.230303	0.516083	1.218182	0.260064
300	30.23636	30.23636	0.630303	1.494956	-2.884848	0.766425	2.393939	0.388132
	SAD 0		SAD 200		SAD 400		SAD 800	
15	0.071355		1.170344		0.724442322		3.801446	

188

18		0.590713	1.016722843	2.182509	
24	0.36157	0.244778	1.886925209	1.540489	
35	0.370413	0.515308	4.041969863	17.03907	
60	1.175467	0.250518	0.423078961	0.987511	
100	2.382296	4.144589	2.309649423	0.57249	
200	3.115407	0.504856	4.746386254	0.958118	
300	7.16E-06	0.864653	3.651273146	2.005807	
	7.476516	8.28576	15.14917487	29.08744	59.99889

$$v = \frac{Vmax\,[S]}{Km + [S](1 + \frac{[I]}{K_I} + \frac{[S]}{K_{IS}})}$$

Substrate + uncompetitive inhibition

	Vmax	61.21975	Km	58.38922	Ki		5	Kis	361.4128
		0		200		400		800	
	0 µM	0 µM fit	200 µM	200 µM fit	400 µM	400 µM fit	800 µM	800 µM fit	
15	12.47879	12.40743	1.248485	1.362433	0.763636	0.720791	-3.78182	0.371177	
18	14.4303	14.2582	-0.49697	1.382134	-0.969697	0.726268	2.206061	0.372624	
24	17.13333	17.4949	0.369697	1.407373	-1.824242	0.733177	-1.50909	0.374434	
35	21.7697	22.14011	-0.33333	1.431535	4.133333	0.739681	17.08485	0.376123	
60	29.79394	28.61847	0.060606	1.452799	-0.266667	0.745317	-0.90909	0.377575	
100	30.52121	32.90351	4.660606	1.462468	2.569697	0.747854	0.70303	0.378225	
200	36.29091	33.1755	1.521212	1.463001	-4.230303	0.747993	1.218182	0.378261	
300	30.23636	30.23636	0.630303	1.456756	-2.884848	0.746357	2.393939	0.377842	
	SAD 0		SAD 200		SAD 400		SAD 800		
15	0.071355		0.113948		0.042845037		4.152995		
18			1.879104		1.695964578		1.833437		
24	0.36157		1.037676		2.557418832		1.883525		
35	0.370413		1.764868		3.393652374		16.70872		
60	1.175467		1.392193		1.01198432		1.286666		
100	2.382296		3.198138		1.821843245		0.324805		
200	3.115407		0.058211		4.978296139		0.839921		
300	7.16E-06		0.826453		3.631205383		2.016097		
	7.476516		10.27059		15.50200452		29.04617	62.29528	

$$v = \frac{Vmax\,[S]}{Km(1 + \frac{[I]}{K_I}) + [S](1 + \frac{[I]}{K_I} + \frac{[S]}{K_{IS}})}$$

Substrate + nonncompetitive inhibition

|	Vmax	61.21975	Km	58.38922	Ki		5	Kis	361.4128
		0		200		400		800	
	0 µM	0 µM fit	200 µM	200 µM fit	400 µM	400 µM fit	800 µM	800 µM fit	
15	12.47879	12.40743	1.248485	0.305124	0.763636	0.154461	-3.78182	0.077714	
18	14.4303	14.2582	-0.49697	0.351742	-0.969697	0.178067	2.206061	0.089593	
24	17.13333	17.4949	0.369697	0.434754	-1.824242	0.220112	-1.50909	0.110753	
35	21.7697	22.14011	-0.33333	0.559107	4.133333	0.283128	17.08485	0.142475	
60	29.79394	28.61847	0.060606	0.75519	-0.266667	0.382644	-0.90909	0.19261	
100	30.52121	32.90351	4.660606	0.938719	2.569697	0.476152	0.70303	0.239811	

200	36.29091	33.1755	1.521212	1.143799	-4.230303	0.581931	1.218182	0.29354
300	30.23636	30.23636	0.630303	1.229067	-2.884848	0.627283	2.393939	0.316929

	SAD 0	SAD 200	SAD 400	SAD 800	
15	0.071355	0.943361	0.609174594	3.859532	
18		0.848712	1.147764224	2.116468	
24	0.36157	0.065057	2.044353952	1.619844	
35	0.370413	0.89244	3.850204737	16.94237	
60	1.175467	0.694584	0.649310813	1.101701	
100	2.382296	3.721887	2.093545406	0.463219	
200	3.115407	0.377413	4.812234102	0.924642	
300	7.16E-06	0.598764	3.512130556	2.07701	
	7.476516	8.142218	15.20658783	29.10479	59.93011

G.6. Compound 4g

Raw data

AR2-22	4g	(TRIS)		
	0 µM	200 µM	400 µM	800 µM
15	11.89091	11.52121	10.53333	9.727273
18	18.15758	17.92727	15.3697	14.07273
24	18.91515	18.71515	16.55152	15.55758
35	24.09697	25.44849	21.56364	19.55758
60	29.29091	28.16364	25.46667	23.14546
100	33.27879	31.67879		29.04242
200	36.29091	33.46667	29.80606	27.61818
300	30.44242	32.27879	30.01818	26.64242
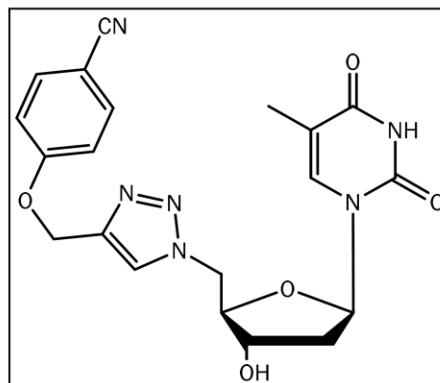
$$v = \frac{Vmax\,[S]}{Km + [S](1 + \frac{[S]}{K_I})}$$

Zero inhibitor

	Vmax	56.43548	Km	46.26325	Ki	428.8007
		calc	SAD			
15	11.89091	13.7006	1.809691			
18	18.15758	15.62376	2.533818			
24	18.91515	18.9152	4.44E-05			
35	24.09697	23.48122	0.615745			
60	29.29091	29.53223	0.241322			
100	33.27879	33.27876	3.19E-05			
200	36.29091	33.24166	3.049247			
300	30.44242	30.44253	0.000108			
			8.250008			

0 inhibitor
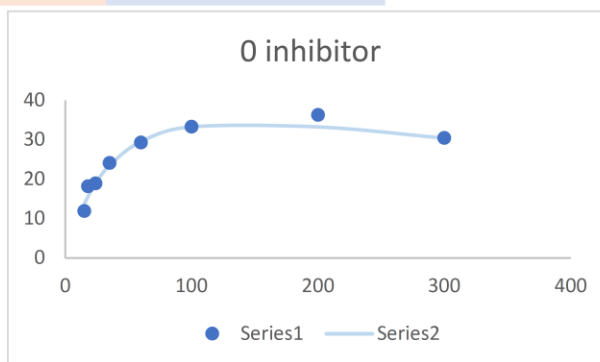
$$v = \frac{Vmax\,[S]}{Km(1 + \frac{[I]}{K_I}) + [S](1 + \frac{[S]}{K_{IS}})}$$

Substrate + competitive inhibition

	Vmax	56.43548	Km	46.26325	Ki	1660.63	Kis	428.8007
			0		200		400	800
	0 µM	0 µM fit	200 µM	200 µM fit	400 µM	400 µM fit	800 µM	800 µM fit
15	11.89091	13.7006	11.52121	12.56733	10.533333	11.60722	9.727273	10.06877
18	18.15758	15.62376	17.92727	14.39056	15.369697	13.3378	14.07273	11.63539
24	18.91515	18.9152	18.71515	17.54964	16.551515	16.36798	15.55758	14.42538
35	24.09697	23.48122	25.44849	22.02254	21.563636	20.73449	19.55758	18.56306
60	29.29091	29.53223	28.16364	28.16364	25.466667	26.91627	23.14546	24.72604
100	33.27879	33.27876	31.67879	32.22015		31.22681	29.04242	29.41321
200	36.29091	33.24166	33.46667	32.70499	29.806061	32.18537	27.61818	31.19415
300	30.44242	30.44253	32.27879	30.14057	30.018182	29.84454	26.64242	29.26959
	SAD 0		SAD 200		SAD 400		SAD 800	
15	1.809691		1.04612		1.073888886		0.341495	

18	2.533818	3.53671	2.031897208	2.437336
24	4.44E-05	1.16551	0.183534704	1.132191
35	0.615745	3.425944	0.829148442	0.994519
60	0.241322	3.32E-07	1.449604596	1.580588
100	3.19E-05	0.541359		0.370788
200	3.049247	0.761675	2.379313131	3.575966
300	0.000108	2.138218	0.173641818	2.627165
	8.250008	12.61554	7.947386966	13.06005	41.87298

$$v = \frac{Vmax\,[S]}{Km + [S](1 + \frac{[I]}{K_I} + \frac{[S]}{K_{IS}})}$$

Substrate + uncompetitive inhibition

	Vmax	56.43548	Km	46.26325	Ki		2314.248	Kis	428.8007
			0		200		400		800
	0 µM	0 µM fit	200 µM	200 µM fit	400 µM	400 µM fit	800 µM	800 µM fit
15	11.89091	13.7006	11.52121	13.41907	10.533333	13.14887	9.727273	12.63986
18	18.15758	15.62376	17.92727	15.25869	15.369697	14.9103	14.07273	14.25915
24	18.91515	18.9152	18.71515	18.38273	16.551515	17.87943	15.55758	16.95121
35	24.09697	23.48122	25.44849	22.66621	21.563636	21.90587	19.55758	20.5286
60	29.29091	29.53223	28.16364	28.25447	25.466667	27.08268	23.14546	25.00837
100	33.27879	33.27876	31.67879	31.66508		30.20067	29.04242	27.64378
200	36.29091	33.24166	33.46667	31.6315	29.806061	30.17011	27.61818	27.61818
300	30.44242	30.44253	32.27879	29.08659	30.018182	27.84629	26.64242	25.65807

|	SAD 0		SAD 200		SAD 400		SAD 800	
15	1.809691		1.897855		2.615537938		2.912585	
18			2.668581		0.459399192		0.186426	
24	4.44E-05		0.332418		1.327913664		1.39363	
35	0.615745		2.782279		0.342231309		0.971026	
60	0.241322		0.090829		1.616016654		1.862913	
100	3.19E-05		0.013705				1.398647	
200	3.049247		1.83517		0.364051602		5.53E-06	
300	0.000108		3.192199		2.171896151		0.984349	
	5.71619		12.81303		6.725150359		9.709581	34.96396

$$v = \frac{Vmax\,[S]}{Km(1 + \frac{[I]}{K_I}) + [S](1 + \frac{[I]}{K_I} + \frac{[S]}{K_{IS}})}$$

Substrate + nonncompetitive inhibition

	Vmax	56.43548	Km	46.26325	Ki		3492.069	Kis	428.8007
			0		200		400		800
	0 µM	0 µM fit	200 µM	200 µM fit	400 µM	400 µM fit	800 µM	800 µM fit
15	11.89091	13.7006	11.52121	12.9644	10.533333	12.30328	9.727273	11.16461
18	18.15758	15.62376	17.92727	14.78672	15.369697	14.03482	14.07273	12.73923
24	18.91515	18.9152	18.71515	17.90876	16.551515	17.00401	15.55758	15.44359
35	24.09697	23.48122	25.44849	22.25018	21.563636	21.14178	19.55758	19.22625
60	29.29091	29.53223	28.16364	28.0437	25.466667	26.69802	23.14546	24.36017

	0 µM	0 µM fit	200 µM	200 µM fit	400 µM	400 µM fit	800 µM	800 µM fit
100	33.27879	33.27876	31.67879	31.71228		30.28664	29.04242	27.78819
200	36.29091	33.24166	33.46667	31.91593	29.806061	30.69189	27.61818	28.50541
300	30.44242	30.44253	32.27879	29.39438	30.018182	28.416	26.64242	26.64243

	SAD 0	SAD 200	SAD 400	SAD 800	
15	1.809691	1.443188	1.769951772	1.43734	
18	2.533818	3.140548	1.334878908	1.333492	
24	4.44E-05	0.806396	0.452490486	0.11399	
35	0.615745	3.198309	0.421859164	0.331322	
60	0.241322	0.119938	1.231353161	1.214717	
100	3.19E-05	0.033489		1.254238	
200	3.049247	1.550734	0.885831253	0.88723	
300	0.000108	2.88441	1.60218339	1.02E-05	
	8.250008	13.17701	6.096364745	6.57234	34.09573

$$v = \frac{Vmax\,[S]}{Km(1 + \frac{[I]}{K_{IC}}) + [S](1 + \frac{[I]}{K_{IU}} + \frac{[S]}{K_{IS}})}$$

Substrate + mixed inhibition				Kic	3738.941			
Vmax	56.43548	Km	46.26325	Kiu	3456.734	Kis	428.8007	

	0		200		400		800	
	0 µM	0 µM fit	200 µM	200 µM fit	400 µM	400 µM fit	800 µM	800 µM fit
15	11.89091	13.7006	11.52121	12.99748	10.533333	12.363	9.727273	11.26335
18	18.15758	15.62376	17.92727	14.8222	15.369697	14.09887	14.07273	12.84517
24	18.91515	18.9152	18.71515	17.94694	16.551515	17.07298	15.55758	15.55775
35	24.09697	23.48122	25.44849	22.28896	21.563636	21.21191	19.55758	19.34257
60	29.29091	29.53223	28.16364	28.07621	25.466667	26.75702	23.14546	24.45858
100	33.27879	33.27876	31.67879	31.73303		30.32453	29.04242	27.85204
200	36.29091	33.24166	33.46667	31.92116	29.806061	30.70155	27.61818	28.52208
300	30.44242	30.44253	32.27879	29.39434	30.018182	28.41593	26.64242	26.64232

	SAD 0	SAD 200	SAD 400	SAD 800	
15	1.809691	1.476264	1.829665201	1.536074	
18	2.533818	3.105076	1.270828468	1.227556	
24	4.44E-05	0.768216	0.521462585	0.000176	
35	0.615745	3.159529	0.351723741	0.215002	
60	0.241322	0.087426	1.290348021	1.313127	
100	3.19E-05	0.054245		1.190384	
200	3.049247	1.545512	0.895491768	0.903901	
300	0.000108	2.884445	1.602248777	0.000105	
	8.250008	13.08071	6.159519785	6.386325	33.87657

G.7. Compound 7

Raw data

AR2-16	7			
	0 uM	200 uM	400 uM	800 uM
20	11.59394	12.03636	12.78182	10.6
40	18.15758	15.99394	16.60606	15.61818
60	20.48485	18.83636	19.61818	17.67879
80	22.82424		22.8303	18.55152
100	24.48485	22.97576	23.26061	21.69091
200	27.60606	22.46061	25.53333	24.29091
300	27.10303	21.79394	22.6	18.93939
350	23.5697	20.5697	20.24242	18.55758
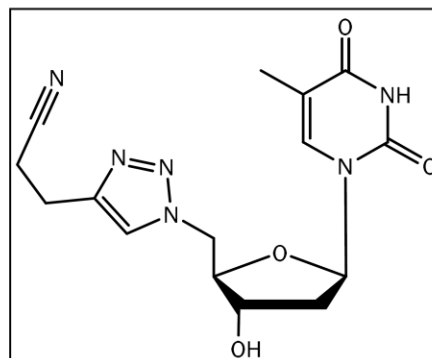
$$v = \frac{Vmax\,[S]}{Km + [S](1 + \frac{[S]}{K_I})}$$

Zero inhibitor

	Vmax	43.40958	Km	60.63849	Ki	600.4879
		calc	SAD			
20	11.59394	10.67826	0.915681			
40	18.15758	16.80865	1.348931			
60	20.48485	20.5678	0.082953			
80	22.82424	22.95339	0.129143			
100	24.48485	24.48485	6E-09			
200	27.60606	26.52984	1.076221			
300	27.10303	25.50921	1.593821			
350	23.5697	24.71914	1.149443			
			6.296192			

0 inhibitor
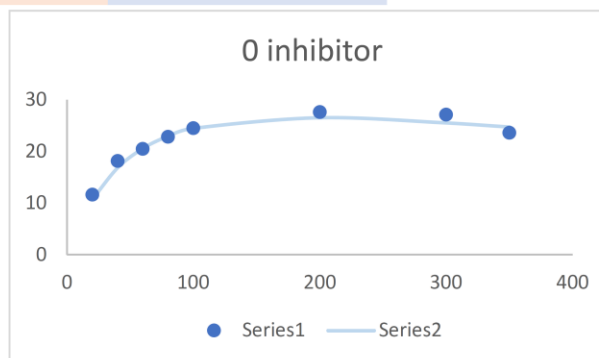
$$v = \frac{Vmax\,[S]}{Km(1 + \frac{[I]}{K_I}) + [S](1 + \frac{[S]}{K_{IS}})}$$

Substrate + competitive inhibition

	Vmax	43.40958	Km	60.63849	Ki	2344.188	Kis	600.4879
		0		200		400		800
	0 µM	0 µM fit	200 µM	200 µM fit	400 µM	400 µM fit	800 µM	800 µM fit
20	11.59394	10.67826	12.03636	10.03944	12.781818	9.472733	10.6	8.511792
40	18.15758	16.80865	15.99394	16.007	16.606061	15.27834	15.61818	14.00342
60	20.48485	20.5678	18.83636	19.7605	19.618182	19.01418	17.67879	17.67879
80	22.82424	22.95339		22.19446	22.830303	21.48411	18.55152	20.19161
100	24.48485	24.48485	22.97576	23.79062	23.260606	23.13467	21.69091	21.92562
200	27.60606	26.52984	22.46061	26.11696	25.533333	25.71673	24.29091	24.95198
300	27.10303	25.50921	21.79394	25.25329	22.6	25.00246	18.93939	24.51546
350	23.5697	24.71914	20.5697	24.51281	20.242424	24.3099	18.55758	23.91399
	SAD 0		SAD 200		SAD 400		SAD 800	
20	0.915681		1.996928		3.309084607		2.088208	

40	1.348931	0.01306	1.327724831	1.614759	
60	0.082953	0.924137	0.604000585	1.16E-09	
80	0.129143		1.346197325	1.640096	
100	6E-09	0.81486	0.125936154	0.234707	
200	1.076221	3.656351	0.183394696	0.661066	
300	1.593821	3.459356	2.402464258	5.576067	
350	1.149443	3.943114	4.067474971	5.356412	
	6.296192	14.80781	9.298802455	17.17132	47.57412

$$v = \frac{Vmax\,[S]}{Km + [S](1 + \frac{[I]}{K_I} + \frac{[S]}{K_{IS}})}$$

Substrate + uncompetitive inhibition

	Vmax	43.40958	Km	60.63849	Ki		2319.505	Kis	600.4879
		0		200		400			800
	0 µM	0 µM fit	200 µM	200 µM fit	400 µM	400 µM fit	800 µM	800 µM fit
20	11.59394	10.67826	12.03636	10.45647	12.781818	10.24371	10.6	9.843148
40	18.15758	16.80865	15.99394	16.26558	16.606061	15.75651	15.61818	14.82833
60	20.48485	20.5678	18.83636	19.7605	19.618182	19.01418	17.67879	17.67879
80	22.82424	22.95339		21.95251	22.830303	21.03527	18.55152	19.41301
100	24.48485	24.48485	22.97576	23.34926	23.260606	22.31434	21.69091	20.49732
200	27.60606	26.52984	22.46061	25.20179	25.533333	24.00036	24.29091	21.91124
300	27.10303	25.50921	21.79394	24.27901	22.6	23.162	18.93939	21.21034
350	23.5697	24.71914	20.5697	23.56223	20.242424	22.50877	18.55758	20.66126
	SAD 0		SAD 200		SAD 400		SAD 800	
20	0.915681		1.579892		2.538107052		0.756852	
40	1.348931		0.271642		0.849551682		0.789851	
60	0.082953		0.924137		0.604000586		3.54E-09	
80	0.129143				1.795030088		0.861499	
100	6E-09		0.373505		0.946262249		1.193588	
200	1.076221		2.741182		1.532974035		2.379672	
300	1.593821		2.485066		0.561997716		2.27095	
350	1.149443		2.992535		2.26634919		2.103683	
	6.296192		11.36796		8.827923409		10.35609	36.84817

$$v = \frac{Vmax\,[S]}{Km(1 + \frac{[I]}{K_I}) + [S](1 + \frac{[I]}{K_I} + \frac{[S]}{K_{IS}})}$$

Substrate + nonncompetitive inhibition

	Vmax	43.40958	Km	60.63849	Ki		5627.457	Kis	600.4879
		0		200		400			800
	0 µM	0 µM fit	200 µM	200 µM fit	400 µM	400 µM fit	800 µM	800 µM fit
20	11.59394	10.67826	12.03636	10.31468	12.781818	9.975041	10.6	9.358721
40	18.15758	16.80865	15.99394	16.24615	16.606061	15.72008	15.61818	14.76394
60	20.48485	20.5678	18.83636	19.89423	19.618182	19.26338	17.67879	18.11455
80	22.82424	22.95339		22.21934	22.830303	21.53078	18.55152	20.27423
100	24.48485	24.48485	22.97576	23.72099	23.260606	23.00335	21.69091	21.69091
200	27.60606	26.52984	22.46061	25.79956	25.533333	25.10841	24.29091	23.83156

	0 µM	0 µM fit	200 µM	200 µM fit	400 µM	400 µM fit	800 µM	800 µM fit
300	27.10303	25.50921	21.79394	24.88446	22.6	24.28957	18.93939	23.18124
350	23.5697	24.71914	20.5697	24.14582	20.242424	23.59849	18.55758	22.57504

	SAD 0	SAD 200	SAD 400	SAD 800	
20	0.915681	1.721687	2.806777481	1.241279	
40	1.348931	0.25221	0.885979464	0.854244	
60	0.082953	1.057868	0.354800657	0.43576	
80	0.129143		1.299518589	1.722717	
100	6E-09	0.745233	0.257253606	3.65E-07	
200	1.076221	3.338957	0.424920027	0.459353	
300	1.593821	3.090517	1.689573507	4.241848	
350	1.149443	3.57612	3.356062249	4.017461	
	6.296192	13.78259	7.71882333	12.97266	40.77027

$$v = \frac{Vmax\,[S]}{Km(1 + \frac{[I]}{K_{IC}}) + [S](1 + \frac{[I]}{K_{IU}} + \frac{[S]}{K_{IS}})}$$

Substrate + mixed inhibition				Kic	5326035		
	Vmax	43.40958	Km	60.63849	Kiu	3504.579	Kis	600.4879

	0		200		400		800	
	0 µM	0 µM fit	200 µM	200 µM fit	400 µM	400 µM fit	800 µM	800 µM fit
20	11.59394	10.67826	12.03636	10.53014	12.781818	10.38607	10.6	10.10945
40	18.15758	16.80865	15.99394	16.44489	16.606061	16.09655	15.61818	15.44234
60	20.48485	20.5678	18.83636	20.02595	19.618182	19.51192	17.67879	18.55916
80	22.82424	22.95339		22.28072	22.830303	21.64635	18.55152	20.48015
100	24.48485	24.48485	22.97576	23.72099	23.260606	23.00335	21.69091	21.69091
200	27.60606	26.52984	22.46061	25.63556	25.533333	24.79961	24.29091	23.28124
300	27.10303	25.50921	21.79394	24.68139	22.6	23.90562	18.93939	22.49172
350	23.5697	24.71914	20.5697	23.94104	20.242424	23.21043	18.55758	21.8753

	SAD 0	SAD 200	SAD 400	SAD 800	
20	0.915681	1.506224	2.395743635	0.490545	
40	1.348931	0.450954	0.509509397	0.175841	
60	0.082953	1.189588	0.106262588	0.880367	
80	0.129143		1.18395086	1.928637	
100	6E-09	0.745233	0.257253444	7.74E-08	
200	1.076221	3.174956	0.733725698	1.009666	
300	1.593821	2.887455	1.305618899	3.552324	
350	1.149443	3.371344	2.968009612	3.317722	
	6.296192	13.32576	6.492064521	11.3551	37.46912

G.8. Compound 8

Raw data

AR2-36	8			
	0 µM	100 µM	200 µM	300 µM
20		12.62424	9.775758	12.0303
40	17.96364	17.44849	17.46667	16.29697
60	22.69697	22.05455		21.13939
80	21.67879	21.99394	23.09697	22.22424
100	25.2303	23.1697	24.37576	24.23636
200	25.70909	27.86667	26.7697	25.73333
300	26.33333	25.73333	26.15152	26.70909
350	20.86061	21.62424	22.07879	21.61212
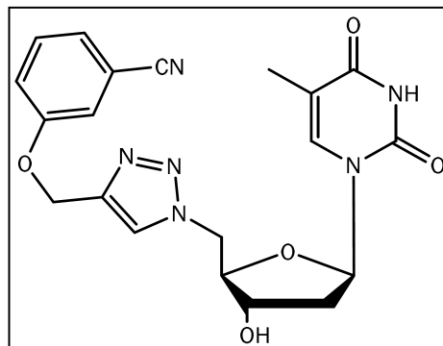
$$v = \frac{Vmax\,[S]}{Km + [S](1 + \frac{[S]}{K_I})}$$

Zero inhibitor

	Vmax	44.61186	Km	62.94042	Ki	475.5634
		calc	SAD			
20		10.64957				
40	17.96364	16.78639	1.17725			
60	22.69697	20.50957	2.187404			
80	21.67879	22.81963	1.140847			
100	25.2303	24.24978	0.980526			
200	25.70909	25.70909	2.58E-06			
300	26.33333	24.23725	2.096085			
350	20.86061	23.28629	2.425688			
			10.0078			

0 inhibitor

(plot: Series1 data points; Series2 fitted curve; x-axis 0 to 400; y-axis 0 to 30)

$$v = \frac{Vmax\,[S]}{Km(1 + \frac{[I]}{K_I}) + [S](1 + \frac{[S]}{K_{IS}})}$$

Substrate + competitive inhibition

	Vmax	44.61186	Km	62.94042	Ki	2.15E+11	Kis	475.5634
			0		100		200	300
	0 µM	0 µM fit	100 µM	100 µM fit	200 µM	200 µM fit	300 µM	300 µM fit
20		10.64957	12.62424	10.64957	9.775758	10.64957	12.0303	10.64957
40	17.96364	16.78639	17.44849	16.78639	17.466667	16.78639	16.29697	16.78639
60	22.69697	20.50957	22.05455	20.50957		20.50957	21.13939	20.50957
80	21.67879	22.81963	21.99394	22.81963	23.09697	22.81963	22.22424	22.81963
100	25.2303	24.24978	23.1697	24.24978	24.375758	24.24978	24.23636	24.24978
200	25.70909	25.70909	27.86667	25.70909	26.769697	25.70909	25.73333	25.70909
300	26.33333	24.23725	25.73333	24.23725	26.151515	24.23725	26.70909	24.23725
350	20.86061	23.28629	21.62424	23.28629	22.078788	23.28629	21.61212	23.28629
	SAD 0		SAD 200		SAD 400		SAD 800	
15	10.64957		1.974673		0.873810561		1.380734	

18		0.662099	0.680281102	0.489416
24	2.187404	1.544979	20.50956552	0.629828
35	1.140847	0.825696	0.277335147	0.595393
60	0.980526	1.08008	0.125981194	0.013413
100	2.58E-06	2.157573	1.060603421	0.024239
200	2.096085	1.496085	1.914267067	2.471843
300	2.425688	1.662052	1.207505864	1.674173
	19.48012	11.40324	25.44184401	7.27904	63.60424

$$v = \frac{Vmax\,[S]}{Km + [S](1 + \frac{[I]}{K_I} + \frac{[S]}{K_{IS}})}$$

Substrate + uncompetitive inhibition

	Vmax	44.61186	Km	62.94042	Ki	2.15E+11	Kis	475.5634
		0		100		200		300
	0 µM	0 µM fit	100 µM	100 µM fit	200 µM	200 µM fit	300 µM	300 µM fit
20		10.64957	12.62424	10.64957	9.775758	10.64957	12.0303	10.64957
40	17.96364	16.78639	17.44849	16.78639	17.466667	16.78639	16.29697	16.78639
60	22.69697	20.50957	22.05455	20.50957		20.50957	21.13939	20.50957
80	21.67879	22.81963	21.99394	22.81963	23.09697	22.81963	22.22424	22.81963
100	25.2303	24.24978	23.1697	24.24978	24.375758	24.24978	24.23636	24.24978
200	25.70909	25.70909	27.86667	25.70909	26.769697	25.70909	25.73333	25.70909
300	26.33333	24.23725	25.73333	24.23725	26.151515	24.23725	26.70909	24.23725
350	20.86061	23.28629	21.62424	23.28629	22.078788	23.28629	21.61212	23.28629
	SAD 0		SAD 200		SAD 400		SAD 800	
15	10.64957		1.974673		0.873810567		1.380734	
18			0.662099		0.680281099		0.489416	
24	2.187404		1.544979		20.50956552		0.629828	
35	1.140847		0.825696		0.277335149		0.595393	
60	0.980526		1.08008		0.125981198		0.013413	
100	2.58E-06		2.157573		1.060603431		0.024239	
200	2.096085		1.496085		1.914267077		2.471843	
300	2.425688		1.662052		1.207505855		1.674173	
	19.48012		11.40324		25.44184404		7.27904	63.60424

$$v = \frac{Vmax\,[S]}{Km(1 + \frac{[I]}{K_I}) + [S](1 + \frac{[I]}{K_I} + \frac{[S]}{K_{IS}})}$$

Substrate + nonncompetitive inhibition

	Vmax	44.61186	Km	62.94042	Ki	2.15E+11	Kis	475.5634
		0		100		200		300
	0 µM	0 µM fit	100 µM	100 µM fit	200 µM	200 µM fit	300 µM	300 µM fit
20		10.64957	12.62424	10.64957	9.775758	10.64957	12.0303	10.64957
40	17.96364	16.78639	17.44849	16.78639	17.466667	16.78639	16.29697	16.78639
60	22.69697	20.50957	22.05455	20.50957		20.50957	21.13939	20.50957
80	21.67879	22.81963	21.99394	22.81963	23.09697	22.81963	22.22424	22.81963
100	25.2303	24.24978	23.1697	24.24978	24.375758	24.24978	24.23636	24.24978
200	25.70909	25.70909	27.86667	25.70909	26.769697	25.70909	25.73333	25.70909

| 300 | 26.33333 | 24.23725 | 25.73333 | 24.23725 | 26.151515 | 24.23725 | 26.70909 | 24.23725 |
| 350 | 20.86061 | 23.28629 | 21.62424 | 23.28629 | 22.078788 | 23.28629 | 21.61212 | 23.28629 |

	SAD 0	SAD 200	SAD 400	SAD 800	
15	10.64957	1.974673	0.873810559	1.380734	
18		0.662099	0.680281108	0.489416	
24	2.187404	1.544979	20.50956551	0.629829	
35	1.140847	0.825696	0.277335158	0.595393	
60	0.980526	1.08008	0.125981206	0.013413	
100	2.58E-06	2.157573	1.060603435	0.024239	
200	2.096085	1.496085	1.914267079	2.471843	
300	2.425688	1.662052	1.207505853	1.674173	
	19.48012	11.40324	25.44184405	7.27904	63.60424

G.9. Compound 10a

Raw data

AR-183	10a			
	0 µM	200 µM	400 µM	800 µM
20	6.833918	5.445614	4.319298	3.94152
40	12.07252	9.334503	8.05731	4.120468
60	16.34386	12.97544	10.18597	7.25731
80	18.19181	13.38129	11.03041	8.57193
100	20.33216	16.3462	13.09006	9.708772
200	24.77544	19.74737	16.56491	12.93333
300	24.34737	21.75205	18.27135	10.00117
350	21.62924	18.7883	15.61053	12.66199
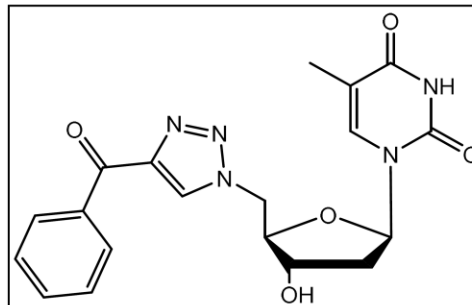
$$v = \frac{Vmax\,[S]}{Km + [S](1 + \frac{[S]}{K_I})}$$

Zero inhibitor

	Vmax	43.73256	Km	98.86999	Ki	616.5011
		calc	SAD			
20	6.833918	7.318106	0.484188			
40	12.07252	12.3656	0.293081			
60	16.34386	15.93081	0.413051			
80	18.19181	18.48657	0.294759			
100	20.33216	20.33216	8.7E-07			
200	24.77544	24.04525	0.730194			
300	24.34737	24.07937	0.267997			
350	21.62924	23.6366	2.007355			
			4.490626			

0 inhibitor

Series1 — Series2
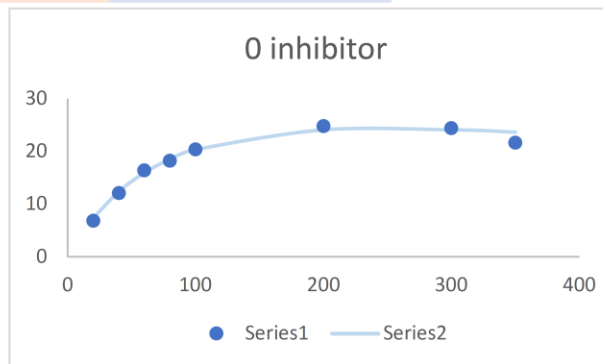
$$v = \frac{Vmax\,[S]}{Km(1 + \frac{[I]}{K_I}) + [S](1 + \frac{[S]}{K_{IS}})}$$

Substrate + competitive inhibition

	Vmax	43.73256	Km	98.86999	Ki		332.3377	Kis	616.5011
		0			200		400		800
	0 µM	0 µM fit	200 µM	200 µM fit	400 µM		400 µM fit	800 µM	800 µM fit
20	6.833918	7.318106	5.445614	4.885814	4.319298		3.66702	3.94152	2.446456
40	12.07252	12.3656	9.334503	8.704514	8.05731		6.716083	4.120468	4.609928
60	16.34386	15.93081	12.97544	11.70315	10.185965		9.248756	7.25731	6.515769
80	18.19181	18.48657	13.38129	14.06469	11.030409		11.34987	8.57193	8.18866
100	20.33216	20.33216	16.3462	15.92648	13.090058		13.09005	9.708772	9.652082
200	24.77544	24.04525	19.74737	20.66502	16.564912		18.11804	12.93333	14.5351
300	24.34737	24.07937	21.75205	21.70872	18.271345		19.76302	10.00117	16.7589
350	21.62924	23.6366	18.7883	21.64759	15.610526		19.96735	12.66199	17.28422
	SAD 0		SAD 200		SAD 400			SAD 800	
20	0.484188		0.5598		0.652277537			1.495064	
40	0.293081		0.629989		1.341227264			0.48946	

60	0.413051	1.272285	0.93720858	0.741541
80	0.294759	0.683408	0.319464299	0.38327
100	8.7E-07	0.41972	3.0106E-06	0.05669
200	0.730194	0.917656	1.553123769	1.601767
300	0.267997	0.043329	1.491671925	6.757726
350	2.007355	2.859284	4.356820424	4.622227
	4.490626	7.385471	6.294976385	16.14775 34.31882

$$v = \frac{Vmax\,[S]}{Km + [S](1 + \frac{[I]}{K_I} + \frac{[S]}{K_{IS}})}$$

Substrate + uncompetitive inhibition

	Vmax	43.73256 Km		98.86999 Ki		339.9146 Kis		616.5011
		0		200		400		800
	0 µM	0 µM fit	200 µM	200 µM fit	400 µM	400 µM fit	800 µM	800 µM fit
20	6.833918	7.318106	5.445614	6.662158	4.319298	6.114128	3.94152	5.25034
40	12.07252	12.3656	9.334503	10.60179	8.05731	9.278351	4.120468	7.424676
60	16.34386	15.93081	12.97544	13.11896	10.185965	11.1508	7.25731	8.577217
80	18.19181	18.48657	13.38129	14.80441	11.030409	12.34544	8.57193	9.266999
100	20.33216	20.33216	16.3462	15.96493	13.090058	13.14209	9.708772	9.708772
200	24.77544	24.04525	19.74737	18.16782	16.564912	14.59929	12.93333	10.48166
300	24.34737	24.07937	21.75205	18.18729	18.271345	14.61186	10.00117	10.48814
350	21.62924	23.6366	18.7883	17.93355	15.610526	14.44763	12.66199	10.40326
	SAD 0		SAD 200		SAD 400		SAD 800	
20	0.484188		1.216544		1.7948298		1.30882	
40	0.293081		1.267292		1.221040979		3.304208	
60	0.413051		0.143518		0.964831444		1.319907	
80	0.294759		1.423124		1.315032734		0.695069	
100	8.7E-07		0.381265		0.052031956		1.32E-08	
200	0.730194		1.57955		1.965626643		2.451674	
300	0.267997		3.564754		3.659486421		0.486969	
350	2.007355		0.854751		1.162898665		2.258733	
	4.490626		10.4308		10.97287998		11.82538 37.71968	

$$v = \frac{Vmax\,[S]}{Km(1 + \frac{[I]}{K_I}) + [S](1 + \frac{[I]}{K_I} + \frac{[S]}{K_{IS}})}$$

Substrate + nonncompetitive inhibition

	Vmax	43.73256 Km		98.86999 Ki		668.4742 Kis		616.5011
		0		200		400		800
	0 µM	0 µM fit	200 µM	200 µM fit	400 µM	400 µM fit	800 µM	800 µM fit
20	6.833918	7.318106	5.445614	5.639877	4.319298	4.587782	3.94152	3.341206
40	12.07252	12.3656	9.334503	9.558319	8.05731	7.789843	4.120468	5.685855
60	16.34386	15.93081	12.97544	12.36306	10.185965	10.10092	7.25731	7.394796
80	18.19181	18.48657	13.38129	14.41137	11.030409	11.80832	8.57193	8.674627
100	20.33216	20.33216	16.3462	15.92648	13.090058	13.09006	9.708772	9.652085
200	24.77544	24.04525	19.74737	19.3007	16.564912	16.11995	12.93333	12.12391

300	24.34737	24.07937	21.75205	19.75296	18.271345	16.74444	10.00117	12.83477
350	21.62924	23.6366	18.7883	19.57668	15.610526	16.70702	12.66199	12.91941

	SAD 0	SAD 200	SAD 400	SAD 800
20	0.484188	0.194263	0.26848414	0.600314
40	0.293081	0.223816	0.267466915	1.565387
60	0.413051	0.612383	0.085041	0.137486
80	0.294759	1.03008	0.777914845	0.102697
100	8.7E-07	0.419717	2.41249E-09	0.056687
200	0.730194	0.446672	0.444964247	0.809419
300	0.267997	1.999088	1.526908006	2.833604
350	2.007355	0.788377	1.096491306	0.257425
	4.490626	5.714395	3.370779156	6.363018	19.93882

Substrate + mixed inhibition

				Kic	556.2873		
Vmax	43.73256	Km	98.86999	Kiu	858.6508	Kis	616.5011

	0		200		400		800	
	0 µM	0 µM fit	200 µM	200 µM fit	400 µM	400 µM fit	800 µM	800 µM fit
20	6.833918	7.318106	5.445614	5.476028	4.319298	4.37482	3.94152	3.119986
40	12.07252	12.3656	9.334503	9.388267	8.05731	7.566452	4.120468	5.450924
60	16.34386	15.93081	12.97544	12.24823	10.185965	9.948528	7.25731	7.232577
80	18.19181	18.48657	13.38129	14.37204	11.030409	11.7556	8.57193	8.617844
100	20.33216	20.33216	16.3462	15.96491	13.090058	13.14206	9.708772	9.708736
200	24.77544	24.04525	19.74737	19.61615	16.564912	16.56491	12.93333	12.63442
300	24.34737	24.07937	21.75205	20.17561	18.271345	17.36103	10.00117	13.57383
350	21.62924	23.6366	18.7883	20.01774	15.610526	17.35988	12.66199	13.71725

	SAD 0	SAD 200	SAD 400	SAD 800
20	0.484188	0.030414	0.055522403	0.821534
40	0.293081	0.053764	0.490857732	1.330456
60	0.413051	0.727204	0.237436805	0.024733
80	0.294759	0.990749	0.725195574	0.045914
100	8.7E-07	0.381289	0.051999361	3.56E-05
200	0.730194	0.131223	1.43731E-07	0.298914
300	0.267997	1.576434	0.910310062	3.572659
350	2.007355	1.229436	1.749349611	1.05526
	4.490626	5.120514	2.47132208	7.149505	19.23197